Interaction mechanisms of epigenetic integrator UHRF1 with TIP60 acetyltransferase

Waseem Ashraf

UNIVERSITÉ DE STRASBOURG

ÉCOLE DOCTORALE DES SCIENCES DE LA VIE ET DE DA SANTE

Laboratoire de Bioimagerie et Pathologies – LBP UMR 7021

THÈSE présentée par :

Waseem ASHRAF

soutenue le : **18 June 2018**

pour obtenir le grade de : **Docteur de l'université de Strasbourg**

Discipline/ Spécialité : DOCTORAT Sciences Pharmaceutiques - Pharmacologie-Pharmacocinétique

Mécanismes d'interaction de l'intégrateur épigénétique UHRF1 avec l'acétyltransférase TIP60

THÈSE dirigée par :

M. MOUSLI Marc	Chargé de recherche, CNRS UMR 7021
M. BRONNER Christian	Chargé de recherche, IGBMC

RAPPORTEURS :

Mme. ARIMONDO Paola	Directrice de recherche, Epigenetic Chemical Biology (EpiChBio), Institut Pasteur
Mme. EYMIN Béatrice	Directrice de recherche, Institut pour l'Avancée des Biosciences, Université Grenoble Alpes

---

AUTRES MEMBRES DU JURY :

Mme DONTENWILL Monique	Directrice de recherches, CNRS UMR 7021
M. BUEB Jean-Luc	Professeur, Université du Luxembourg

ACKNOWLEDGEMENTS

Many people have helped me in the completion of this project and I want to thank them all in my humble acknowledgement.

First and foremost, I would like to express my gratitude to my mentor Dr. Marc MOUSLI for his valuable and continuous support during the last four years. His kind suggestions, encouragement and constructive criticism helped me immensely during the project and enabled me to develop the skills needed through this journey. Secondly, I would also like to thank my co-supervisor Dr. Christian BRONNER for his valuable time, worthy advices and insightful comments regarding the project.

I also extend my gratitude to Prof. Yves MELY, the director of LBP for accepting me in the lab and providing the technical insights to the project.

I am also very thankful to Dr. Paola ARIMONDO, Dr. Béatrice EYMIN, Dr. Monique DONTENWILL and Prof. Jean-Luc BUEB for accepting our request to evaluate this thesis. Their comments will certainly be an added value to our work.

I am also grateful to our collaborators Dr. Christian D. MULLER and Dr. Ali HAMICHE for giving me access to their labs and providing me the research facilities required for this project.

I take this opportunity to thank Dr. Hugues DE ROCQUIGNY, Dr. Ludovic RICHERT and Dr. Pascal DIDIER for their help in setting up and analyzing the FILM experiments and I am also thankful to the members of Plateforme d'Imagerie Quantitative, specially Romain VAUCHELLES, Dr. Philippe CARL, Dr. Philippe RONDE for helping me in confocal microscopy and live cell imaging. I am also grateful to Khalid OUARARHNI and Abdulkhaleg IBRAHIM for their guidance in protein purification. I also thank the permanent members of LBP notably Dr. Eleonore REAL, Dr. Emmanuel BOUTANT and Thiebault LEQUEU for healthy discussions and support in lab. I am also thankful to Marlyse WERNERT and Ingrid BARTHEL for their help in administrative procedures.

Sincere thanks to the past and current labmates Faisal, Maaz, Rajhans, Avisek, Redouane, Lesia, Manu, Sarwat, Nedal, Salah, Marianna, Sacha, Hassan, Yosuke, Krishna, Kamal… and many others for generously sharing their knowledge and keeping a joyable company in the lab. A special

mention to Liliana and Tanveer for their endless laughs and reliable company during the good or bad times, which created timeless memories. I would also like to thank my friends in Strasbourg Zahid, Ikram Ullah, Adnan, Abdul Kareem, Tajith, Naveed, Akmal, Abdul Wahid, Arslan, Salman, Asad, Bilal, Imtiaz, Abid, Hira, Sara, Fareeha, Ramandeep, Camille (and many more) who made this journey easier for me and made my stay in France a memorable experience of my life.

I would also like to acknowledge the Higher Education Commission of Pakistan and Campus France for providing me the financial support to pursue my studies in France.

Finally, I would like to express my deepest gratitude to my family members: my parents, younger brother and sister for their unconditional love, care, support and encouragement throughout my life. In the end, I dedicate this work to my parents as they are the sole inspiration for my achievements.

TABLE OF CONTENTS

LIST OF ABBREVIATIONS ..... **v**

1 - INTRODUCTION **1**

1.1 Epigenetics 1

1.1.1 Chromatin Organization 1

1.1.2 Epigenetic Mechanisms 3

1.2 Ubiquitin like with PHD and Ring Finger domains 1 (UHRF1) 9

1.2.1 Structure of UHRF1 9

1.2.2 Roles of UHRF1 in Cells 14

1.2.3 Post Translational Modification on UHRF1 19

1.2.4 UHRF1 Regulation and its Role in Cancer 21

The epigenetic integrator UHRF1: on the road to become a universal biomarker for cancer (Review Article)…..……22

1.2.5 UHRF1 - A Drugable Target for Anticancer Therapy 40

1.2.6 UHRF1 Partners 41

1.3 Histones / Lysine Acetylation 43

1.3.1 Histone Acetyltransferase 44

1.3.2 Histone Deacetylases 45

1.3.3 Bromodomain proteins 45

1.4 Tat Interactive Protein 60 kDa (TIP60) 45

1.4.1 Structure of TIP60 46

1.4.2 TIP60 as a Lysine Acetyltransferase 49

1.4.3 TIP60 role in DNA Damage Response 52

1.4.4 TIP60 as Transcriptional Regulator 56

1.4.5 TIP60 as Cell Cycle Regulator 60
1.4.6 TIP60 Regulation in Cells 61
1.4.7 Post Translational Modifications Regulating TIP60 Activities 62
1.4.8 TIP60 Deregulation in Cancer 64
1.5 UHRF1-TIP60 interaction and its putative roles in cells 65
1.5.1 DNMT1 Stability 66
1.5.2 p53-Mediated Apoptosis and Cell Cycle Arrest 69
2 - OBJECTIVES 72
3 - MATERIALS AND METHODS 76
3.1 Materials 76
3.1.1 Cell lines 76
3.1.2 Antibodies 76
3.1.3 Plasmid Constructs 78
3.2 Methods 79
3.2.1 Cell Culture 79
3.2.2 Transfection 79
3.2.3 Cell Lysis and Protein Extraction 80
3.2.4 Western Blot 80
3.2.5 Co-Immunoprecipitation 81
3.2.6 Recombinant Protein Expression and Pull-down assays 81
3.2.7 DNA Damage (Double Strand Break) Induction 82
3.2.8 Förster Resonance Energy Transfer (FRET)-Fluorescence Lifetime Imaging Microscopy (FLIM) 83
3.2.9 Confocal Microscopy 85
3.2.10 Global DNA Methylation Assay 87

3.2.11 Cell Cycle Analysis 88

3.2.12 Apoptosis Analysis 88

4 - RESULTS 90

4.1 Interaction of the epigenetic integrator UHRF1 with the MYST domain of TIP60 inside the cell (Manuscript I) 90

4.1.1 Supplementary Results 107

ADDITONAL RESULTS 112

4.2 Interaction of TIP60 and UHRF1 at DNA damage area 113

4.2.1 Introduction 113

4.2.2 Results 113

4.2.3 Discussion 122

4.3 Consequences of TIP60 overexpression in HeLa Cells 124

4.3.1 Introduction 124

4.3.2 Results 125

4.3.3 Discussion 133

5 - CONCLUSION AND PERSPECTIVES 139

6 - REFERENCES 151

LIST OF PUBLICATIONS 166

7 - ANNEXURE 169

7.1 **Manuscript II** 170

7.2 **Manuscript III** 207

8 - RÉSUMÉ DE THÈSE 230

LIST OF ABBREVIATIONS

5-mC	5-methylcytosine
Acetyl CoA	Acetyl-Coenzyme A
ATF3	Activating transcription factor 3
ATM	Ataxia telangiectasia mutated (ATM)
BAX	Bcl-2-Associated X Protein
BCL2	B Cell Lymphoma
BRCA1	Breast Cancer 1
BrdU	5-Bromo-2'-deoxyuridine
Caspase	Cysteine Aspartate Protease
CDK	Cyclin kinase dependent
CpG	Cytosine-phosphate Guanine
DAPI	4',6-diamidino-2-phenylindole
DMEM	Dulbecco's modified Eagle's medium
DNA	Deoxyribonucleic Acid
DNMT1	DNA Methyltransferase 1
DSB	Double Strand Break
E2F1	E2F Transcription Factor 1
EDTA	Ethylenediaminetetraacetic acid
EdU	5-Ethynyl-2´-deoxyuridine
eGFP	enhanced Green Fluorescent Protein
FA	Fanconi Anemia
FACS	Fluorescence-activated cell sorting
FANCD2	Fanconi Anemia Complementation Group D2
FLIM	Fluorescence Lifetime Imaging Microscopy
FRET	Fluorescence Resonance Energy Transfer
FRET	Förster Resonance Energy Transfer
H2K5Ac	Histone 2 Lysine 5 Acetylation
H3K9me2	Histone 3 Lysine 9 dimethylation

H3K9me3	Histone 3 Lysine 9 trimethylation
H4K16Ac	Histone 4 Lysine 16 Acetylation
HAT	Histone Acetyltransferase
HDAC1	Histone Deacetylase 1
HMT	Histone Methyltransferase
HR	Homologous Recombination
ICBP90	Inverted CCAAT box Binding Protein of 90 kDa
ICL	Interstrand Crosslinks
IPTG	isopropyl-1-thio-b-D-galactopyranoside
mad1	mitotic check point proteins
MBD	methyl-CpG binding domain proteins
Mdm2	Mouse double minute 2
miRNA	microRNA
MYST	MOZ, Ybf2/Sas3, Sas2 and Tip60
ncRNA	non-coding RNA
NFκB	Nuclear Factor Kappa B
NHEJ	Non-Hhomologous End Joining
NLS	Nuclear Localization Signal
NR	Nuclear Receptor
PARP	Poly-ADPribose Polymerase
PCNA	Proliferation Cell Nuclear Antigen
PHD	PlantHomeo Domain
PI	Propidium iodide
PMSF	Phenylmethylsulfonyl fluoride
PUMA	p53 upregulated modulator of apoptosis
RING	Really Intersting New Gene
SAM	S-adenosyl methionine
SRA	Set and Ring Associated
Tet	Ten Eleven Translocation
TIP60	Tat Interactive Protein 60 kDa
TSGs	Tumor Suppressor Genes

TTD	Tandem Tudor Domain
UBL	Ubiquitin-Like Domain
UHRF1	Ubiquitin like with PHD and Ring Finger domains 1
USP7 also known as **HAUSP**	Ubiquitin-specific-processing protease 7 or Herpesvirus-associated ubiquitin-specific protease
γH2AX	Phosphorylated gamma Histone H2AX protein

INTRODUCTION

1 - INTRODUCTION

1.1 Epigenetics

Scientists have always been intrigued by the diversity of cellular function that arise from a single genome in the human body. Failure of classical genetics to explain that how an embryonic stem cell leads to well differentiated, specialized cells in the human body despite having a similar genetic makeup led to the foundation of a new field called "Epigenetics". This term was first introduced by Conrad Waddington in 1939 who described it as "the causal interactions between genes and their products, which bring the phenotype into being" (Esteller, 2008). Since then, it is redefined in many ways; Riggs *et al* defined it as "the study of mitotically and/or meiotically heritable changes in gene function that cannot be explained by changes in DNA sequence" (Riggs *et al.*, 1996) and later Bird tried to summarize epigenetic events as "the structural adaptation of chromosomal regions so as to register, signal or perpetuate altered activity states" (Bird, 2007).

Epigenetics serves as an extra layer of control over the genetic sequence, which can turn a gene "on" or "off" in the cells. Epigenetics related mechanisms are important for normal development and maintenance of tissue-specific gene expression patterns in humans. Disruption of these processes can lead to altered gene function and various anomalies including malignant cellular transformation.

1.1.1 Chromatin Organization

In eukaryotes, epigenetic phenomena are mostly linked to the arrangement of genomic DNA into chromatin, a complex and dynamic structure primarily formed by the association between DNA, histone proteins in nucleosome and some non-histone proteins. Nucleosome is the basic structural unit of chromatin, which is made up of 147 base pair of DNA coiled around a histone octamer, comprising of two copies of each core histone proteins H2A, H2B, H3 and H4. Linker H1 histone protein seals the DNA coiling around the core histone proteins and many such nucleosomes fold and condense into higher order chromatin structures called chromosomes in the nucleus of eukaryotic cells (Figure 1) (Cole *et al.*, 2016).

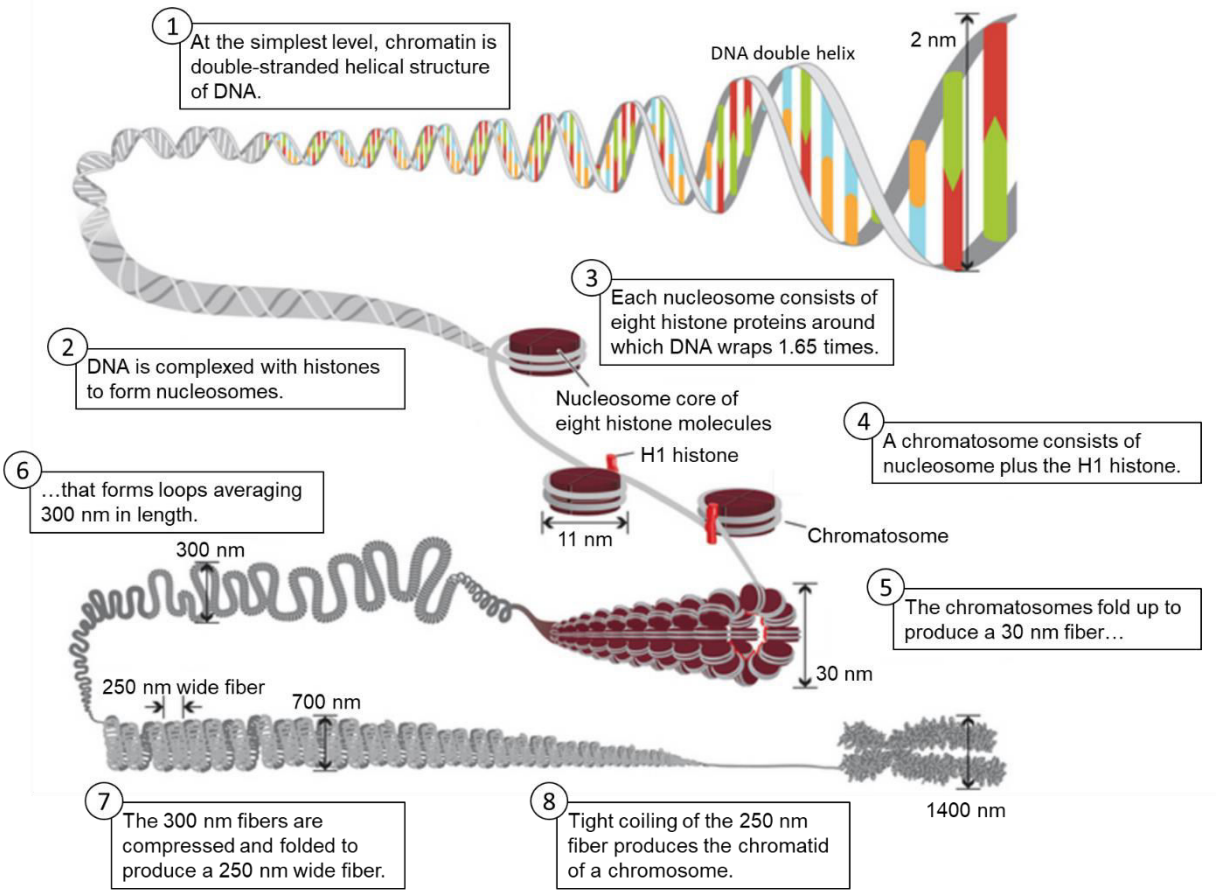

Figure 1: Chromatin organization in eukaryotes. DNA is wrapped around the histone octamer to form a nucleosome and many nucleosomes condense together to form the chromosome. Adapted from Genetics: A Conceptual Approach, 2nd Edition (Pierce, 2012) Courtesy: Nature Education

The compactness of chromatin structure determines the accessibility of DNA to cellular machinery for transcription. Euchromatin structures have loosely packed DNA around the core histone proteins, which allows the binding of transcription factors and are therefore, the sites of active transcription. On the other hand, heterochromatin structures have DNA tightly packed to the histone proteins which reduces the access of transcriptional machinery and thus these areas are repressed regions of gene function (Figure 2) (Allis and Jenuwein, 2016).

Chromatin structure can be mainly affected by the following mechanisms:

1. DNA methylation
2. Post-translational modifications at the N-terminal tails of histones by chromatin-modifying enzymes
3. ATP-dependent chromatin remodeling by different complexes, which can alter the chromatin structure by modifying the interaction between DNA and histones.

4. Exchange of histone variants *i.e.,* H2A to H2A.Z

These changes in the chromatin structure can affect the transcription, replication, recombination and DNA repair mechanisms in the cell.

Various modifications at histones N-terminal tails (including acetylation, methylation, ubiquitination and phosphorylation) regulate the gene expression and are involved in many cellular processes (Figure ***2***). Current studies have indicated that disproportionate global histone modifications may lead to various pathologies because of irregularities in gene expression (Allis and Jenuwein, 2016).

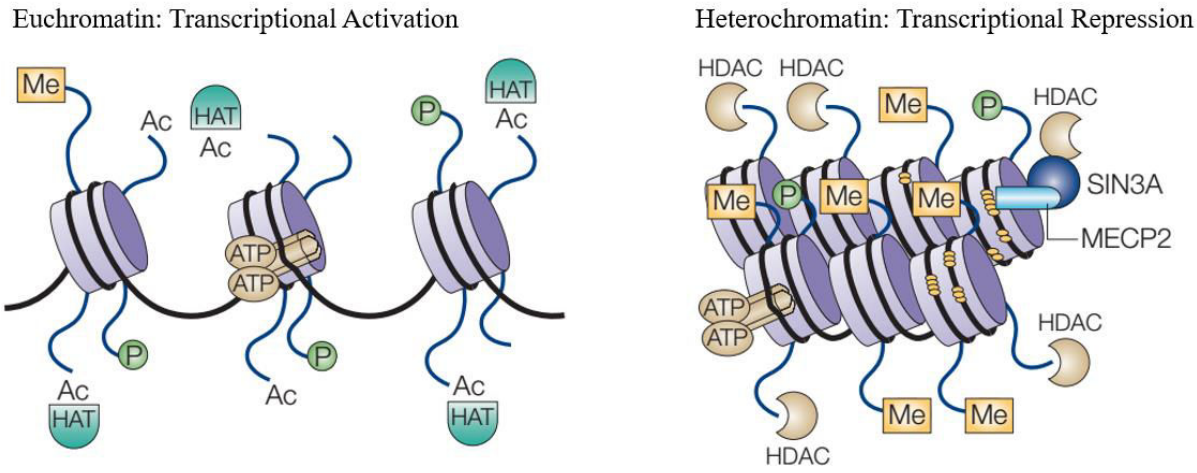

Figure 2: Effect of chromatin structure on transcriptional activity. Loose coiling of DNA or relaxed configuration of chromatin allows active transcription of genes. Tight coiling or compact configuration of chromatin repress the transcriptional activity of genes. Adapted from (Johnstone, 2002)

1.1.2 Epigenetic Mechanisms

DNA methylation, histone modifications, histone variants and non-coding RNA (ncRNA) activity represent the major mechanisms of epigenetic regulation in humans.

1.1.2.1 DNA Methylation

DNA methylation was first discovered by Rollin Hotchkiss in 1948 when he detected 5-methylcytosine (5mC) in calf thymus DNA (Hotchkiss, 1948) and later many studies linked DNA methylation to inheritable mechanisms of gene regulation and cell differentiation (Holliday and Pugh, 1975, Riggs, 1975, Compere and Palmiter, 1981). Today, DNA methylation is a well-recognized and extensively studied epigenetic factor playing important

role in genomic stability, transcriptional regulation, genomic imprinting, X chromosome inactivation and many important developmental processes in humans (Jurkowska *et al.*, 2011).

In mammals, methylation mostly occurs at C5 position on cytosine adjacent to guanosine nucleotide, commonly represented as CpG dinucleotides in genome. DNA methylation is carried out by a group of specific enzymes called DNA methyltransferases (DNMTs) which transfer the methyl group from a methyl group donating cofactor *S*-adenosyl-L-methionine (SAM) to the targeted cytosine (Figure 3) (Robertson, 2005).

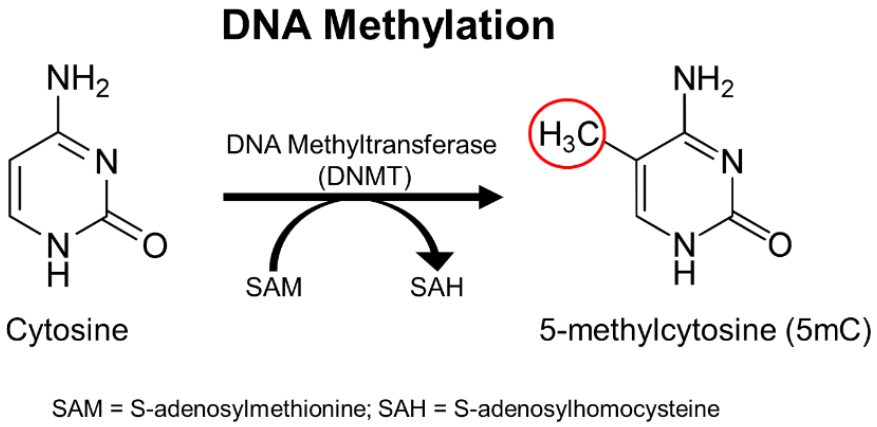

Figure 3: Methylation of cytosine to 5-methylcytosine by the DNA methyltransferase

There are two major classes of DNMTs in mammalian cells (i) maintenance DNA methyltransferase and (ii) *de novo* DNA methyltransferases (Jin and Robertson, 2013). Maintenance DNA methyltransferase (DNMT1) methylates the hemi-methylated DNA generated after DNA replication and maintains the methylation pattern on the newly formed daughter strand by help of other epigenetic partners such as Ubiquitin like with PHD and ring finger domains 1 (UHRF1) and proliferation cell nuclear antigen PCNA. UHRF1 identifies the hemi-methylated DNA by recognizing the methylation marks on parent strand, plus the absence of methylation on daughter strand and recruits DNMT1 for proper establishment of DNA methylation patterns (Bostick *et al.*, 2007, Arita *et al.*, 2008, Avvakumov *et al.*, 2008) On the other hand, *de novo* methyltransferases (DNMT3a, DNMT3b) have equal preferences for hemi or un-methylated DNA but are primarily involved in establishing new pattern of DNA methylation on the genome. DNMTL is another member of this DNMT family lacking the catalytic active domain and helps DNMT3a and DNMT3b to modulate their activities (Xu *et al.*, 2010). DNMT1, DNMT3a and DNMT3b are essential proteins for cells as knock out of

these genes in mammals lead to embryonic development failure and death (Li *et al.*, 1992, Okano *et al.*, 1999, Liao *et al.*, 2015).

DNA methylation primarily occurs on CpG dinucleotides and almost 70-80% of CpG dinucleotides can be methylated in a human cell genome (Bird, 2002). These methylated CpG dinucleotides are not randomly distributed within the genome but are more localized within the repetitive elements (satellite DNAs, interspersed repeat), centromeres and coding region of functional genes. Methylation of CpG dinucleotides in these areas prevents the genomic instability and aberrant initiation of transcription within the gene body (Figure 4) (Portela and Esteller, 2010, Biswas and Rao, 2017). While most of the non-methylated CpG dinucleotides are in the promoter region of active genes where CpG dinucleotides are concentrated in a form of "CpG islands (CGI)". CpG islands are region of 550 bp of DNA which have GC content of at least 50% and have observed to expected CpG ratio of greater than 0.6 (Jurkowska *et al.*, 2011). Approximately, 70% of human gene promoters contain CGIs which are mostly unmethylated for active gene expression. During development and differentiation around 6% of them get methylated in a tissue specific manner to allow specific gene expression needed for the function of those tissues (Portela and Esteller, 2010, Jurkowska *et al.*, 2011).

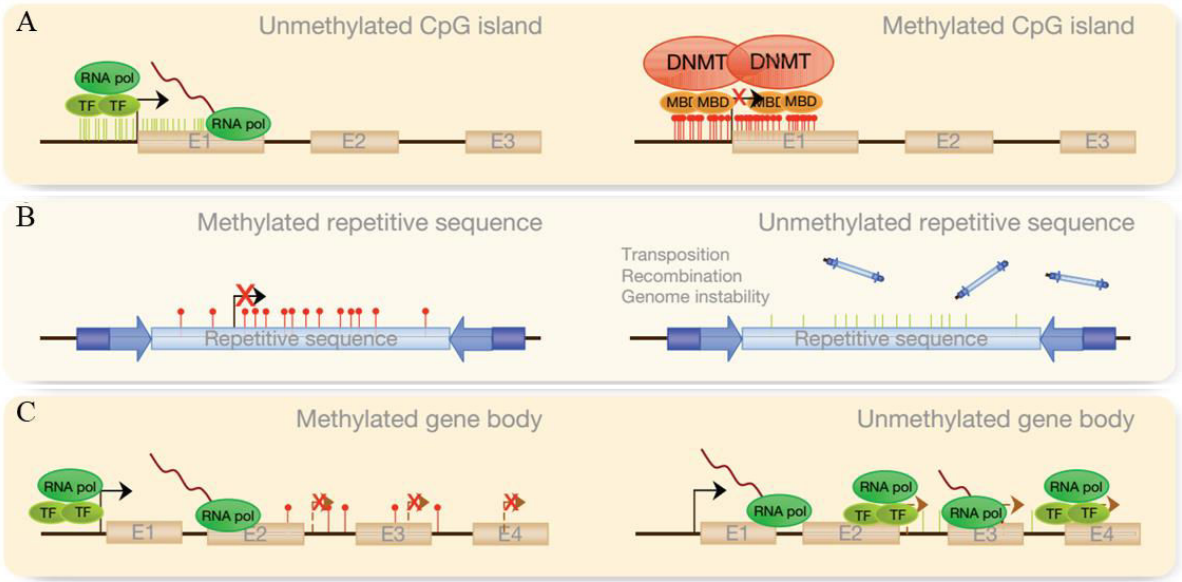

Figure 4: Effect of DNA methylation on transcription. A, CpG islands at the promoter region of active genes are usually unmethylated and allow the binding of transcriptional machinery for transcription and function (Left). However, the promoters of repressed genes are methylated by DNMTs and occupied by methyl-CpG binding domain (MBD) proteins, which maintain the methylation patterns and inhibit transcription (Right). B, Methylation at repetitive sequence is important for chromosomal stability. Repetitive

sequences are hypermethylated (Left) to prevent transposition, translocation and recombination leading to genomic instability which occur when these sequences are hypomethylated (Right). C, Methylation at gene body is also important for the error free transcription, as it prevents the initiation of transcription from incorrect sites (Left). Unmethylated gene body can lead to activation of transcription from multiple intragenic sites which can compromise the gene function (Right). Adapted from (Portela and Esteller, 2010)

Irregularities in methylation pattern, especially in promoters, can lead to serious abnormalities including malignant transformation of cells. In cancers, two seemingly opposite pattern of DNA methylation are observed which together contribute to tumorigenesis. Firstly, CpG in promoter region of various tumor suppressor genes (TSGs) (such as *p16*, *p73*, *BRCA1*, *TIMP3*) are hypermethylated in cancer, inhibiting the expression of these genes and thus leading to unopposed proliferation of transformed cells (Merlo *et al.*, 1995, Pei *et al.*, 2011, Stefansson *et al.*, 2011, Guan *et al.*, 2013). Secondly, a global hypomethylation is observed in many cancer cells, which promotes the expression of oncogenes and aggravates tumor production by inducing genomic instability (Figure 4) (Rodriguez *et al.*, 2006, Dawson and Kouzarides, 2012).

1.1.2.2 Histone Modifications

Histones octamer provides an inherently positive charge base for the effective binding of negatively charged DNA in nucleosome. Histone core proteins consist of a C-terminal globular structure domain and an N-terminal tail, which protrudes out of nucleosome. This N-terminal tail is rich in lysine and arginine residues and can undergo a variety of posttranslational modifications such as acetylation, methylation, ubiquitination, sumoylation and phosphorylation (Inbar-Feigenberg *et al.*, 2013). These posttranslational modifications have been known for a long time to affect the expression of genes by dynamically regulating the structure of chromatin or binding of the non-histone effector proteins to the histone code (Figure 5) (Allfrey *et al.*, 1964, Dawson and Kouzarides, 2012).

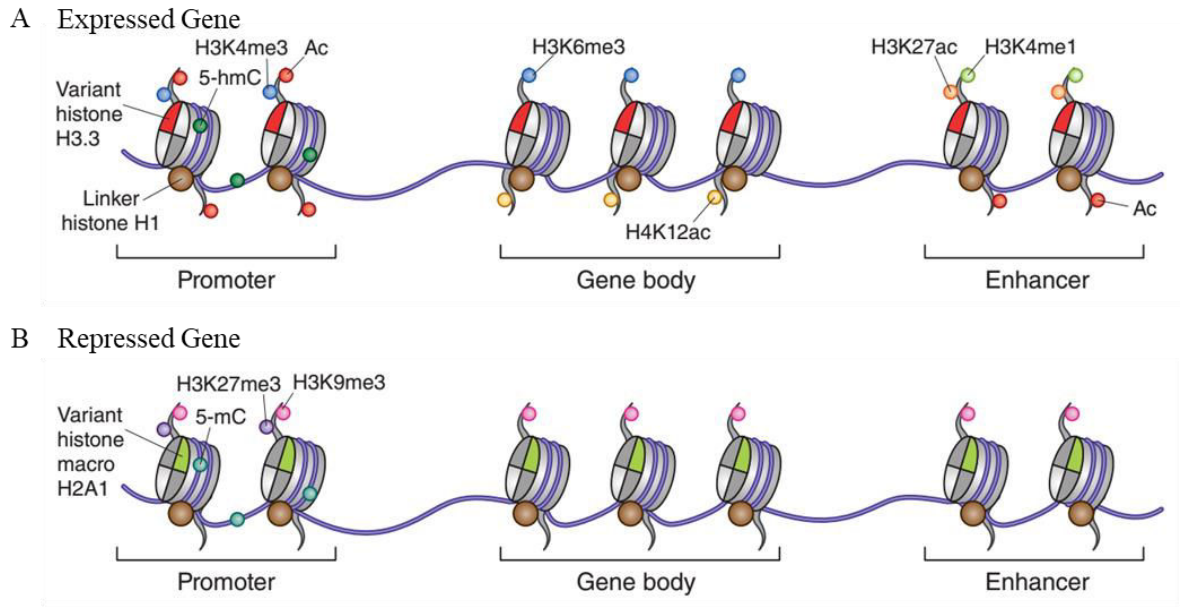

Figure 5: Effect of histone modifications on gene function. A, Histone modifications such as methylation at H3K4, H3K6, and acetylation at H3K27 promote gene function by relaxing the chromatin. B, Repressive histone marks such as trimethylation at H3K9 or H3K27 inhibit gene function by compacting the chromatin structure. Adapted from (Jakovcevski and Akbarian, 2012)

1.1.2.3 Regulatory Non-coding RNAs

In eukaryotes, almost 75% of the genomic DNA is transcribed into RNA and out of it only 3% encodes for protein. The remaining non-coding RNAs are believed to play an important role in epigenetic regulation of gene expression (Figure 6) (Djebali *et al.*, 2012, Inbar-Feigenberg *et al.*, 2013). These non-coding RNAs are characterized into different classes according to the size and the roles they play in cell. Micro RNA (miRNA 19-24 bp) and long non-coding (lnc RNA >200 bp) are well studied classes of non-coding RNAs (Esteller, 2011). miRNAs are single-stranded RNAs produced from precursor RNA by the action of two RNase III family enzymes called DROSHA and DICER. Mature miRNAs bind to the target mRNA of single or multiple genes and lead to their degradation or repression by cellular machinery. Different miRNAs can also target various epigenetic modifiers such as DNMTs or histone methyltransferases and thus affect the epigenome of cells. (Biswas and Rao, 2017).

Lnc RNAs make up the largest proportion of mammalian non-coding transcriptome and mediate epigenetic modifications by acting as molecular chaperones or scaffolds to recruit chromatin remodeling complexes to specific loci on genome (Esteller, 2011). The expression patterns of lncRNAs are tissue specific and have also been shown to play a role in lineage

specific gene expression and other developmental processes such as X-chromosome inactivation and genomic imprinting (Ponting *et al.*, 2009).

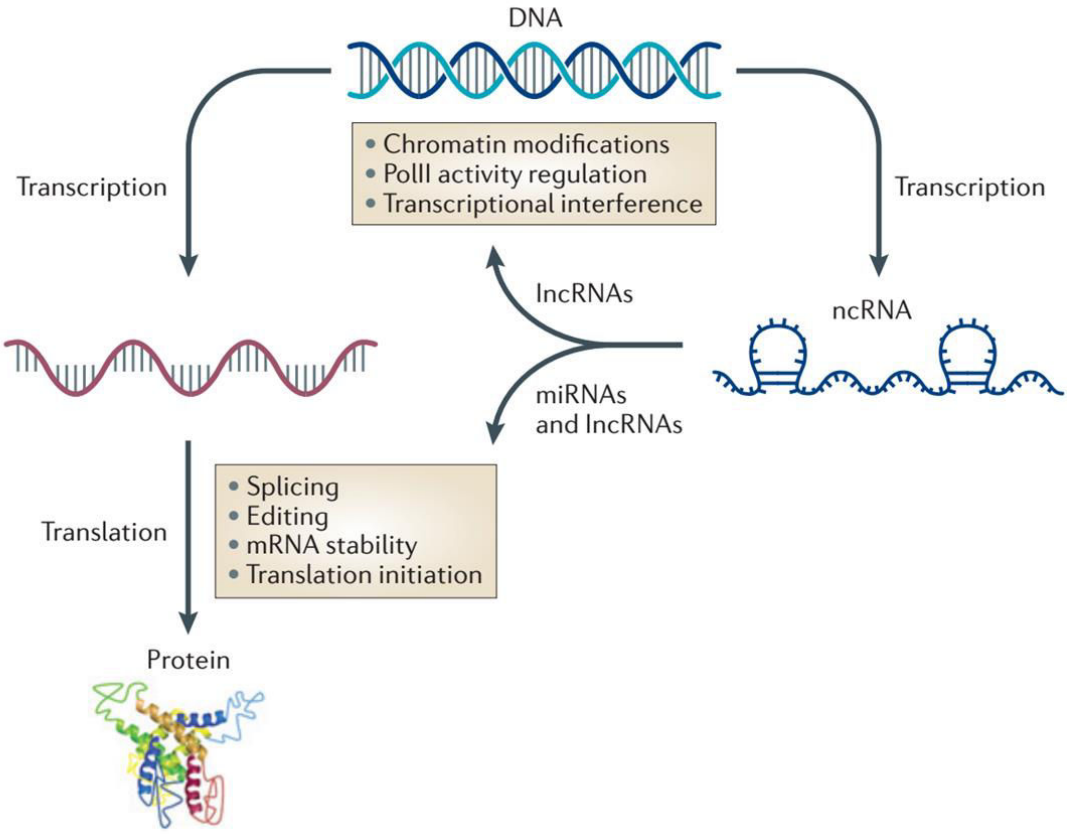

Figure 6: Regulatory effects of non-coding RNAs. Non-coding RNAs are transcribed from the DNA and they interfere in the gene function by altering the chromatin organization, transcriptional activity or stability of mRNA. Adapted from (Wahlestedt, 2013)

Ubiquitin like with PHD and ring finger domains 1 (UHRF1) is an important nuclear protein, which interacts with multiple epigenetic marks on chromatin and coordinates the activities of different proteins involved in DNA methylation and histone modifications. Through its different domains it reads the DNA methylation and histone methylation marks (H3K9me2/3) and can also ubiquitinate histone proteins. It is an integral unit of the epigenetic code replication machinery interacting with other chromatin modifiers. Next section details the structure and function of UHRF1 protein in epigenetics and its role in cancer.

1.2 Ubiquitin like with PHD and Ring Finger domains 1 (UHRF1)

Ubiquitin like with PHD and ring finger domains 1 (UHRF1) was first isolated from Jurkat cells in 2000, as a novel protein binding to an inverted CCAAT box in the promoter region of *topoisomerase IIα* gene and was thus named as Inverted CCAAT Box-binding Protein of 90 kDa (ICBP90) (Hopfner *et al.*, 2000). Initially, it was recognized as a transcription factor modulating the expression of topoisomerase IIα and actively involved in proliferation of cells (Hopfner *et al.*, 2000). But now, UHRF1 is well known as a multifunctional nuclear protein involved in epigenetic modulation, DNA damage response and regulation of stability and functions of other proteins (Alhosin *et al.*, 2011, Alhosin *et al.*, 2016, Ashraf *et al.*, 2017b).

UHRF1 protein has two isoforms. The major isoform of UHRF1 (isoform 1) is 793 amino acid long protein coded by a gene mapped at location 19p13.3 in the genome (Hopfner *et al.*, 2000). The second isoform of UHRF1 results from initiation of translation at an early start codon resulting in longer protein with additional 13 amino acids at N-terminus (Zhang *et al.*, 2016a).

UHRF1 is an evolutionary conserved protein with remarkable similarity of 98% and 73.6% with its rhesus and mouse orthologues, respectively (Bronner *et al.*, 2007). Within the UHRF family, UHRF1 is 53% identical to UHRF2, which is another important member of this family (Bronner *et al.*, 2007).

1.2.1 Structure of UHRF1

UHRF1 is a multidomain protein with special characteristic features (Figure 7). At its N-terminal is ubiquitin-like domain (UBL) followed by a tandem tudor domain (TTD) and plant homeodomain (PHD). At the C-terminus of PHD is the set and ring associated (SRA) domain followed by the really interesting new gene (RING) domain near the C terminus of UHRF1 protein.

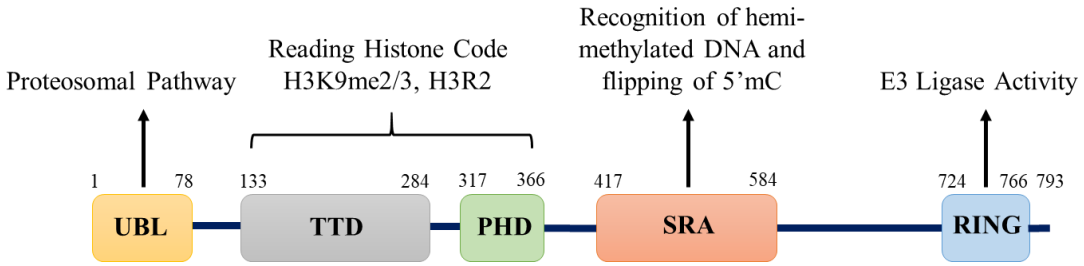

Figure 7: Structure of UHRF1 protein with its five major domains: UBL (ubiquitin-like domain), TTD (tandem tudor Domain), PHD (plant homeodomain), SRA (set and ring finger associated) and RING (really interesting new gene).

1.2.1.1 Ubiquitin-like Domain (UBL)

UBL domain is the N-terminal domain of UHRF1. It is structurally identical (35%) to ubiquitin by having characteristic α-helix and β-sheet folds (Figure 8) and is believed to have similar roles in protein stability, protein-protein interaction and transcriptional regulation. It has two structurally conserved lysine residues K31 and K50 at its surface (like ubiquitin, K29 and K48), the latter of which can be polyubiquitinated and can serve as signal for proteasomal degradation of protein (Bronner *et al.*, 2007). Recently, role of UBL domain of UHRF1 has also been reported in recruitment and localization of DNMT1 for the maintenance of methylation (Li *et al.*, 2018).

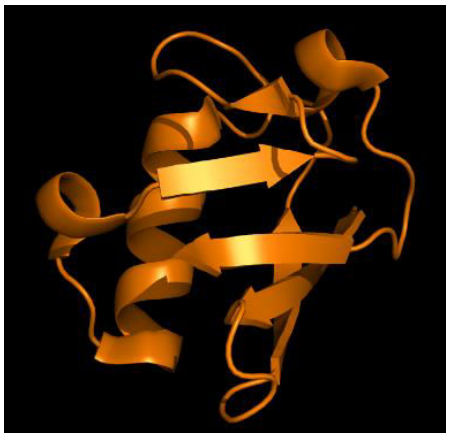

Figure 8: Crystal structure of Ubiquitin-like Domain of UHRF1 showing characteristic α-helix and β-sheet folds. Adapted from structure deposited at RCSB protein data bank. PDB ID: 2FAZ

1.2.1.2 Tandem Tudor Domain (TTD)

TTD helps UHRF1 to recognize the multivalent histones states of heterochromatin and plays an important role in functioning of UHRF1. It is made up of two subdomains (TTD_N and TTD_C)

and each subdomain has a characteristic five-stranded β-barrel moiety in its structure (Nady *et al.*, 2011). TTD_N aromatic cage (Phe-152, Tyr-188, and Tyr-191) identifies the di and trimethylammonium moiety of H3K9 by the help of two other polar residues Asn-194 and Asp-145, which provide the necessary charge for the stabilization of this interaction. Specificity of UHRF1 to recognize the H3K9me3 is governed by a peptide-binding groove between the two subdomains of TTD, which establishes close contacts with the neighboring residues of H3 methylated lysine. Therefore, posttranslational modifications on adjacent histone residues (such as H3K4 methylation or H3T6 phosphorylation) can alter the specific binding of H3K9me3 between the two tudor subdomains and, thus, can affect the association of UHRF1 with H3K9me3 (Nady *et al.*, 2011).

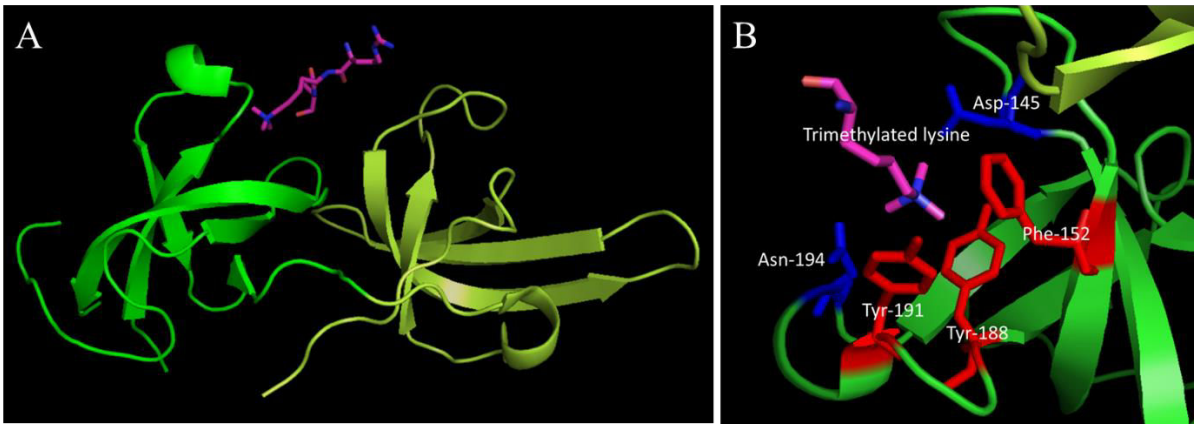

Figure 9: Crystal structure of TTD domain of UHRF1. A, Subdomains of TTD (TTD_N and TTD_C indicated in green and lemon color respectively) with trimethylated lysine (indicated in magenta). B, Aromatic cage of TTD_N Phe-152, Tyr-188, and Tyr-191 (indicated in red) along with Asn-194 and Asp-145 (indicated in blue) serve as binding pocket for trimethylated lysine residue. Adapted from structure deposited at RCSB protein data bank. PDB ID: 3DB3 (Nady *et al.*, 2011)

1.2.1.3 Plant Homeodomain (PHD)

A pre PHD motif at N-terminal differentiates the PHD of UHRF1 from the canonical PHD found in other proteins. A zinc atom coordinates with four cysteines residue (Cys-302, 305, 313 and 316 shown in red color) in the initial loop region to form this pre PHD motif which is linked to the canonical PHD structure by a single helical turn (Figure 10). Canonical PHD region of UHRF1 consists of a small α-helix, double stranded anti-parallel β-sheet and three loops coordinated by three other zinc atoms to form a rod shaped structure (Hu *et al.*, 2011, Rajakumara *et al.*, 2011). PHD domain of UHRF1 specifically recognizes the H3R2 motif in

chromatin, which is considered essential for UHRF1 to perform its functions (Hu *et al.*, 2011, Rajakumara *et al.*, 2011).

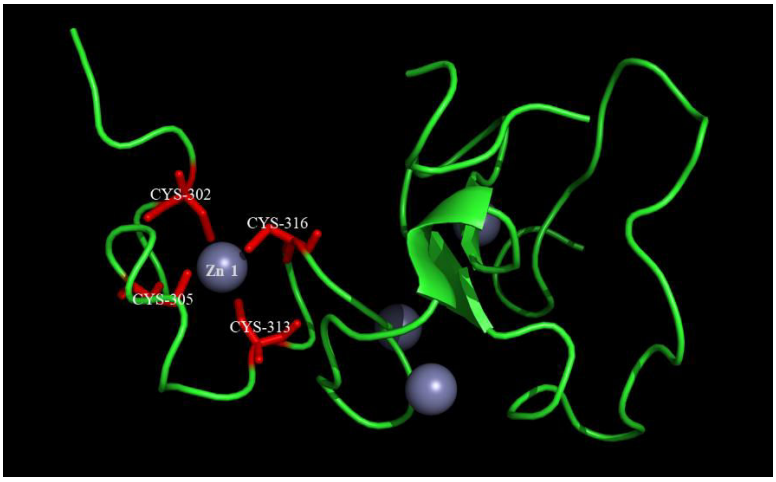

Figure 10: Crystal structure showing pre PHD motif linked to canonical PHD domain of UHRF1. Adapted from structure deposited at RCSB protein data bank. PDB ID: 3SHB (Hu *et al*., 2011)

1.2.1.4 Set and Ring Associated (SRA) Domain

SRA domain is unique characteristic of UHRF family proteins allowing them to interact with the hemi-methylated DNA. In UHRF1, SRA domain consists of a β-barrel flanked by α-helical structures with a basic inner surface. Crystallization studies of SRA with DNA duplex have revealed SRA as a hand grasping the hemi-methylated DNA duplex. The palm of the hand is a specific binding pocket to accommodate the flipped methyl cytosine while the finger (489-491 residues) and thumb (444-496 residues) forms two specific loops which project into major and minor groove of DNA double helix to read the nucleotides in the CpG duplex (Figure 11) (Avvakumov *et al.*, 2008). The Finger is a specific NKR (N-489, K-490 and R-491) motif, which recognizes 5-mC in hemi-methylated DNA and flips the methylated cytosine into the binding pocket. The binding pocket is highly selective for flipped methylated cytosine where it is stabilized by stacking interactions of Tyr-478 and Tyr-466 while conformational arrangement of surrounding amino acids does not allow thymine or non-methylated cytosine to fit into this pocket (Avvakumov *et al.*, 2008). NKR finger also makes contact with the non-methylated cytosine in hemi-methylated CpG motif and acts as key for UHRF1 to differentiate between hemi and fully methylated CpG motif. Presence of second methylated cytosine in fully methylated CpG motif create a sterical hindrance for NKR finger interaction and thus decreases the affinity of UHRF1 for fully methylated DNA (Avvakumov *et al.*, 2008).

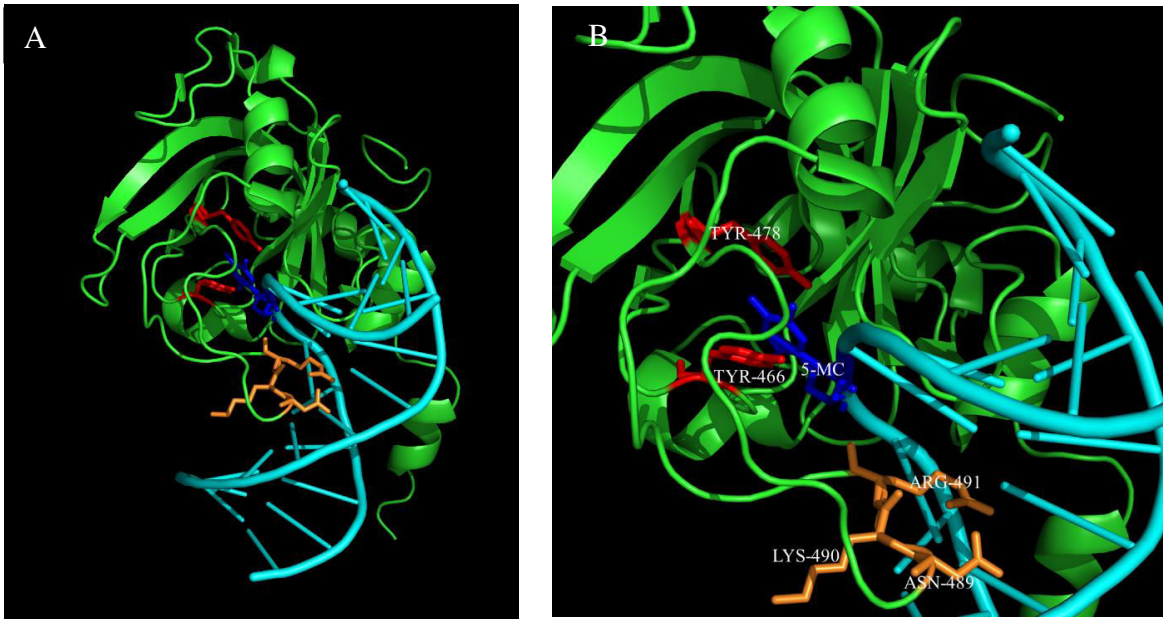

Figure 11: A, Crystal structure showing SRA domain of UHRF1 (green in color) in complex with hemi-methylated DNA (cyan in color). B, Zoomed image showing 5-MC (blue in color) flipped out of DNA duplex and stacked between tyrosine 466 and 478 (red in color). NKR finger (orange in color) projects into major groove of DNA. Adapted from structure deposited at RCSB protein data bank. PDB ID: 3CLZ (Avvakumov *et al*., 2008)

1.2.1.5 Really Interesting New Gene (RING) Domain

RING domain at the C-terminus, is the only enzymatic domain present in UHRF1 possessing the E3 ligase activity (Tauber and Fischle, 2015). It is rich in cysteine residues, which form two zinc fingers surrounded by α-helix structures to interact with the substrates (Figure 12). By the help of this domain, UHRF1 ubiquitinates variety of proteins including itself and thus modulate the activity and stability of its substrates (Tauber and Fischle, 2015).

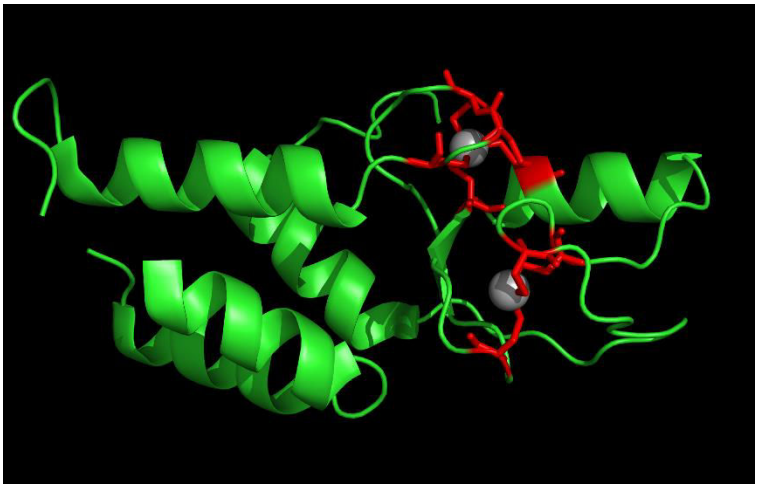

Figure 12: Crystal structure of RING domain of UHRF1. Cysteine residues (red in color) interact with zinc atoms (grey in color) to form zinc fingers necessary for interaction with substrates. Adapted from structure deposited at RCSB protein data bank. PDB ID: 3FL2

1.2.2 Roles of UHRF1 in Cells

1.2.2.1 UHRF1 in Epigenetic Modifications

UHRF1 is an important epigenetic modifier with a well-established role in DNA methylation. In 2007, Bronner *et al* and Bostick *et al* first reported UHRF1 as a part of epigenetic complex maintaining the methylation pattern on DNA after replication (Bostick *et al.*, 2007, Bronner *et al.*, 2007). It was revealed that UHRF1 directly interacts with DNMT1 and is essential for loading of DNMT1 to chromatin during the S phase in order to perform its DNA methylation function (Bostick *et al.*, 2007). Knock-down of UHRF1 impaired the loading of DNMT1 to chromatin and led to global hypomethylation (Bostick *et al.*, 2007). UHRF1 has high affinity for hemi-methylated DNA and identifies the hemi-methylated CpG motif through its specialized SRA domain (Sharif *et al.*, 2007). It was confirmed by the structural studies that SRA domain of UHRF1 specifically recognizes the methylated cytosine on the parent DNA strand and flips it out of the double helix, serving as guide for DNMT1 to locate the target cytosine on newly formed DNA strands (Arita *et al.*, 2008, Avvakumov *et al.*, 2008, Hashimoto *et al.*, 2008).

Recent studies have revealed that UHRF1 interactions with N-terminal histone tail are also playing important role in maintenance of DNA methylation (Figure 13). Besides interaction of SRA domain with hemi-methylated DNA, UHRF1-TTD association with H3K9me3 or H3K4 is also essential for UHRF1 loading onto the chromatin and subsequent DNA methylation

(Karagianni *et al.*, 2008, Rottach *et al.*, 2010, Nady *et al.*, 2011, Rothbart *et al.*, 2012). Similarly, studies also signified the role of PHD in UHRF1 mediated control of DNA methylation where PHD binds to H3R2 (unmodified arginine) on chromatin and helps UHRF1 to repress genes by hypermethylation (Rajakumara *et al.*, 2011, Wang *et al.*, 2011). It is also reported that UHRF1 enhances DNMT1 association with chromatin through its E3 ligase catalytic activity. UHRF1 ubiquitinates H3K18, which is recognized by the ubiquitin interacting motif (UIM) of DNMT1, facilitating its anchoring on the chromatin (Qin *et al.*, 2015).

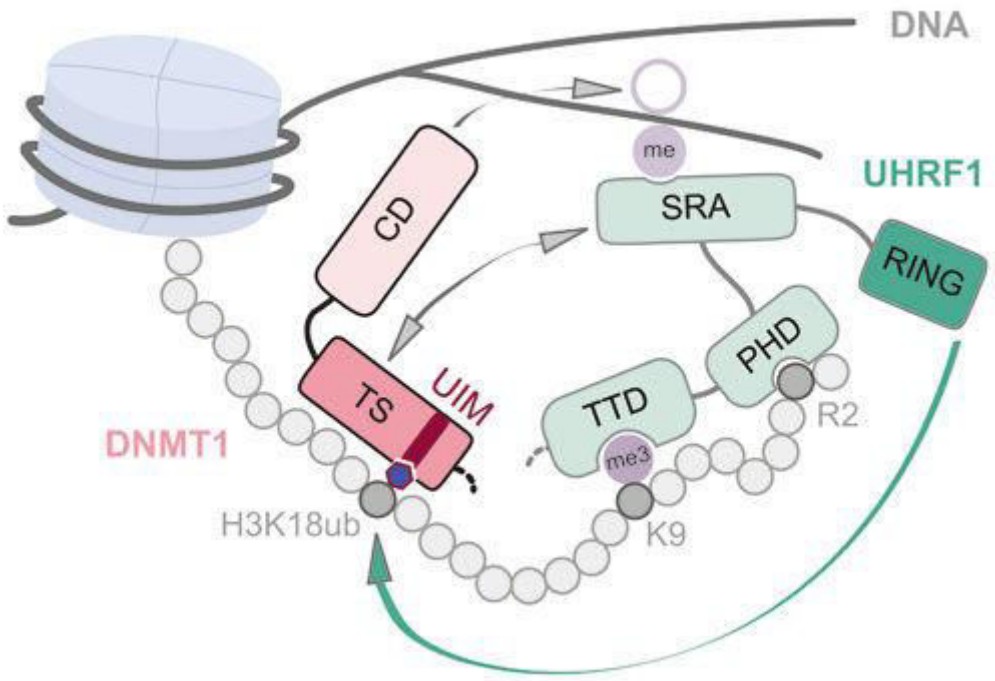

Figure 13: Schematic diagram of UHRF1 domains (indicated in green) interaction with chromatin to maintain the DNA methylation. TTD interacts with H3K9me3 and PHD interacts with H3R2on chromatin. SRA domain of UHRF1 identifies hemi-methylated DNA, flips methylated-cytosine out of DNA duplex and recruits DNMT1 to the chromatin. RING domain ubiquitinates H3K18, which serves as an anchor for ubiquitin interaction motif (UIM) of DNMT1 (indicted in red) to enrich DNMT1 on the chromatin for its catalytic activity on nascent cytosine in CpG motif. Adapted from (Qin *et al.*, 2015).

A recent study also reported that DNA replication machinery also recruits UHRF1 directly to replication sites besides hemi-methylated DNA and histone epigenetic marks. DNA ligase 1 (LIG1) is methylated by G9a and GLP methyltransferases, which mimics H3K9me2/3 in binding to the TTD of UHRF1. This binding of LIG1 to TTD of UHRF1 brings UHRF1 to the replication sites of DNA for maintenance of DNA methylation (Ferry *et al.*, 2017).

According to the latest reports, UHRF1 conformation also defines its recruitment to the chromatin. TTD in UHRF1 can intramolecularly interact with C-terminal polybasic region (PBR) or "spacer" between SRA and RING domain while PHD can interact with SRA domain to attain an "occluded" or "closed" conformation; a state in which UHRF1 loading to chromatin is less likely to occur (Figure 14) (Gelato *et al.*, 2014, Zhang *et al.*, 2015, Fang *et al.*, 2016). Cellular molecules such as phosphatidylinositol 5-phosphate (PI5P), hemi-methylated DNA or ubiquitin-specific-processing protease 7 (USP7) (also known as Herpes virus-associated ubiquitin-specific protease - HAUSP) can disrupt these intramolecular interactions and "open" UHRF1 for its loading to chromatin (Gelato *et al.*, 2014, Zhang *et al.*, 2015, Fang *et al.*, 2016). PI5P and USP7 directly associate with spacer, releasing the TTD and PHD domain for binding with H3K9me3 and H3R2 marks, respectively and thus allosterically regulate the loading of UHRF1 on chromatin. The open conformation also helps UHRF1 to interact with DNMT1 and bring it to the chromatin for methylation function (Fang *et al.*, 2016).

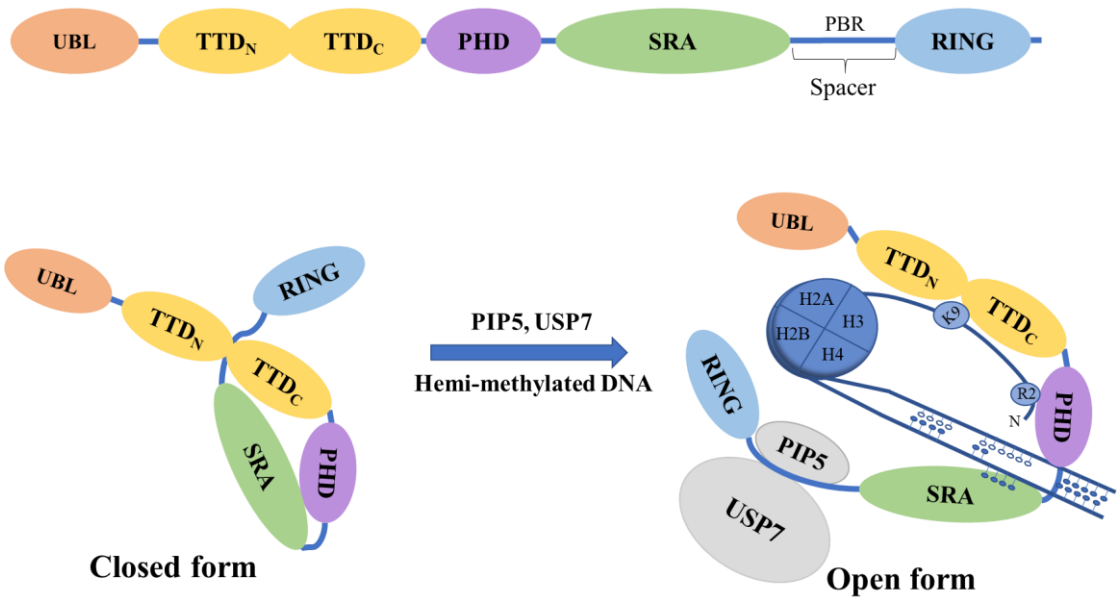

Figure 14: UHRF1 conformational changes during the DNA methylation. During S phase, association of PIP5, USP7 and hemi-methylated DNA "open" the UHRF1 for interaction with chromatin. Adapted from (Gelato *et al.*, 2014, Zhang *et al.*, 2015, Fang *et al.*, 2016).

1.2.2.2 UHRF1 in DNA Damage Response

Besides its role in DNA methylation and histone modifications, UHRF1 is also involved in cellular response to DNA damage in order to maintain the genome integrity and stability. It has been reported in earlier studies that cells lacking UHRF1 have higher sensitivity to genotoxic

agents while over expression of UHRF1 in cancer cells render them resistant to anticancer therapy (Muto *et al.*, 2002, Arima *et al.*, 2004, Li *et al.*, 2009, Mistry *et al.*, 2010, Yang *et al.*, 2013).

Recently, the role of UHRF1 has been observed in identification of interstrand crosslinks (ICLs) and initiation of repair mechanisms dealing with such DNA damages (Liang *et al.*, 2015, Tian *et al.*, 2015). ICLs arise when the nitrogenous bases on the opposite strands are covalently linked by the action of different extrinsic or intrinsic bifunctional alkylating agents. Such DNA lesions are difficult to repair and extremely toxic to cells as they prevent the opening of strands during replication and transcription. Many anticancer drugs are alkylating agents, which induce ICLs to kill the proliferating tumor cells. ICLs are also induced naturally in cells and repaired by distinct Fanconi anemia (FA) DNA repair pathway. Deregulation of this repair mechanism can also predispose the cells to malignant transformation (Deans and West, 2011). It was observed in *in vivo* and *in vitro* experiments that UHRF1 senses the ICLs through its SRA domain and then recruits the major effector proteins such as FANCD2 for its repair (Figure 15) (Liang *et al.*, 2015). Besides recruiting components of Fanconi anemia pathway, UHRF1 also recruits ERCC1 and MUS81 nucleases through a direct contact to the site of ICL damage (Tian *et al.*, 2015). These nucleases are essential for the initiation of repair pathway as they cleave and remove the cross-linked sites from the DNA, which is subsequently repaired by the appropriate pathway (Tian *et al.*, 2015). However, knockdown of UHRF1 increases the sensitivity of cells to alkylating agents such as mitomycin C and abolishes the recruitment of effector proteins (Liang *et al.*, 2015).

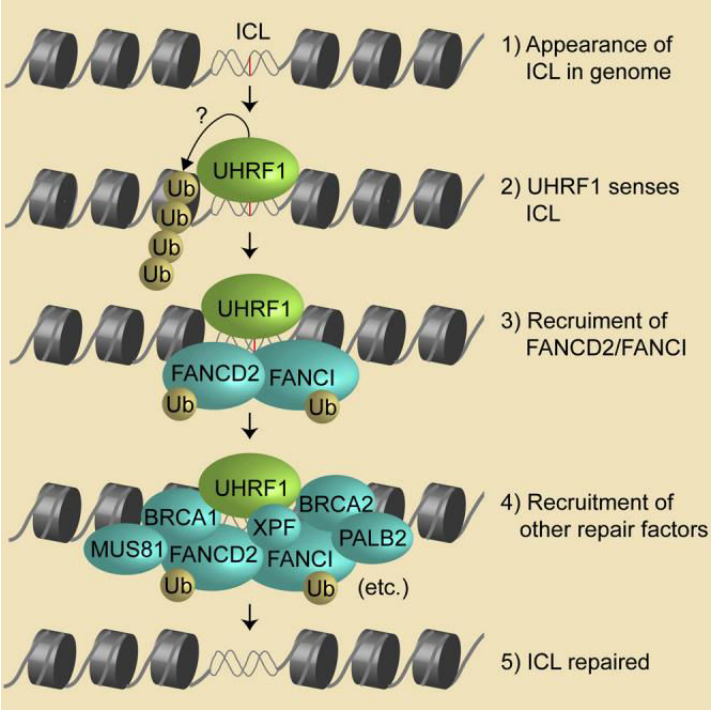

Figure 15: UHRF1 role in interstrand cross link (ICL) repair. UHRF1 identifies the ICLs and recruits the FANCD2 and other effector proteins to repair the damage. Adapted from (Liang *et al.*, 2015).

UHRF1 is also linked to DNA damage response against the double strand breaks where it facilitates the repair by homologous recombination pathway (Zhang *et al.*, 2016a). DNA double strand break (DSB) is one of the most commonly occurring form of DNA damage in cells, which is also difficult to repair. There are two major pathways to repair DSBs (i) homologous recombination (HR) and (ii) non-homologous end joining (NHEJ). Homologous recombination pathway utilizes undamaged sister chromatid or homologous chromosome as template to ensures accurate repair of the damaged DNA and therefore it dominates in S and G2 phase. Non-homologous end joining on the other hand uses no or limited homology to rejoin the damage DNA and therefore can lead to mutation in the repaired DNA (Helleday *et al.*, 2014). The decision to proceed the DSB repair by HR or NHEJ pathway depends on the occupancy of BRCA1 or 53BP1 protein at the site of damage. BRCA1 facilitates the repair through HR pathway while 53BP1 promotes repair mechanisms through NHEJ pathway (Daley and Sung, 2014). During S phase UHRF1 accumulates at the site of damage and decides the interplay between BRCA1 and 53BP1 for associated DNA damage response. Mechanistically, UHRF1 is phosphorylated at S674 (S661 in isoform 1) by CDK2/cyclin in response to DSBs during S phase which allows it to interact with BRCA1 (Figure 16) (Zhang *et al.*, 2016a). BRCA1 by utilizing its BRCT domain recruits phosphorylated UHRF1 to DSB site where it ubiquitinates

the replication timing regulatory factor 1 (RIF1). RIF1 is an important chromatin associated protein that interacts with 53BP1 and favors the repair through NHEJ pathway. Polyubiquitination of RIF1 at K63 by UHRF1 disrupts the RIF1 foci formation at the DSBs and its association with 53BP1, triggering the repair mechanism to proceed by HR pathway (Zhang *et al.*, 2016a).

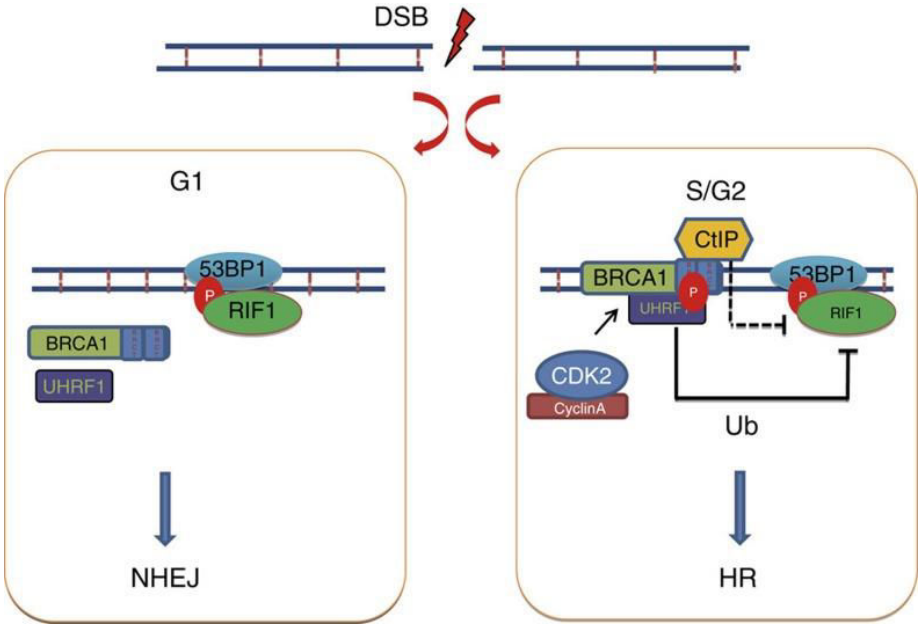

Figure 16: UHRF1 favors the DSB repair through HR pathway in S/G2 phase of cell cycle. In G1 phase DSBs repair mostly occur by NHEJ pathway. RIF1 is recruited to the site of damage which serves as guide for 53BP1 to initiate the damage response. In S/G2 phase, UHRF1 is phosphorylated by CDK2/cyclinA in response to DSBs and later recruited to damaged area by BRCA1. UHRF1 ubiquitinates the RIF1 and prevents the anchorage of 53BP1 to facilitate the repair by HR pathway. Adapted from (Zhang *et al.*, 2016a).

1.2.3 Post Translational Modification on UHRF1

Like many proteins, UHRF1 undergoes different posttranslational modifications, which affect its stability and function. Few of the important posttranslational modifications regulating UHRF1 are described hereafter.

1.2.3.1 Phosphorylation of UHRF1

Phosphorylation plays a key role in regulating the activity and stability of UHRF1 during the cell cycle. UHRF1 phosphorylation at Ser-298 by protein kinase A (PKA) in cAMP signaling pathway enhances its ability to activate topoisomerase IIα expression which is one of the major events involved in the G1/S transition (Trotzier *et al.*, 2004). Similarly, UHRF1 has many

consensus motifs for protein kinase 2 (PK2) which also facilitates G1/S phase transition by increasing the transcriptional activity of UHRF1 through phosphorylation (Bronner *et al.*, 2004). Ser-298 phosphorylation is also implicated in the binding of UHRF1 with H3 tail and thus regulates the function of UHRF1 in DNA methylation (Arita *et al.*, 2012). During S phase UHRF1 is phosphorylated at Ser-661 by cyclin A2/cyclin dependent kinase 2, which is important for its normal function and embryogenesis in zebrafish. Loss of Ser-661 phosphorylation decreases the cytoplasmic fraction of UHRF1 and induces death during the zebrafish embryogenesis (Chu *et al.*, 2012). Phosphorylation at Ser-639 (isoform 1) or Ser-652 (isoform 2) plays a key role in regulating the stability of UHRF1. During M phase, cyclin B/CDK1 phosphorylates UHRF1 at Ser-639 which reduces UHRF1 association with deubiquitinating enzyme ubiquitin specific peptidase 7 (USP7), leading to degradation of UHRF1 (Ma *et al.*, 2012). Recently PIM1, a serine/threonine protein kinase has also been discovered as regulator of UHRF1, which phosphorylates UHRF1 at Ser-298 (isoform 1) and induces degradation of UHRF1 to promote cellular senescence (Yang *et al.*, 2017a). UHRF1 phosphorylation at its N-terminal Ser-95 (isoform 1) in response to DNA damage also predisposes it to be degraded by proteasomal degradation pathway after its ubiquitination by $SCF^{\beta\text{-}TrCP}$ E3 ligase (Chen *et al.*, 2013).

1.2.3.2 Ubiquitination of UHRF1

Like many other short-lived proteins, UHRF1 levels in cells are regulated by the ubiquitin-mediated proteasomal degradation pathway. UHRF1 is polyubiquitinated by its intrinsic E3 ligase activity or by other E3 ligase enzymes such as $SCF^{\beta\text{-}TrCP}$ and targeted for degradation by proteasomes (Jenkins *et al.*, 2005, Chen *et al.*, 2013). UHRF1 intrinsic E3 ligase activity lies in its RING domain where Cys-724 & His-741 are playing important role in UHRF1's ability to auto-ubiquitinate itself (Jenkins *et al.*, 2005). It is interesting to note that presence of natural substrate like unmodified histones or nucleosomes diminish the auto-ubiquitination activity of UHRF1 and increase the stability of UHRF1 (Karagianni *et al.*, 2008). Similarly, presence of deubiquitinating enzyme like ubiquitin specific peptidase 7 (USP7) in the complex also increases the life of UHRF1 protein and prevents its degradation by deubiquitinating UHRF1 during the S phase (Felle *et al.*, 2011, Ma *et al.*, 2012). Different posttranslational modifications on UHRF1, like phosphorylation in M phase, interfere in USP7 protective relationship with UHRF1 and thus promote the degradation of UHRF1 (Ma *et al.*, 2012).

1.2.4 UHRF1 Regulation and its Role in Cancer

UHRF1 is mostly expressed in proliferating cells while little or no UHRF1 is found in dormant or quiescent cells (Hopfner *et al.*, 2000). In most of cancer cells, UHRF1 is overexpressed and is believed to have an oncogenic role in tumor progression. It facilitates proliferation of cells and represses the activities of tumor suppressor genes (TSGs) in transformed cells (Bronner *et al.*, 2007). High levels of UHRF1 in cancer tissues as compared to adjacent normal cells, can serve as valuable diagnostic and prognostic marker for the detection of cancer and evaluation of its treatment (Ashraf *et al.*, 2017b).

The epigenetic integrator UHRF1: on the road to become a universal biomarker for cancer

Waseem Ashraf[1], Abdulkhaleg Ibrahim[2], Mahmoud Alhosin[3,4,5], Liliyana Zaayter[1], Khalid Ouararhni[2], Christophe Papin[2], Tanveer Ahmad[1], Ali Hamiche[2], Yves Mély[1], Christian Bronner[2,*] and Marc Mousli[1,*]

[1] Laboratory of Biophotonics and Pharmacology, Faculty of Pharmacy, University of Strasbourg, Illkirch, Cedex, France

[2] Institute of Genetics and Molecular and Cellular Biology, University of Strasbourg, Illkirch-Graffenstaden, France

[3] Department of Biochemistry, Faculty of Sciences, King Abdulaziz University, Jeddah, Saudi Arabia

[4] Cancer Metabolism and Epigenetic Unit, King Abdulaziz University, Jeddah, Saudi Arabia

[5] Cancer and Mutagenesis Unit, King Fahd Centre for Medical Research, King Abdulaziz University, Jeddah, Saudi Arabia

[*] These authors are co-last authors

***Correspondence to**: Marc Mousli, **email**: marc.mousli@unistra.fr*

Keywords: cancer, biomarkers, epigenetics, UHRF1, DNA methylation

***Received**: February 03, 2017* ***Accepted**: April 02, 2017* ***Published**: April 24, 2017*

ABSTRACT

Cancer is one of the deadliest diseases in the world causing record number of mortalities in both developed and undeveloped countries. Despite a lot of advances and breakthroughs in the field of oncology still, it is very hard to diagnose and treat the cancers at early stages. Here in this review we analyze the potential of Ubiquitin-like containing PHD and Ring Finger domain 1 (UHRF1) as a universal biomarker for cancers. UHRF1 is an important epigenetic regulator maintaining DNA methylation and histone code in the cell. It is highly expressed in a variety of cancers and is a well-known oncogene that can disrupt the epigenetic code and override the senescence machinery. Many studies have validated UHRF1 as a powerful diagnostic and prognostic tool to differentially diagnose cancer, predict the therapeutic response and assess the risk of tumor progression and recurrence. Highly sensitive, non-invasive and cost effective approaches are therefore needed to assess the level of UHRF1 in patients, which can be deployed in diagnostic laboratories to detect cancer and monitor disease progression.

INTRODUCTION

In cancer, the prognosis of the disease is highly dependent on the type and location of the cancer along with the stage at which it is diagnosed. The survival rate and the treatment response is better if the cancer is diagnosed early when the tumor is localized and small. Nowadays many biomolecules and epigenetic patterns are being explored as "biomarkers" to help in early diagnosis of cancers along with currently employed techniques of imaging and cytology [1]. An ideal biomarker for cancer detection must be able to differentiate between normal and tumoral cells and it should be able to predict the malignant potential and prognosis of the disease.

All cells of a multicellular mammalian organism, except germinal cells, contain the same DNA in terms of nucleotide sequence. Considering the fact that DNA is the layer of heredity and cell identity, how can cell diversity and differentiation arise from the same DNA sequence is an important question challenging the scientific community. Epigenetics is the research field that tries to answer this question by deciphering a tremendous number of cellular mechanisms of gene regulation embedded in the chromatin but not related to changes in DNA sequences. In other words, it refers to external modifications of DNA that turn *genes* "on" or "off. At the molecular level, "off" means that the genes are silenced, by means of DNA methylation and histone methylation, *e.g.,* di- and tri-methylation of lysines 9 & 27 of histone H3 (H3K9me2, H3K9me3, H3K27me2, H3K27me3) as well as chromatin structure, micro RNA and histone variants [2-5]. However, gene expression does not function as a simple "on-off" dichotomy but rather through a complex language dictated by the degree of DNA methylation and a set of epigenetic

marks appearing on the N-terminal tails of histones present in the nucleosome [3]. This complex language allows the cell to express genes as a function of precise needs during cell cycle or during lifespan and no more or less than it is required for the cell to work adequately. This complex language is profoundly modified in various diseases, including cancer [3-5].

Indeed, cancer cells exhibit profound changes in epigenetic profiles, as much on the DNA methylation side as on histone code side [6]. Cancer cells undergo global DNA hypomethylation, whereas some regions, on the contrary, undergo hypermethylation, *e.g.* promoters of tumor suppressor genes [7, 8]. On the histone code versant, several modifications have been reported in various types of cancer [9].

There are increased evidences that DNA methylation appears as an ideal biomarker for various types of cancers [10-13]. DNA methylation in mammals preferentially occurs in a CpG context, meaning that both DNA strands are methylated in an asymmetrical manner, which represents one of the layers of epigenetic information. Methylation of cytosine is slightly mutagenic, explaining the loss of CpG sites in mammalian genomes during evolution. As a consequence, CpG sites in human genome are globally found 3–4 times less often than statistically expected, except in CpG islands, which are often located in gene promoters [2, 14].

The mechanism of inheritance of the methylation patterns is relatively well documented regarding DNA but is still elusive concerning histones, although several models are under investigation for definitive validation [15]. Duplication of DNA methylation patterns in a CpG context, is subjected to prior DNA replication generating hemi-methylated DNA, *i.e.,* only one DNA strand is methylated, a state that is specifically recognized by Ubiquitin-like containing PHD and Ring Finger domain protein 1 (UHRF1) [16-20]. The sensing of hemi-methylated DNA by UHRF1, induces the recruitment of DNA methyltransferase 1 (DNMT1) which methylates the opposite unmethylated DNA strand, and consequently CpG dinucleotides are methylated on both strands. Through these properties, the tandem UHRF1/DNMT1 plays a role during cell proliferation and therefore in development and cancer [21].

THE EPIGENETIC INTEGRATOR UHRF1

Structure of UHRF1

Among the different epigenetic modulators, UHRF1, which is also known as Inverted CCAAT box Binding Protein of 90 kDa (ICBP90) or nuclear protein of 95kDa (Np95) [22-24] has gained a considerable attention during the past few years because of its high expression in most of the cancers and its ability to link important epigenetic processes such as DNA methylation and histone modifications [25].

Initially, UHRF1 was identified as a transcription factor regulating the expression of topoisomerase IIα by binding to an inverted CCAAT box located in its promoter [22]. UHRF1 was further shown to critically participate in various epigenetic processes by its different structural domains (Figure 1). Indeed, UHRF1 is composed of an N-terminal ubiquitin-like domain that is coming before the tandem tudor domain (TTD) and plant homeodomain (PHD). These domains are followed by the unique set and ring associated (SRA) domain and the really interesting new gene (RING) finger domain at the C-terminus [25]. Except for the RING domain exhibiting an E3 ligase activity towards histone H3 on lysine 23 or on lysine 18, no further enzymatic activity has been so far identified for any of the other domains. Instead, interesting binding activities were identified for each domain conferring unique capacities of readout [26-28]. One key property of UHRF1 is its ability to sense the presence of hemi-methylated DNA at the replication fork, thanks to the SRA domain [19, 20]. Concomitantly, it can also sense the di- and tri- methylated lysine 9 of histone H3 (H3K9me2/H3K9me3) in the chromatin by help of its tandem tudor domain [29-31]. Association of UHRF1 with methylated H3K9 through TTD facilitates the maintenance of DNA methylation but primarily it is the SRA domain that recruits UHRF1 to hemi-methylated DNA [32]. Indeed, we have shown that the binding of SRA domain does not induce distortion of the DNA, which is in favor of a sliding behavior along the DNA seeking for hemi-methylated CpG sites and subsequent flipping of the methylated cytosine, thus facilitating the recruitment of DNMT1 [33, 34]. It has also been shown that UHRF1, through its SRA domain, is capable of recognizing hydroxymethylcytosine [35]. The relevance of this latter remains elusive but it might bring new insights in DNA methylation maintenance, once resolved.

Beside this role, UHRF1 is considered to play a pivotal role in the epigenetic inheritance as it coordinates the action of different chromatin modifying proteins [36]. It interacts, among many others, with DNA methyltransferases (DNMTs), proliferating cell nuclear antigen (PCNA), histone deacetylase 1 (HDAC1), ubiquitin specific protease 7 (USP7), euchromatic histone-lysine N methyltransferase 2 (G9a/EHMT2) and Tat Interacting Protein 60 (Tip60) to maintain DNA methylation patterns and histone epigenetic marks in various physiological and pathological conditions [18, 19, 37-42]. Together with its partners, UHRF1 ensures the regulation, through "silencing" of a high number of tumor suppressor genes and long non-coding RNAs, including *RB1* [43], *p16* (*CDKN2A)* [44-48], *CDH13* and *SHP1* [49], *SOCS3* and *3OST2* [50], *BRCA1* [51], *CDX2, RUNX3, FOXO4, PPARG* and *PML* [52, 53], *MEG3* [54]

and *14-3-3σ* [55]. Moreover, *KISS1*, functioning as a metastasis suppressor in various cancers, also looks to be under the control of UHRF1 [56]. Altogether, these studies highlight UHRF1 as a conductor of tumor suppressor gene silencing in cancers through a DNA methylation-dependent mechanism.

UHRF1 as a tumor promoter

UHRF1 is mostly expressed in proliferating cells, while it is not found in fully differentiated tissues [22]. Levels of UHRF1 expression positively co-relate with the proliferative potential of cells. In cancer cells, UHRF1 is overexpressed and promotes the proliferation and dedifferentiation of cells [22]. In non-cancerous proliferating cells, UHRF1 expression is cell cycle regulated and peaks in late G1 and G2/M phase, while in cancerous cells, UHRF1 is continuously expressed at all stages of cell cycle [57]. UHRF1 is considered to be essential for G1/S phase transition as its depletion or down-regulation by activation of p53/p21$^{Cip1/WAF1}$ dependent DNA damage response leads to cell cycle arrest at the G1/S phase transition [58, 59]. Similarly, in another study it has been reported that depletion of UHRF1 in HCT116 cells leads to the activation of DNA damage response with subsequent cell cycle arrest at G2/M phase and induction of caspase 8-dependent apoptosis [60]. Conversely, overexpression of UHRF1 in human fibroblasts or its orthologue Np95 in terminally differentiated mouse myotubes facilitates the entry of these cells in S-phase and induces cell proliferation [43, 58].The possibility that UHRF1 behaves as an oncogene has been questioned for a while [61]. However, it is now clearly demonstrated through a recent series of studies that UHRF1 is a tumor promoter. Indeed, it was shown that overexpressed UHRF1 causes DNA hypomethylation, a hallmark of cancer cells; instead of normal maintenance of DNA methylation. Overexpressed UHRF1, through its E3 ligase activity, ubiquitinylates DNMT1 and DNMT3. Thus, by destabilizing and delocalizing them, UHRF1 induces global DNA hypomethylation [62, 63].

Several studies have also revealed that disruption of UHRF1 function results in hypersensitivity to DNA damage [64-69] supporting the idea that UHRF1 plays a critical role in the maintenance of genome stability. This is not surprising, considering that a native protein has first a physiological role before a deleterious role. The deleterious role is coming from an abnormal level of UHRF1 rather than from its function itself.

The abnormally high level of UHRF1 may result from the aberrant activity of various transcription factors regulating the expression of UHRF1 in cancers (Figure 2). E2F transcription factor 1 (E2F1) and E2F transcription factor 8 (E2F8) are upregulated in many cancers and stimulate *UHRF1* expression by directly binding to different sites in its promoter region [37, 57, 70]. Specificity protein 1 (SP1) and Forkhead Box M1 (FOXM1) also potentiate UHRF1 expression in different cancers [71, 72]. Repression of SP1 activity by T3 receptor pathway activation downregulates UHRF1, relieves p21 from UHRF1-mediated silencing and induces cell cycle arrest at G0/G1 phase in liver cancer cells [71]. Similarly, our recent study suggests that activation of highly expressed membrane integrin CD47 in astrocytoma activates NFκB-mediated signaling and UHRF1 expression, which in turn represses p16, thereby strengthening the tumor promoter role of UHRF1 [48]. High UHRF1 levels are also attributed to downregulation of its epigenetic regulator H3K9 methyltransferase (G9a) in various cancers which works along with Yin Yang transcription factor 1 (YY1) as negative upstream regulator of UHRF1 [73].

Besides increased expression of *UHRF1*, increased stability of *UHRF1 mRNA* through down-regulation of regulatory micro RNAs and increased stability of UHRF1 protein also contribute to abnormal high levels of UHRF1 in different cancers (Figure 2) [8, 74-79]. UHRF1 protein levels are controlled in normal cells by coordination of ubiquitinylating and deubiquitinylating enzymes which

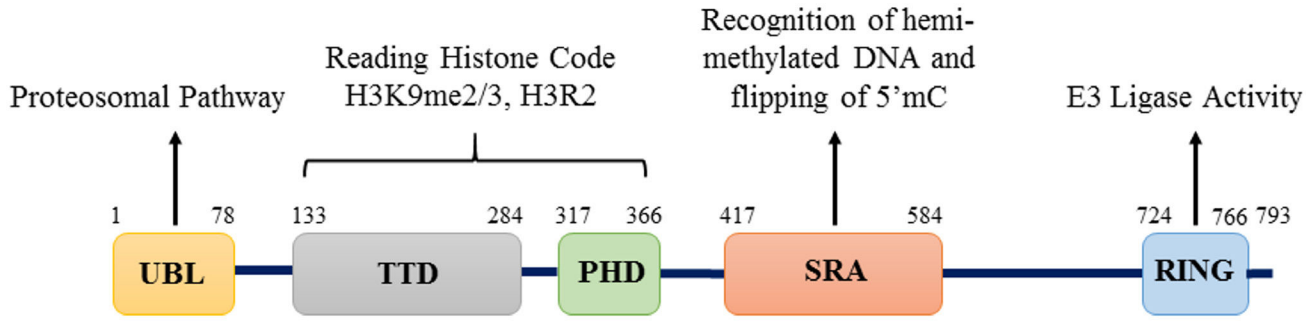

Figure 1: Structure of UHRF1 protein. Structure of UHRF1 protein showing the different domains and their functions. The protein contains 793 amino acids and five major domains: UBL (ubiquitin-like) domain, TTD (Tandem Tudor Domain), PHD (Plant Homeodomain), SRA (Set and Ring Associated) domain and RING (Really Interesting New Gene) domain.

regulate its proteosomal degradation (Figure 2). $SCF^{\beta\text{-}TrCP}$ E3 ligase or intrinsic activity of UHRF1 RING domain can induce degradation of UHRF1 by ubiquitinylation [26, 65]. Phosphorylation of serine residue at 108 by casein kinase 1δ helps $SCF^{\beta\text{-}TrCP}$ E3 ligase to recognize and ubiquitinate UHRF1 for degradation [65]. On the other hand, UHRF1 is stabilized and recruited to chromatin by its association with deubiquitinating enzyme USP7. M phase specific kinase CDK1-cyclin B which phosphorylates UHRF1 at serine 652 in the interacting region of USP7 can disrupt this association and lead to degradation of UHRF1 [40, 80]. Considering that USP7 is upregulated in many cancers, this might be one of the possible reason for high levels of UHRF1 in cancer cells [81-83]. UHRF1 is also stabilized by its interaction with long noncoding RNA UPAT (UHRF1 Protein Associated Transcript), which promotes colon tumorigenesis through inhibition of UHRF1 degradation [84]. Pharmacological inhibition of heat shock protein (HSP90) also destabilizes UHRF1 and suppress cancer cell proliferation predicting a role of HSP90 in UHRF1 turnover [85]. Altogether these events result in abnormal high level of UHRF1 in cancers which appears now to be exploitable as a biomarker.

We will now review the potential of UHRF1 to fulfil the features of a biomarker in various types of cancer.

UHRF1 EXPRESSION IN DIFFERENT CANCERS

UHRF1 in lung cancer

Lung cancer is the most common and fatal among different types of cancers with an average 5-year survival rate of around 15% [86]. According to latest data, over 1.8 million new cases of lung cancer were reported worldwide in 2012, while in the same year the death toll of lung cancer was around 1.59 million [86]. High smoking incidences and late diagnosis of cancer are major factors contributing to its high mortality rate. Various novel proteins are now being investigated, in search of a superior biomarker and

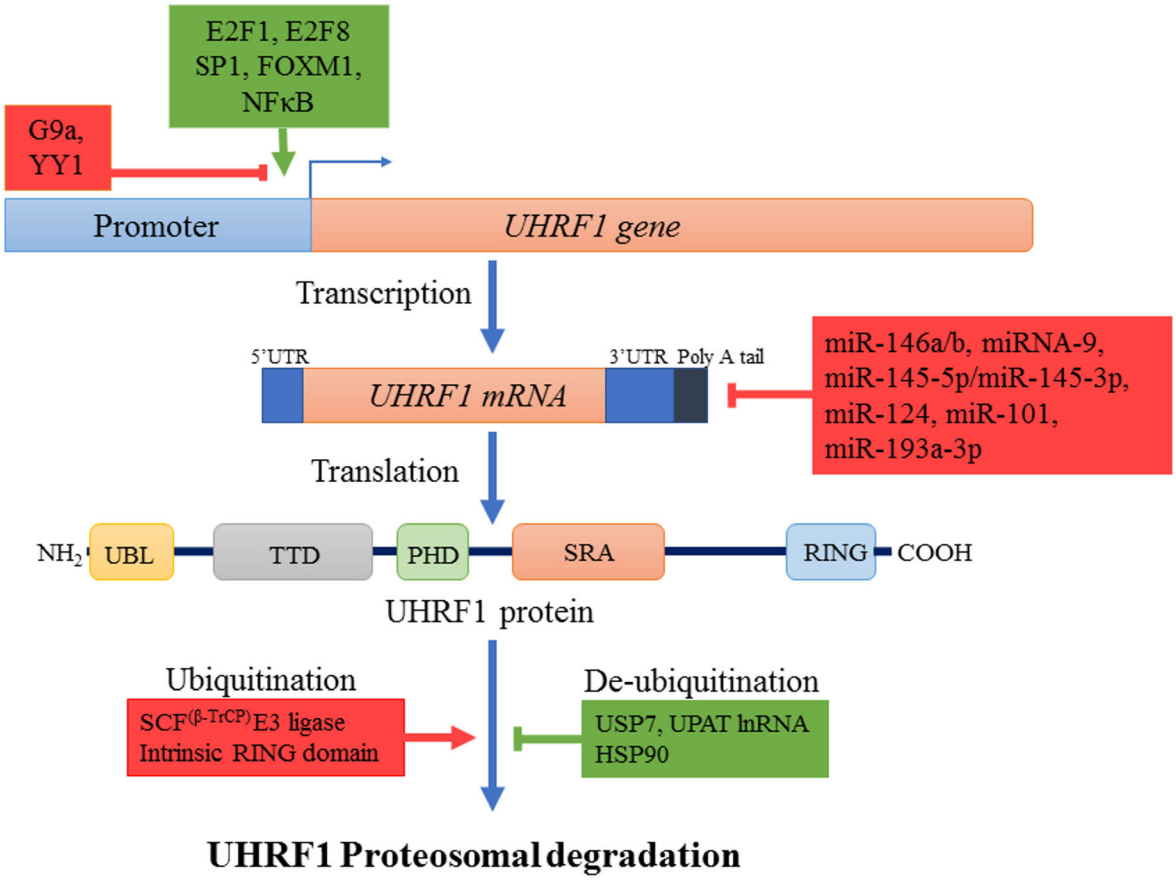

Figure 2: Regulation mechanisms of UHRF1. Different transcription factors like E2F1, E2F8, Sp1, FOXM1, NFκB (indicated in green) enhance while others such as YY1 along with lysine methyl transferase G9a (indicated in red) repress the expression of *UHRF1* at transcription level. Many small non-coding microRNAs also decrease *UHRF1* expression by destabilizing *UHRF1 mRNA* through binding to 3'UTR region. UHRF1 protein is degraded by proteosomal pathway after autoubiquitinylation or ubiquitinylation by $SCF^{\beta\text{-}TrCP}$ E3 ligase. Ubiquitinylated UHRF1 is stabilized in cells by USP7, HSP90 or UPAT lnRNA. Increased transcription factor expression, downregulation of miRNAs and increased levels of stabilizing factors (all indicated in green) result in overexpression of UHRF1.

among them UHRF1 has shown encouraging results. Immunohistochemistry (IHC) analysis of 322 lung cancer tissues from Japan and 56 samples from US, revealed an overexpression of UHRF1 in all histological types of non-small cell lung cancer (NSCLC) especially in non-adenocarcinomas [87]. Transcript analysis of samples also showed marked increase of UHRF1 mRNA in 70% of lung cancer cases. As enhanced expression significantly correlated with the advanced stages and malignancy of the cancer, authors proposed UHRF1 as a prognostic biomarker for lung cancer [87]. Similarly, a recent study in Taiwan has predicted a six-gene signature including *ABCC4*, *ADRBK2*, *KLHL23*, *PDS5A*, *UHRF1* and *ZNF551* as better prognostic marker in NSCLC for overall survival time and treatment outcome [88].

UHRF1 overexpression was also confirmed in another study including 105 NSCLC tissues (55 adenocarcinomas and 50 squamous cell carcinomas) along with DNMT1, DNMT3A and DNMT3B [89]. This overexpression resulted in silencing of tumor suppressor genes such as *RASSF1* and *p16*, via promoter hypermethylation in 32.4% and 26% of cases, respectively. Accordingly, in a cell model of lung cancer, knockdown of UHRF1 in A549 cells prevented the tumor suppressor genes *RASSF1*, *CYGB*, and *CDH13* promoters from hypermethylation [89].

UHRF1 in liver cancer

Hepatocellular carcinoma (HCC) is one of the most prevalent cancers with multiple etiological factors and is the second leading cause of cancer related deaths worldwide [86]. So far, many studies have been carried out to understand the complex nature and poor prognosis of this disease but it is still elusive. A recent study reported overexpression of UHRF1 in HCC of various etiologies and described UHRF1 as an oncogene, that drives global DNA hypomethylation by delocalizing DNMT1 [62]. In this study, expression of UHRF1 was assessed in 109 human HCC cases by qPCR and results revealed abnormally high expression of UHRF1 (averagely 2-fold higher than normal) in 95.41% (104/109) of the cases [62]. UHRF1 protein levels in samples were also in accordance with mRNA levels and were found significantly higher in 73% of tumors but were barely detectable in normal tissue

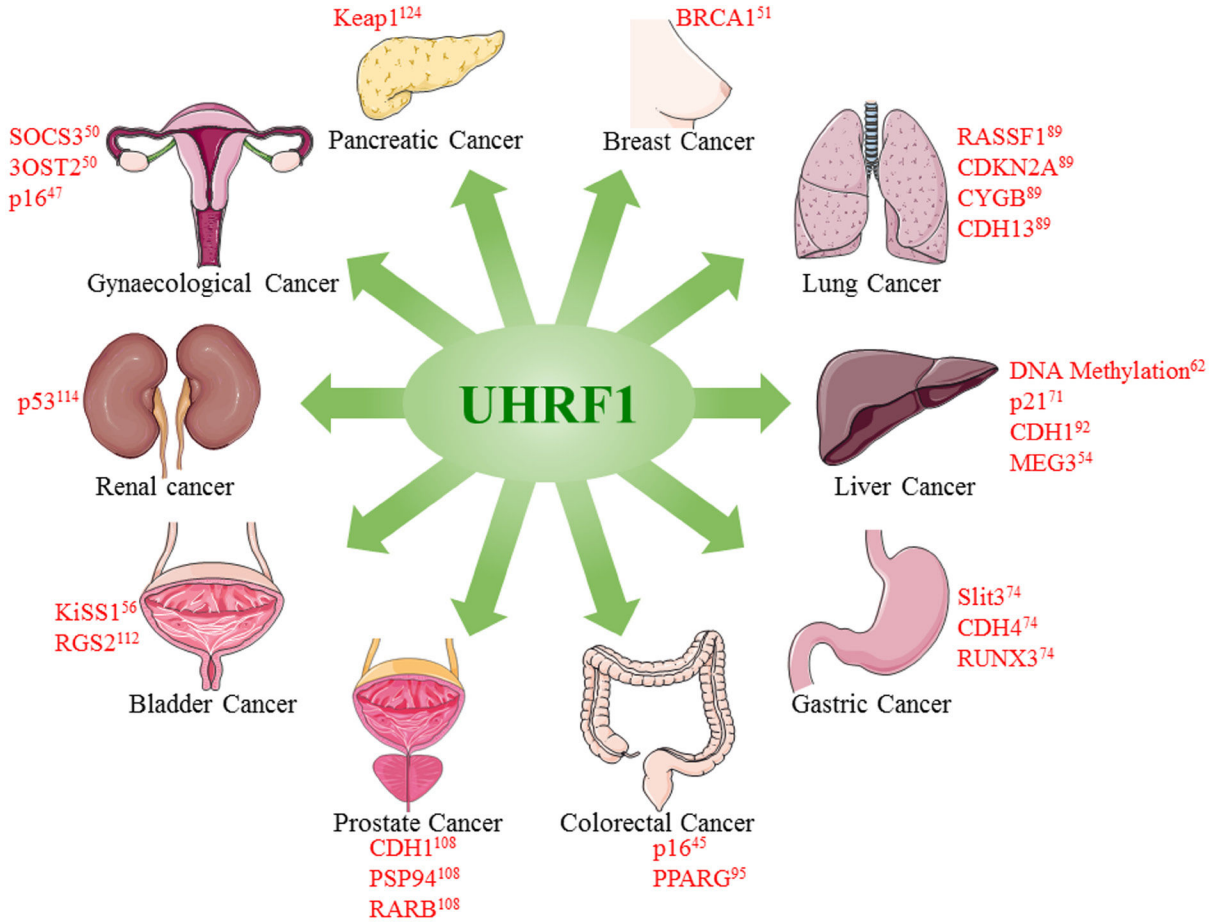

Figure 3: Overexpression of UHRF1 promotes tumorigenesis in different cancers. UHRF1 overexpression leads to epigenetic abnormalities including DNA methylation and downregulation of tumor suppressor genes or lnRNAs. Figure is made using images taken with permission from Servier Medical Arts http://servier.com/Powerpoint-image-bank.

samples [62]. Tumors with higher expression of UHRF1 also had poor prognosis with higher recurrence rate, alpha fetoprotein, microvascular invasion and lower survival rate emphasizing the diagnostic and prognostic potential of UHRF1 in HCC [62]. Similarly, high levels of UHRF1 mRNA were reported in 160 HCC patients notably during later stages II & III of cancer [71]. UHRF1 protein level were also significantly upregulated in 75.7% (52 of 70) of samples when analyzed by western blot [71]. Results were further confirmed by immunohistochemistry analysis of 136 HCC tissue samples which showed high expression of UHRF1 in tumor samples, positively correlating with tumor size, fetoprotein levels and HBV infection [71]. The diagnostic and prognostic capacities of UHRF1, as a novel biomarker in HCC, were also highlighted by a study on Chinese population including 68 HCC specimens [90]. In this study, significantly higher levels of UHRF1 were found in HCC samples by HPLC compared with the adjacent non-cancerous tissues. Of note, the levels of UHRF1 correlated with distant metastasis, tumor area and HBV [90]. Furthermore, elevated levels of UHRF1 also predicted poor prognosis as after 5 years of follow up, the survival rate in high UHRF1 expression group was 29.8% as compared with 81% in low UHRF1 expression group [90]. Another group also reported similar findings where UHRF1 mRNA expression was found significantly increased in 67% (54/80, $P < 0.05$) of HCC specimens [91]. Immunohistochemical staining of 102 pairs of HCC samples included in study also revealed significantly higher staining of UHRF1 protein in cancerous tissues (57.8% vs 32.7%) when compared to non-cancerous tissue. Like previous studies, overexpression of UHRF1 positively correlated with tumor size, staging and poor survival rate of patients [92].

On a cellular aspect, knockdown of UHRF1 inhibited the tumor growth *in vivo* and *in vitro* and induced cell cycle arrest at G2/M phase confirming the oncogenic potential of UHRF1. Targeting of UHRF1 also decreased the migration and invasion of cancer cells by hampering endothelial to mesenchymal transition (EMT) as evidenced by up regulation of (EMT opposing) E-cadherin and down regulation of (EMT favoring) β-catenin, vimentin, N-cadherin and snail in UHRF1 knockdown cells [92]. Overexpression of UHRF1 in hepatocellular carcinoma also negatively regulated the levels of tumor suppressive long non-coding RNA maternally expressed gene 3 (MEG3) via promoter hypermethylation which exerts its tumor suppressive role by induction of p53 [54, 93].

UHRF1 in gastric cancer

Gastric cancer is one of the most fatal cancers among all malignant diseases, and is accounted for approximately 723,000 world-wide deaths each year. Eastern Asian countries like China, Japan, Taiwan and Philippines have higher incidences of gastric cancer as compared with western countries [86]. In 2013, a study reported high levels of UHRF1 in gastric cancers and explored miR-146a/b mediated regulation of UHRF1 as a novel therapeutic approach in preventing metastasis and treating such cancers [74]. Immunohistochemistry staining of 106 gastric tumors revealed higher expression of UHRF1 in cancer tissues compared with adjacent normal tissues, which correlated with poor differentiation, cancer staging, increased lymph node and tissue metastasis [74]. Kaplan-Meier analysis showed that patients with higher expression of UHRF1 had poor prognosis and shorter overall survival time as compared with patients having relatively lower expression of UHRF1, suggesting abnormal high levels of UHRF1 as independent diagnostic and prognostic marker for gastric cancer [74].

At the cellular level, overexpression of UHRF1 was observed in aggressive gastric cancer cell lines (GC9811-P and MKN28M), which has been suggested to enhance the proliferating capacity of these cells [74]. Reduced levels of UHRF1, induced by miR-146a/b, reactivated tumor suppressor genes like *SLIT3*, *CDH4*, and *RUNX3* via promoter hypomethylation [74]. Consistently, with this notion, same authors further explored the prognostic value of UHRF1 expression in a study including 238 gastric cancer patients [52]. Immunohistochemistry labelling for UHRF1 was found positive in 82% of samples and significantly correlated with poor differentiation and metastasis. Indeed, patients with higher expression of UHRF1 had a very low 5-year survival rate of 19% as compared to patients with negative (38%) or low expression of UHRF1 (30%) suggesting UHRF1 as a significant predictor of gastric cancer prognosis [52].

UHRF1 in colorectal cancer

Epigenetic silencing of tumor suppressor genes via promoter hypermethylation is commonly reported besides the genetic aberrations in colorectal carcinogenesis and many mechanisms have been proposed for this deregulation. UHRF1 overexpression in colorectal cancer has been observed in several studies and is considered to be involved in promoter hypermethylation mediated repression of TSGs [7, 8, 94]. Wang *et al* first reported the overexpression of UHRF1 in colorectal cancer and suggested its use as a biomarker and a possible therapeutic target for diagnosis and treatment of colorectal cancer [45]. The authors observed a significantly increased UHRF1 expression at both transcriptomic and proteomic levels in colon cancer tissues and found positive association of this overexpression with metastasis, poor clinical staging and *p16* silencing [45]. Overexpression of UHRF1 was also observed in LoVo, DLD1, SW480 and SW620 colon cancer cell lines. Inhibition of UHRF1 in these cells led to upregulation of *p16*, decreased proliferation and migration capacity, as well as cell cycle arrest at G0/G1 and apoptosis [45]. Similarly, in colorectal cells,

overexpressed UHRF1 negatively regulated peroxisome proliferator-activated receptor gamma *(PPARG),* through epigenetic-dependent mechanisms [95]. The consequences were increased endothelial to mesenchymal transition (EMT), growth and cell viability. Furthermore, prognostic values were more significant when both UHRF1 overexpression and PPARG down-regulation were taken into account [95]. Another study in which 231 colorectal cancer tissues and 40 adenoma specimens were analyzed for UHRF1 levels reported similar results [96]. Indeed, immunohistochemistry showed high expression of UHRF1 in the nucleus of 65.8% (152/231) colorectal cancer tissues and of 87.5% (35/40) adenoma samples while little or no expression was found in normal colonic mucosa [96]. Expression of UHRF1 positively correlated with the depth of invasion and E2F-1 levels [96]. So far it is not yet clear why UHRF1 is up-regulated in cancer but some interesting leads are emerging. For instance, an inverse relationship between the levels of UHRF1 and the regulatory miRNA-9 has been reported in colorectal cells, for which high levels of UHRF1 are associated with poor survival rate of patients [75].

UHRF1 in breast cancer

Like for other cancers, many studies have reported the association of UHRF1 with breast cancer which is one of the leading causes of cancer related deaths in women world-wide, killing around 0.5 million women each year [86]. In 2003, we first reported increased expression of UHRF1 in breast cancer tissues and found a relationship between its expression and pathological grade of cancer [57]. Later UHRF1 overexpression in breast cancer patients was reported by cDNA microarray and qRT-PCR [37]. Overexpressed UHRF1 was further confirmed by the immunohistochemical staining and correlated with poor differentiation of tumors [37]. Recently, a study has investigated UHRF1 as a diagnostic and prognostic marker for breast cancer [97]. In this study, 62 tissue samples were analyzed and compared with 24 adjacent non-cancerous tissues. Higher expression of UHRF1 was observed at both mRNA and protein level in cancerous tissues which significantly correlated with stage of disease and c-erb2 status but was independent of age, menopause, estrogen and progesterone receptor levels [97].

The origin of the enhanced UHRF1 expression in breast cancer remains elusive in contrast to the down-stream events. Notably, increased expression of UHRF1 in breast cancers is believed to aggravate the pathogenesis by silencing *BRCA1* and modulating the estrogen receptor-α expression [51, 98]. UHRF1 overexpression also increased the proliferation and migration potential of breast cancer cells as exogenous expression of UHRF1 in MDA-MB-231 breast cancer cells facilitated their passage through the cell cycle by induction of cyclin D1 and prevention of apoptosis [99]. UHRF1 also confers radioresistance to breast cancer cells by promoting the expression of DNA damage repair proteins Lupus Ku autoantigen protein p70 (Ku-70) and Lupus Ku autoantigen protein p80 (Ku-80) repairing the chromosomal aberrations and also by down-regulating the expression of BAX and other pro-apoptotic proteins [100]. Similarly, it has been observed that specific inhibition of UHRF1, by mRNA targeting, decreased the oncogenic capacity in breast cancer cells and increased their sensitivity to chemotherapy [101, 102].

UHRF1 in gynecological tumors

UHRF1 expression in cervical cancer is also a good indicator for cellular proliferation and malignancy. Notably, an analysis of 99 cervical biopsies showed UHRF1 as a useful biomarker to discriminate low grade intraepithelial lesions from normal tissues with a sensitivity of 71.4% and to discriminate low grade intraepithelial lesions from high grade intraepithelial lesions with a sensitivity of 97.6% [103]. Another study on cervical squamous cell carcinoma (CSCC) also reported high expression of UHRF1 at both mRNA and protein level in 47 samples and found that silencing of UHRF1 in cervical cancer cells inhibited cell proliferation and induced apoptosis [104]. The reasons why UHRF1 is overexpressed in cervical cancer, is still not yet elucidated and again it is rather the downstream events that have been deciphered in cellular models. Indeed, polyphenolic extracts from plant sources were found to downregulate UHRF1 in the cervical cancer HeLa cell line [47]. This in turn upregulated the tumor suppressor gene *p16* and ultimately halted the progression of the cell cycle and induced apoptosis [47]. Moreover, UHRF1 overexpression in HeLa cells was shown to decrease their radio-sensitivity to γ-radiation by increasing the expression of the DNA repair proteins XRCC4, thus, enhancing the capability of these cells to repair the DNA damaged by radiation [105]. It is remarkable to notice that a paradigm is emerging concerning the decreased sensitivity of cancer cells to chemotherapy through control of the DNA repair machinery by UHRF1.

Besides cervical cancer, the diagnostic and prognostic capabilities of UHRF1 as biomarker have also been evaluated in ovarian cancer, which is the major worldwide contributor in gynecological tumors posing serious threat to the life of women. In a study including 80 samples from ovarian cancer tissues, significantly higher expression of UHRF1 was found at both transcriptomic and protein levels in tumors as compared with adjacent normal tissues. Knockdown of UHRF1 in ovarian cancer cells inhibited their proliferation and induced apoptosis, suggesting UHRF1 as a general indicator of malignancy and an attractive therapeutic target for ovarian cancers [106].

UHRF1 in prostate cancer

Prostate cancer undergoes profound epigenetic modifications via aberrant DNA methylation and histone post-translational modifications resulting in silencing of tumor suppressor genes [107]. Expression analysis by immunohistochemistry in tissue microarrays of 226 prostate tumor samples revealed significant overexpression of UHRF1 in almost half of tissue samples [108]. This overexpression correlated with poor clinical prognosis as patients with high expression of UHRF1 had reduced median survival rates (10.4 years) as compared to patients with low expression of UHRF1 (12.4 years) [108]. Recently Wan *et al* reported similar results after analyzing expression of UHRF1 in 225 prostate cancer specimens [109]. UHRF1 staining was found in 47.1% of specimens which positively correlated with the Gleason score and the pathological stage of the disease [109]. Patients with higher levels of UHRF1 were found to be at higher risk for biochemical recurrence after radical prostatectomy. Mean biochemical recurrence (BCR) free time in UHRF1-positive patients was around 23.0 months versus 38.9 months in UHRF1-negative patients while 5-year BCR-free survival rate was 12.4% in UHRF1-positive patients as compared with 51.8% in UHRF1-negative patients. These results support UHRF1 as a valuable independent prognostic factor to predict prostate cancer outcome after radical prostatectomy [109].

At the cellular level, overexpression of UHRF1 has also been reported in aggressively proliferating, androgen-independent cell lines of prostate cancer (DU145 and PC3), while low expression of UHRF1 was found in immortalized normal prostate epithelial cells (LHS) or androgen-dependent prostate adenocarcinoma cells with low metastatic potential (LNCaP and 22Rv1 cells) [108, 109]. Overexpression of UHRF1 accompanied with downregulation of tumor suppressor genes and increased expression of EZH2 (H3K27 methyltransferase) in prostate cancer cells contributed to the poor clinical prognosis and lethal progression disease. UHRF1 also recruited SUV39H1 (H3K9 methyltransferase) and DNMTs to the promoter region of many tumor suppressor genes *(CDH1, PSP94, RARB)* resulting in increased methylation of histones and DNA with subsequent silencing of TSGs [108]. Altogether these results suggest that UHRF1 may serve as a useful biomarker and therapeutic target for prostate cancer as it plays an important role in epigenetic silencing of TSGs via histone and DNA modifications

UHRF1 in bladder cancer

UHRF1 has also been described as a 'novel' diagnostic and prognostic marker for the bladder cancer, which is the second most common cancer of the urinary system [110]. Expression of UHRF1 was found significantly increased in the cancer cells and was positively correlated with histological and pathological grade, as higher expression was observed in later stages of cancer. Increased expression of UHRF1 was also associated with poor prognosis of disease as patients having higher levels of UHRF1 had poor survival rate and higher recurrence [110]. UHRF1 levels evaluated by qRT-PCR or immunohistochemistry based detection methods in surgical sections showed UHRF1 as a specific and sensitive biomarker for bladder cancer. Significantly higher levels of UHRF1 were detectable in specimens with non-invasive or superficially invasive cancers at very early stages compared to normal cells [110]. Similarly, in non-muscle-invasive bladder cancer (NMIBC) increased expression of UHRF1 was found in cancer cells, which was directly related with tumor malignancy [111]. Indeed, patients with UHRF1 overexpression had shorter survival duration (mean survival time 42.59 months) and higher incidences of recurrence (41 out of 70 cases) as compared with patients with relatively lower expression of UHRF1, who had greater survival time (mean survival time 71.36 months) and lower chances of recurrence (29 out of 70 cases) [111]. This suggests UHRF1 as an independent prognostic marker for the bladder cancers.

Other studies reported similar overexpression of UHRF1 in bladder cancers and in invasive cell lines, such as 253J, T24, KU7, along with silencing of tumor suppressor genes *e.g., KISS1* and *RGS2* [56, 112, 113]. Altogether, these studies emphasize UHRF1 as an attractive biomarker and therapeutic target for bladder cancers.

UHRF1 in renal cancer

Each year 338,000 new cases of kidney cancers, with a majority of renal cell carcinomas (RCC) are reported worldwide with a high prevalence in developed countries [86]. First evidence of UHRF1 overexpression in kidney tumors has been reported by Unoki *et al* [110]. By investigating mRNA levels, UHRF1 overexpression was found to be associated with several characteristics of kidney tumor patients, including 5-year survival rates, pathological staging and histological grade [110]. Later Ma *et al* found elevated levels of UHRF1 mRNA in 70% of RCC cases [114]. Overexpression was further confirmed by staining of UHRF1 in histological samples, which showed 74.2 % positive staining in RCC carcinoma tissues [114]. Similarly, UHRF1 overexpression, in metastatic renal cancer tissues as compared with non-metastatic tissues, correlated with downregulation of non-coding miR-146a-5p, which targets UHRF1 transcription [115]. However, another miRNA might also be involved in UHRF1 overexpression in RCC. Indeed, miRNA-101 has also been shown to regulate UHRF1 expression since its downregulation leads to UHRF1 upregulation [78]. Interestingly, in this study UHRF1 overexpression

was confirmed in sunitinib-treated RCC tissues and was associated with shorter overall survival after surgery for RCC [78].

UHRF1 in other cancers

Few studies have also predicted UHRF1 as a diagnostic and prognostic marker for various other types of cancers. Representational difference analysis (RDA) of different pathological grades of astrocytoma revealed *UHRF1* and four other genes to be differentially expressed in astrocytoma cancer tissues [116]. Results were confirmed by qPCR analysis in which 7 normal brain tissues, 9 grade I (pilocytic astrocytoma), 9 grade II (low grade astrocytoma), 11 grade III (anaplastic astrocytoma), and 22 grade IV (glioblastoma multiforme) samples were analyzed. Significant overexpression of UHRF1 was observed in cancerous tissues as compared with normal cells showing the possibility to use this differential expression of UHRF1 as a diagnostic marker for astrocytoma [116].

The diagnostic and prognostic value of UHRF1 has also been evaluated in medulloblastoma, a common malignant brain tumor. Out of 168 formalin-fixed, paraffin-embedded medulloblastoma, high levels of UHRF1 were found in 108 cases while lower expression of UHRF1 was observed in the remaining 60 samples, whilst normal cerebellum tissue samples lacked UHRF1 staining [117]. Kaplan–Meier survival analysis showed that patients with high levels of UHRF1 had poor overall survival and progression free survival rate illustrating UHRF1 as a potential independent prognostic marker for medulloblastoma [117].

UHRF1 has also been proposed as a biomarker and potential therapeutic target for gallbladder cancer, which is well known for its poor prognosis and high mortality rate [118]. Immunohistochemical results showed UHRF1-positive staining in 63.2% of cancerous tissue samples [118]. UHRF1 was overexpressed in cancerous tissues and correlated with the advanced stage and lymph node metastasis. Enhanced expression of UHRF1 was also observed at both mRNA and protein level in GBC-SD and NOZ cell lines and depletion of UHRF1 by siRNA or shRNA markedly reduced their migration potential *in vitro* and tumor forming capabilities [118]. Interestingly, knockdown of UHRF1 promoted the expression of *promyelocytic leukemia protein* (PML) and *p21* (*CDKN1A)* tumor suppressor genes, resulting in cell cycle arrest at G1 [118]. UHRF1 depletion also induced apoptosis in these cells by activating both intrinsic and extrinsic pathways for apoptosis, in accordance with previous studies suggesting that UHRF1 exhibits anti-apoptotic properties [119]. All this information suggests an oncogenic role of UHRF1 in gallbladder cancer and increased expression of UHRF1 as an independent biomarker for diagnosis and a therapeutic target of gallbladder cancers.

Correlation of UHRF1 expression with tumorigenesis has also been demonstrated in laryngeal squamous cell carcinomas (LSCC), through analysis of 60 LSCC samples [120]. UHRF1 overexpression was found in 78.3% (47/60) of cancer tissue samples, whereas remaining 13 samples had relatively lower expression of UHRF1 and in normal tissues, UHRF1 expression was barely detectable [120]. UHRF1 overexpression also correlated with the histological and pathological stages of cancer and was found in undifferentiated cells in advanced stages of cancer [120].

Similar findings were reported in esophageal squamous cell carcinoma (ESCC) where increased expression of UHRF1 was observed in 67% of human ESCC samples and overexpression positively correlated with advanced pathological and histological stages of the cancer, poor differentiation and lymph node metastasis [121]. Accordingly, overexpressed UHRF1 was also related to the radiotherapy resistance in patients with ESCC. Furthermore, results were validated by lentivirus mediated targeting of UHRF1 by shRNA in a TE-1 cell line inducing radio-sensitivity and apoptosis in ESCC derived cell line [121]. Another cohort study of 160 ESCC patients demonstrated that UHRF1 is as an attractive prognostic marker and potential target for cancer therapy as high levels of UHRF1 corresponded to poor survival rate [122].

High levels of UHRF1 have also been reported in several studies on pancreatic cancer, supporting the use of UHRF1 as a diagnostic marker for pancreatic cancer. For instance, power blot assay identified UHRF1 among differentially expressed proteins in pancreatic adenocarcinoma, which is extremely aggressive and difficult to diagnose with survival rate of less than 5% in five years [123]. Moreover, UHRF1 was selectively overexpressed in pancreatic adenocarcinoma tissues while it was not detectable in normal pancreatic tissue or chronic pancreatitis specimens [123]. UHRF1 overexpression was found at both proteomic and transcriptomic level in 80% of pancreatic ductal adenosarcoma cases and high UHRF1 levels correlated with neoplastic grade and lesion [123]. Similarly, UHRF1 overexpression was observed in 86% (114 of 132) of malignant pancreatic tumors samples [124] and 158 pancreatic cancer samples [125]. Furthermore, high UHRF1 levels positively correlated with short survival time of patients [124, 125]. All these results suggest UHRF1 as a valuable independent diagnostic marker for pancreatic cancer in clinical settings.

Similar findings were reported in thyroid cancers cells as microarray analysis showed significant upregulation of UHRF1 to identify gene expression profile that favors the progression of well differentiated tumors to aggressive, poorly differentiated or undifferentiated cancer cells [126]. UHRF1 levels were significantly higher in both differentiated and poorly differentiated cancer cells as compared with normal cells, suggesting a good

Table 1: Summary of studies describing diagnostic and prognostic potential of UHRF1 in various cancers

Cancer	Methods	Potential of UHRF1	Downregulated TSGs	Reference
Lung Cancer	qRT-PCR, IHC	UHRF1 overexpression relates to tumor stages, metastasis and poor prognosis.	*RASSF1, p16, CYGB CDH13*	[87-89]
Liver Cancer	qRT-PCR, IHC, Immunoblot assay, HPLC	UHRF1 overexpression relates to tumor size, metastasis, α-fetoprotein, relapse and short survival time.	*p21, CDH1, MEG3*	[54, 62, 71, 90-92]
Gastric Cancer	qRT-PCR, IHC	UHRF1 overexpression relates to poor differentiation, tumor stages, metastasis and low survival rate.	*SLIT3, CDH4, RUNX3, p16, FOXO4, PPARG, BRCA1, PML*	[52, 74]
Colorectal Cancer	qRT-PCR, IHC	UHRF1 overexpression relates to metastasis, tumor stage, E2F1 levels and poor survival rate.	*p16, PPARG*	[45, 75, 95, 96]
Breast Cancer	qPCR, Western Blot, IHC	UHRF1 overexpression relates to tumor stages, low survival rate and resistance to radiotherapy.	*BRCA1*	[37, 51, 97, 100]
Cervical Cancer	qRT-PCR, Western Blot, IHC	UHRF1 overexpression relates to tumor stages, poor prognosis and resistance to radiotherapy.	*p16*	[47, 103-105]
Ovarian Cancer	qRT-PCR, Western Blot	UHRF1 overexpression relates to progression of cancer.		[106]
Prostate Cancer	qRT-PCR IHC	UHRF1 overexpression relates to high Gleason score, tumor stages, recurrence and low survival rate.	*CDH1, PSP94, RARB*	[107-109]
Bladder Cancer	qRT-PCR, IHC	UHRF1 overexpression relates to tumor stages, risk of recurrence and low survival rate.	*KISS1, RGS2*	[56, 76, 77, 110-113]
Renal Cell Carcinoma	qRT-PCR, Western Blot, IHC	UHRF1 overexpression relates to tumor stages of cancer, drug (sunitinib) resistance and low survival rate	*p53*	[78, 114, 115]
Astrocytoma	RDA, qRT-PCR	UHRF1 overexpression relates to stages of cancer.		[116]
Medulloblastoma	IHC	UHRF1 overexpression relates to shorter survival and progression free time.		[117]
Gall Bladder Carcinoma	qRT-PCR, Western Blot, IHC	UHRF1 overexpression relates to tumor stages and lymph node metastasis.	*PML, p21*	[118]
Laryngeal Squamous Cell Carcinoma	qRT-PCR, IHC	UHRF1 overexpression relates to tumor stages, metastasis and low survival rate.		[120]
Esophageal Squamous Cell Carcinoma	qRT-PCR, IHC	UHRF1 overexpression relates to poor differentiation, pathological stage, low survival rate and resistance to radiotherapy.		[121, 122]
Pancreatic Carcinoma	qRT-PCR, IHC	UHRF1 overexpression relates to tumor size, metastasis, stages of cancer and low survival rate.	*RASSF1, p16, KEAP1*	[123-125]
Thyroid Cancer	qRT-PCR, IHC	UHRF1 overexpression relates to tumor stage.		[126, 127]

Abbreviations: qRT-PCR: quantitative reverse-transcriptase polymerase chain reaction; IHC: immunohistochemistry; RDA: representational difference analysis

diagnostic value for UHRF1 in thyroid cancers [126]. These results were in agreement with another study in a Chinese population showing high expression of UHRF1 in poorly differentiated anaplastic thyroid cancer cells versus papillary thyroid cancer and normal cells [127]. Targeting UHRF1 in these cells resulted in suppression of dedifferentiation and stem cell marker expression such as CD97, SOX2, OCT4 and NANOG, highlighting UHRF1 as an attractive target for thyroid cancer therapy [127].

CONCLUSIONANDFUTUREDIRECTIONS

UHRF1 overexpression is found in majority, if not all, of cancers, thus predicting UHRF1 as an independent universal diagnostic and prognostic biomarker for cancer detection, disease progression and therapeutic response monitoring (Table 1). High UHRF1 mRNA and protein levels are detected in early stages of many tumors suggesting UHRF1 as a valuable diagnostic marker for the timely detection of cancers. It is also employed to predict the prognosis of cancer as high level of UHRF1 is generally correlated to poor survival rate, resistance to therapy and recurrence of malignancy.

UHRF1 levels have been well correlated with Ki67 and PCNA which are widely used proliferation markers in cancers [52, 95, 104]. However, UHRF1 overexpression is a better diagnosis and prognostic biomarker in cancers as compared with Ki67 and PCNA since it fulfills the requirement of an independent factor. However, so far no universal biomarker is available for cancer early-onset diagnostic. Ratio of Ki67-staining vs UHRF1-staining might differentiate well between normal proliferating cells and cancer cells. Indeed, overexpression of UHRF1 is maintained throughout the cell cycle in cancer cells but not in normal cells [57]. Thus, one might expect that UHRF1-staining should be lower than Ki67 in normal tissues and as much as Ki67 or above in cancer cells. This interesting direction requires further investigations but may represent the basis for the development of a diagnostic kit.

UHRF1 overexpression has also proven to be a barrier to cure cancer because of its ability to silence tumor suppressor genes depending on the cancer type (Figure 3) or to counteract pro-apoptotic genes and to induce therapy resistance. It is therefore essential to target UHRF1 overexpression to achieve therapeutic goals in cancer patients. Many strategies can be designed to target UHRF1, including use of small molecules [128]. Therefore, following UHRF1 levels in fluids or tissues during cancer treatment could be of help in a theranostic context.

Abbreviations

UHRF1: ubiquitin-like containing PHD and Ring Finger domain protein 1; DNMT1: DNA methyltransferase 1; qRT-PCR: quantitative reverse-transcriptase polymerase chain reaction; IHC: immunohistochemistry; RDA: representational difference analysis; NSCLC: non-small cell lung cancer; HCC: hepatocellular carcinoma, NMIBC: non-muscle-invasive bladder cancer; RCC: renal cell carcinoma; ESCC: esophageal squamous cell carcinoma; LSCC: laryngeal squamous cell carcinomas.

ACKNOWLEDGMENTS

Our work on UHRF1 was supported by the Agence National de la Recherche (ANR Fluometadn), the Fondation pour la Recherche Médicale (FRM DCM20111223038), Ligue contre le Cancer and by the grant ANR-10-LABX-0030-INRT, a French State fund managed by the Agence Nationale de la Recherche under the frame program Investissements d'Avenir ANR-10-IDEX-0002-02.

CONFLICT OF INTEREST

All authors report no conflicts of interest.

REFERENCES

1. Sandoval J, Peiro-Chova L, Pallardo FV, Garcia-Gimenez JL. Epigenetic biomarkers in laboratory diagnostics: emerging approaches and opportunities. Expert Rev Mol Diagn. 2013; 13: 457-71. doi: 10.1586/erm.13.37.
2. Jeltsch A, Jurkowska RZ. New concepts in DNA methylation. Trends Biochem Sci. 2014; 39: 310-8. doi: 10.1016/j.tibs.2014.05.002.
3. Zane L, Sharma V, Misteli T. Common features of chromatin in aging and cancer: cause or coincidence? Trends Cell Biol. 2014; 24: 686-94. doi: 10.1016/j.tcb.2014.07.001.
4. Lawrence M, Daujat S, Schneider R. Lateral Thinking: How Histone Modifications Regulate Gene Expression. Trends Genet. 2016; 32: 42-56. doi: 10.1016/j.tig.2015.10.007.
5. Zink LM, Hake SB. Histone variants: nuclear function and disease. Curr Opin Genet Dev. 2016; 37: 82-9. doi: 10.1016/j.gde.2015.12.002.
6. Dawson MA, Kouzarides T. Cancer epigenetics: from mechanism to therapy. Cell. 2012; 150: 12-27. doi: 10.1016/j.cell.2012.06.013.
7. Alhosin M, Sharif T, Mousli M, Etienne-Selloum N, Fuhrmann G, Schini-Kerth VB, Bronner C. Down-regulation of UHRF1, associated with re-expression of tumor suppressor genes, is a common feature of natural compounds exhibiting anti-cancer properties. J Exp Clin Cancer Res. 2011; 30: 41. doi: 10.1186/1756-9966-30-41.
8. Alhosin M, Omran Z, Zamzami MA, Al-Malki AL, Choudhry H, Mousli M, Bronner C. Signalling pathways in UHRF1-dependent regulation of tumor suppressor genes in cancer. J Exp Clin Cancer Res. 2016; 35: 174. doi: 10.1186/s13046-016-0453-5.
9. Chervona Y, Costa M. Histone modifications and cancer: biomarkers of prognosis? Am J Cancer Res. 2012; 2: 589-97.
10. Amacher DE. A 2015 survey of established or potential epigenetic biomarkers for the accurate detection of human cancers. Biomarkers. 2016; 21: 387-403. doi:

10.3109/1354750X.2016.1153724.

11. Angulo JC, Lopez JI, Ropero S. DNA Methylation and Urological Cancer, a Step Towards Personalized Medicine: Current and Future Prospects. Mol Diagn Ther. 2016; 20: 531-49. doi: 10.1007/s40291-016-0231-2.
12. Lam K, Pan K, Linnekamp JF, Medema JP, Kandimalla R. DNA methylation based biomarkers in colorectal cancer: A systematic review. Biochim Biophys Acta. 2016; 1866: 106-20. doi: 10.1016/j.bbcan.2016.07.001.
13. Wu P, Cao Z, Wu S. New Progress of Epigenetic Biomarkers in Urological Cancer. Dis Markers. 2016; 2016: 9864047. doi: 10.1155/2016/9864047.
14. Willbanks A, Leary M, Greenshields M, Tyminski C, Heerboth S, Lapinska K, Haskins K, Sarkar S. The Evolution of Epigenetics: From Prokaryotes to Humans and Its Biological Consequences. Genet Epigenet. 2016; 8: 25-36. doi: 10.4137/GEG.S31863.
15. Probst AV, Dunleavy E, Almouzni G. Epigenetic inheritance during the cell cycle. Nat Rev Mol Cell Biol. 2009; 10: 192-206. doi: 10.1038/nrm2640.
16. Bostick M, Kim JK, Esteve PO, Clark A, Pradhan S, Jacobsen SE. UHRF1 plays a role in maintaining DNA methylation in mammalian cells. Science. 2007; 317: 1760-4. doi: 10.1126/science.1147939.
17. Sharif J, Muto M, Takebayashi S, Suetake I, Iwamatsu A, Endo TA, Shinga J, Mizutani-Koseki Y, Toyoda T, Okamura K, Tajima S, Mitsuya K, Okano M, et al. The SRA protein Np95 mediates epigenetic inheritance by recruiting Dnmt1 to methylated DNA. Nature. 2007; 450: 908-12. doi: 10.1038/nature06397.
18. Arita K, Ariyoshi M, Tochio H, Nakamura Y, Shirakawa M. Recognition of hemi-methylated DNA by the SRA protein UHRF1 by a base-flipping mechanism. Nature. 2008; 455: 818-21. doi: 10.1038/nature07249.
19. Avvakumov GV, Walker JR, Xue S, Li Y, Duan S, Bronner C, Arrowsmith CH, Dhe-Paganon S. Structural basis for recognition of hemi-methylated DNA by the SRA domain of human UHRF1. Nature. 2008; 455: 822-5. doi: 10.1038/nature07273.
20. Hashimoto H, Horton JR, Zhang X, Bostick M, Jacobsen SE, Cheng X. The SRA domain of UHRF1 flips 5-methylcytosine out of the DNA helix. Nature. 2008; 455: 826-9. doi: 10.1038/nature07280.
21. Kent B, Magnani E, Walsh MJ, Sadler KC. UHRF1 regulation of Dnmt1 is required for pre-gastrula zebrafish development. Dev Biol. 2016; 412: 99-113. doi: 10.1016/j.ydbio.2016.01.036.
22. Hopfner R, Mousli M, Jeltsch JM, Voulgaris A, Lutz Y, Marin C, Bellocq JP, Oudet P, Bronner C. ICBP90, a novel human CCAAT binding protein, involved in the regulation of topoisomerase IIalpha expression. Cancer Res. 2000; 60: 121-8.
23. Hopfner R, Mousli M, Garnier JM, Redon R, du Manoir S, Chatton B, Ghyselinck N, Oudet P, Bronner C. Genomic structure and chromosomal mapping of the gene coding for ICBP90, a protein involved in the regulation of the topoisomerase IIalpha gene expression. Gene. 2001; 266: 15-23.
24. Hopfner R, Mousli M, Oudet P, Bronner C. Overexpression of ICBP90, a novel CCAAT-binding protein, overcomes cell contact inhibition by forcing topoisomerase II alpha expression. Anticancer Res. 2002; 22: 3165-70.
25. Bronner C, Krifa M, Mousli M. Increasing role of UHRF1 in the reading and inheritance of the epigenetic code as well as in tumorogenesis. Biochem Pharmacol. 2013; 86: 1643-9. doi: 10.1016/j.bcp.2013.10.002.
26. Jenkins Y, Markovtsov V, Lang W, Sharma P, Pearsall D, Warner J, Franci C, Huang B, Huang J, Yam GC, Vistan JP, Pali E, Vialard J, et al. Critical role of the ubiquitin ligase activity of UHRF1, a nuclear RING finger protein, in tumor cell growth. Mol Biol Cell. 2005; 16: 5621-9. doi: 10.1091/mbc.E05-03-0194.
27. Nishiyama A, Yamaguchi L, Sharif J, Johmura Y, Kawamura T, Nakanishi K, Shimamura S, Arita K, Kodama T, Ishikawa F, Koseki H, Nakanishi M. Uhrf1-dependent H3K23 ubiquitylation couples maintenance DNA methylation and replication. Nature. 2013; 502: 249-53. doi: 10.1038/nature12488.
28. Qin W, Wolf P, Liu N, Link S, Smets M, La Mastra F, Forne I, Pichler G, Horl D, Fellinger K, Spada F, Bonapace IM, Imhof A, et al. DNA methylation requires a DNMT1 ubiquitin interacting motif (UIM) and histone ubiquitination. Cell Res. 2015; 25: 911-29. doi: 10.1038/cr.2015.72.
29. Hashimoto H, Horton JR, Zhang X, Cheng X. UHRF1, a modular multi-domain protein, regulates replication-coupled crosstalk between DNA methylation and histone modifications. Epigenetics. 2009; 4: 8-14.
30. Nady N, Lemak A, Walker JR, Avvakumov GV, Kareta MS, Achour M, Xue S, Duan S, Allali-Hassani A, Zuo X, Wang YX, Bronner C, Chedin F, et al. Recognition of multivalent histone states associated with heterochromatin by UHRF1 protein. J Biol Chem. 2011; 286: 24300-11. doi: 10.1074/jbc.M111.234104.
31. Karagianni P, Amazit L, Qin J, Wong J. ICBP90, a novel methyl K9 H3 binding protein linking protein ubiquitination with heterochromatin formation. Mol Cell Biol. 2008; 28: 705-17. doi: 10.1128/MCB.01598-07.
32. Zhao Q, Zhang J, Chen R, Wang L, Li B, Cheng H, Duan X, Zhu H, Wei W, Li J, Wu Q, Han JD, Yu W, et al. Dissecting the precise role of H3K9 methylation in crosstalk with DNA maintenance methylation in mammals. Nat Commun. 2016; 7: 12464. doi: 10.1038/ncomms12464.
33. Greiner VJ, Kovalenko L, Humbert N, Richert L, Birck C, Ruff M, Zaporozhets OA, Dhe-Paganon S, Bronner C, Mely Y. Site-Selective Monitoring of the Interaction of the SRA Domain of UHRF1 with Target DNA Sequences Labeled with 2-Aminopurine. Biochemistry. 2015; 54: 6012-20. doi: 10.1021/acs.biochem.5b00419.

34. Kilin V, Gavvala K, Barthes NP, Michel BY, Shin D, Boudier C, Mauffret O, Yashchuk V, Mousli M, Ruff M, Granger F, Eiler S, Bronner C, et al. Dynamics of Methylated Cytosine Flipping by UHRF1. J Am Chem Soc. 2017; 139: 2520-8. doi: 10.1021/jacs.7b00154.

35. Frauer C, Hoffmann T, Bultmann S, Casa V, Cardoso MC, Antes I, Leonhardt H. Recognition of 5-hydroxymethylcytosine by the Uhrf1 SRA domain. PLoS One. 2011; 6: e21306. doi: 10.1371/journal.pone.0021306.

36. Unoki M, Brunet J, Mousli M. Drug discovery targeting epigenetic codes: the great potential of UHRF1, which links DNA methylation and histone modifications, as a drug target in cancers and toxoplasmosis. Biochem Pharmacol. 2009; 78: 1279-88. doi: 10.1016/j.bcp.2009.05.035.

37. Unoki M, Nishidate T, Nakamura Y. ICBP90, an E2F-1 target, recruits HDAC1 and binds to methyl-CpG through its SRA domain. Oncogene. 2004; 23: 7601-10. doi: 10.1038/sj.onc.1208053.

38. Achour M, Fuhrmann G, Alhosin M, Ronde P, Chataigneau T, Mousli M, Schini-Kerth VB, Bronner C. UHRF1 recruits the histone acetyltransferase Tip60 and controls its expression and activity. Biochem Biophys Res Commun. 2009; 390: 523-8. doi: 10.1016/j.bbrc.2009.09.131.

39. Kim JK, Esteve PO, Jacobsen SE, Pradhan S. UHRF1 binds G9a and participates in p21 transcriptional regulation in mammalian cells. Nucleic Acids Res. 2009; 37: 493-505. doi: 10.1093/nar/gkn961.

40. Ma H, Chen H, Guo X, Wang Z, Sowa ME, Zheng L, Hu S, Zeng P, Guo R, Diao J, Lan F, Harper JW, Shi YG, et al. M phase phosphorylation of the epigenetic regulator UHRF1 regulates its physical association with the deubiquitylase USP7 and stability. Proc Natl Acad Sci U S A. 2012; 109: 4828-33. doi: 10.1073/pnas.1116349109.

41. Dai C, Shi D, Gu W. Negative regulation of the acetyltransferase TIP60-p53 interplay by UHRF1 (ubiquitin-like with PHD and RING finger domains 1). J Biol Chem. 2013; 288: 19581-92. doi: 10.1074/jbc.M113.476606.

42. Pacaud R, Brocard E, Lalier L, Hervouet E, Vallette FM, Cartron PF. The DNMT1/PCNA/UHRF1 disruption induces tumorigenesis characterized by similar genetic and epigenetic signatures. Sci Rep. 2014; 4: 4230. doi: 10.1038/srep04230.

43. Jeanblanc M, Mousli M, Hopfner R, Bathami K, Martinet N, Abbady AQ, Siffert JC, Mathieu E, Muller CD, Bronner C. The retinoblastoma gene and its product are targeted by ICBP90: a key mechanism in the G1/S transition during the cell cycle. Oncogene. 2005; 24: 7337-45. doi: 10.1038/sj.onc.1208878.

44. Achour M, Jacq X, Ronde P, Alhosin M, Charlot C, Chataigneau T, Jeanblanc M, Macaluso M, Giordano A, Hughes AD, Schini-Kerth VB, Bronner C. The interaction of the SRA domain of ICBP90 with a novel domain of DNMT1 is involved in the regulation of VEGF gene expression. Oncogene. 2008; 27: 2187-97. doi: 10.1038/sj.onc.1210855.

45. Wang F, Yang YZ, Shi CZ, Zhang P, Moyer MP, Zhang HZ, Zou Y, Qin HL. UHRF1 promotes cell growth and metastasis through repression of p16(ink(4)a) in colorectal cancer. Ann Surg Oncol. 2012; 19: 2753-62. doi: 10.1245/s10434-011-2194-1.

46. Achour M, Mousli M, Alhosin M, Ibrahim A, Peluso J, Muller CD, Schini-Kerth VB, Hamiche A, Dhe-Paganon S, Bronner C. Epigallocatechin-3-gallate up-regulates tumor suppressor gene expression via a reactive oxygen species-dependent down-regulation of UHRF1. Biochem Biophys Res Commun. 2013; 430: 208-12. doi: 10.1016/j.bbrc.2012.11.087.

47. Krifa M, Alhosin M, Muller CD, Gies JP, Chekir-Ghedira L, Ghedira K, Mely Y, Bronner C, Mousli M. Limoniastrum guyonianum aqueous gall extract induces apoptosis in human cervical cancer cells involving p16 INK4A re-expression related to UHRF1 and DNMT1 down-regulation. J Exp Clin Cancer Res. 2013; 32: 30. doi: 10.1186/1756-9966-32-30.

48. Boukhari A, Alhosin M, Bronner C, Sagini K, Truchot C, Sick E, Schini-Kerth VB, Andre P, Mely Y, Mousli M, Gies JP. CD47 activation-induced UHRF1 over-expression is associated with silencing of tumor suppressor gene p16INK4A in glioblastoma cells. Anticancer Res. 2015; 35: 149-57.

49. Sheng Y, Wang H, Liu D, Zhang C, Deng Y, Yang F, Zhang T, Zhang C. Methylation of tumor suppressor gene CDH13 and SHP1 promoters and their epigenetic regulation by the UHRF1/PRMT5 complex in endometrial carcinoma. Gynecol Oncol. 2016; 140: 145-51. doi: 10.1016/j.ygyno.2015.11.017.

50. Chen H, Zhang C, Sheng Y, Yao S, Liu Z, Zhang C, Zhang T. Frequent SOCS3 and 3OST2 promoter methylation and their epigenetic regulation in endometrial carcinoma. Am J Cancer Res. 2015; 5: 180-90.

51. Jin W, Chen L, Chen Y, Xu SG, Di GH, Yin WJ, Wu J, Shao ZM. UHRF1 is associated with epigenetic silencing of BRCA1 in sporadic breast cancer. Breast Cancer Res Treat. 2010; 123: 359-73. doi: 10.1007/s10549-009-0652-2.

52. Zhou L, Shang Y, Jin Z, Zhang W, Lv C, Zhao X, Liu Y, Li N, Liang J. UHRF1 promotes proliferation of gastric cancer via mediating tumor suppressor gene hypermethylation. Cancer Biol Ther. 2015; 16: 1241-51. doi: 10.1080/15384047.2015.1056411.

53. Guan D, Factor D, Liu Y, Wang Z, Kao HY. The epigenetic regulator UHRF1 promotes ubiquitination-mediated degradation of the tumor-suppressor protein promyelocytic leukemia protein. Oncogene. 2013; 32: 3819-28. doi: 10.1038/onc.2012.406.

54. Zhuo H, Tang J, Lin Z, Jiang R, Zhang X, Ji J, Wang P, Sun B. The aberrant expression of MEG3 regulated by UHRF1 predicts the prognosis of hepatocellular carcinoma. Mol Carcinog. 2016; 55: 209-19. doi: 10.1002/mc.22270.

55. Qin L, Dong Z, Zhang JT. Reversible epigenetic regulation of 14-3-3sigma expression in acquired gemcitabine resistance by uhrf1 and DNA methyltransferase 1. Mol Pharmacol. 2014; 86: 561-9. doi: 10.1124/mol.114.092544.

56. Zhang Y, Huang Z, Zhu Z, Zheng X, Liu J, Han Z, Ma X, Zhang Y. Upregulated UHRF1 promotes bladder cancer cell invasion by epigenetic silencing of KiSS1. PLoS One. 2014; 9: e104252. doi: 10.1371/journal.pone.0104252.

57. Mousli M, Hopfner R, Abbady AQ, Monte D, Jeanblanc M, Oudet P, Louis B, Bronner C. ICBP90 belongs to a new family of proteins with an expression that is deregulated in cancer cells. Br J Cancer. 2003; 89: 120-7. doi: 10.1038/sj.bjc.6601068.

58. Bonapace IM, Latella L, Papait R, Nicassio F, Sacco A, Muto M, Crescenzi M, Di Fiore PP. Np95 is regulated by E1A during mitotic reactivation of terminally differentiated cells and is essential for S phase entry. J Cell Biol. 2002; 157: 909-14. doi: 10.1083/jcb.200201025.

59. Arima Y, Hirota T, Bronner C, Mousli M, Fujiwara T, Niwa S, Ishikawa H, Saya H. Down-regulation of nuclear protein ICBP90 by p53/p21Cip1/WAF1-dependent DNA-damage checkpoint signals contributes to cell cycle arrest at G1/S transition. Genes Cells. 2004; 9: 131-42.

60. Tien AL, Senbanerjee S, Kulkarni A, Mudbhary R, Goudreau B, Ganesan S, Sadler KC, Ukomadu C. UHRF1 depletion causes a G2/M arrest, activation of DNA damage response and apoptosis. Biochem J. 2011; 435: 175-85. doi: 10.1042/BJ20100840.

61. Bronner C, Achour M, Arima Y, Chataigneau T, Saya H, Schini-Kerth VB. The UHRF family: oncogenes that are drugable targets for cancer therapy in the near future? Pharmacol Ther. 2007; 115: 419-34. doi: 10.1016/j.pharmthera.2007.06.003.

62. Mudbhary R, Hoshida Y, Chernyavskaya Y, Jacob V, Villanueva A, Fiel MI, Chen X, Kojima K, Thung S, Bronson RT, Lachenmayer A, Revill K, Alsinet C, et al. UHRF1 overexpression drives DNA hypomethylation and hepatocellular carcinoma. Cancer Cell. 2014; 25: 196-209. doi: 10.1016/j.ccr.2014.01.003.

63. Jia Y, Li P, Fang L, Zhu H, Xu L, Cheng H, Zhang J, Li F, Feng Y, Li Y, Li J, Wang R, Du JX, et al. Negative regulation of DNMT3A de novo DNA methylation by frequently overexpressed UHRF family proteins as a mechanism for widespread DNA hypomethylation in cancer. Cell Discov. 2016; 2: 16007. doi: 10.1038/celldisc.2016.7.

64. Muto M, Fujimori A, Nenoi M, Daino K, Matsuda Y, Kuroiwa A, Kubo E, Kanari Y, Utsuno M, Tsuji H, Ukai H, Mita K, Takahagi M, et al. Isolation and Characterization of a Novel Human Radiosusceptibility Gene, NP95. Radiat Res. 2006; 166: 723-33. doi: 10.1667/RR0459.1.

65. Chen H, Ma H, Inuzuka H, Diao J, Lan F, Shi YG, Wei W, Shi Y. DNA damage regulates UHRF1 stability via the SCF(beta-TrCP) E3 ligase. Mol Cell Biol. 2013; 33: 1139-48. doi: 10.1128/MCB.01191-12.

66. Tian Y, Paramasivam M, Ghosal G, Chen D, Shen X, Huang Y, Akhter S, Legerski R, Chen J, Seidman MM, Qin J, Li L. UHRF1 contributes to DNA damage repair as a lesion recognition factor and nuclease scaffold. Cell Rep. 2015; 10: 1957-66. doi: 10.1016/j.celrep.2015.03.038.

67. Zhang H, Liu H, Chen Y, Yang X, Wang P, Liu T, Deng M, Qin B, Correia C, Lee S, Kim J, Sparks M, Nair AA, et al. A cell cycle-dependent BRCA1-UHRF1 cascade regulates DNA double-strand break repair pathway choice. Nat Commun. 2016; 7: 10201. doi: 10.1038/ncomms10201.

68. Liang CC, Zhan B, Yoshikawa Y, Haas W, Gygi SP, Cohn MA. UHRF1 is a sensor for DNA interstrand crosslinks and recruits FANCD2 to initiate the Fanconi anemia pathway. Cell Rep. 2015; 10: 1947-56. doi: 10.1016/j.celrep.2015.02.053.

69. Wang KY, Chen CC, Tsai SF, Shen CJ. Epigenetic Enhancement of the Post-replicative DNA Mismatch Repair of Mammalian Genomes by a Hemi-mCpG-Np95-Dnmt1 Axis. Sci Rep. 2016; 6: 37490. doi: 10.1038/srep37490.

70. Park SA, Platt J, Lee JW, Lopez-Giraldez F, Herbst RS, Koo JS. E2F8 as a Novel Therapeutic Target for Lung Cancer. J Natl Cancer Inst. 2015; 107: djv151. doi: 10.1093/jnci/djv151.

71. Wu SM, Cheng WL, Liao CJ, Chi HC, Lin YH, Tseng YH, Tsai CY, Chen CY, Lin SL, Chen WJ, Yeh YH, Huang CY, Chen MH, et al. Negative modulation of the epigenetic regulator, UHRF1, by thyroid hormone receptors suppresses liver cancer cell growth. Int J Cancer. 2015; 137: 37-49. doi: 10.1002/ijc.29368.

72. Sanders DA, Gormally MV, Marsico G, Beraldi D, Tannahill D, Balasubramanian S. FOXM1 binds directly to non-consensus sequences in the human genome. Genome Biol. 2015; 16: 130. doi: 10.1186/s13059-015-0696-z.

73. Kim KB, Son HJ, Choi S, Hahm JY, Jung H, Baek HJ, Kook H, Hahn Y, Kook H, Seo SB. H3K9 methyltransferase G9a negatively regulates UHRF1 transcription during leukemia cell differentiation. Nucleic Acids Res. 2015; 43: 3509-23. doi: 10.1093/nar/gkv183.

74. Zhou L, Zhao X, Han Y, Lu Y, Shang Y, Liu C, Li T, Jin Z, Fan D, Wu K. Regulation of UHRF1 by miR-146a/b modulates gastric cancer invasion and metastasis. FASEB J. 2013; 27: 4929-39. doi: 10.1096/fj.13-233387.

75. Zhu M, Xu Y, Ge M, Gui Z, Yan F. Regulation of UHRF1 by microRNA-9 modulates colorectal cancer cell proliferation and apoptosis. Cancer Sci. 2015; 106: 833-9. doi: 10.1111/cas.12689.

76. Matsushita R, Yoshino H, Enokida H, Goto Y, Miyamoto K, Yonemori M, Inoguchi S, Nakagawa M, Seki N. Regulation of UHRF1 by dual-strand tumor-suppressor microRNA-145 (miR-145-5p and miR-145-3p): Inhibition of bladder cancer cell aggressiveness. Oncotarget. 2016; 7: 28460-87. doi: 10.18632/oncotarget.8668.

77. Wang X, Wu Q, Xu B, Wang P, Fan W, Cai Y, Gu X, Meng F. MiR-124 exerts tumor suppressive functions on the cell

proliferation, motility and angiogenesis of bladder cancer by fine-tuning UHRF1. FEBS J. 2015; 282: 4376-88. doi: 10.1111/febs.13502.

78. Goto Y, Kurozumi A, Nohata N, Kojima S, Matsushita R, Yoshino H, Yamazaki K, Ishida Y, Ichikawa T, Naya Y, Seki N. The microRNA signature of patients with sunitinib failure: regulation of UHRF1 pathways by microRNA-101 in renal cell carcinoma. Oncotarget. 2016; 7: 59070-86. doi: 10.18632/oncotarget.10887.
79. Deng W, Yan M, Yu T, Ge H, Lin H, Li J, Liu Y, Geng Q, Zhu M, Liu L, He X, Yao M. Quantitative proteomic analysis of the metastasis-inhibitory mechanism of miR-193a-3p in non-small cell lung cancer. Cell Physiol Biochem. 2015; 35: 1677-88. doi: 10.1159/000373981.
80. Zhang ZM, Rothbart SB, Allison DF, Cai Q, Harrison JS, Li L, Wang Y, Strahl BD, Wang GG, Song J. An Allosteric Interaction Links USP7 to Deubiquitination and Chromatin Targeting of UHRF1. Cell Rep. 2015; 12: 1400-6. doi: 10.1016/j.celrep.2015.07.046.
81. Zhao GY, Lin ZW, Lu CL, Gu J, Yuan YF, Xu FK, Liu RH, Ge D, Ding JY. USP7 overexpression predicts a poor prognosis in lung squamous cell carcinoma and large cell carcinoma. Tumour Biol. 2015; 36: 1721-9. doi: 10.1007/s13277-014-2773-4.
82. Song MS, Salmena L, Carracedo A, Egia A, Lo-Coco F, Teruya-Feldstein J, Pandolfi PP. The deubiquitinylation and localization of PTEN are regulated by a HAUSP-PML network. Nature. 2008; 455: 813-7. doi: 10.1038/nature07290.
83. Nicholson B, Suresh Kumar KG. The multifaceted roles of USP7: new therapeutic opportunities. Cell Biochem Biophys. 2011; 60: 61-8. doi: 10.1007/s12013-011-9185-5.
84. Taniue K, Kurimoto A, Sugimasa H, Nasu E, Takeda Y, Iwasaki K, Nagashima T, Okada-Hatakeyama M, Oyama M, Kozuka-Hata H, Hiyoshi M, Kitayama J, Negishi L, et al. Long noncoding RNA UPAT promotes colon tumorigenesis by inhibiting degradation of UHRF1. Proc Natl Acad Sci U S A. 2016; 113: 1273-8. doi: 10.1073/pnas.1500992113.
85. Ding G, Chen P, Zhang H, Huang X, Zang Y, Li J, Li J, Wong J. Regulation of Ubiquitin-like with Plant Homeodomain and RING Finger Domain 1 (UHRF1) Protein Stability by Heat Shock Protein 90 Chaperone Machinery. J Biol Chem. 2016; 291: 20125-35. doi: 10.1074/jbc.M116.727214.
86. Ferlay J, Soerjomataram I, Dikshit R, Eser S, Mathers C, Rebelo M, Parkin DM, Forman D, Bray F. Cancer incidence and mortality worldwide: sources, methods and major patterns in GLOBOCAN 2012. Int J Cancer. 2015; 136: E359-86. doi: 10.1002/ijc.29210.
87. Unoki M, Daigo Y, Koinuma J, Tsuchiya E, Hamamoto R, Nakamura Y. UHRF1 is a novel diagnostic marker of lung cancer. Br J Cancer. 2010; 103: 217-22. doi: 10.1038/sj.bjc.6605717.
88. Huang P, Cheng CL, Chang YH, Liu CH, Hsu YC, Chen JS, Chang GC, Ho BC, Su KY, Chen HY, Yu SL. Molecular gene signature and prognosis of non-small cell lung cancer. Oncotarget. 2016; 7: 51898-907. doi: 10.18632/oncotarget.10622.
89. Daskalos A, Oleksiewicz U, Filia A, Nikolaidis G, Xinarianos G, Gosney JR, Malliri A, Field JK, Liloglou T. UHRF1-mediated tumor suppressor gene inactivation in nonsmall cell lung cancer. Cancer. 2011; 117: 1027-37. doi: 10.1002/cncr.25531.
90. Liang D, Xue H, Yu Y, Lv F, You W, Zhang B. Elevated expression of UHRF1 predicts unfavorable prognosis for patients with hepatocellular carcinoma. Int J Clin Exp Pathol. 2015; 8: 9416-21.
91. Chen X, Cheung ST, So S, Fan ST, Barry C, Higgins J, Lai KM, Ji J, Dudoit S, Ng IO, Van De Rijn M, Botstein D, Brown PO. Gene expression patterns in human liver cancers. Mol Biol Cell. 2002; 13: 1929-39. doi: 10.1091/mbc.02-02-0023.
92. Liu X, Ou H, Xiang L, Li X, Huang Y, Yang D. Elevated UHRF1 expression contributes to poor prognosis by promoting cell proliferation and metastasis in hepatocellular carcinoma. Oncotarget. 2017; 8: 10510-22. doi: 10.18632/oncotarget.14446.
93. Chang L, Wang G, Jia T, Zhang L, Li Y, Han Y, Zhang K, Lin G, Zhang R, Li J, Wang L. Armored long non-coding RNA MEG3 targeting EGFR based on recombinant MS2 bacteriophage virus-like particles against hepatocellular carcinoma. Oncotarget. 2016; 7: 23988-4004. doi: 10.18632/oncotarget.8115.
94. Shen L, Toyota M, Kondo Y, Lin E, Zhang L, Guo Y, Hernandez NS, Chen X, Ahmed S, Konishi K, Hamilton SR, Issa JP. Integrated genetic and epigenetic analysis identifies three different subclasses of colon cancer. Proc Natl Acad Sci U S A. 2007; 104: 18654-9. doi: 10.1073/pnas.0704652104.
95. Sabatino L, Fucci A, Pancione M, Carafa V, Nebbioso A, Pistore C, Babbio F, Votino C, Laudanna C, Ceccarelli M, Altucci L, Bonapace IM, Colantuoni V. UHRF1 coordinates peroxisome proliferator activated receptor gamma (PPARG) epigenetic silencing and mediates colorectal cancer progression. Oncogene. 2012; 31: 5061-72. doi: 10.1038/onc.2012.3.
96. Kofunato Y, Kumamoto K, Saitou K, Hayase S, Okayama H, Miyamoto K, Sato Y, Katakura K, Nakamura I, Ohki S, Koyama Y, Unoki M, Takenoshita S. UHRF1 expression is upregulated and associated with cellular proliferation in colorectal cancer. Oncol Rep. 2012; 28: 1997-2002. doi: 10.3892/or.2012.2064.
97. Geng Y, Gao Y, Ju H, Yan F. Diagnostic and prognostic value of plasma and tissue ubiquitin-like, containing PHD and RING finger domains 1 in breast cancer patients. Cancer Sci. 2013; 104: 194-9. doi: 10.1111/cas.12052.
98. Macaluso M, Montanari M, Noto PB, Gregorio V, Bronner C, Giordano A. Epigenetic modulation of estrogen receptor-

alpha by pRb family proteins: a novel mechanism in breast cancer. Cancer Res. 2007; 67: 7731-7. doi: 10.1158/0008-5472.CAN-07-1476.

99. Li XL, Xu JH, Nie JH, Fan SJ. Exogenous expression of UHRF1 promotes proliferation and metastasis of breast cancer cells. Oncol Rep. 2012; 28: 375-83. doi: 10.3892/or.2012.1792.

100. Li X, Meng Q, Rosen EM, Fan S. UHRF1 confers radioresistance to human breast cancer cells. Int J Radiat Biol. 2011; 87: 263-73. doi: 10.3109/09553002.2011.530335.

101. Yan F, Tan XY, Geng Y, Ju HX, Gao YF, Zhu MC. Inhibition effect of siRNA-downregulated UHRF1 on breast cancer growth. Cancer Biother Radiopharm. 2011; 26: 183-9. doi: 10.1089/cbr.2010.0886.

102. Fang L, Shanqu L, Ping G, Ting H, Xi W, Ke D, Min L, Junxia W, Huizhong Z. Gene therapy with RNAi targeting UHRF1 driven by tumor-specific promoter inhibits tumor growth and enhances the sensitivity of chemotherapeutic drug in breast cancer in vitro and in vivo. Cancer Chemother Pharmacol. 2012; 69: 1079-87. doi: 10.1007/s00280-011-1801-y.

103. Lorenzato M, Caudroy S, Bronner C, Evrard G, Simon M, Durlach A, Birembaut P, Clavel C. Cell cycle and/or proliferation markers: what is the best method to discriminate cervical high-grade lesions? Hum Pathol. 2005; 36: 1101-7. doi: 10.1016/j.humpath.2005.07.016.

104. Ge TT, Yang M, Chen Z, Lou G, Gu T. UHRF1 gene silencing inhibits cell proliferation and promotes cell apoptosis in human cervical squamous cell carcinoma CaSki cells. J Ovarian Res. 2016; 9: 42. doi: 10.1186/s13048-016-0253-8.

105. Li XL, Meng QH, Fan SJ. Adenovirus-mediated expression of UHRF1 reduces the radiosensitivity of cervical cancer HeLa cells to gamma-irradiation. Acta Pharmacol Sin. 2009; 30: 458-66. doi: 10.1038/aps.2009.18.

106. Yan F, Wang X, Shao L, Ge M, Hu X. Analysis of UHRF1 expression in human ovarian cancer tissues and its regulation in cancer cell growth. Tumour Biol. 2015; 36: 8887-93. doi: 10.1007/s13277-015-3638-1.

107. Adjakly M, Ngollo M, Dagdemir A, Judes G, Pajon A, Karsli-Ceppioglu S, Penault-Llorca F, Boiteux JP, Bignon YJ, Guy L, Bernard-Gallon D. Prostate cancer: The main risk and protective factors-Epigenetic modifications. Ann Endocrinol (Paris). 2015; 76: 25-41. doi: 10.1016/j.ando.2014.09.001.

108. Babbio F, Pistore C, Curti L, Castiglioni I, Kunderfranco P, Brino L, Oudet P, Seiler R, Thalman GN, Roggero E, Sarti M, Pinton S, Mello-Grand M, et al. The SRA protein UHRF1 promotes epigenetic crosstalks and is involved in prostate cancer progression. Oncogene. 2012; 31: 4878-87. doi: 10.1038/onc.2011.641.

109. Wan X, Yang S, Huang W, Wu D, Chen H, Wu M, Li J, Li T, Li Y. UHRF1 overexpression is involved in cell proliferation and biochemical recurrence in prostate cancer after radical prostatectomy. J Exp Clin Cancer Res. 2016; 35: 34. doi: 10.1186/s13046-016-0308-0.

110. Unoki M, Kelly JD, Neal DE, Ponder BA, Nakamura Y, Hamamoto R. UHRF1 is a novel molecular marker for diagnosis and the prognosis of bladder cancer. Br J Cancer. 2009; 101: 98-105. doi: 10.1038/sj.bjc.6605123.

111. Yang GL, Zhang LH, Bo JJ, Chen HG, Cao M, Liu DM, Huang YR. UHRF1 is associated with tumor recurrence in non-muscle-invasive bladder cancer. Med Oncol. 2012; 29: 842-7. doi: 10.1007/s12032-011-9983-z.

112. Ying L, Lin J, Qiu F, Cao M, Chen H, Liu Z, Huang Y. Epigenetic repression of regulator of G-protein signaling 2 by ubiquitin-like with PHD and ring-finger domain 1 promotes bladder cancer progression. FEBS J. 2015; 282: 174-82. doi: 10.1111/febs.13116.

113. Saidi S, Popov Z, Janevska V, Panov S. Overexpression of UHRF1 gene correlates with the major clinicopathological parameters in urinary bladder cancer. Int Braz J Urol. 2017; 43: 224-9. doi: 10.1590/S1677-5538.IBJU.2016.0126.

114. Ma J, Peng J, Mo R, Ma S, Wang J, Zang L, Li W, Fan J. Ubiquitin E3 ligase UHRF1 regulates p53 ubiquitination and p53-dependent cell apoptosis in clear cell Renal Cell Carcinoma. Biochem Biophys Res Commun. 2015; 464: 147-53. doi: 10.1016/j.bbrc.2015.06.104.

115. Wotschofsky Z, Gummlich L, Liep J, Stephan C, Kilic E, Jung K, Billaud JN, Meyer HA. Integrated microRNA and mRNA Signature Associated with the Transition from the Locally Confined to the Metastasized Clear Cell Renal Cell Carcinoma Exemplified by miR-146-5p. PLoS One. 2016; 11: e0148746. doi: 10.1371/journal.pone.0148746.

116. Oba-Shinjo SM, Bengtson MH, Winnischofer SM, Colin C, Vedoy CG, de Mendonca Z, Marie SK, Sogayar MC. Identification of novel differentially expressed genes in human astrocytomas by cDNA representational difference analysis. Brain Res Mol Brain Res. 2005; 140: 25-33. doi: 10.1016/j.molbrainres.2005.06.015.

117. Zhang ZY, Cai JJ, Hong J, Li KK, Ping Z, Wang Y, Ng HK, Yao Y, Mao Y. Clinicopathological analysis of UHRF1 expression in medulloblastoma tissues and its regulation on tumor cell proliferation. Med Oncol. 2016; 33: 99. doi: 10.1007/s12032-016-0799-8.

118. Qin Y, Wang J, Gong W, Zhang M, Tang Z, Zhang J, Quan Z. UHRF1 depletion suppresses growth of gallbladder cancer cells through induction of apoptosis and cell cycle arrest. Oncol Rep. 2014; 31: 2635-43. doi: 10.3892/or.2014.3145.

119. Abbady AQ, Bronner C, Trotzier MA, Hopfner R, Bathami K, Muller CD, Jeanblanc M, Mousli M. ICBP90 expression is downregulated in apoptosis-induced Jurkat cells. Ann N Y Acad Sci. 2003; 1010: 300-3.

120. Pi JT, Lin Y, Quan Q, Chen LL, Jiang LZ, Chi W, Chen HY. Overexpression of UHRF1 is significantly associated with poor prognosis in laryngeal squamous cell carcinoma.

Med Oncol. 2013; 30: 613. doi: 10.1007/s12032-013-0613-9.

121. Yang C, Wang Y, Zhang F, Sun G, Li C, Jing S, Liu Q, Cheng Y. Inhibiting UHRF1 expression enhances radiosensitivity in human esophageal squamous cell carcinoma. Mol Biol Rep. 2013; 40: 5225-35. doi: 10.1007/s11033-013-2559-6.

122. Nakamura K, Baba Y, Kosumi K, Harada K, Shigaki H, Miyake K, Kiyozumi Y, Ohuchi M, Kurashige J, Ishimoto T, Iwatsuki M, Sakamoto Y, Yoshida N, et al. UHRF1 regulates global DNA hypomethylation and is associated with poor prognosis in esophageal squamous cell carcinoma. Oncotarget. 2016; 7: 57821-31. doi: 10.18632/oncotarget.11067.

123. Crnogorac-Jurcevic T, Gangeswaran R, Bhakta V, Capurso G, Lattimore S, Akada M, Sunamura M, Prime W, Campbell F, Brentnall TA, Costello E, Neoptolemos J, Lemoine NR. Proteomic analysis of chronic pancreatitis and pancreatic adenocarcinoma. Gastroenterology. 2005; 129: 1454-63. doi: 10.1053/j.gastro.2005.08.012.

124. Abu-Alainin W, Gana T, Liloglou T, Olayanju A, Barrera LN, Ferguson R, Campbell F, Andrews T, Goldring C, Kitteringham N, Park BK, Nedjadi T, Schmid MC, et al. UHRF1 regulation of the Keap1-Nrf2 pathway in pancreatic cancer contributes to oncogenesis. J Pathol. 2016; 238: 423-33. doi: 10.1002/path.4665.

125. Cui L, Chen J, Zhang Q, Wang X, Qu J, Zhang J, Dang S. Up-regulation of UHRF1 by oncogenic Ras promoted the growth, migration, and metastasis of pancreatic cancer cells. Mol Cell Biochem. 2015; 400: 223-32. doi: 10.1007/s11010-014-2279-9.

126. Pita JM, Banito A, Cavaco BM, Leite V. Gene expression profiling associated with the progression to poorly differentiated thyroid carcinomas. Br J Cancer. 2009; 101: 1782-91. doi: 10.1038/sj.bjc.6605340.

127. Wang BC, Lin GH, Wang B, Yan M, He B, Zhang W, Yang AK, Long ZJ, Liu Q. UHRF1 suppression promotes cell differentiation and reduces inflammatory reaction in anaplastic thyroid cancer. Oncotarget. 2016. doi: 10.18632/oncotarget.10674.

128. Myrianthopoulos V, Cartron PF, Liutkeviciute Z, Klimasauskas S, Matulis D, Bronner C, Martinet N, Mikros E. Tandem virtual screening targeting the SRA domain of UHRF1 identifies a novel chemical tool modulating DNA methylation. Eur J Med Chem. 2016; 114: 390-6. doi: 10.1016/j.ejmech.2016.02.043.

1.2.5 UHRF1 - A Drugable Target for Anticancer Therapy

UHRF1 overexpression along with its involvement in silencing of TSGs and inducing resistance to anticancer therapy in cancer cells make UHRF1 an attractive target for therapy (Bronner *et al.*, 2007, Unoki *et al.*, 2009a, Alhosin *et al.*, 2011, Alhosin *et al.*, 2016). Many studies have reported that downregulation of UHRF1 or its knockdown leads to increase expression of TSGs and induces cell cycle arrest and apoptosis in cancer cells. It has also been seen that knockdown of UHRF1, in therapy resistant tumors, increases the response of anticancer therapy and improves the prognosis of disease (Ashraf *et al.*, 2017b, Sidhu and Capalash, 2017).

Different bioactive compounds have been reported to target UHRF1 expression. Polyphenolic compounds such as epigallocatechin-3-gallate, anthocyanins and luteolin were reported to downregulate UHRF1 in cancer cells and activate the expression of TSGs like $p16^{INK4A}$ and *p73* to induce apoptosis and growth arrest in these cells (Achour *et al.*, 2013, Krifa *et al.*, 2013, Krifa *et al.*, 2014, Alhosin *et al.*, 2015). Other natural compounds such as thymoquinone, naphthazarin (5,8-dihydroxy-l,4-naphthoquinone) and Shikonin (a naphthoquinone isolated from Chinese traditional medicine Zi Cao) have also been reported to target UHRF1 expression and to induce apoptosis in cancer cells by activation of $p16^{INK4A}$, p53-p21 and p73 dependent pathways (Alhosin *et al.*, 2010, Jang *et al.*, 2015b, Kim *et al.*, 2015b). Similarly, curcumin and hinokitiol possess an anticancer effect by targeting UHRF1 and DNMT1 interaction in cancer cells, which releases TSGs from repression because of promoter hypomethylation (Parashar and Capalash, 2016, Seo *et al.*, 2017).

In search of specific inhibitor for UHRF1, a study screened around 2200 molecules on HeLa cells stably expressing UHRF1-eGFP and reported 17-allylamino-17-demethoxygeldanamycin (17-AAG) as the most promising molecule inhibiting the activity of UHRF1 in these cells (Ding *et al.*, 2016). 17-AAG is a known inhibitor of HSP90 (90-kDa heat-shock protein) and has shown to exert its anticancer affect by deregulating the stability of UHRF1. Treatment of cells with 17-AAG increases the ubiquitination and proteasomal degradation of UHRF1 as a consequence of HSP90 inhibition predicting the role of HSP90 in stability of UHRF1 (Ding *et al.*, 2016). Recently, one direct inhibitor of UHRF1 has also been reported in the scientific literature, which targets UHRF1 SRA domain for DNA methylation modulation. NSC232003 is a uracil derivative, which fits into the 5-methylcytosine recognition pocket of UHRF1 and

inhibits its interaction with hemi-methylated DNA (Myrianthopoulos *et al.*, 2016). Treatment of cells with NSC232003, also interferes in UHRF1 interaction with DNMT1 and results in global DNA hypomethylation. This molecule can therefore serve as lead to develop specific molecules targeting UHRF1 for anticancer therapy (Myrianthopoulos *et al.*, 2016).

1.2.6 UHRF1 Partners

UHRF1 works inside the nucleus in a multiprotein complex to perform its function. It is loaded on to the chromatin in association with PCNA and DNMT1 to play a role in DNA methylation. Different other epigenetic modifiers like histone acetyltransferase, histone deacetylase, deubiquitinase, ubiquitinase, histone methyltransferase and demethylase are also reported to be the component of this complex.

Table 1: Interacting Partners of UHRF1

DNMT1	Maintenance of DNA methylation.
DNM3a, DNMT3b	Involved in *de novo* methylation
PCNA	Auxiliary protein for DNA polymerase δ and serves as scaffold for recruitment of other proteins involved in DNA replication, epigenetic modulation and DNA repair.
TIP60 (Histone acetyltransferase)	Acetylates lysine residue on histone and non-histone proteins. Involved in epigenetic modulation, DNA damage repair and transcriptional regulation.
HDAC1	Deacetylates histone and non-histone proteins. Regulates chromatin structure and stability of other proteins.
USP7	Deubiquitinates protein and increases stability of UHRF1.
SCFβ-TrCP	E3 ubiquitin ligase involved in ubiquitination of UHRF1 and compromising its stability after DNA damage.
Euchromatic histone lysine methyltransferase 2 (EHMT2) also known as G9a	Methylates lysine residues on histone H3. Involved in chromatin regulation, recruitment of epigenetic modulators and transcriptional repression.
Suppressor of variegation 3-9 homolog 1 (SUV39H1) (Histone methyltransferase)	Mainly methylates lysine 9 of histone H3 along with other substrates. Involved in transcriptional repression and heterochromatin formation.

Enhancer of Zeste 2 Polycomb Repressive Complex 2 Subunit (EZH2) (Histone methyltransferase)	Mainly involved in methylation of lysine 27 residue of histone H3. Involved in transcriptional repression and heterochromatin formation.
BRCA1	Involved in DNA damage repair
PARP1	Involved in DNA damage response, transcriptional regulation and UHRF1 relationship with DNMT1.
Protein arginine methyltransferase 5 (PRMT5)	Methylates arginine on histone and non-histone proteins. Involved in transcriptional repression of tumor suppressor genes.
DNA ligase 1 (LIG1)	Involved in DNA replication, DNA damage repair and recruits UHRF1 for maintenance of DNA methylation during replication phase.
Methyl-CpG binding domain 4, DNA glycosylase (MBD4)	Involved in DNA repair response, apoptosis, transcriptional regulation and play a role in regulation of DNMT1 in association with UHRF1 and USP7.

Among these proteins, TIP60 is an important partner of UHRF1 in this epigenetic complex, which is associated with multiple cellular processes through its lysine-acetyltransferase activity. Lysine acetylation is one of the major post-translational modifications on proteins having profound effects on the epigenome and metabolome of cells. It is reversible and tightly regulated in cells by the activity of acetyltransferases and deacetylases. Lysine acetylation, its role in epigenome and TIP60 mediated acetylation effects will be detailed in the next section.

1.3 Histones / Lysine Acetylation

Acetylation of lysine in the proteins is one of the most extensively studied modification, which can regulate dynamics and functions of proteins. Lysine acetylation at N-terminal tail of histones can affect the DNA coiling and chromatin structure and thus can affect the function of many genes (Struhl, 1998, Kouzarides, 2007). Besides histones, lysines are acetylated on many other non-histone proteins, which are implicated in a wide array of biological processes. Dysregulation of acetylation or acetyltransferase activity in cells have been related to many human diseases (Choudhary *et al.*, 2009).

Acetylation is a dynamic process involving the exchange of a hydrogen atom on the ε-NH_3^+ group of lysine by the acetyl group provided by co-substrate acetyl Coenzyme A (AcCoA) (Figure 17).

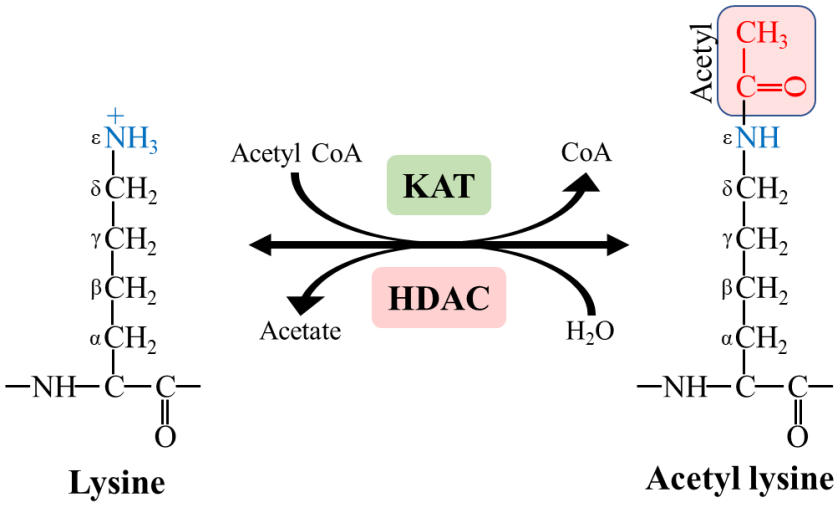

Figure 17: Acetylation and deacetylation of ε-amino group of lysine residue. Lysine acetyltransferase (KAT) transfer the acetyl group (indicated in red) to amino group (indicated in blue) while enzymes like histone deacetylase (HDAC) remove the acetyl group from acetylated lysine.

In histones, acetylation reduces the overall affinity of the histones proteins towards the negatively charged DNA resulting in loosened chromatin structure with more accessibility to the transcriptional machinery for gene expression (Figure 18). Besides transcription factors, different regulator proteins can also easily access the relaxed chromatin sites with or without the help of specialized reader domain, which makes the acetylation of histone an important

'switch' to control transcription and other important activities such as DNA replication and DNA damage repair processes (Verdin and Ott, 2015).

Histone acetylation is dynamically controlled by two classes of enzymes; the 'writer' histone acetyl transferases (HATs) and the 'eraser' histone deacetylases (HDACs) while bromodomain containing proteins are 'reader' of this epigenetic mark.

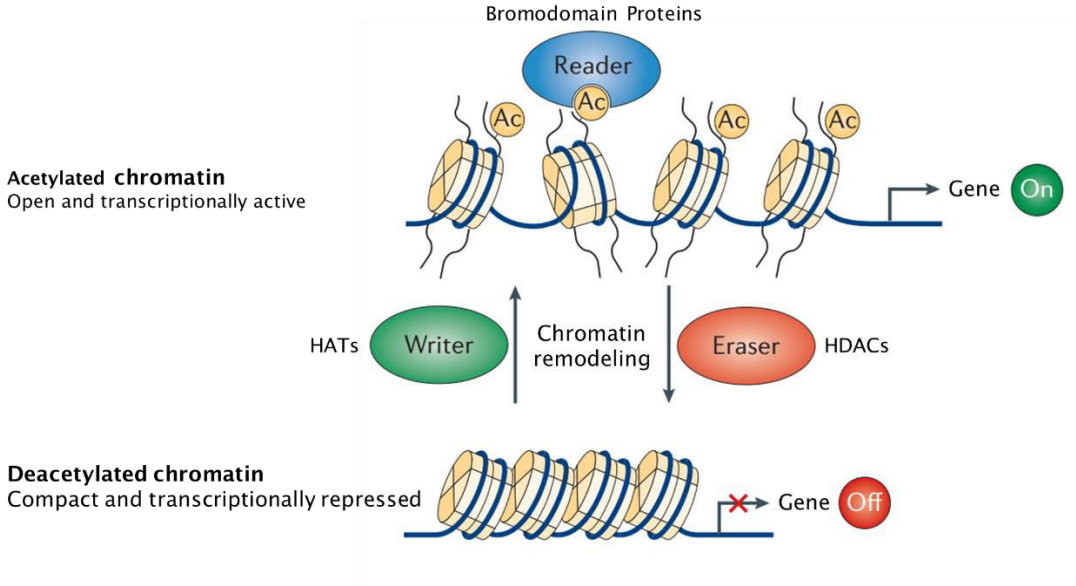

Figure 18: Histone acetylation in relation to chromatin structure and gene expression. Acetylation of histone leads to relaxed chromatin structure and active gene transcription while deacetylation leads to compact chromatin with repression of gene transcription. Adapted from (Verdin and Ott, 2015)

1.3.1 Histone Acetyltransferase

Histone acetyltransferases (HATs) catalyze the transfer of acetyl group from acetyl-coenzyme A (acetyl-CoA) (co-factor) to lysine residues of histones and other proteins. Many HATs have been discovered so far which are classified according to their preferred location, structural and functional similarities (Simon *et al.*, 2016). Type A HATs include the acetyltransferase, which are localized in nucleus and include five major subfamilies. MYST family (named after initial letter of members MOZ, YBF2/SAS3, SAS2 and TIP60) is one of the most important and largest family of acetyl transferases (Wapenaar and Dekker, 2016). The members of this family have remarkable sequence similarity with each other and contain a conserved catalytic domain in their structures. The GNAT (Gcn5-related N-acetyltransferases) is another important HAT family with Gcn5, PCAF (p300/CBP associated factor), Elp, Hpa2/3, and Nut1 as its members. p300 and CBP (CREB-PCAF binding protein) constitute the p300/CBP family of HATs which

acetylate the proteins by distinct Theorell−Chance mechanism. Other HATs include enzymes from transcriptional co-activators and steroid receptor co-activators family which have key roles in variety of cellular activities (Wapenaar and Dekker, 2016).

Type B HATs (KAT1, HAT4) are predominantly located in cytoplasm where they acetylate newly synthesized histone proteins and help them to translocate to nucleus where they can be deacetylated again and added to the newly form chromatin structures (Simon *et al.*, 2016).

1.3.2 Histone Deacetylases

Histone deacetylases (HDACs) catalyze the amide hydrolysis of acetylated lysines leading to non-acetylated proteins. They are categorized into four major classes i.e. class I Rpd3-like proteins, class II Hda1-like proteins, class III Sir2-like proteins and the class IV proteins including HDAC11 (Yoon and Eom, 2016). Class I, II, IV HDACs require a zinc molecule as cofactor for their catalytic activity while class III HDACs utilize NAD+ as cofactor for their activity. Because of their dysregulation and involvement in various cellular processes, so far four HDAC inhibitors have been approved for anti-cancer therapy while many are being explored in different clinical trials for their use against neurodegenerative, inflammatory or cardiovascular disease in clinical settings (Holbert and Marmorstein, 2005, Yoon and Eom, 2016).

1.3.3 Bromodomain proteins

Bromodomain is conserved protein-protein interaction module described as ‘reader’ of the acetylated proteins. This domain is found in 42 different types of proteins including HATs, component of chromatin remodeling complexes and transcriptional regulators. This shows the role of bromodomain in wide array of cellular activities (Fujisawa and Filippakopoulos, 2017). Bromodomains consists of several α-helices linked by loops forming a hydrophobic cavity that specifically recognizes acetylated lysines on proteins. Dysfunction and dysregulation of BRD proteins has also been reported in many diseases, including cancer (Fujisawa and Filippakopoulos, 2017).

1.4 Tat Interactive Protein 60 kDa (TIP60)

TIP60 was initially identified as an interacting partner of HIV-1 Tat protein in yeast two-hybrid system and thus got its name as **T**at **I**nteracting **P**rotein 60kDa (TIP60) (Kamine *et al.*, 1996).

It is also symbolized as lysine acetyltransferase 5 (KAT5) and now is a well characterized member of MYST family of acetyl transferases. TIP60 acetylates histone and non-histone proteins and plays a key role in chromatin remodeling, DNA damage response, transcriptional regulation and apoptosis. Despite the remarkable sequence and functional similarity with other members of MYST family, several cellular functions are specific to TIP60 and cannot be compensated by other members of the MYST family (Sapountzi *et al.*, 2006, Judes *et al.*, 2015). Indeed, it is an essential gene, as homozygous deletion of TIP60 in mice results in development failure and early embryonic lethality at blastocyst stage of embryogenesis (Hu *et al.*, 2009).

1.4.1 Structure of TIP60

TIP60 is encoded by *HTATIP* gene, which consists of 14 exons and located at 11q13.1 position in human genome (Sapountzi *et al.*, 2006). So far, four splice variants of TIP60 have been known encoding different isoforms (Figure 19). Isoform 1 is the longest isoform of TIP60 having an additional 33 amino acids at its N terminal because of inclusion of intron 1 in translation (Legube and Trouche, 2003). Isoform 2 (TIP60α) is the most studied and well characterized isoform of TIP60 having 513 amino acids. It is the main isoform of TIP60, which is actively involved in different cellular activities (Sapountzi *et al.*, 2006). Isoform 3 (TIP60β) is the truncated version of isoform 2 lacking the proline rich region encoded by exon 5 (Ran and Pereira-Smith, 2000, Sheridan *et al.*, 2001). Isoform 4 is encoded by transcript variant having intron 1 but is lacking exon 5 in its sequence.

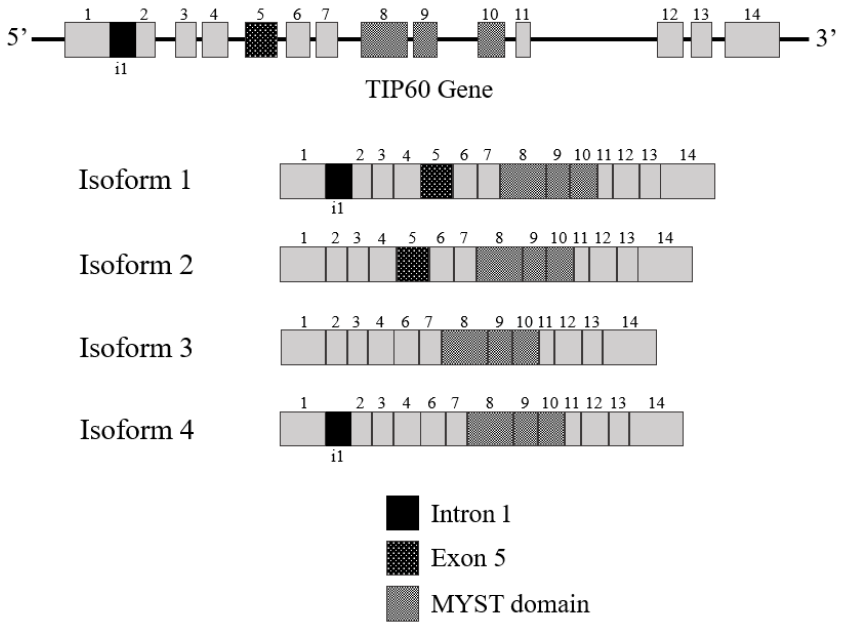

Figure 19: Schematic structure of *TIP60* gene and the resulting isoforms produced after differential splicing.

TIP60 is a multidomain protein which has a conserved chromodomain at its N-terminus and a conserved MYST domain near the C-terminus (Figure 20).

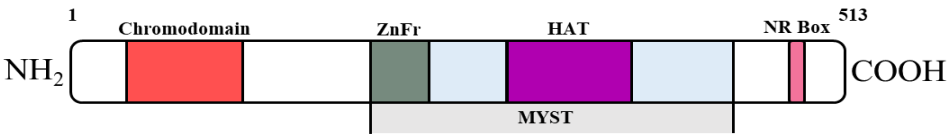

Figure 20: Schematic structure of TIP60 protein

Chromodomain is specific hydrophobic module present in variety of proteins helping them to interact with methylated lysines on histones or RNA molecules (Figure 21) (Akhtar *et al.*, 2000, Nielsen *et al.*, 2002, Pray-Grant *et al.*, 2005). TIP60 chromodomain can read both active and repressive methylated lysines marks (H3K4me / H3K9me3) on histones, which is necessary for TIP60 mediated DNA damage response or chromatin remodeling at the promoter region of different genes.

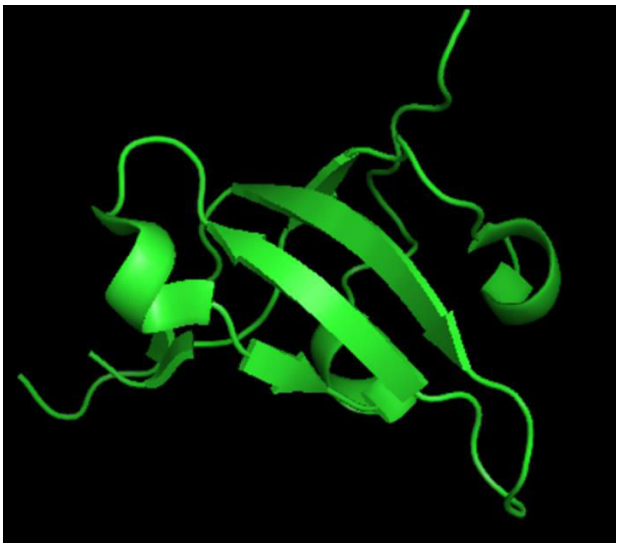

Figure 21: Crystal structure of an N-terminal HTATIP fragment containing the chromodomain of TIP60. Adapted from structure deposited at RCSB protein data bank. PDB ID: 4QQG

Indeed, TIP60 acts as 'translator' by reading out the histone marks through chromodomain and conveying the message to downstream effectors through its enzymatic MYST domain (Sun *et al.*, 2009, Jang *et al.*, 2015a, Kim *et al.*, 2015a). The MYST domain is the functional enzymatic domain of TIP60 and it is conserved in all the MYST family members (Voss and Thomas, 2009). Within the MYST family, TIP60 is closely related to MOF (males absent on the first) protein as evident by the 47% sequence similarity between the two proteins. Both the proteins have a similar chromodomain at N-terminus besides having conserved MYST domain near the C-terminus of proteins (Su *et al.*, 2016). Inside the MYST domain resides catalytic HAT domain responsible for its acetyl transferase activity (Figure 22). Besides HAT domain, MYST regions also harbor a CCHC type zinc finger motif which is necessary for interaction with other proteins (Kim *et al.*, 2007, Putnik *et al.*, 2007, Kim *et al.*, 2008).

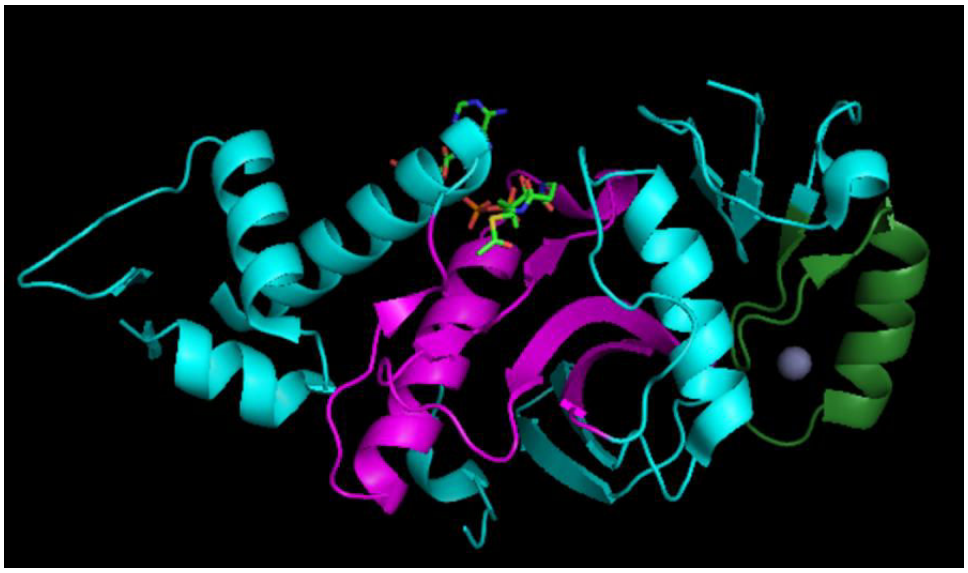

Figure 22: Crystal structure of TIP60 MYST domain. Green color region indicates the zinc finger of MYST domain in association with zinc atom (indicated in grey color). Magenta color indicates the conserved histone acetyltransferase (HAT) domain in association with Acetyl CoA (indicated in red color). Adapted from structure deposited at RCSB protein data bank. PDB ID: 2OU2

At C-terminus, TIP60 also has a nuclear receptor (NR) interacting box in its structure, enabling it to interact with nuclear receptor on the nuclear membrane (Gaughan *et al.*, 2001).

1.4.2 TIP60 as a Lysine Acetyltransferase

The exact catalytic mechanism by which MYST family proteins acetylate their substrate is still not completely known even though many studies have tried to uncover the details of this mechanism by using ESA1, a yeast homologue of TIP60 as a model. Initially it was believed that MYST acetyltransferases acetylate lysine residue on substrates through a distinct 'ping pong' mechanism in which acetyl group is first transferred from acetyl CoA to an amino acid (Cys-369 in *H. sapiens* TIP60) in the catalytic site of the enzyme and later this acetyl group is transferred to the lysine residue on the targeted protein (Yan *et al.*, 2000, Yan *et al.*, 2002). However, a study countered this mechanism and showed that enzyme can acetylate substrate via a direct attack mechanism; forming a ternary complex between enzyme, acetyl CoA and substrate (Berndsen *et al.*, 2007, Wapenaar and Dekker, 2016). Conserved Glu-338 of Esa1 (403 in TIP60) attracts a proton from ε-amine of lysine to facilitate the nucleophilic attack on the acetyl carbonyl-carbon of acetyl-CoA (Berndsen *et al.*, 2007).

1.4.2.1 Acetyltransferase Activity on Histones

After its discovery, acetyltransferase activity of TIP60 was first determined by Yamamoto and Horikoshi in 1997, who described TIP60 as a substrate specific acetyltransferase for H2A, H3 and H4 core histone proteins (Yamamoto and Horikoshi, 1997). Next year, Kimura and Horikoshi reported Lys-5 of histone H2A, Lys-14 of histone H3, and Lys-5, 8, 12, 16 of histone H4 as preferred sites of acetylation by TIP60 (Kimura and Horikoshi, 1998). Although TIP60 preferentially acetylates lysine residues preceded by glycine or alanine amino acids, so far no consensus motif for recognition of substrate lysine has been identified for TIP60 (Kimura and Horikoshi, 1998). It was also observed that TIP60 readily acetylated the histones amino terminal tail *in vitro,* however this activity was drastically reduced when the whole nucleosome was used as a substrate. This predicts that TIP60 alone is insufficient to acetylate histones packed in nucleosomes and needs help from other proteins to do this job (Yamamoto and Horikoshi, 1997). Indeed, it was found that TIP60 works in collaboration with at least 16 other protein subunits to form a multiprotein chromatin remodeler complex which is named as TIP60 acetyltransferase complex or human TIP60-NuA4 complex (Figure 23) (Doyon and Cote, 2004). TIP60 is playing a central role in this complex through its acetyltransferase activity while other protein subunits offer ATPase, DNA helicase and DNA binding activities and help TIP60 in its enzymatic activity on chromatin (Sapountzi *et al.*, 2006). The molecular composition of human TIP60-NuA4 complex suggests that it is functionally evolved through fusion of two distinct yeast complexes; one having histone acetyltransferase activity (NuA4) and other having ATP dependent chromatin remodeling (SWR1) capability (Auger *et al.*, 2008). Therefore, TIP60-NuA4 complex is also involved in ATP dependent H2AZ/H2B dimer exchange besides acetylation of histones and play an important role in regulation of transcription, DNA damage response, apoptosis and chromatin remodeling which correlate to TIP60 regulated pathways (Ikura *et al.*, 2000, Doyon and Cote, 2004, Auger *et al.*, 2008).

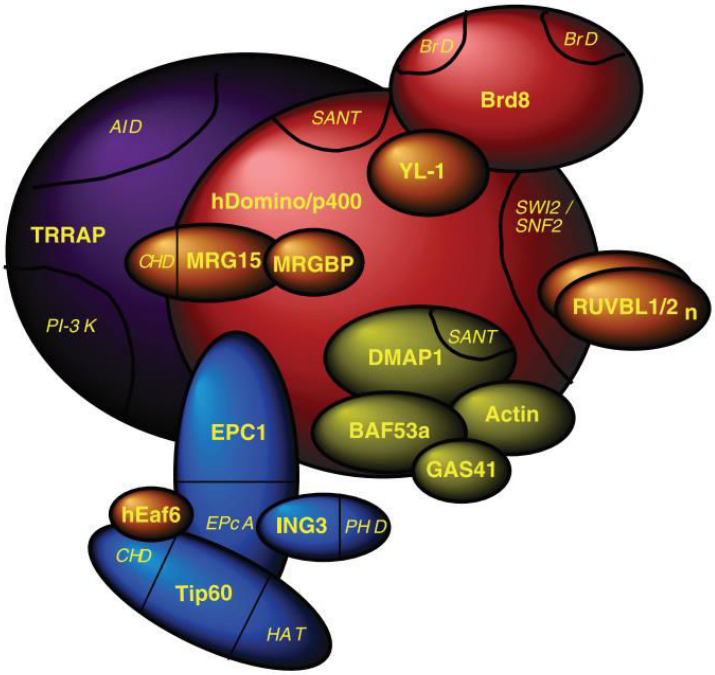

Figure 23: Schematic diagram of TIP60-NuA4 complex. Different proteins of this complex are indicated with their respective domains, which suggest the involvement of this complex in multiple cellular functions. Adapted from (Doyon and Cote, 2004 and Auger et al., 2008)

TIP60-NuA4 complex activity on chromatin is also influenced by other nuclear proteins. Transcriptional factors like c-MYC and E2F1 proteins recruit TIP60 and four other component of TIP60-NuA4 complex (TRRAP, p400, Tip48, and Tip49) to their target genes and through TIP60-mediated acetylation facilitate G1/S phase transitions and proliferation (Frank *et al.*, 2003, Taubert *et al.*, 2004).

1.4.2.2 Acetyltransferase Activity on Non-Histone Proteins

Besides histone, TIP60 can acetylate various non-histone proteins including different post-translational modifiers, transcription factors and epigenetic modulators. However, unlike histones most of the non-histone proteins can be acetylated directly by TIP60 independent of NuA4 or multiprotein complex (Yamada, 2012). Ataxia telangiectasia mutated (ATM), p53, c-MYC, p21, DNMT1 and androgen receptor are some of important non-histone substrates of TIP60 (Gaughan *et al.*, 2002, Patel *et al.*, 2004, Sun *et al.*, 2005, Sykes *et al.*, 2006, Tang *et al.*, 2006, Sun *et al.*, 2007, Du *et al.*, 2010, Lee *et al.*, 2013a). TIP60 regulates the functions of these proteins in cell through acetylation, which affects the activity and stability of these proteins. TIP60 acetylates and activates ataxia telangiectasia mutated (ATM) protein kinase

after DNA damage which can initiate a DNA damage response through phosphorylation of proteins involved in DNA repair and cell cycle regulations (Sun *et al.*, 2005). TIP60 is also involved in transcriptional regulation by interaction and activation of nuclear hormone receptors, p53, c-MYC and nuclear factor-κB (NF-κB) regulated pathways through its enzymatic activity. Abnormalities in function of these proteins can lead to serious pathologies including cancer (Judes *et al.*, 2015).

1.4.3 TIP60 role in DNA Damage Response

Cellular machinery is continuously at work to maintain the integrity of human genome which suffers thousands of DNA injuries per day in a cell. Different kinds of DNA lesions arise from various exogenous agents such as exposure to ultra violet (UV) light, ionizing radiation and genotoxic chemicals or endogenous factors including replication mistakes, free radical species and erroneous enzymatic conversions (Helleday *et al.*, 2014). Cellular response to these lesions varies with the kind of damage induce by the genotoxic elements. If damage is repairable, cells initiate an appropriate DNA repair mechanism to fix the DNA but if damage is irreparable then either senescence or apoptosis is induced to arrest or remove the damaged cell (d'Adda di Fagagna, 2008, Helleday *et al.*, 2014).

TIP60 is involved in double strand breaks repair mechanisms and is implicated to direct and facilitate the repair by HR pathway. It plays important role at different steps of the repair pathway by being involved in remodeling of chromatin, acetylation of histones and acetylation of ataxia telangiectasia mutated (ATM) which is an important modulator of DNA repair pathway. By initiating the DNA damage response and protecting the cell from genetic instability, TIP60 prevents the transforming events which might lead to cancer (Xu and Price, 2011).

1.4.3.1 TIP60-mediated Histone Acetylation and Recruitment of DNA Repair Proteins

In 2000, Ikura *et al* first reported the involvement of TIP60 in DNA damage response and revealed that expression of mutated TIP60, lacking its acetyltransferase activity resulted in defective double strand break repair in the irradiated HeLa cells (Ikura *et al.*, 2000). Later, it was reported that TIP60 along with p400/domino, another important member of TIP60-NuA4 complex is involved in chromatin remodeling by selectively exchanging the histone variant at the damage site, which facilitates the repair mechanism (Kusch *et al.*, 2004). This predicts that TIP60 is involved in various steps of DNA repair process and is an essential protein for DNA

damage response. Through its acetylation activity TIP60 changes the surface charge distribution and spatial arrangement of molecules on chromatin and governs the chromatin remodeling as well as the recruitment of repair protein complexes on damage sites. Indeed, TIP60 mediated acetylation of histone 4 lysine 16 (H4K16Ac) and histone 2A lysine 15 (H2AK15Ac) acts as molecular switch to decide whether the DNA repair from the double strand break will proceed through HR or NHEJ pathway (Figure 24) (Tang *et al.*, 2013, Jacquet *et al.*, 2016). This decision is dependent on the occupancy of BRCA1 or 53BP1 protein at the DNA damage site. BRCA1 facilitates the repair through HR pathway while 53BP1 promotes repair mechanisms through NHEJ pathway (Daley and Sung, 2014). 53BP1 interacts with H4K20me2 at DNA damage site, which is necessary for 53BP1 loading to chromatin and repair mechanism initiated by it. However, acetylation of adjacent lysine residue at H4K16 by TIP60 inhibits the interaction of 53BP1 with H4K20me2 through steric hindrance (Tang *et al.*, 2013). Besides H4K20me, 53BP1 is also dependent on H2AK15Ub for its recruitment to DSBs. TIP60 also acetylates H2AK15 which in turn blocks its ubiquitination by RNF168 and prevents 53BP1 loading. It is interesting to note that H2AK15Ac increases in response to DSBs in S/G2 phase, which is in coherence with the HR pathway dominance in these phases of cell cycle (Jacquet *et al.*, 2016).

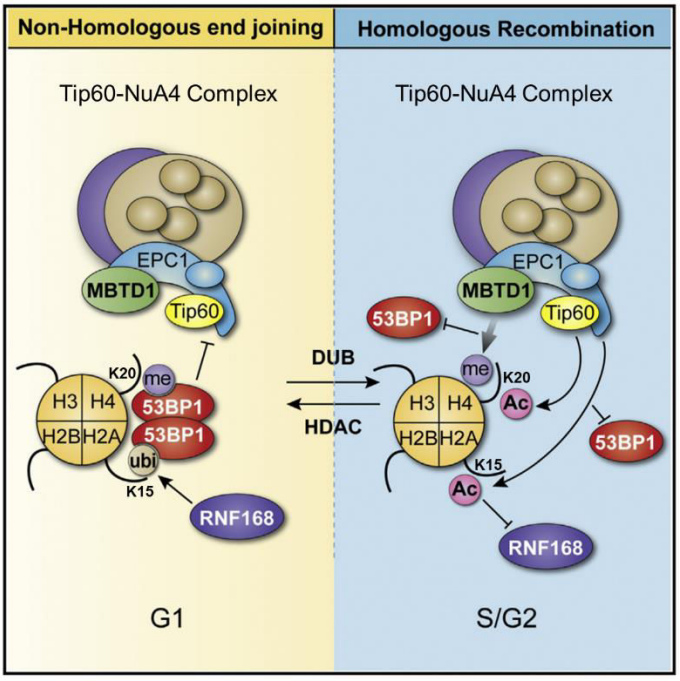

Figure 24: Model for TIP60-NuA4 complex mediated response to DSBs. In G1 phase 53BP1 accumulates at the chromatin through its interaction with H4K20me and H2AK15Ub to promote the repair through NHEJ pathway. In S/G2 phase TIP60-

mediated acetylation of H4K16 and H2Ak15 prevents the recruitment of 53BP1 to facilitate the repair through HR pathway. Adapted from (Jacquet *et al.*, 2016)

TIP60 also acetylates histone variant H2AX at lysine 5 and mediates its release after ubiquitination by UBC13 in early stages of DNA repair (Ikura *et al.*, 2007). ZNF688 interaction with TIP60 directs this acetylation and promotes chromatin relaxation after H2AX eviction, which is necessary for DNA repair process (Hu *et al.*, 2013). TIP60 mediated acetylation of H2AXK5Ac is also essential for dynamic accumulation of NBS1 to the damaged area. NBS1, as a part of MRN complex along with MRE11 and RAD50 protein, functions as sensor of DBS and initiates downstream signaling for DNA damage response (Ikura *et al.*, 2015).

1.4.3.2 TIP60 in ATM Activation

Ataxia telangiectasia mutated (ATM) protein kinase is a key component of signal transduction pathway activated by DNA damage. In response to DSBs, ATM kinase is converted from inactive ATM dimer to an active monomeric ATM and then phosphorylates multiple proteins involved in the DNA damage response, including NBS1, p53, CHK2, and SMC1 (Lavin *et al.*, 2005). These phosphorylated proteins in turn, activate cell-cycle checkpoints and initiate DNA repair. Loss of functional or active ATM leads to defect in DNA repair and increased sensitivity to genotoxic stress (Lavin *et al.*, 2005).

TIP60 is reported to be crucial for the activation of ATM in response to DSBs related DNA damage response (Sun *et al.*, 2005). Indeed, TIP60 interacts with C-terminal FATC domain of ATM by the help of FOXO3a protein and acetylates Lys-3016 to activate ATM (Sun *et al.*, 2007, Adamowicz *et al.*, 2016). TIP60 mediated K3016 acetylation is specific to DNA damage response as mutation of K3016 or loss of TIP60 acetyltransferase activity abolish ATM mediated phosphorylation of p53 and CHK2 and downstream signaling related to DNA damage response (Sun *et al.*, 2007). Cancer cells can target this FOXO3a-TIP60 complex mediated ATM activation by NOTCH1 protein. This allows them to escape the DNA damage induced cell death and continue proliferation (Adamowicz *et al.*, 2016).

1.4.3.3 TIP60 Role in DNA Damage Response to Interstrand Cross Links (ICL)

TIP60 also plays a role in DNA damage response to interstrand cross link (ICL) in Fanconi anemia pathway (Renaud *et al.*, 2016). ICLs bridge the complementary strands with irreversible covalent linkages and prevent the opening of double helix during DNA replication. Replication forks cannot pass through this obstacle, resulting in one or two DSBs around the

stalled replication fork. Repair of these DSBs is usually proceeded with HR pathway in normal cells to maintain the genomic integrity as repair by NHEJ can lead to deleterious genomic abrasions. TIP60 interacts with FANCD2, the major effector protein of this repair mechanism, which relocates TIP60 to the chromatin to rescue the ICL damaged cells (Hejna *et al.*, 2008, Hejna *et al.*, 2010). FANCD2 helps in loading of TIP60 to the chromatin where it acetylates the H4K16 to initiates the repair by HR pathway (Renaud *et al.*, 2016). In Fanconi anemia pathway deficient cells, absence of FANCD2 leads to impaired loading of TIP60 which in turn perturbs the acetylation of H4K16. This favors the accumulation of 53BP1 at H4K20me2 site and repair by NHEJ pathway predisposing these cells to oncogenic mutations (Renaud *et al.*, 2016). TIP60 also binds to the promoter area of FANCD2 and BRCA1 to upregulate their expression and response in ICL repair (Su *et al.*, 2017).

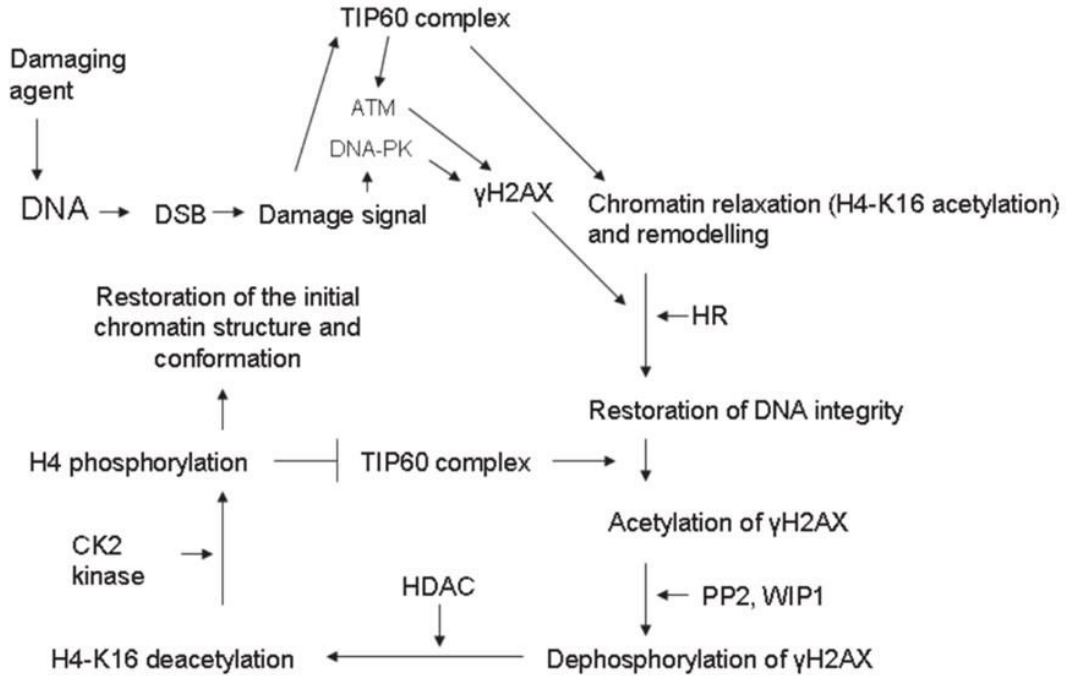

Figure 25: Sequential involvement of TIP60 at various steps of DNA damage response Adapted from (Szumiel and Foray, 2011)

1.4.3.4 TIP60 Activation on DNA Damage

As TIP60 is critically involved in DNA damage response, it is important to know how it is activated and recruited to the DNA damage site. Sun *et al* reported that TIP60 interacts with H3K9me3 signature on histones through its chromodomain and this interaction is responsible for the activation of acetyltransferase activity of TIP60 in response to DSBs (Sun *et al.*, 2009).

Normally H3K9me3 is abundant in heterochromatin and occupied by HP1β through its chromodomain. Upon DNA damage HP1β is phosphorylated at its chromodomain by casein kinase 2 (CK2), which releases HP1β from H3K9me3. Exposed H3K9me3 sites are then available to interact and activate TIP60 (Sun *et al.*, 2009).

However, this does not explain how TIP60 is activated in euchromatin as H3K9me3 signature is less abundant in relaxed chromatin. H3K9me3 sites are also regulated during the response to DSBs and open state of chromatin is initially repressed for a moment to inhibit transcription and facilitate the loading of repair complexes (Ayrapetov *et al.*, 2014). A complex containing H3K9 methyltransferase SUV39H1, HP1 and KAP1 is enriched to the site of damage as an initial response which methylates nascent H3K9 residue. This methylation further increases the loading of SUV39H1/HP1/KAP1 complex to chromatin through interaction of HP1 with H3K9me3 resulting in spread of H3K9me3 to tens of kilobases around DSB (Ayrapetov *et al.*, 2014). This transient repressed state achieved by H3K9me3 is then reversed by TIP60, which acetylates ATM and H4 as described earlier. Later, ATM on activation phosphorylates KAP1 of SUV39H1/HP1/KAP1 complex, leading to release of this complex from chromatin as a negative feedback mechanism (Ayrapetov *et al.*, 2014). It was also discovered that chromatin remodeling also enhances phosphorylation of TIP60 at tyrosine 44 by c-abl kinase, which increase TIP60 activity in response to DNA damage (Kaidi and Jackson, 2013).

Recently it has also been reported that small DSB-induced RNAs (diRNA) are also produced as a result of DNA damage, which are complementary to the sequences surrounding these break sites (Wang and Goldstein, 2016). These diRNAs tend to recruit TIP60 to the damage site through their association with AGO2 and facilitate H4 acetylation and chromatin remodeling. This diRNA-mediated TIP60 activation serves an additional layer of sequence specific RNA component to the DNA damage response (Wang and Goldstein, 2016).

1.4.4 TIP60 as Transcriptional Regulator

TIP60 also act as transcriptional regulator by regulating the activity of various proteins either directly or through its association with other transcription modulators. It can promote the activity of gene by facilitating its expression through chromatin relaxation or interaction with different transcription factors serving as coactivator. Similarly, it can also inhibit a gene function by regulating the transcription factors for that gene or facilitating the transcription repressors activity at the promoter of that gene.

1.4.4.1 TIP60 mediated transcriptional regulation inhibiting cancers

One of the most important non-histone target of TIP60 is p53 protein which is a major transcriptional factor and is implicated in many diseases including cancer. In 2004, a study reported involvement of TIP60 in p53 pathway and found that knockdown of TIP60 resulted in downregulation of p53 dependent, p21 activation and growth arrest (Legube *et al.*, 2004). TIP60 was described as transcription coactivator, helping p53 to induce the activation of p21. TIP60 also regulated basal level of p53 in cells by interfering with its degradation through MDM2 mediated ubiquitination (Legube *et al.*, 2004). Later it was found that TIP60 can acetylate Lys-120 in the DNA binding domain of p53 as a result of direct interaction between the two proteins after DNA damage. Interestingly, this K120 acetylation is indispensable for p53 mediated proapoptotic response while p53 mediated growth arrest can proceed without this posttranslational modification (Tang *et al.*, 2006). Acetylated-K120 form of p53 accumulates at the promoters of BAX and PUMA to initiate transcription and proapoptotic response while nonacetylated p53 appeared at the promoters of p21 to promote growth arrest. This information predicts TIP60-mediated acetylation of p53 as regulatory switch to decide whether the outcome of p53 activation will be a proapoptotic response or cell cycle arrest (Sykes *et al.*, 2006). TIP60 mediated activation of p53 is influenced by inhibitor of growth (ING) family of proteins. ING3 as the part of TIP60-NuA4 complex aids in activation of p53-transactivated promoter such BAX and p21and helps to regulate p53 mediated cell cycle control and apoptosis (Nagashima *et al.*, 2003). While ING5 serves as cofactor for TIP60 to acetylate p53 at K120 and consequently promotes apoptosis through BAX activation (Liu *et al.*, 2013a).

Along with p53, TIP60 can also acetylate Lys-161 and -163 in p21 structure which is necessary for the G1-phase cell cycle arrest induced by p21 in response to DNA damage (Figure 26). This acetylation increases the stability of p21 as it prevents ubiquitination and thus proteasomal degradation of p21 (Lee *et al.*, 2013a). TIP60 coactivator function on p21 promoter in p53 dependent pathway is regulated by p400, another subunit of TIP60-NuA4 complex in normal cells. p400 physically blocks TIP60 acetyltransferase activity through direct interaction and positions H2A.Z on promoter of p21 to repress its expression. However, in response to DNA damage or genotoxic stress, p400 and H2A.Z are evicted from the p21 promoter and TIP60 is recruited which increases the expression of p21 to induce cell cycle arrest (Gevry *et al.*, 2007, Park *et al.*, 2010).

TIP60 also interacts with $p14^{ARF}$ and increases the tumor suppressor role of both proteins (Figure 26). $p14^{ARF}$ can induce a p53-independent, G2-phase cell cycle arrest in response to genotoxic stress by TIP60-mediated activation of ATM/ATR/CHK signaling pathways (Eymin *et al.*, 2006). Further, increased association of $p14^{ARF}$ with TIP60 in response to DNA damage inhibits TIP60 dependent degradation of retinoblastoma protein and triggers it antiproliferative response to DNA damage (Leduc *et al.*, 2006).

Besides inducing the activity of tumor suppressor genes, TIP60 can regulate oncogenic transcription factors like c-MYB or STAT3 (Figure 26) (Xiao *et al.*, 2003, Zhao *et al.*, 2012). c-MYB is a proto-oncogene transcription factor involved in proliferation and differentiation of hematopoietic progenitor cells. TIP60 interacts with c-MYB through its HAT domain and in acetylation independent manner inhibits the transcriptional activity of c-MYB by recruiting HDAC1 and HDAC2 to the targeted promoters (Zhao *et al.*, 2012). For instance, in leukemias TIP60 is found downregulated, which promotes c-MYB driven leukemogenesis by inducing the expression of target genes such as *c-myc* (Zhao *et al.*, 2012). Similarly, STAT3 is also a transcription factor involved in cell cycle progression, apoptosis and cell motility in response to cytokines and growth factors. Study has shown that TIP60 through its direct association with STAT3, represses STAT3-mediated transcriptional activation of targeted genes and also recruits HDAC7 to the targeted promoters for further repression of transcription (Figure 26) (Xiao *et al.*, 2003).

1.4.4.2 TIP60 mediated transcriptional regulation favoring oncogenesis

TIP60 can also acetylate and coactivate different oncogenes to facilitate their tumor supportive effect in certain conditions (Figure 26). One such transcription factor regulated by TIP60 is c-MYC oncoprotein. TIP60 can acetylate c-MYC protein, which can increase the stability and chromatin loading of c-MYC at the targeted promoters (Patel *et al.*, 2004). c-MYC through its direct association with TIP60 also brings TIP60 and subunits of its complex (TRRAP, p400, TIP48 and TIP49) to chromatin where TIP60-mediated H4 acetylation opens the chromatin for active transcription (Frank *et al.*, 2003). Indeed, human T-cell lymphotropic virus type 1 (HTLV-1) enhances transforming potential of c-MYC by stabilizing its association with TIP60 through its p30II oncoprotein (Figure 26). This association transcriptionally activates genes for G1/S-phase transition and multinucleation contributing to adult T-cell leukemogenesis (Awasthi *et al.*, 2005).

TIP60 is also demonstrated as direct regulator of E2F1, another transcription factor involved in multiple cellular pathways (Figure 26). TIP60 stabilizes E2F1 by acetylation on Lys-120 and 125 in cells exposed to cisplatin induced genotoxic stress and TIP60/E2F1 complex initiates accumulation of excision repair cross-complementing group 1 (ERCC1) known to repair platinum-DNA adducts (Van Den Broeck *et al.*, 2012). E2F1 can also recruit TIP60 and other subunits of TIP60 complex (TRRAP, p400, Tip48, and Tip49) to E2F1 targeted promoters for chromatin acetylation necessary for downstream signaling (Taubert *et al.*, 2004).

TIP60 also acts as coactivator for nuclear factor-kappa B (NFκB) family which is involved in expression of several genes required in development, apoptosis, inflammatory responses and oncogenesis. It binds directly to RelA/p65 subunit of NFκB family and is recruited to promoters of targeted genes (*IL-6*, *IL-8*, *C-IAP1* and *XIAP*) by this association. Relaxation of chromatin by acetylation of histones H3 and H4 leads to enhance expression of these genes involved in oncogenesis (Kim *et al.*, 2012). NF-kB p50 can recruit TIP60/pontin complex to the promoters of tumor suppressor gene *KAI1* to induce its transcription. However, enhanced levels of nuclear β-catenin in cancer along with downregulation of TIP60 leads to accumulation of repressive β-catenin/reptin complex on *KAI1* promoters lowering its transcription and function to promote tumor progression (Figure 26) (Kim *et al.*, 2005).

TIP60 also physically and functionally interacts with steroid hormone nuclear receptors and coregulates the activity of these receptors (Brady *et al.*, 1999). TIP60 has a LXXLL motif near its C terminus through which it interacts with ligand binding domain of androgen receptor (AR) and enhances AR-mediated transactivation (Brady *et al.*, 1999, Gaughan *et al.*, 2001). TIP60 dependent acetylation also increases the transcriptional activity of AR, which is reversed by deacetylation carried out by HDAC1 (Gaughan *et al.*, 2002). AR signaling is crucial in prostate cancers and increased activity of AR is often related to progression of prostate cancer. High levels of TIP60 have been reported in castration resistant prostate cancer cells where TIP60 promotes cancer progression by hormone independent AR activation while silencing of TIP60 leads to cell cycle arrest at G1 phase (Figure 26) (Shiota *et al.*, 2010).

Like AR, TIP60 also acts as a ligand dependent coactivator for progesterone receptor (PR) and estrogen receptors (ER) (Brady *et al.*, 1999). A study has reported TIP60 as an essential moderator for estrogen-induced transcription of a subset of estrogen receptor alpha (ERα) target genes in human cells. Active histone methylation marks on target genes help to recruit

TIP60 on chromatin, which after acetylation of histones promote the expression of target genes (Jeong *et al.*, 2011). Similarly, TIP60 can interact with estrogen receptor beta (ERβ) and can modulate transcriptional activity of ERβ1 at the AP-1 site and estrogen-response element (ERE) site in an estradiol-independent manner (Lee *et al.*, 2013b).

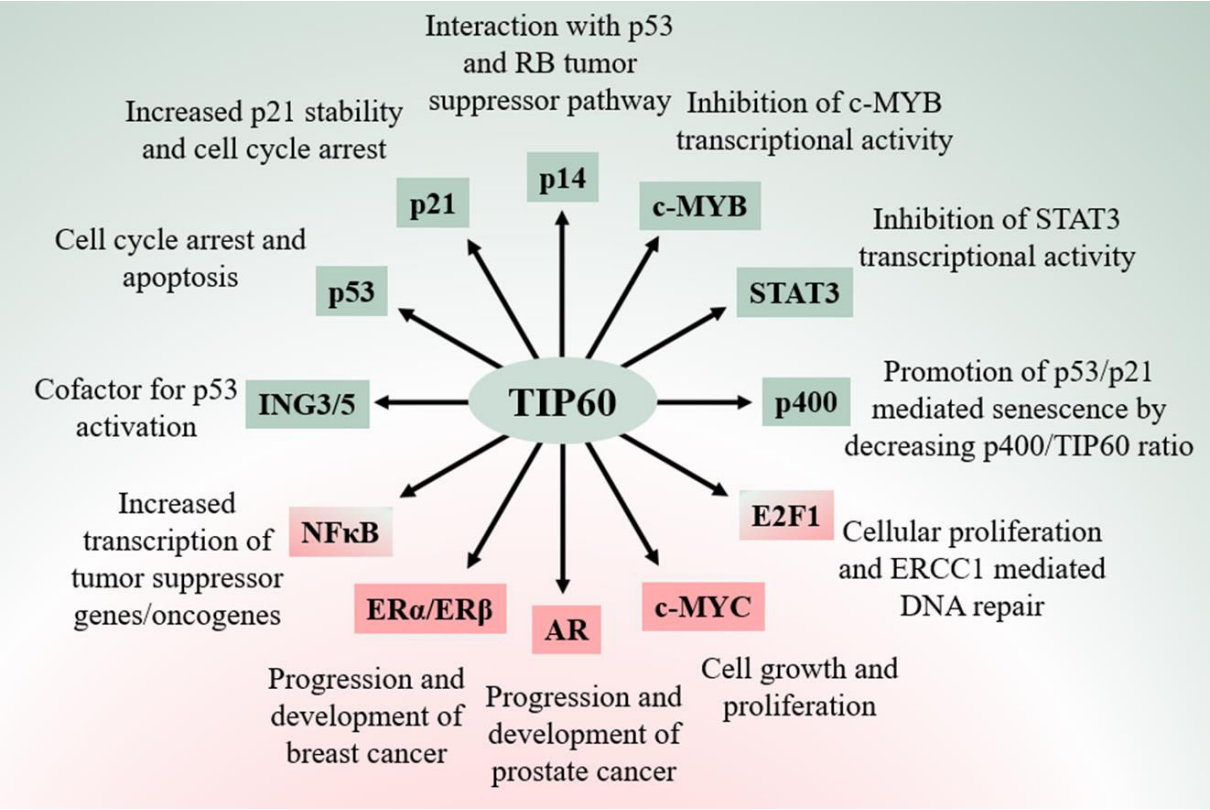

Figure 26: Summary of TIP60 interaction with other proteins in reference to its role in cancer. Green boxes represent antitumor activities while red boxes indicate pre-oncogenic roles of TIP60. Adapted from (Avvakumov and Cote, 2007, Judes *et al.*, 2015)

1.4.5 TIP60 as Cell Cycle Regulator

TIP60 is involved in different/multiple cell cycle checkpoints and thus plays a vital role in regulation of cell cycle related events. At G1/S phase transition TIP60-mediated activation of histones genes is necessary to synthesize the new histone proteins needed during the replication of genome. Mechanistically, cyclin E activates nuclear protein, coactivator of histone transcription (NPAT) at the end of G1 phase which recruits TIP60 to the histone genes for H4 acetylation and subsequently induces the histone gene expression (DeRan *et al.*, 2008). Similarly, TIP60 maintains enough pool of dNTPs at the site of DNA damage and replication during S phase through its association with the ribonucleotide reductase (Niida *et al.*, 2010). TIP60 is also necessary for the error free repair of DNA damages occurring during the

replication phase of cell cycle (Jacquet *et al.*, 2016). In the M phase of cell cycle, TIP60 also ensures accurate segregation of chromatin by inducing the expression of mitotic check point proteins mad1 and mad2 and maintaining the activity of acetylated Aurora B protein (Li *et al.*, 2004, Mo *et al.*, 2016).

1.4.6 TIP60 Regulation in Cells

TIP60 being a pleiotropic protein is very tightly regulated in cells and its expression, stability and activity in cells are controlled by variety of mechanisms. TIP60 expression is positively regulated by circadian transcription factor clock, which binds to the E boxes present in the promoter region of TIP60 gene and induces its expression (Miyamoto *et al.*, 2008). While other E boxes binding transcription factors such as c-MYC, Twist, and USF1 have no effect on expression of TIP60 (Miyamoto *et al.*, 2008).

TIP60 protein has a short half-life varying from 30 to 120 mins, depending upon the cell type and its condition (Legube *et al.*, 2002, Sapountzi *et al.*, 2006). Normally, low levels of TIP60 are maintained in the cell through its regulation via the proteasomal degradation pathways. Mouse double minute 2 (Mdm2), p300/CBP-associated E4-type ubiquitin-ligase, E3 identified by differential display (EDD1/UBR5) and Cullin-3 (Cul3) ubiquitin ligase are well known to ubiquitinate TIP60 and induce its degradation (Legube *et al.*, 2002, Col *et al.*, 2005, Bhoumik *et al.*, 2008, Subbaiah *et al.*, 2016). In the absence of stimulating signal for TIP60 activity, Mdm2 acts as a negative regulator of TIP60 and targets it for proteasomal degradation after mono or polyubiquitination. But upon DNA damage by UV irradiation, TIP60 is stabilized in cells and Mdm2 mediated degradation of TIP60 is inhibited (Legube *et al.*, 2002). It is also known that many cellular proteins influence this degradation of TIP60. For instance, activating transcription factor-2 (ATF2) promotes degradation of TIP60 in coordination with Cul3 ubiquitin ligase (Miyamoto *et al.*, 2008). However, DNA damage inhibits this ATF2-Cul3-mediated degradation pathway of TIP60 and stimulates ATM activation (Bhoumik *et al.*, 2008).

TIP60 proteasomal degradation is also influenced by different viral proteins. HIV Tat protein facilitates degradation of TIP60 inside the affected cell through proteasomal pathway by p300/CBP-associated E4-type ubiquitin-ligase (Col *et al.*, 2005). This ubiquitination of TIP60 is independent of p300/CBP acetyltransferase activity and neutralizes the TIP60-mediated apoptosis in response to DNA damage. This shows a role of HIV-1 Tat protein in making cell

resistant to genotoxic stress by targeting TIP60 (Col *et al.*, 2005). Similarly, human papilloma virus (HPV) utilizes its E6 oncoprotein to attenuate TIP60 and p53 dependent apoptotic pathways by destabilizing TIP60 in cervical cells. Indeed, HPV E6 protein employs EDD1 E3 ligase for ubiquitination and subsequent proteasomal degradation of TIP60 to promote cell proliferation and survival in cervical cancers (Jha *et al.*, 2010, Subbaiah *et al.*, 2016).

TIP60 is stabilized and its levels are increased when it is functionally needed in cell. Early adipogenesis requires elevated levels of TIP60, which are achieved by the deubiquitinase activity of USP7 (Gao *et al.*, 2013). In cellular response to genotoxic stress USP7 also stabilizes TIP60 for p53 dependent apoptosis (Dar *et al.*, 2013). Activating transcription factor 3 (ATF3), a common stress mediator has been recently discovered to facilitate this deubiquitination of TIP60. ATF3 directly binds to TIP60 and increases the acetyltransferase activity of TIP60 facilitating the activation of ATM dependent signaling response to DNA damage (Cui *et al.*, 2015).

1.4.7 Post Translational Modifications Regulating TIP60 Activities

Like ubiquitination, many other post-translational modifications affect the functions of TIP60 by regulating its enzymatic activity and localization.

1.4.7.1 Phosphorylation of TIP60

Initially it was identified that TIP60 is phosphorylated at Ser-86 and 90 when it is overexpressed in an insect cell line and acetyltransferase activity of TIP60 is modulated by this phosphorylation (Lemercier *et al.*, 2003). Authors discovered that Ser-90 lies within the consensus sequence for cyclin B/cdc2 whose activity dominates in the G2/M phase of cell cycle (Lemercier *et al.*, 2003). Recently it is elaborated that TIP60 upon activation by cyclin B/cdc2 dependent phosphorylation acetylates Aurora B protein, which ensures robust and error free segregation of chromosomes during the metaphase-anaphase transition (Mo *et al.*, 2016).

Ser-86 phosphorylation of TIP60 is important for its role in p53 dependent apoptotic pathways in response to DNA damage. Glycogen synthase kinase 3 (GSK3) is identified to be responsible for this phosphorylation (Charvet *et al.*, 2011). Indeed, it is reported that inhibition of GSK3 or addition of phosphorylation resistant TIP60 mutant S86A resulted in failure of TIP60 to acetylate p53 at K120 which is necessary for activation of PUMA and induction of apoptosis (Charvet *et al.*, 2011). Furthermore, it is reported that GSK3-mediated phosphorylation of

TIP60 Ser-86 is also necessary for the induction of growth factor deprivation related autophagy (Lin *et al.*, 2012a). In absence of extracellular growth factors and nutrients, cells activate a self-eating catabolic process of autophagy to recycle unnecessary proteins and organelles for survival. GSK3 is activated in cells under serum deprivation and increases Ser-86 phosphorylation of TIP60, that in turn activates unc-51 like autophagy activating kinase 1 (ULK1) by acetylation, leading to formation of autophagosomes (Lin *et al.*, 2012a, Lin *et al.*, 2012b).

TIP60 is also phosphorylated on various tyrosine residues, which regulates its activities. TIP60 phosphorylation at Tyr-158 by p38α kinase is mandatory for TIP60 dependent acetylation of p53 and induction of apoptosis (Xu *et al.*, 2014). While phosphorylation at Tyr-44 by abl kinase in response to genotoxic stress is essential for ATM acetylation and activation of DNA damage check points and survival (Kaidi and Jackson, 2013). Interestingly, abl kinase can also phosphorylates TIP60 at Tyr-327 upon environmental or endoplasmic reticulum (ER) stress and thus compromises TIP60 acetyltransferase activity through binding with the scaffolding protein FE65 which is implicated in Alzheimer's disease. This binding with FE65 also affects the subcellular localization of TIP60 and leads to G0/G1 arrest and apoptosis (Shin and Kang, 2013). p38 can also phosphorylate TIP60 at Thr-158 to activate p38-regulated/activated protein kinase (PRAK) mediated senescence in response to oncogenes showing tumor suppressor role of TIP60 (Zheng *et al.*, 2013).

1.4.7.2 Acetylation of TIP60

TIP60 acetylation at multiple sites is also known to govern its function. TIP60 is capable to auto-acetylate itself at different lysine residues including Lys-76, 80, 104, 150, 187, 327 and 383 in response to DNA damage (Wang and Chen, 2010, Yang *et al.*, 2012). Autoacetylation of TIP60 leads to the dissociation of TIP60 oligomers and increases its interaction with substrates while deacetylation of TIP60 by enzyme such as SIRT1 reduces the enzymatic activity of TIP60 acetyltransferase (Wang and Chen, 2010). Among the acetylated lysine residues, Lys-327 has gained a considerable attention as it lies within the MYST domain of TIP60. A study has shown that mutation at Lys-327 (K327R or K327Q) drastically reduces the enzymatic activity of TIP60 making it unable to auto-acetylated itself or acetylate H4 histones (Yang *et al.*, 2012). During the development of regulatory T cells, this autoacetylation of K327

serves as an important molecular switch allowing TIP60 to interact and activate FOXP3, which is the master regulator of Treg development (Xiao *et al.*, 2014).

TIP60 is also reported to be acetylated by p300/CBP acetyltransferase on Lys-268 and 282 in zinc finger domain under the influence of HIV-1 Tat protein, however the effects of this acetylation are not fully elucidated (Col *et al.*, 2005).

1.4.7.3 Sumoylation of TIP60

Like many other modifications, sumoylation of TIP60 is playing a key role in TIP60-p53 mediated signaling (Cheng *et al.*, 2008, Naidu *et al.*, 2012). Indeed, it was reported that UV irradiation induces site-specific sumoylation of TIP60 at Lys-430 and 451 via SUMO-conjugating enzyme UBC9. This sumoylation orchestrate the relocation of TIP60 to the promyelocytic leukemia (PML) bodies, which is essential for DNA damage repair response via the p53-dependent pathway (Cheng *et al.*, 2008). Another enzyme E3 SUMO-protein ligase PIAS4 (PIASy) was also shown to sumoylate TIP60 at Lys-430 and 451 and augmented the p53 K120 acetylation and apoptosis (Naidu *et al.*, 2012).

1.4.8 TIP60 Deregulation in Cancer

TIP60 is found downregulated in multiple cancers and low levels of TIP60 are often positively correlated with the cancer proliferation and metastasis suggesting a tumor suppressive role of TIP60. A prominent evidence of TIP60 down regulation in cancer emerged from a study analyzing the levels of p53 related genes in tumors. It was found that *TIP60* mRNA levels were significantly decreased in colon and lung carcinomas (ME *et al.*, 2006). Later Gorrini *et al* narrated TIP60 as haplo-insufficient tumor suppressor protein counteracting c-MYC induced lymphomagenesis in mice. In this study authors also analyzed *TIP60* mRNA levels in human samples and found decreased expression of *TIP60* in ductal breast carcinoma, head and neck squamous cell carcinoma (HNSCC) and low-grade B-cell lymphomas. TIP60 protein levels were also found decreased in breast, colon, gastric and lung carcinomas. Indeed, analysis of a large cohort included in this study confirmed these findings as loss of TIP60 nuclear staining was observed in 72% (129/179) of breast carcinoma samples which positively correlated to the pathological grade of the cancer (Gorrini *et al.*, 2007). TIP60 is playing important role in modulating the DNA repair after genotoxic stress and thus TIP60 downregulation has been extensively studied in relation to breast cancers (Bassi *et al.*, 2016). Loss of TIP60 results in genomic instability, that promotes tumorigenesis. Besides DNA repair, TIP60 also exerts its

tumor suppressive role by inhibiting cell migration and invasion (Bassi *et al.*, 2016). Recently miR-22 has been discovered as key regulator of TIP60, as it targets the 3'UTR region of *TIP60* mRNA for degradation. Elevated levels of miR-22 have been reported in breast cancer specimen which by downregulation of TIP60 exacerbates epithelial-mesenchymal transition (EMT) and metastasis (Pandey *et al.*, 2015). TIP60 mRNA and proteins have also been found downregulated in metastatic prostate cancer cells as compared to normal or non-metastatic cancer cells (Kim *et al.*, 2005). Similarly, *TIP60* mRNA was found significantly downregulated in primary colorectal cancer specimen which also correlated with larger tumor size, poor differentiation, distant metastasis and higher TNM staging (Sakuraba *et al.*, 2009). Later it was revealed by Mattera *et al* that ratio of p400/TIP60 expression is critical for colorectal cancer cell proliferation. p400 functionally hampers TIP60-mediated apoptosis and DNA damage response in genotoxic stress. Therefore, higher p400/TIP60 ratio in TIP60 downregulation facilitates tumor progression and proliferation (Mattera *et al.*, 2009). Sakuraba *et al* also reported downregulation of TIP60 in 61% (28/46) specimens of primary gastric cancer correlating with age, depth of invasion and lymph node metastasis. These findings predict that downregulation of TIP60 promotes the gastric oncogenesis (Sakuraba *et al.*, 2011). Reduced expression of TIP60 has also been observed in melanoma and is described as independent prognostic marker for melanomas. Analysis of 448 cases of melanoma revealed significantly reduced levels of TIP60 in cancer, correlating with poor five-year disease specific survival in primary ($P = 0.016$) and metastatic ($P = 0.027$) melanoma patients (Chen *et al.*, 2012). It was also observed that enforced expression of TIP60 in melanoma cells increases the response to chemotherapy (Chen *et al.*, 2012). Similar results have been reported in lung, breast and pancreatic cells where enhanced expression of TIP60 improved the chemotherapeutic response in lung, breast and pancreatic carcinomas by reducing malignant cell proliferation and invasion potential (Ravichandran and Ginsburg, 2015, Yang *et al.*, 2017b).

1.5 UHRF1-TIP60 interaction and its putative roles in cells

In 2009, our lab first reported the presence of TIP60 and UHRF1 in the same macromolecular epigenetic complex along with DNMT1 (Achour *et al.*, 2009). TIP60 was found to be colocalized with UHRF1/DNMT1 complex in Jurkat cells and targeting of UHRF1 by siRNA enhanced the levels of TIP60 in these cells. However, despite the increased levels of TIP60 on UHRF1 downregulation, acetylation of H2AK5 was drastically decreased suggesting a cooperative role of these proteins in execution of their normal functions (Achour *et al.*, 2009).

After that the interaction between UHRF1 and TIP60 was reported in few other studies (Du *et al.*, 2010, Dai *et al.*, 2013) describing the role of both the proteins in regulation of stability and functions of other important proteins in the nucleus.

1.5.1 DNMT1 Stability

DNA methylation patterns are maintained on the daughter strand after DNA replication by a well-coordinated action of an epigenetic complex comprising of different nuclear protein including DNMT1, UHRF1, PCNA, USP7, TIP60 and HDAC1 (Figure 27) (Du *et al.*, 2010). DNMT1 is a key player in reproducing those methylation marks on the newly formed daughter strand by the help of UHRF1, which reads the pattern on parent strand and recruits the DNMT1 to the target cytosine on daughter strand for methylation. After completion of methylation function, DNMT1 levels are downregulated and maintained at low level during the cell cycle by the coordinated function of TIP60 and UHRF1 (Du *et al.*, 2010). Mechanistically, TIP60 acetylates DNMT1 in the late S phase and triggers the degradation mechanism of DNMT1. TIP60-mediated acetylation stimulates the UHRF1 to use its E3 ligase activity to ubiquitinate the acetylated DNMT1, which is later degraded by the proteasomal pathway. DNMT1 is stabilized in the cells during DNA replication by its association with USP7 and HDAC1 which deubiquitinates and deacetylates DNMT1 respectively to prevent the UHRF1-TIP60 mediated degradation of DNMT1. However, as the cell progress to the late S phase or G2 phase, levels of TIP60 are increased and the association between DNMT1 and USP7 is reduced which promotes the degradation of DNMT1 by increased acetylation and unopposed ubiquitination (Du *et al.*, 2010). Later, it was revealed that USP7 binds to the lysine residues in the KG linker region of DNMT1 to prevent its ubiquitination and this binding is drastically reduced when these lysine residues are acetylated by TIP60 (Cheng *et al.*, 2015). Previous studies have also reported that DNMT1 stability is also reduced in response to DNA damage or oncogenic insult (Shamma *et al.*, 2013, Huang *et al.*, 2014). DNA damage response can activate ATM which can directly bind to DNMT1 along with TIP60 and UHRF1, and promotes the acetylation dependent ubiquitination of DNMT1 (Shamma *et al.*, 2013). Similarly, RGS6 prevents the cells from RAS induced oncogenic stress by increasing the TIP60 mediated degradation of DNMT1 to inhibit proliferation. (Huang *et al.*, 2014).

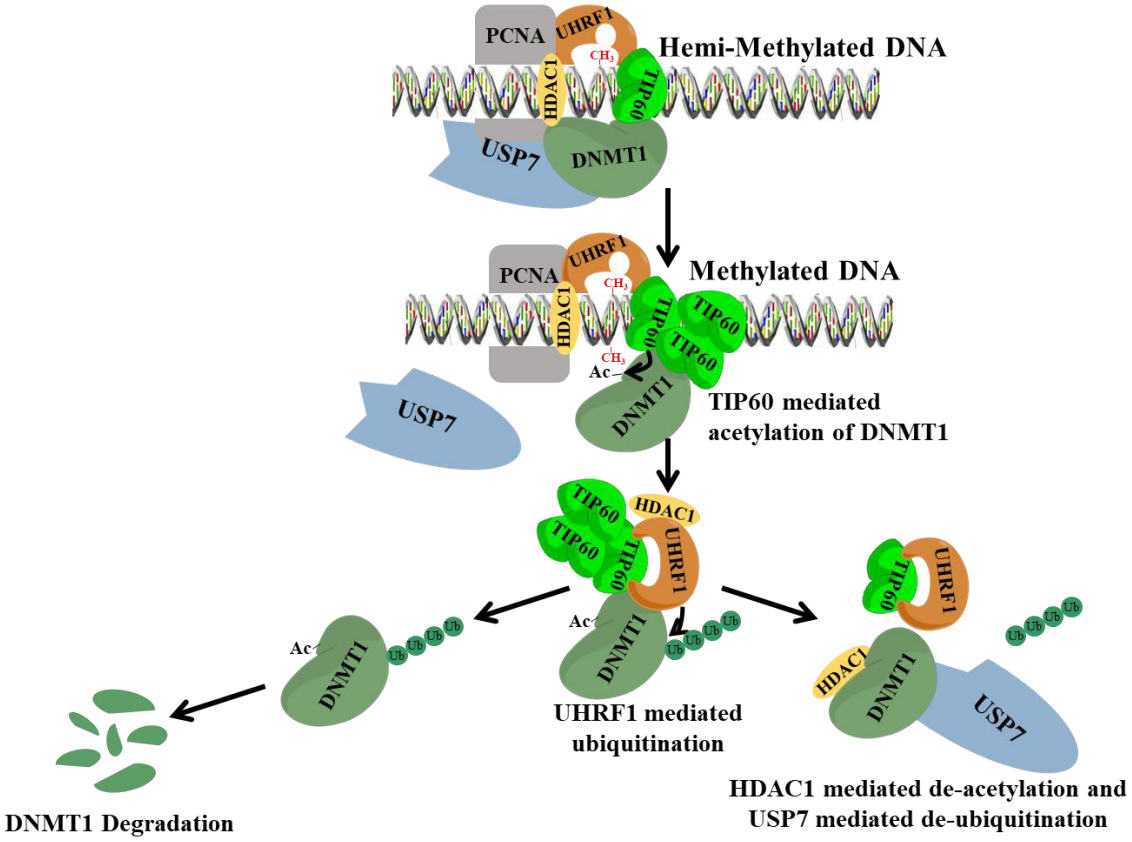

Figure 27: A model for DNMT1 regulation by posttranslational modifications. After the DNA methylation, TIP60 levels are increased which acetylates the DNMT1 and decreases the association between DNMT1 and USP7. Loss of USP7 promotes ubiquitination of DNMT1 by UHRF1, which promotes its proteasomal degradation. HDAC1, by deacetylation can prevent this degradation of DNMT1 and increase the half-life of DNMT1 in cells. Adapted from (Du et al., 2010)

Here it is interesting to note that though both UHRF1-TIP60 are involved in destabilizing DNMT1 in cells, but implication of this downregulation is different in cancers. TIP60 is mostly downregulated in cancer and is believed to have a tumor suppressive role in cancers. Recently it is reported that overexpression of TIP60 in cancers cells decreases the metastatic potential of these cells by destabilizing the highly expressed DNMT1 (Figure 28) (Zhang *et al.*, 2016b). Epithelial to mesenchymal transition (EMT) is an important step in cancer metastasis and is described as transition of polarized, immotile, adhered epithelial cells to motile and invasive mesenchymal-like cells, which are capable of dissemination to multiple organs. Transcription factors like SNAIL2 promote EMT by inducing the expression of genes responsible for mesothelial like phenotypes (*FN1, SNAI2*) and repressing the genes responsible for epithelial phenotype (*EpCAM*) in cancer cells. SNAIL2 recruits DNMT1 to the promoters of epithelial genes and suppress their expression by promoter hypermethylation to facilitate metastasis.

Enhanced expression of TIP60 in cancer cells targets the DNMT1 for degradation and inhibits DNMT1-SNAIL mediated EMT by increasing the expression of epithelial phenotype supporting genes like EpCAM (Zhang *et al.*, 2016b).

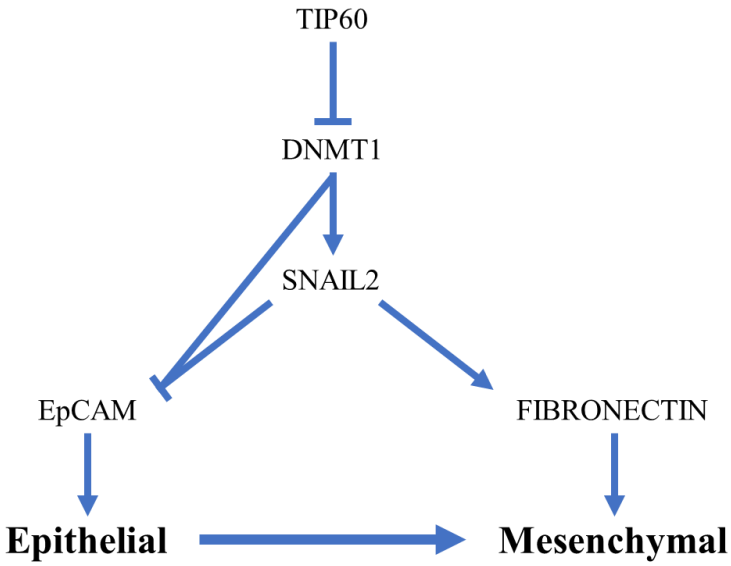

Figure 28: A model for TIP60-mediated inhibition of EMT.

TIP60 destabilizes DNMT1 and inhibits SNAIL2-driven EMT. Decreased level of TIP60 increases SNAIL2 and fibronectin level along with hypermethylation of EpCAM promoter, which facilitates EMT. Adapted From (Zhang et al., 2016)

UHRF1 on the other hand is overexpressed in cancers and can promote oncogenesis by destabilizing DNMT1. A study reported that overexpression of UHRF1 in zebrafish model led to global hypomethylation after degradation of DNMT1 (Figure 29) (Mudbhary *et al.*, 2014). p53 mediated senescence initiated in response to this global methylation, however this senescence was ablated by an unknown mechanism and increase UHRF1 levels promoted proliferation and oncogenesis. It is speculated that global DNA hypomethylation released the promoter of different oncogenes from repressive state and transformed the normal cells to cancerous cells (Mudbhary *et al.*, 2014).

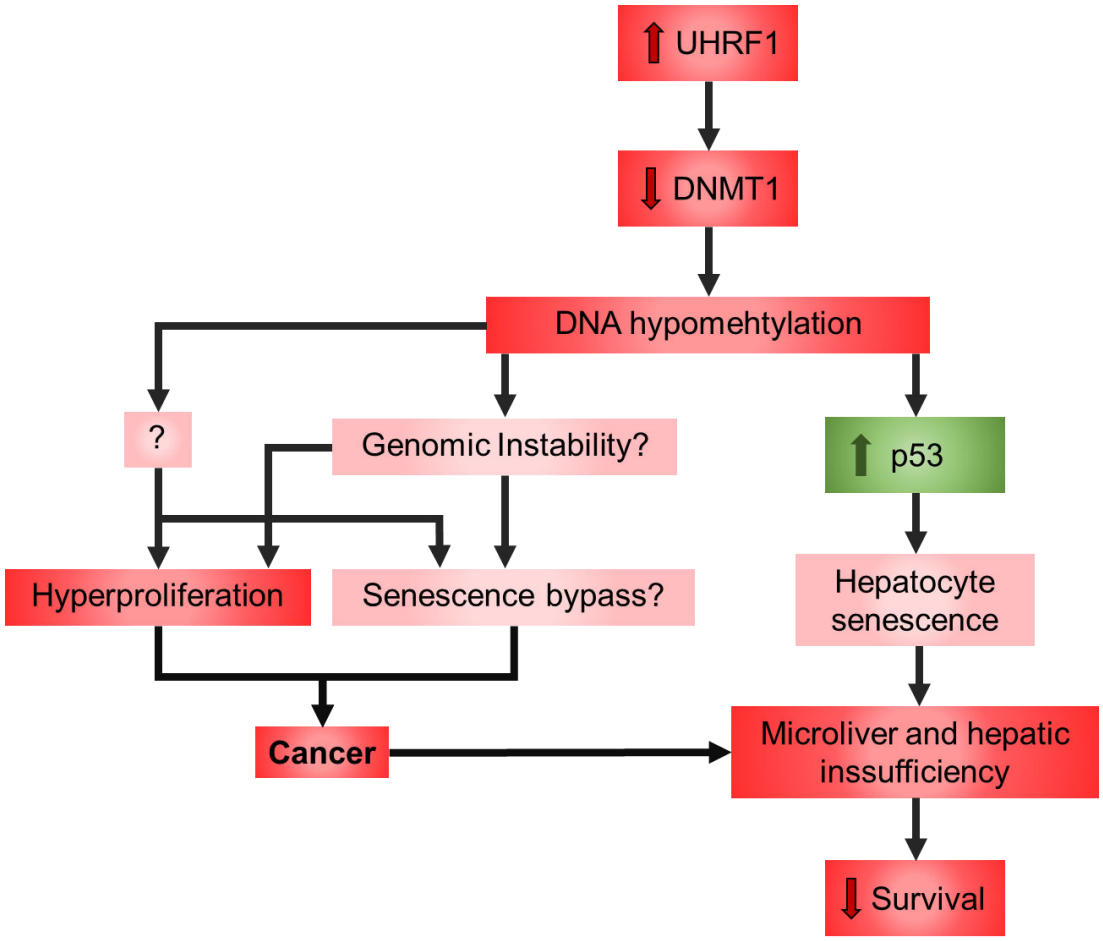

Figure 29: Model of relationship between UHRF1 overexpression and hepatocellular carcinoma. Overexpressed UHRF1 in cancers targets DNMT1 for degradation, leading to overall DNA hypomethylation and genomic instability. Adapted from (Mudbhary et al., 2014)

TIP60 and UHRF1 together play a role to destabilize DNMT1 but because of their seemingly opposite roles in cancer makes the interaction of these two proteins interesting to be further explored specially in cancer cells.

1.5.2 p53-Mediated Apoptosis and Cell Cycle Arrest

As described earlier TIP60 plays an important role in activation of p53 mediated apoptosis and cell cycle arrest. A recent study has reported that a direct interaction between UHRF1 and TIP60 can negatively regulate the interplay between TIP60-p53 and lead to tumorigenesis (Figure 30) (Dai *et al.*, 2013). It is reported that UHRF1 directly interacts with TIP60 through its SRA-RING domain and induces degradation independent ubiquitination of TIP60. This association of UHRF1 with TIP60 compromises the ability of TIP60 to acetylate p53 at K120

and hampers the apoptosis induced by the activation of p53. It was also found that downregulation of UHRF1 increases TIP60-mediated activation of p53 leading to induction of PUMA and p21, to induce apoptosis and cell cycle arrest respectively (Dai *et al.*, 2013).

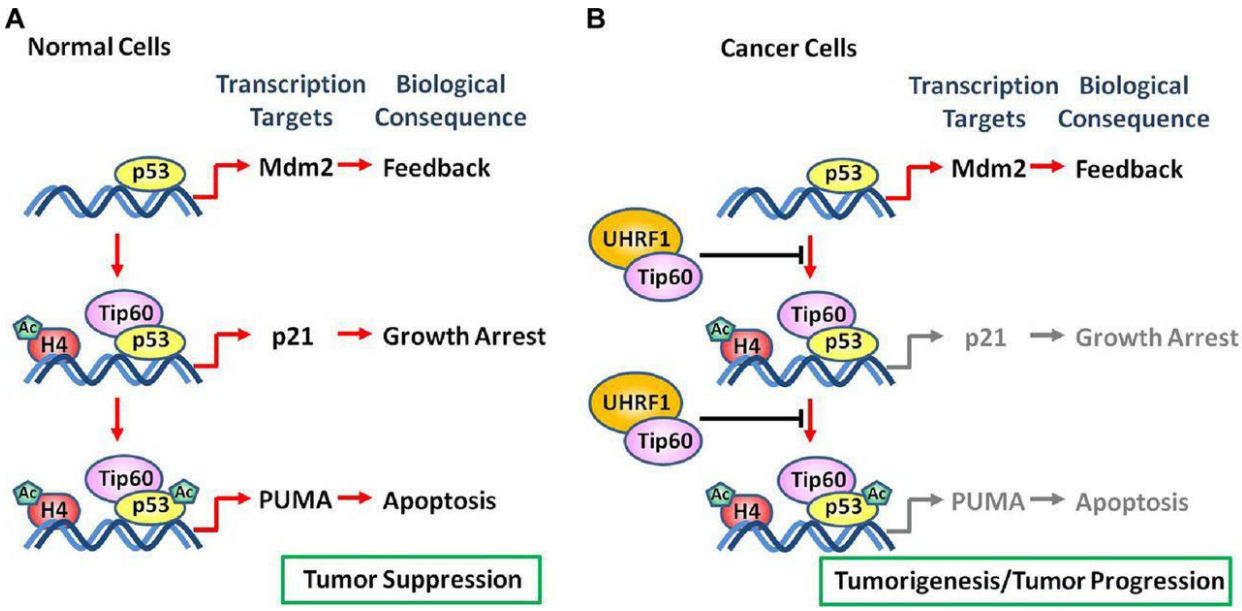

Figure 30: A model for tumor progression in cells with UHRF1 overexpression. Normally TIP60 can activate p53 in acetylation independent and dependent manner to induce growth arrest and apoptosis respectively. However, overexpression of UHRF1 blocks the TIP60-mediated activation of p53 and thus promotes proliferation by inhibiting the induction of growth arrest or apoptosis in transformed cells.

As beside their individual role in epigenetics, UHRF1 and TIP60 are reported to be involved in multiple cellular functions including their coordination in regulation of stability and function of other important proteins like DNMT1 and p53. Abnormalities to these processes can play a critical role in the development of cancers and other pathologies. Therefore, it is imperative to study this interaction further, to explore its role and functional dynamics in cells.

OBJECTIVES

2 - OBJECTIVES

Epigenetics is a relatively new and rapidly expanding field of biology, unveiling the previously hidden mechanisms of gene regulation. Extensive amount of research is being carried out to understand the epigenetic processes such as DNA methylations, histone modifications and non-coding RNAs activities in order to regulate the gene expression and cell function. This knowledge is of great importance as it not only provides us the basic understanding of developmental and functional procedures but also enable us to treat different pathologies.

Epigenetic machinery comprises of wide array of proteins, which are able to read, write or erase epigenetic marks on chromatin and can affect its nuclear organization and functions. These proteins mostly work in a multiprotein complex where their activities are well coordinated and regulated. UHRF1 is one such important integrator of epigenetic machinery, which links the DNA methylation and histone modifications by its interaction with different proteins in the nucleus. It is upregulated in most of cancers and is linked to aberrant methylation patterns leading to repression of tumor suppressor genes and unchecked proliferation.

TIP60, a histone acetyltransferase of MYST family was found to be present in the same complex with UHRF1 by our team and later both proteins were reported to play a key role in degradation of DNMT1 in cells. Besides, this a study also reported that UHRF1 hinders the TIP60 mediated activation of p53 in cancer cells to promote tumorigenesis. Therefore, this project was designed to get a better understanding of this UHRF1-TIP60 interaction in cells as it will help to decipher the roles of these proteins in normal and cancer cells.

The key objectives of this project were:

1. To visualize the interaction between UHRF1 and TIP60 inside the cells by fluorescent lifetime imaging microscopy (FLIM). TIP60 and UHRF1 are known to be present in the same epigenetic complex with DNMT1 and together they are linked to S phase related activities such as epigenetic code replication and DNA damage response. So, studying the interaction of these proteins during the S phase of cell cycle can help to understand the function of these proteins together in this phase of cell cycle.
2. To identify the domains of TIP60 interacting with UHRF1.
3. TIP60 is well known to play a role in DNA damage repair through homologous recombination (HR) pathway and recently role of UHRF1 has also been predicted in

DNA damage identification and initiation of DNA damage response. The aim of this project was to also study the colocalization of TIP60 and UHRF1 on DNA double strand breaks in order to check if both proteins work in coherence with each other during the DNA damage response or not?

4. To check the effect of TIP60 overexpression in cancer cells. TIP60 is believed to exert a tumor suppressive role by directly inhibiting the proliferation or augmenting the response of other TSGs. TIP60 is found downregulated in most of the cancer cells and overexpression of TIP60 in such tumor cells might restore the normal functional of other TSGs and can prevent the proliferation of cancer cells.

MATERIALS AND METHODS

3 - MATERIALS AND METHODS

3.1 Materials

3.1.1 Cell lines

HeLa

HeLa (ATCC® CCL-2™) is one of the earliest human cell line derived from patient named Henrietta Lacks, who died of cervical cancer in 1951. These are adherent cervical adenocarcinoma cells transformed with human papilloma (HPV) genome.

3.1.2 Antibodies

Name	**Host Organism**	**Source**	**Type**
Primary Antibodies			
Anti-UHRF1	Mouse	Engineered in lab as described previously in (Hopfner *et al.*, 2000)	Monoclonal
Anti-DNMT1	Mouse	Stressgen, Canada & Proteogenix, France (PTG-MAB0079)	Monoclonal
Anti-eGFP	Mouse	Thermo Fisher Scientific (A-11120) and Proteintech (66002-1-Ig)	Monoclonal
Anti-mCherry	Rabbit	Genetex (GTX 59788)	Polyclonal
Anti-TIP60	Rabbit	Genetex (GTX 112197)	Polyclonal
Anti-p73	Mouse	BD Biosciences Pharmingen (558785)	Monoclonal
Anti-p53	Mouse	BD Biosciences Pharmingen (554293)	Monoclonal
Anti-GAPDH	Mouse	Merck Millipore (MAB 374)	Monoclonal

Anti-His	Mouse	IGBMC & ThermoFisher Scientific (MA1-21315)	Monoclonal
Anti-GST	Mouse	IGBMC	Monoclonal
Anti-Flag	Mouse	Sigma Aldrich (A8592-1MG) HRP linked	Monoclonal
Anti-Caspase 3	Rabbit	Cell Signaling Technology, Danvers, MA, USA (9661)	Polyclonal
Anti-PARP	Mouse	BD Biosciences Pharmingen (51-6639GR)	Monoclonal
anti BCL2	Mouse	Merck-Millipore (05-826)	Monoclonal
Anti-p21	Rabbit	Santa Cruz Biotechnology (sc-397)	Polyclonal
Anti-BAX	Rabbit	Merck Millipore (AB2930)	Polyclonal
Anti-γH2A.X	Rabbit	Abcam Cat (ab2893)	Polyclonal
Secondary Antibodies			
Anti-Mouse	Goat	HRP Conjugate Promega France (W4021)	Polyclonal
Anti-Rabbit	Goat	HRP Conjugate Promega France (W4011)	Polyclonal
Anti-Mouse	Goat	ThermoFisher Scientific Alexa-568 (A11031)	Polyclonal
Anti-Rabbit	Goat	ThermoFisher Scientific Alexa-488 (A11008)	Polyclonal

3.1.3 Plasmid Constructs

Name	Tag	Resistance	Vector Backbone	Promoter
eGFP	eGFP	Kanamycin		CMV
TIP60WT-eGFP	eGFP at C-terminus	Kanamycin	pEGFP-N1	CMV
TIP60ΔCRD-eGFP	eGFP at C-terminus	Kanamycin	pEGFP-N1	CMV
TIP60ΔZnFr-eGFP	eGFP at C-terminus	Kanamycin	pEGFP-N1	CMV
TIP60ΔHAT-eGFP	eGFP at C-terminus	Kanamycin	pEGFP-N1	CMV
TIP60ΔMYST-eGFP	eGFP at C-terminus	Kanamycin	pEGFP-N1	CMV
TIP60ΔNLS1-eGFP	eGFP at C-terminus	Kanamycin	pEGFP-N1	CMV
TIP60ΔNLS2-eGFP	eGFP at C-terminus	Kanamycin	pEGFP-N1	CMV
TIP60ΔNLS1&2-eGFP	eGFP at C-terminus	Kanamycin	pEGFP-N1	CMV
mCherry	mCherry	Ampicillin	pCMV-mCherry	CMV
UHRF1-mCherry	mCherry at C-terminus	Kanamycin	pCMV-mCherry	CMV
GST	GST	Ampicillin	pGEX	tac
GST-UHRF1	GST at N-terminus	Ampicillin	pGEX-4T1	tac
His-TIP60WT	6xHis at N-terminus	Ampicillin	pET-15b	T7
His-TIP60ΔCRD	6xHis at N-terminus	Ampicillin	pET-15b	T7
His-TIP60ΔZnFr	6xHis at N-terminus	Ampicillin	pET-15b	T7
His-TIP60ΔHAT	6xHis at N-terminus	Ampicillin	pET-15b	T7

His-TIP60ΔMYST	6xHis at N-terminus	Ampicillin	pET-15b	T7
His-TIP60(MYST)	6xHis at N-terminus	Ampicillin	pET-15b	T7
Flag-TIP60(MYST)	Flag at N-terminus	Ampicillin	pET-15b	T7

3.2 Methods

3.2.1 Cell Culture

Cell lines were cultured and maintained in Dulbecco's modified Eagle's medium (DMEM + GlutaMAX, Gibco, Lifetech, France) supplemented with 10% of heat inactivated fetal bovine serum and mixture of penicillin (100 U/ml) and streptomycin (100 U/ml) (penicillin/streptomycin: Invitrogen Corporation Pontoise, France) at 37°C in 5% CO_2 in a humidified environment.

3.2.2 Transfection

Transient transfection of the foreign DNA was carried out by jetPEI® (Polyplus) DNA transfection reagent which has minimum toxicity towards the mammalian cells. It is made up of linear polyethylenimine molecules that cover up the DNA to form positively charged particles. These particles interact with anionic proteoglycans on cell membrane and are taken inside the cell via endocytosis. PEI also protects the DNA integrity in endosomes and later releases the DNA into cytoplasm for subsequent transportation to nucleus and transcription.

For transfection, two solutions were prepared according to manufacturer's protocol: one containing the DNA (plasmid) in 150 mM of NaCl while the other containing JetPEI reagent in 150 mM of NaCl. JetPEI solution was added to DNA solution and incubated for 20 mins to allow the formation of DNA-PEI particles which were added later drop by drop into the culture media. For all samples in one experiment, cells were transfected with equal amount of DNA.

3.2.3 Cell Lysis and Protein Extraction

Cells were lysed 24 hr after transfection to collect the proteins. Briefly, adherent cells were washed with PBS and trypsinized to collect the cells in fresh DMEM. Cells were pellet down by centrifugation at 500 g for 5 min and were lysed by an ice-cold lysis buffer of following composition: 10 mM Tris-HCl pH 7.5, 150 mM NaCl, 1 mM EDTA and 1% NP40 supplemented with protease inhibitors (complete mini EDTA free protease inhibitor cocktail tablets, Roche Germany 11836170001). Samples were incubated on ice for 20 min to ensure complete lysis of the cells and later centrifuged at 14000 g for 20 min at 4°C to remove all the debris.

The extracted proteins were quantified by the help of colorimetric Bradford assay which is based on the color changes in Coomassie brilliant blue G-250 dye in response to different concentration of proteins. This color change is because of interaction of acidic Coomassie dye with arginine and aromatic amino acids in proteins. Color change is proportional to the amount of proteins and is measured by the difference of absorption at 595 nm. Proteins samples were relatively quantified from the standard curve obtained by the known concentration of bovine serum albumin (BSA).

3.2.4 Western Blot

To check the expression of proteins, 40 µg of protein lysate of different samples were loaded on to 10% or 12.5% of SDS-PAGE for separation in Tris-Glycine running buffer (25 mM Tris, 192 mM glycine, 0.1% SDS, pH 8.8) by using Bio-Rad minigel system. Prior to loading on the gel, proteins were mixed with Laemmli sample buffer (Bio-Rad, 1610747) and dithiothreitol (DTT) and were denatured by heating at 95°C for 5 min. Separated proteins were transferred to the previously activated polyvinylidene difluoride (PVDF) membranes in Tris-Glycine transfer buffer (25mM Tris, 192mM glycine, 30% ethanol, pH 6.8). Membranes were blocked by 3% blotting-grade blocker (Bio-Rad 1706404) in Tris Buffered Saline, with Tween® 20, pH 8.0 (TBS-T) (SIGMA-T9039) for 1 hr at room temperature. Membranes were incubated with primary antibodies at 4°C and later washed three times with TBS-T buffer, before incubation with secondary antibodies for 1 hr. After washing again with TBS-T for three times the samples were visualized by using chemiluminescent ECL system (Clarity™ ECL western blotting substrate, Biorad, 170-5060) on ImageQuant™ LAS 4000 system (GE Healthcare).

3.2.5 Co-Immunoprecipitation

For co-immunoprecipitation, HeLa cells are transfected as described earlier and 24 hr post transfection, cells are lysed by freeze shock and sonication method to collect the proteins. Briefly, cells after trypsinization are collected and centrifuged to form a pellet, which was resuspended in 0.5 mL of PBS supplemented with protease inhibitor cocktail (complete mini EDTA free protease inhibitor cocktail tablets, Roche Germany 11836170001). Cells were then frozen in liquid nitrogen and allowed to defreeze slowly on ice. After de-freezing, fragile cells were sonicated at maximum power for five seconds on ice and process was repeated for five times with 30 seconds interval. The lysed cells were then centrifuged at 14000 g for 25 mins at 4°C to remove the debris. 40 µg of proteins from each sample were saved as "input" controls while 800 µg to 1 mg of proteins from each sample were used for the immunoprecipitation experiments. Respective antibodies for the immunoprecipitation of proteins were added to those samples and incubated on rotor for 2 hr at 4°C. Later, 50 µL of magnetic Dynabeads® Protein A (ThermoFisher Scientific, Norway 10002D) were added to the mixture after equilibration with the same buffer to pull down the protein complexes bound with antibodies. Beads were washed five times with the fresh buffer to remove the unbound proteins in the samples. After washing, the protein complexes were denatured and analyzed through Western blot.

3.2.6 Recombinant Protein Expression and Pull-down assays

Recombinant proteins for the pull-down experiments were expressed in BL21 (DE3) pLysS transfected cells. For GST and GST-UHRF1 proteins, the expression was induced by 1 mM of isopropyl-1-thio-β-D-galactopyranoside (IPTG) after O.D of transfected bacterial culture reached between 0.5-0.6. Bacterial cells were grown at 25°C for 4 hours and were later collected by centrifugation. Pelleted cells were lysed by sonication in PBS containing 0.5% Triton x-100, 1mM EDTA, lysozyme (0.5mg/ml), 0.1 mM PMSF (phenylmethylsulfonyl fluoride) and protease inhibitors cocktail. After lysis of cells, the debris was removed by centrifugation and the GST proteins were captured by incubation with Glutathione Sepharose 4B beads (GE Healthcare Life Sciences 17-0756-05) for 2 hr at 4°C. Next, the beads were washed with fresh lysis buffer for five times and later the GST proteins bound to beads were eluted by glutathione buffer (glutathione 10 mM, NaCl 200 mM, pH 8.0). The eluted proteins were concentrated and further purified by using Amicon Ultra-15 (30 kDa and 10 kDa) filter

units. His-tag proteins were purified similarly after expression in BL21 (DE3) pLysS transfected cells by using Ni-NTA agarose beads (Qiagen 30230) in appropriate buffers.

For pull-down experiments the His tagged proteins were immobilized on Ni-NTA beads in PBS interaction buffer containing 0.1% triton x-100 and 30mM imidazole along with protease inhibitor cocktail. Equal quantities of GST and GST-UHRF1 were added to these immobilized proteins and incubated for 2 hr at 4°C with rotation. Next, the beads were washed five times with fresh interaction buffer to remove the unbound proteins and the complex was then analyzed by western blotting to see the association between proteins.

3.2.7 DNA Damage (Double Strand Break) Induction

To study the interaction of endogenous UHRF1 and TIP60 at DSBs, localized DNA damage was induced by micro-irradiation as described in Nature protocols (Suzuki *et al.*, 2011). HeLa cells were seeded on 18 mm cover glass in six well plate with a density of 10^5 cells per well. Cells were pre-sensitized by incubating them with 10 µM of 5-bromo-2'-deoxyuridine (BrdU) for 48 hr. BrdU gets incorporated into the replicating DNA as thymidine analogue and makes DNA more prone to damage on irradiation with UVC. Before micro-irradiation, cells were washed with PBS and covered by 25 mm isopore (polycarbonate) hydrophilic membrane of 5.0 µm pore size (Merck Millipore TMTP02500) to create localized spots of DNA damage. Cells were irradiated with UVC at a dose of 40 J s^{-1} for 30 seconds by using Stratalinker® UV Crosslinker (Stratalinker Model 1800) and were later fixed by using 3.7% paraformaldehyde at different time intervals (5, 15, 30 and 60mins) after irradiation. Fixed cells were then labelled by immunofluorescence and observed by confocal microscopy.

DNA damage response was also observed in cells overexpressing TIP60-eGFP and UHRF1-mCherry through live cell imaging. Briefly, cells were seeded on 18 mm cover glass and transfected as mentioned earlier. Twenty-four hours post transfection, cells were pre-sensitized by incubation with Hoechst 33258 (Molecular Probes, H3569) (5µg/ml) containing DMEM for 10 mins. Micro-irradiation and time-lapse imaging was done by using an iMIC microscope (Till Photonics) equipped with an Olympus 60x (1.45 NA) objective. DNA damage was induced along a pre-selected line within the nucleus by a Toptica laser iBEAM 405 nm with a power set to 10% and dwell time of 20 ms/µm. Cells were maintained at 37°C with 5% CO_2 in humidified atmosphere during the laser induced micro-irradiation and image acquisition.

3.2.8 Förster Resonance Energy Transfer (FRET)-Fluorescence Lifetime Imaging Microscopy (FLIM)

Interaction between TIP60 and UHRF1 inside the cells was studied by the FRET-FLIM technique. FRET is the non-radiative transfer of energy from excited donor fluorophore to the non-excited acceptor fluorophore through dipole-dipole coupling. This transfer of energy results in the quenching of donor fluorophore and changes the fluorescence intensity and lifetime of both fluorophores. Major prerequisite to use this technique for the study of interaction between the two proteins are following:

(1) absorption spectrum of the acceptor fluorophore must overlap with the emission spectrum of the donor fluorophore (Figure 31 A). Direct excitation of the acceptor fluorophore is avoided when donor fluorophore is excited by the laser.

(2) the two fluorophores should be in close vicinity of each other (< 10nm) within the Förster radius, for the efficient transfer of energy from donor to acceptor fluorophore (Figure 31 B).

Among the different fluorophores pairs used for different FRET analysis, eGFP and mCherry form the most common pair where eGFP serves as donor and mCherry acts as an acceptor fluorophore. To study the interaction between TIP60 and UHRF1 proteins, we tagged wild type and mutant TIP60 proteins with eGFP at their C-terminus while UHRF1 was tagged with mCherry at its C-terminus.

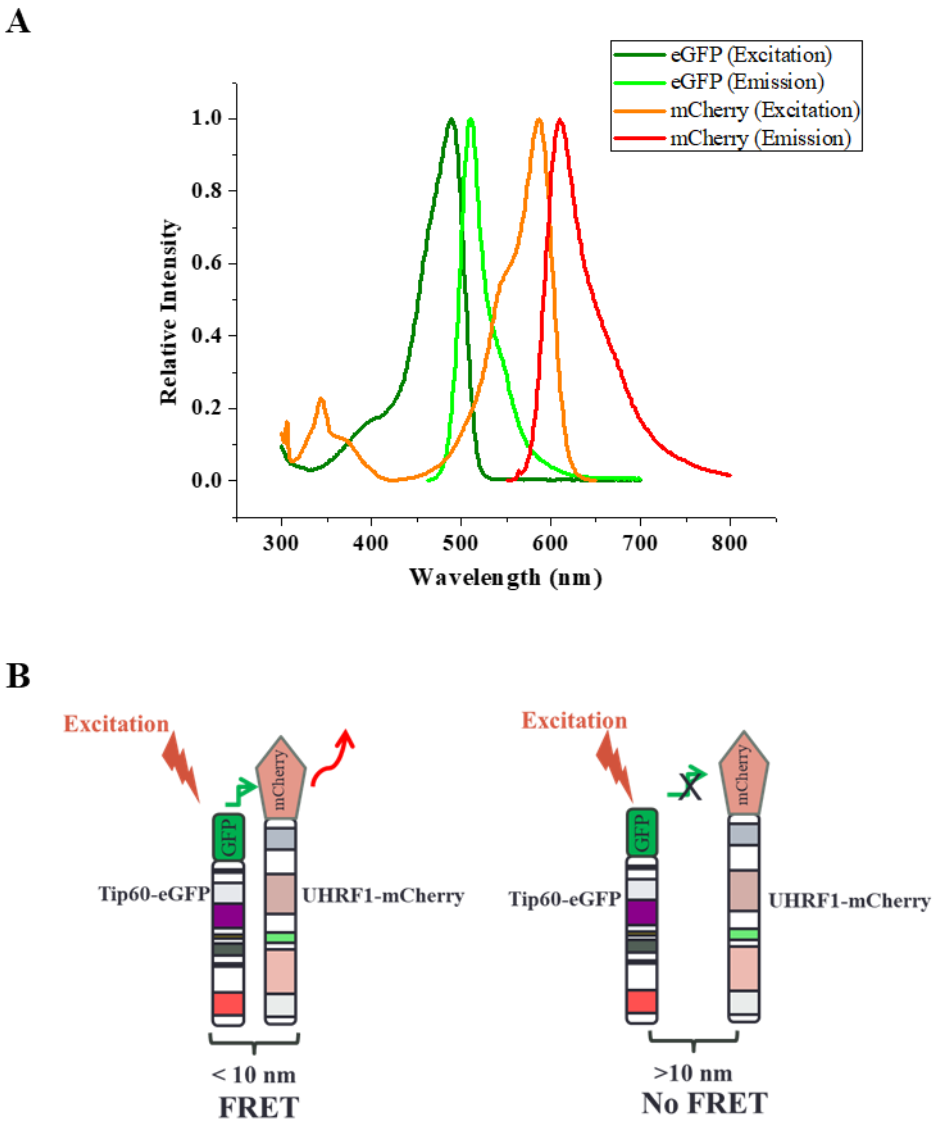

Figure 31: Two major prerequisite for FRET based experiments. A, Excitation spectrum of mCherry (represented by orange color) falls within the emission spectrum of eGFP (represented by light green color). B, Schematic model for the FRET between eGFP labeled TIP60 and mCherry labeled UHRF1. Transfer of energy occurs only when the two fluorophores are in close contact with each other and the distance between them is less than 10 nm.

In our experiments, we used Fluorescence Lifetime Imaging Microscopy (FLIM) to quantitatively analyze the FRET by measuring the changes in lifetime of donor (eGFP) fluorophore in the presence of acceptor (mCherry) molecule. By FLIM we can visualize the FRET, as it generates an image based on the lifetime of donor fluorophore recorded at each pixel. FLIM-based FRET measurements are advantageous as compared to intensity-based

FRET measurements as they are insensitive to the concentration of the fluorophores and thus insensitive to the variation in expression of fluorophore tagged proteins.

For FLIM experiments, 10^5 cells were seeded in 35 mm, high glass bottom grid-50 (Ibidi 81148) wells and were co-transfected with 0.75 µg TIP60-eGFP and 0.75 µg UHRF1-mCherry plasmids by using jetPEI™ reagent as described earlier to express the proteins. Cells were later fixed with 3.7% of paraformaldehyde and proceeded for FLIM measurements.

FLIM measurements were made on homemade two-photon excitation scanning microscope system which is based on an Olympus IX70 inverted microscope with an Olympus 60X 1.2 NA water immersion objective operating in the descanned fluorescence collection mode as described previously (El Meshri *et al.*, 2015). Two-photon excitation at 930 nm was provided by an Insight DeepSee laser (Spectra Physics). Photons were collected using a short pass filter with a cut-off wavelength of 680 nm (F75-680, AHF, Germany) and a band-pass filter of 520 ± 17 nm (F37-520, AHF, Germany). The fluorescence was directed to a fiber coupled APD (SPCM-AQR-14-FC, Perkin Elmer), which was connected to a time-correlated single photon counting module (SPC830, Becker & Hickl, Germany).

The data of the FLIM data were analyzed using the SPCImage v 4.0.6 (Becker & Hickel) software. The Förster resonance energy transfer (FRET) efficiency was calculated according to following formula

$$E = 1- (\tau_{DA}/\tau_D),$$

where τ_{DA} is lifetime of donor (eGFP) in the presence of acceptor (mCherry) and τ_D is the lifetime of donor in the absence of acceptor.

3.2.9 Confocal Microscopy

Cellular localization of the fluorophore tagged proteins, identification of the cells in S-phase and the accumulation of UHRF1 and TIP60 at the sites of double strand breaks was analyzed by the help of confocal microscopy. Confocal microscopy offers better optical resolution as compared to traditional wide field optical microscopy by using spatial pinhole to filter out-of-focus light in image formation.

HeLa cells were co-transfected as described earlier to express the fluorescent tagged proteins and DAPI (4',6-diamidino-2-phenylindole) was used to stain the nucleus of cells after fixation with 3.7% paraformaldehyde.

All samples were imaged with a Leica SPE confocal microscope equipped with a 63× 1.4NA oil immersion objective (HXC PL APO 63× 1.40 OIL CS). The images were further processed with Image J software.

For identification of the cells in S-phase, cells were incubated with 10 µM 5-ethynyl-2´-deoxyuridine (EdU) containing media for 20 mins before fixation with 3.7% paraformaldehyde. EdU is a thymidine analogue, that is incorporated into the replicating DNA in cells going through S-phase. The incorporated EdU in these cells is later identified by a copper catalyzed Click-iT reaction between alkyne group in EdU and azide moiety coupled to alexa 647 fluorophore by utilizing Click-iT® EdU Imaging Kits (ThermoFischer Scientific C10340). To check whether the cells imaged by FLIM were in S-phase or not, the same cells were re-imaged after EdU-alexa 647 labeling by confocal microscopy. The same cells were located by the help of grid present on the bottom of the ibidi wells in which the cells were seeded (Figure 32).

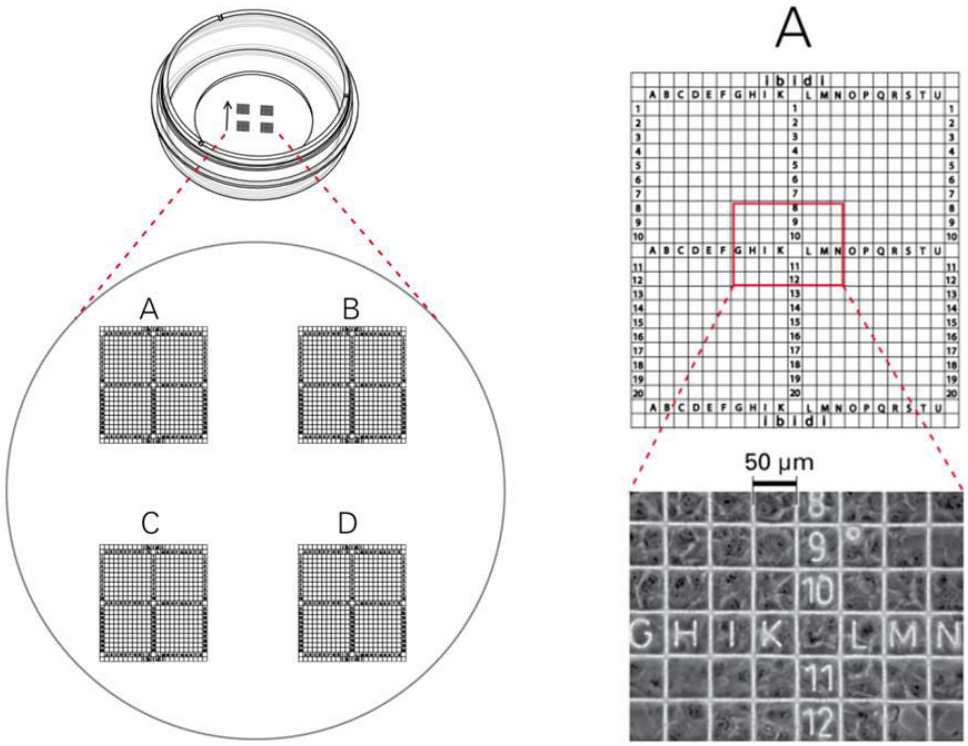

Figure 32: Schematic diagram of 35 mm glass bottom ibidi well showing the location grid used for the imaging the same cell in FLIM and confocal microscopy.

For DNA damage studies, the cells after fixation were first permeabilized by 0.5% triton X-100 in PBS for 10 mins and later blocked with 1% BSA in PBS, prior to immunofluorescence labelling of proteins. Next the cells were incubated with anti-UHRF1 (4 µg/mL), anti-Tip60 (8 µg/mL), or anti-γH2A.X (4 µg/mL) antibodies in PBS for 4 hr and were later incubated with secondary antibodies tagged with alexa fluorophores (1:250 dilution) to visualize the proteins. Cells were also stained with DAPI to identify the DNA in nucleus of the cells.

3.2.10 Global DNA Methylation Assay

For global methylation assay, HeLa cells were transfected with TIP60-eGFP and 24 hr post-transfection, cells were lysed to extract DNA by help of QIAamp® DNA Kit (Qiagen). 200 µg of purified DNA was later used to check the global methylation levels. Sigma's Imprint® methylated DNA quantification kit (Sigma-Aldrich, MDQ1-96RXN) was used to quantify the methylation levels in the DNA samples along with the positive control supplied with the kit.

3.2.11 Cell Cycle Analysis

Cell cycle analysis was performed using flow cytometry. Briefly cells transfected with TIP60-eGFP were compared to control HeLa cells or HeLa cells treated with transfecting agent. Cells were seeded in 6-well plate and were transfected with TIP60eGFP as described earlier. After 24 hr of transfection, cells were washed with PBS and harvested after mild trypsinization. Later, cells were fixed with BD cellfix (BD Biosciences) reagent and incubated with FxCycle™ (Thermo Fisher Scientific, F10797) PI/RNase staining solution for 20 min before analysis. Flow cytometry was carried out by guava easyCyte™ flow cytometer (Merck Millipore) and results were analyzed by InCyte Software for Guava® (Merck Millipore).

3.2.12 Apoptosis Analysis

Apoptosis analysis was performed using flow cytometry. Briefly cells transfected with TIP60-eGFP were compared to control cells or HeLa cells treated with transfecting agent JetPEI. Cells were collected after mild trypsinization and incubated with PI (Miltenyi Biotec) and annexin V-iFluor™ 350 conjugate (AAT Bioquest®, Inc) for analysis through guava easyCyte™ flow cytometer (Merck Millipore). Results were analyzed by InCyte Software for Guava® (Merck Millipore).

3.2.13 Molecular Docking Studies

For molecular docking studies, Cluspro docking server was used (https://cluspro.bu.edu). Molecular structures used for docking predictions were obtained from RCSB Protein Data Bank (https://www.rcsb.org). For UHRF1 PBR region and USP7, 5C6D structure was used at PDB (https://www.rcsb.org/structure/5C6D) while for TIP60 MYST domain it was 2OU2 (https://www.rcsb.org/structure/2OU2). UHRF1 PBR region was taken as fixed receptor molecule and modeled with chains of USP7 and TIP60 protein which served as ligand in the preset settings on the website.

RESULTS

4 - RESULTS

4.1 Interaction of the epigenetic integrator UHRF1 with the MYST domain of TIP60 inside the cell

UHRF1 is a key epigenetic integrator protein in cellular machinery, that serves as bridge to link the DNA methylation and histone modifications together. It works in a multiprotein macromolecular complex and is involved in variety of cellular activities including DNA methylation maintenance, DNA damage response, chromatin remodeling, regulation of stability and functions of other proteins. TIP60 is one of the important proteins found in this complex with UHRF1 and together they have been reported to modulate the stability of DNMT1 and the functional dynamics of p53 protein.

In this manuscript, we have tried to shed more light onto this interaction between UHRF1 and TIP60. Our results confirmed the presence of both proteins together in the same complex and for the first time we were able to visualize this interaction inside the cells by FLIM. Our results also revealed that UHRF1 interacts with MYST domain of TIP60 and this interaction takes place in S phase of cell cycle. The results of our study also predicted a tumor suppressive role of TIP60 whose overexpression in cells downregulated the UHRF1 and DNMT1, which are promising targets of anticancer therapy.

Ashraf et al. Journal of Experimental & Clinical Cancer Research (2017) 36:188
DOI 10.1186/s13046-017-0659-1

Journal of Experimental & Clinical Cancer Research

RESEARCH Open Access

Interaction of the epigenetic integrator UHRF1 with the MYST domain of TIP60 inside the cell

Waseem Ashraf[1], Christian Bronner[2], Liliyana Zaayter[1], Tanveer Ahmad[1], Ludovic Richert[1], Mahmoud Alhosin[3,4], Abdulkhaleg Ibrahim[2,5], Ali Hamiche[2], Yves Mely[1] and Marc Mousli[1*]

Abstract

Background: The nuclear epigenetic integrator UHRF1 is known to play a key role with DNMT1 in maintaining the DNA methylation patterns during cell division. Among UHRF1 partners, TIP60 takes part in epigenetic regulations through its acetyltransferase activity. Both proteins are involved in multiple cellular functions such as chromatin remodeling, DNA damage repair and regulation of stability and activity of other proteins. The aim of this work was to investigate the interaction between UHRF1 and TIP60 in order to elucidate the dialogue between these two proteins.

Methods: Biochemical (immunoprecipitation and pull-down assays) and microscopic (confocal and fluorescence lifetime imaging microscopy; FLIM) techniques were used to analyze the interaction between TIP60 and UHRF1 in vitro and in vivo. Global methylation levels were assessed by using a specific kit. The results were statistically analyzed using Graphpad prism and Origin.

Results: Our study shows that UHRF1, TIP60 and DNMT1 were found in the same epigenetic macro-molecular complex. In vitro pull-down assay showed that deletion of either the zinc finger in MYST domain or deletion of whole MYST domain from TIP60 significantly reduced its interaction with UHRF1. Confocal and FLIM microscopy showed that UHRF1 co-localized with TIP60 in the nucleus and confirmed that both proteins interacted together through the MYST domain of TIP60. Moreover, overexpression of TIP60 reduced the DNA methylation levels in HeLa cells along with downregulation of UHRF1 and DNMT1.

Conclusion: Our data demonstrate for the first time that TIP60 through its MYST domain directly interacts with UHRF1 which might be of high interest for the development of novel oncogenic inhibitors targeting this interaction.

Keywords: Cancer, Epigenetics, Fluorescence lifetime imaging microscopy (FLIM), Fluorescence resonance energy transfer (FRET), Protein-protein interaction, TIP60, UHRF1, Cell cycle

Background

Ubiquitin-like containing PHD and RING Finger domains 1 (UHRF1) is a multi-domain nuclear protein that plays an important role in epigenetics through the maintenance of DNA methylation patterns during DNA replication [1, 2]. UHRF1 senses hemi-methylated strand through its SRA domain and then recruits the DNA methyltransferase 1 (DNMT1) to duplicate the methylation patterns on the newly formed daughter strand [3–5]. Besides the readout of DNA methylation marks, UHRF1 also reads histone post-translational modifications (H3K9me2/3) via its tandem tudor and PHD domains and ubiquitinylates histone H3 at lysine 23 by its C-terminal RING domain [6–9]. UHRF1 is highly expressed in proliferating cells as compared with differentiated cells and its level peaks during the G1/S phase transition and G2/M phase of the cell cycle [1, 10]. In cancer cells, UHRF1 is mostly up-regulated and its levels are maintained constant throughout the cell cycle. The high levels of UHRF1 found in variety of cancers are often

* Correspondence: marc.mousli@unistra.fr
[1]Laboratoire de Biophotonique et Pharmacologie, UMR 7213 CNRS, Faculté de Pharmacie, Université de Strasbourg, 74, Route du Rhin, 67401 Illkirch Cedex, France
Full list of author information is available at the end of the article

correlated to the epigenetically silencing of tumor suppressor genes, poor prognosis and aggressiveness of the tumor [11–15]. UHRF1 is stabilized in the cells by its association with the ubiquitin specific protease 7 (USP7 or HAUSP) which prevents the proteasomal degradation of UHRF1 [16]. UHRF1 also plays an important role in regulating the stability and functions of other proteins such as DNMT1, promyelocytic leukemia protein (PML) and p53 through its interaction with other proteins such as the Tat-interacting protein 60 kDa (TIP60), USP7 and histone deacetylase 1 (HDAC1) [17–20]. UHRF1 and TIP60 were shown to be in the same epigenetic complex and to play an important role in regulating the stability and activity of DNMT1 [19, 21]. DNMT1 is acetylated by TIP60 which allows UHRF1 to ubiquitinylate DNMT1 and induce its down-regulation [19].

TIP60, initially identified as a partner of the HIV-1 Tat protein, is an evolutionary conserved and ubiquitously expressed acetyltransferase of the MYST family [22–25]. The TIP60 protein contains several domains (Fig. 1a, (i)), including a chromodomain and MYST domain endowed with acetyltransferase activity. Through these domains, TIP60 acetylates both histone and non-histone proteins. Tip60 also interacts with androgenic receptors and transcription factors and is involved in a variety of cellular activities including DNA damage response, chromatin remodeling, gene transcription, cell cycle regulation and apoptosis [26–29]. It also mediates the progression of the cell cycle by facilitating the G1/S phase transition, maintaining the genome integrity during the G1 and S phase and ensuring the faithful chromatin segregation during the M phase [30–33]. TIP60 also plays a role in regulating the activities of p53 in an acetylation-dependent and independent manner [18]. TIP60 mediated K120 acetylation in DNA binding region of p53 is necessary for the induction of apoptosis through Bcl 2-associated X protein (BAX) and p53 upregulated modulator of apoptosis (PUMA) pathway. The knockdown of TIP60 has been shown to abrogate the p21-induced cell cycle arrest after the activation of the tumor suppressor gene p53 in response to DNA damage [34–36]. Of note, UHRF1 by its direct interaction with TIP60 through the SRA and RING domains is thought to perturb the association between TIP60 and p53, preventing this latter from an acetylation-dependent activation and antitumor response [18]. Thus, a new anticancer strategy would be to restore p53 function by hindering UHRF1 to interact with TIP60. Although, the literature [18, 21] clearly suggests the occurrence of such an interaction in cells, its final demonstration is still lacking.

In order to further explore this interaction in cells and identify its determinants, we performed Fluoresecence Lifetime Imaging Microscopy (FLIM) experiments to demonstrate that UHRF1 and TIP60 physically interacts inside the cells. Through the use of deletion mutants of TIP60, we identified the key role of the MYST domain in its interaction with the UHRF1. This interaction also occurs in the S phase of the cell cycle during DNA replication.

Methods

Cell cultures

HeLa cells (ATCC, CCL-2 Amp, HeLa; Cervical Adenocarcinoma; Human) were cultured in Dulbecco's modified Eagle's medium (DMEM + GlutaMAX, Gibco, Lifetech, France) supplemented with 10% of heat inactivated fetal bovine serum and mixture of penicillin (100 U/ml) and streptomycin (100 U/ml) (penicillin/streptomycin: Invitrogen Corporation Pontoise, France) at 37 °C in 5% CO_2. Transfection of the plasmids in HeLa cells was carried by the jetPEI™ reagent (Life Technologies, Saint Aubin, France) according to the manufacturer's protocol.

Plasmid constructs

For HeLa cell transfection, UHRF1 was cloned into pCMV-mCherry vector to express UHRF1-mCherry protein while the TIP60 wild-type and mutants were cloned into a pEGFP-N1 plasmid to express eGFP-labeled TIP60 proteins in cells. For protein purification, UHRF1 was cloned into pGEX-4 T-1 to get the recombinant GST-UHRF1 fusion protein as described in [1]. For in vitro studies, TIP60 wild-type (TIP60-WT) and mutant TIP60 proteins were cloned into pET15b vector with XhoI and BamHI restriction sites to purify His tagged TIP60WT/mutants from bacteria.

Antibodies

Antibodies used in this study include the mouse monoclonal anti-UHRF1 engineered as described previously [1], mouse monoclonal anti-DNMT1 (Stressgen Canada), rabbit polyclonal anti-TIP60 (Genetex GTX 112197), rabbit polyclonal anti-mCherry (Genetex GTX 59788), mouse monoclonal anti-eGFP (Thermo Fisher Scientific A-11120 & Proteintech 66,002–1-Ig), and mouse monoclonal anti-GAPDH (Merck Millipore MAB 374). Mouse monoclonal anti-His and mouse monoclonal anti-GST antibodies were engineered in our core facilities (IGBMC, Illkirch, France).

Protein purification and pull-down assays

For protein purification, the plasmids were transfected in BL21 cells and cells were allowed to grow at 37 °C until the absorbance of the culture reached 0.5–0.6. Expression of the proteins was induced by the addition of 1 mM isopropyl-1-thio-β-D-galactopyranoside (IPTG) and the cells were further incubated at 25 °C for 4 h before collecting the proteins. GST-tagged UHRF1 protein

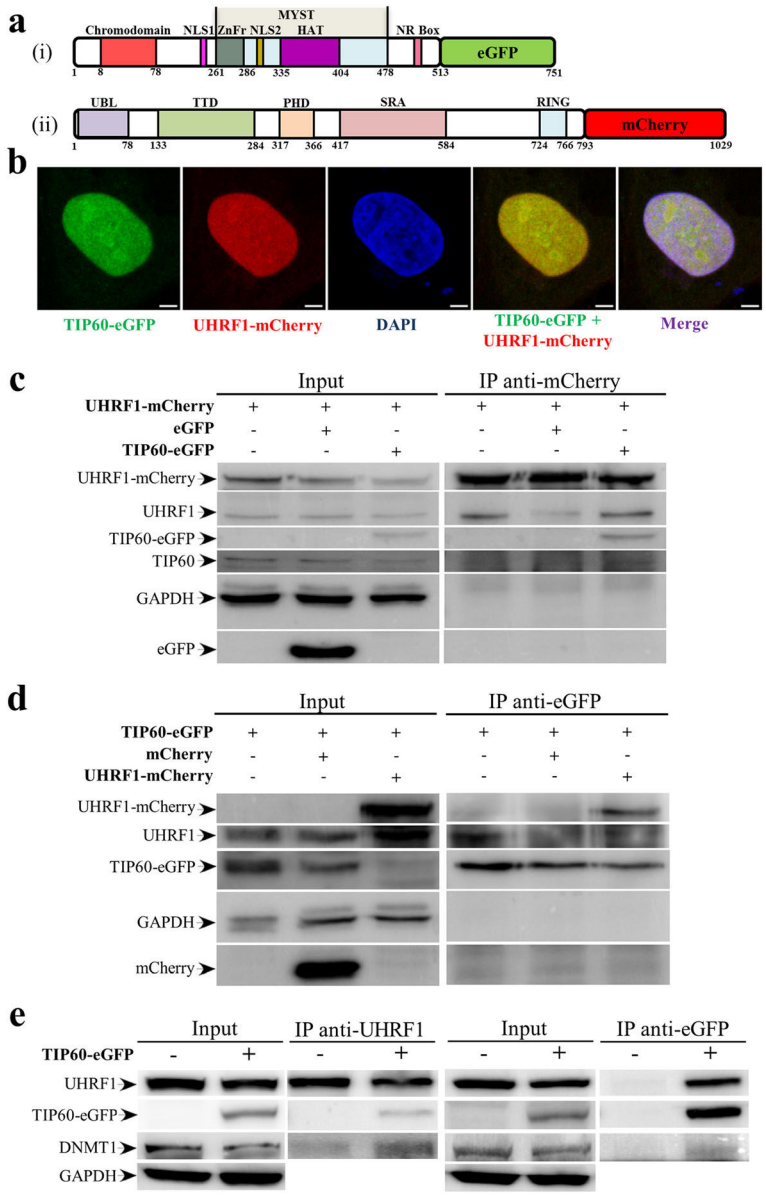

Fig. 1 TIP60 interacts with UHRF1 and DNMT1 in HeLa cells. **a** Schematic diagram of TIP60 wild type tagged with eGFP (i) and UHRF1 tagged with mCherry (ii) at their C-terminus. **b** Transfection of TIP60-eGFP and UHRF1-mCherry in the nucleus of HeLa cells. White bar indicates size of 5 μm. **c** Immunoprecipitation of UHRF1-mCherry with anti-mCherry antibody co-immunoprecipitating exogenous TIP60-eGFP and endogenous TIP60. **d** Reciprocal immunoprecipitation of TIP60-eGFP with anti-eGFP antibody co-immunoprecipitating exogenous UHRF1-mCherry and endogenous UHRF1. **e** DNMT1 co-immunoprecipitate with UHRF1 and TIP60-eGFP using anti-UHRF1 and anti-eGFP antibody respectively

was purified from the cell lysate using Glutathione Sepharose 4B beads (GE Healthcare Life Sciences 17–0756-05) while the His-tagged wild-type and mutant TIP60 proteins were purified using Ni-NTA agarose beads (Qiagen 30,230) in appropriate buffers. Wild-type and mutant TIP60 proteins were immobilized on the Ni-NTA agarose beads and equal quantity of GST-UHRF1 was added in PBS containing 30 mM imidazole and 0.1% triton to study protein-protein interaction. The immobilized beads were washed five times before being analyzed by SDS-PAGE.

Fluorescence lifetime imaging microscopy (FLIM)

For FLIM measurements, 10^5 cells were seeded in a μ-dish 35 mm, glass bottom grid-50 (Ibidi 81,148) wells and were co-transfected with 0.75 μg TIP60-eGFP and 0.75 μg UHRF1-mCherry plasmids by using jetPEI™ reagent as described in manufacturer's protocol. After 24 h of transfection, cells were incubated for 20 min with 10 μM 5-ethynyl-2′-deoxyuridine (EdU) containing media before fixation with 3.7% paraformaldehyde. After fixation, cells were analyzed with a homemade two-photon excitation

scanning microscope based on an Olympus IX70 inverted microscope with an Olympus 60X 1.2 NA water immersion objective operating in the descanned fluorescence collection mode as described [37]. Two-photon excitation at 930 nm was provided by an Insight DeepSee laser (Spectra Physics). Photons were collected using a short pass filter with a cut-off wavelength of 680 nm (F75–680, AHF, Germany) and a band-pass filter of 520 ± 17 nm (F37–520, AHF, Germany). The fluorescence was directed to a fiber coupled APD (SPCM-AQR-14-FC, Perkin Elmer), which was connected to a time-correlated single photon counting module (SPC830, Becker & Hickl, Germany). FLIM data were analyzed using the SPCImage v 4.0.6 (Becker & Hickel) software. The Förster resonance energy transfer (FRET) efficiency was calculated according to $E = 1- (\tau_{DA}/\tau_{D})$, where τ_{DA} is lifetime of donor (eGFP) in the presence of acceptor (mCherry) and τ_{D} is the lifetime of donor in the absence of acceptor.

Confocal microscopy

The cells imaged by FLIM were also imaged by confocal microscopy. The same cells could be imaged by both techniques, by locating the cells with the help of coordinates on the ibidi well. Prior to confocal microscopy the cells in S phase were labeled with the Click-iT® EdU Alexa Fluor® 647 Imaging Kit (Thermo Fisher Scientific USA C10340) according to the manufacturer's protocol. For transfection and localization analysis, cells were co-transfected with TIP60-eGFP WT/mutants and UHRF1-mCherry and were labeled with DAPI after fixation to stain the nucleus. All samples were imaged with a Leica SPE equipped with a 63× 1.4NA oil immersion objective (HXC PL APO 63×/1.40 OIL CS). The images were further processed with Image J software.

Immunoprecipitation and western blotting

For Western blot, cells were harvested 24 h post-transfection by mild trypsinization. After washing with PBS, cells were lysed by ice cold lysis buffer 10 mM Tris-HCl pH 7.5, 150 mM NaCl, 1 mM EDTA and 1% NP40 supplemented with protease inhibitors (complete mini EDTA free protease inhibitor cocktail tablets, Roche Germany 11,836,170,001). Cell lysates (40 μg of the protein) were loaded onto 10% SDS-PAGE gels after denaturation for 5 min in Laemmli sample buffer (Bio-Rad Laboratories USA 1610747). The proteins were identified by anti-UHRF1, anti-eGFP, anti-DNMT1 and anti-GAPDH antibodies with overnight incubation at 4 °C. Primary antibodies were labeled with secondary anti-mouse (Promega, W402B) or anti-rabbit antibodies (Promega, W401B) conjugated with horseradish peroxidase and were visualized with the chemiluminescent ECL system (Clarity™ ECL western blotting substrate, Biorad, 170–5060) on an Image Quant LAS 4000 apparatus. Images were analyzed using the Image Studio Lite (Li-Core Biosciences, USA). For co-immunoprecipitation, the cells were collected and lysed by freeze shock and sonication in PBS supplemented with protease inhibitor cocktail tablet. A fraction of 40 μg of protein from each lysate was saved to serve as input control while 800 μg to 1 mg of protein lysate was incubated with appropriate antibodies for 4 h at 4 °C for subsequent immunoprecipitation. After washing and equilibration, 50 μL of Dynabeads® Protein A (Thermo Fisher Scientific Norway 10002D) were added to the lysate-antibody mixture and incubated for 1 h at 4 °C. Beads were collected later and washed five times in lysis buffer. They were then resuspended in Laemmli sample buffer (Bio-Rad Laboratories, USA). Proteins denatured by heating at 95 °C for 5 min were analyzed through Western blotting.

Global DNA Methylation analysis

HeLa cells were transiently transfected with TIP60-eGFP and mutants and were analyzed for global methylation levels by using Sigma's Imprint® Methylated DNA Quantification Kit Sigma-Aldrich). Briefly DNA was extracted from the cells using QIAamp® DNA Kit (Qiagen) and 200 ng of purified DNA were used for global DNA methylation level analysis according to the manufacturer's protocol.

Statistical analysis

The results were statistically analyzed using GraphPadPrism (version 5.04) and Origin (version 8.6).

Results

UHRF1 and TIP60 interaction inside the cells

In order to study the interaction between TIP60 and UHRF1, we expressed eGFP-tagged TIP60 (Fig. 1a, (i)) and mCherry-tagged UHRF1 (Fig. 1a, (ii)) in HeLa cells. The two proteins were expressed and co-localized with DAPI inside the nucleus of HeLa cells as seen by the merge (Fig. 1b). The interaction between UHRF1 and TIP60 proteins was assessed in vitro by co-immunoprecipitation experiments. Immunoprecipitating UHRF1-mCherry by using anti-mCherry antibody led to the co-immunoprecipitation of both endogenous TIP60 and exogenous TIP60-eGFP while free eGFP which was co-transfected with UHRF1-mCherry did not co-immunoprecipitate with it (Fig. 1c). This shows specific interaction of UHRF1-mCherry with endogenous TIP60 and exogenous TIP60-eGFP. Similarly, reciprocal co-immunoprecipitation experiments were performed by immunoprecipitating TIP60-eGFP with anti-eGFP antibody in cells (Fig. 1d). Immunoprecipitation of TIP60-eGFP led to co-immunoprecipitation of UHRF1-mCherry and endogenous UHRF1 while it did not immunoprecipitate free mCherry suggesting specific interaction between UHRF1 and TIP60 in the cells. Therefore, we can

assume that tagged proteins correctly localize in the nucleus of HeLa cells and can mimic the interaction pattern of endogenous proteins. It is interesting to note that UHRF1-mCherry co-expression resulted in lower levels of TIP60-eGFP recombinant protein (Fig. 1d) as compared with cells transfected with TIP60-eGFP or co-transfected with mCherry alone.

LikeTIP60, DNMT1 has also been reported to be associated with UHRF1 in the same protein complex [21]. So, in order to check the presence of DNMT1 in UHRF1/TIP60 complex, we also performed co-immunoprecipitation experiments. DNMT1 co-immunoprecipitated with the UHRF1 in normal HeLa cells or cells with overexpressed TIP60-eGFP (Fig. 1e). Overexpressed TIP60-eGFP also interacted with endogenous DNMT1 as DNMT1 co-immunoprecipitated with TIP60-eGFP along with UHRF1 showing the presence of the three proteins together in the same complex (Fig. 1e). This supports that the tag of TIP60-eGFP does not hinder it to adequately interact with its partners like DNMT1.

However, the results obtained with immunoprecipitation cannot confirm the interaction of proteins in vivo and do not explain the presence or absence of a close dialogue between the two proteins inside the cell.

Therefore, we studied the interaction between UHRF1 and TIP60 in cells using the FLIM-FRET technique which allows monitoring of very close contact (< 10 nm) between two proteins inside a cell. TIP60-eGFP served as the FRET pair donor because of the mono-exponential decay and high quantum yield of eGFP while the UHRF1-mCherry served as the FRET pair acceptor in these experiments as the absorption spectrum of mCherry falls in the emission spectrum of the eGFP. FRET occurs only when the two fluorophores are in close proximity to each other and can be unambiguously evidenced by a decrease of lifetime of the donor. By using FLIM microscopy, the lifetime of eGFP is calculated and color coded in each pixel of the image. The red to blue color covers lifetime ranging from 1.8 ns to 2.8 ns. FLIM images were recorded for TIP60-eGFP transfected cells (Fig. 2a, (i)) and cells co-transfected with TIP60-eGFP and UHRF1-mCherry (Fig. 2a, (ii)). The resulting distributions of fluorescent lifetimes are given in (Fig. 2a, (iii)). The average lifetime of TIP60-eGFP was 2.52 ± 0.01 ns in the cells transfected with TIP60-eGFP alone (Fig. 2b) or co-transfected with free mCherry (data not shown). However, the lifetime of eGFP was significantly reduced when TIP60-eGFP was co-transfected with UHRF1-mCherry in 1:1 ratio (Fig. 2b). The average lifetime of eGFP in co-transfected cells was 2.15 ± 0.02 ns, which corresponds to a mean FRET efficiency of 14.3 ± 0.6% (Fig. 2b). Altogether, these findings demonstrate that TIP60-eGFP interacts with UHRF1-mCherry in HeLa cells.

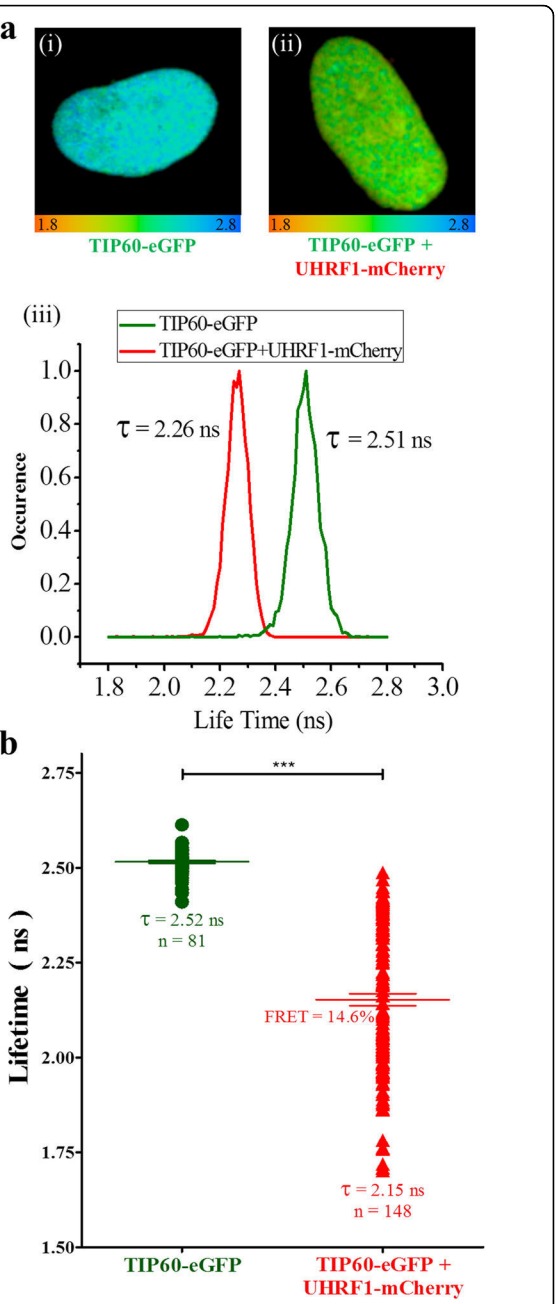

Fig. 2 Interaction of TIP60-eGFP with UHRF1-mCherry evidenced by FRET-FLIM. **a** 25 μm × 25 μm FLIM images of HeLa cells transfected with TIP60eGFP (i) or co-transfected with TIP60-eGFP and UHRF1-mCherry (ii) and lifetime distribution curve (iii). Color coded images indicate the fluorescence lifetime of TIP60-eGFP at each pixel. Color scale codes for lifetimes ranging from 1.8 ns (red) to 2.8 ns (blue). **b** Fluorescence lifetimes in TIP60-eGFP (●) and TIP60-eGFP + UHRF1-mCherry co-transfected cells (▲). Values are means ± SEM from five independent experiments. For statistical analysis, a Student's *t*-test was performed (*** $P < 0.001$)

UHRF1 and TIP60 interaction occurs during S phase of the cell cycle

UHRF1 localization and its association with other proteins dynamically changes during the cell cycle. NP95, the murine homologue of UHRF1 associates with PCNA and chromatin in early and mid S phase of cell cycle. Moreover UHRF1 interaction with DNMT1 for maintenance of DNA methylation pattern is also dependent on the S phase of cell cycle and is more pronounced in mid and late S phase of cell cycle [38–40]. Since both UHRF1 and TIP60 are also regulating the DNMT1 levels [19] and TIP60 is also playing important roles during the G1/S phase transition and S phase of the cell cycle [30, 33], we focused on S phase to decipher the interaction between UHRF1 and TIP60. Therefore, we labeled S phase cells undergoing DNA replication with EdU (thymidine analogue) for 15 min before fixation and then, we performed FLIM analysis (Fig. 3). After this, S phase cells were identified using alexa 647 labeling for confocal microscopy study. Different sub-phases of S phase were identified by the characteristic staining of EdU which gets incorporated into the genome at the sites of active replication [41]. Early S phase cells have numerous replication foci in the nucleus as evident by bright and abundant EdU labeling in nucleus of HeLa cells (Fig. 3a). In mid S phase the replication foci are more localized to periphery of nucleus and surrounding the nucleolus (Fig. 3b) while in late S phase, very few irregular replication foci are found in nucleus at heterochromatin regions of genome (Fig. 3c). The lifetime of the TIP60-eGFP was found to be decreased in the different sub-phases of the S phase (Fig. 3a-c). When the average lifetime of TIP60-eGFP in S phase cells was compared to the total cells, it was decreased to 2.12 ± 0.03 ns and the overall FRET efficiency increased to 16.0 ± 1.2% in the S phase positive cells (Fig. 3d). These results confirm UHRF1/ TIP60 interaction during the S phase of cell cycle.

TIP60 interacts with UHRF1 through its MYST domain

It is known that UHRF1 interacts with TIP60 through its SRA and RING domains and hinders the association of TIP60 with p53 and K120 acetylation of p53 [18]. However, the TIP60 domain responsible for its interaction with UHRF1 remains to be determined. Therefore, in this study we performed in vitro pull-down assay to identify the domain of TIP60 that is responsible for interaction with UHRF1. For this, we used His-tagged mutants of the TIP60 (Fig. 4a) immobilized on Nickel NTA agarose beads and the GST-UHRF1. We observed that full length UHRF1 interacted with TIP60WT in the presence of 150 mM NaCl (Fig. 4b-c) until 500 mM NaCl (data not shown) supporting a strong interaction between both proteins. Deletion of the TIP60 zinc finger domain or the whole MYST domain significantly reduced its association with GST-UHRF1 in the pull-down assay (Fig. 4b-c). In contrast, deletion of the chromodomain and HAT domains did not significantly affect their interaction with UHRF1. Recombinant TIP60 MYST domain also had a strong association with UHRF1 like the wild type TIP60 protein (Fig. 4b-c) and this interaction was stable up to 1 M NaCl salt concentration (data not shown) predicting the TIP60 MYST domain is playing a key role in this interaction.

The FLIM-FRET technique employing different mutants of TIP60 tagged with eGFP (Fig. 5a) was further used to identify the interacting domain of TIP60 with UHRF1-mCherry inside the nucleus of HeLa cells. TIP60-eGFP wild type and mutants were co-transfected with UHRF1-mCherry and the lifetime of eGFP was measured to assess the interaction. We found that the interaction of TIP60 and UHRF1 was marginally affected by removal of TIP60 chromodomain as the average FRET of TIP60ΔCRD-eGFP co-transfected with UHRF1-mCherry was of 12.2 ± 1.3% as compared to 14.3 ± 0.6% for TIP60WT-eGFP (Fig. 5b). All other mutations affecting the MYST domain of TIP60 strongly perturbed the interaction of these mutants with UHRF1. Indeed, the lifetime of TIP60ΔZnFr-eGFP, TIP60ΔHAT-eGFP and TIP60ΔMYST-eGFP co-transfected with UHRF1-mCherry was 2.49 ± 0.01 ns, 2.46 ± 0.01 ns and 2.49 ± 0.01 ns, respectively which is quite similar to that in control sample with 2.52 ± 0.01 ns (Fig. 5b). To check whether this loss of interaction is not a result of an alteration of subcellular localization, we performed a confocal microscopy analysis of co-transfected HeLa cells. We observed that TIP60WT-eGFP and its mutants including TIP60ΔCRD-eGFP, TIP60ΔZnFr-eGFP, TIP60ΔHAT-eGFP and TIP60ΔMYST-eGFP are localized in the nucleus of HeLa cells (Fig. 6). It is also important to note that TIP60WT and mutants co-localized with UHRF1-mCherry as shown in merge panels and were closely associated to DNA labeled by DAPI. This indicates that the loss of interaction between TIP60ΔZnFr, TIP60ΔHAT and TIP60ΔMYST with UHRF1 is not due to protein delocalization.

In order to check the heterogeneity of lifetime populations in TIP60-eGFP wild type or TIP60ΔCRD-eGFP co-transfected cells showing FRET, the FLIM images were also analyzed by a two-component model: $F(t) = \alpha_1 e_1^{-t/\tau} + \alpha_2 e_2^{-t/\tau}$ [37]. This analysis provides the distribution and population of TIP60-eGFP molecules interacting with UHRF1-mCherry (having FRET) and the TIP60-eGFP molecules which are free in nucleus without having interaction with UHRF1-mCherry (having no FRET). The lifetime for the long lifetime component (τ_2) (having no FRET) was fixed according to the lifetime of eGFP in only TIP60-eGFP transfected samples, while the lifetime (τ_1) of the short

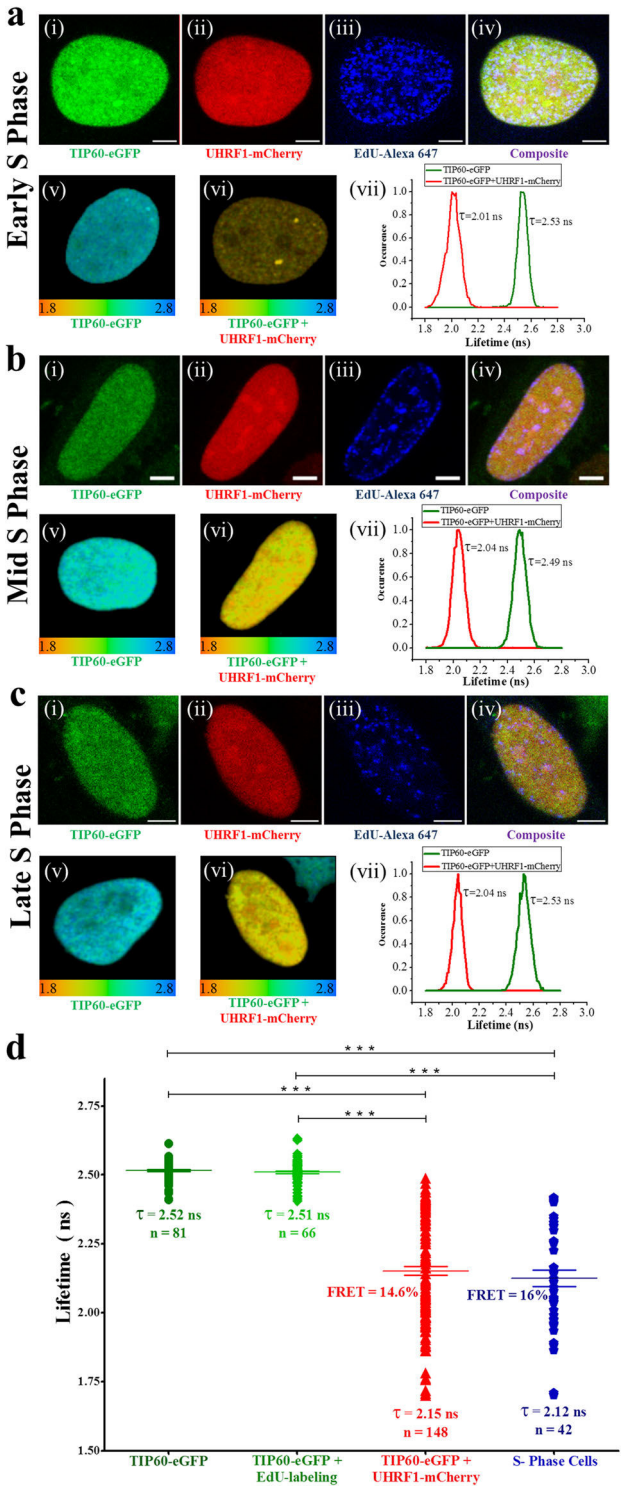

Fig. 3 Interaction between TIP60-eGFP and UHRF1-mCherry in S phase of cell cycle. **a-c** TIP60-eGFP interaction with UHRF1-mCherry in early, mid and late S phases of cell cycle, respectively. Confocal images of cells labeled with TIP60-eGFP, UHRF1-mCherry, EdU-Alexa 647 and merge, respectively (i - iv). The white bar indicates size of 5 μm. 25 μm × 25 μm FLIM images of HeLa cells transfected with TIP60-eGFP (v) or co-transfected with TIP60-eGFP and UHRF1-mCherry (vi) and lifetime distribution curves of the respected cells (vii). Color scale codes for lifetimes ranging from 1.8 ns (red) to 2.8 ns (blue). **d** Fluorescence lifetime distributions of TIP60-eGFP (●), TIP60-eGFP EdU labeled cells (◆), total TIP60-eGFP + UHRF1-mCherry co-transfected cells (▲) and co-transfected cells in S-phase of cell cycle (⬟). Values are means ± SEM from five independent experiments. For statistical analysis, a Student's *t*-test was performed (*** $P < 0.001$)

component (having FRET) and the populations of both component (α_1 and α_2) were obtained from the fits. The short lifetime component (τ_1) in TIP60WT-eGFP and TIP60ΔCRD-eGFP samples having FRET because of interaction with UHRF1-mCherry are shown in green or warmer color in FLIM images (Fig. 7a-b). The lifetime distribution curves of these FRET components for TIP60WT-eGFP and TIP60ΔCRD-eGFP are depicted in Fig. 7c. The mean value of the short lifetime component in TIP60WT-eGFP samples was 1.33 ± 0.01 ns and the average FRET calculated for this component was 45 ± 0.6% indicating close association of TIP60-eGFP with UHRF1-mCherry in HeLa cells. The mean value of the short component in TIP60ΔCRD-eGFP was 1.4 ± 0.03 ns and the average FRET calculated for this component was 43 ± 1.1% (Fig. 7c). Though the short lifetime component had almost similar values in TIP60WT-eGFP and TIP60ΔCRD-eGFP samples, the values of its corresponding population were different in the two samples as shown in Fig. 7d-e. TIP60WT-eGFP had higher population (α_1) of interacting short lifetime component as compared to TIP60ΔCRD-eGFP as its mean value in TIP60WT-eGFP was 37.5 ± 1.2% while it was 19 ± 0.3% in TIP60ΔCRD-eGFP as indicated from their respective distribution curves (Fig. 7f). This shows that TIP60ΔCRD-eGFP can interact with UHRF1-mCherry inside the nucleus but with less efficiency than TIP60WT-eGFP.

TIP60 overexpression down-regulates UHRF1 and DNMT1

Down-regulation of TIP60 has been reported in many cancers [42–45] and TIP60 has a well-established role in regulation of DNMT1. So, we investigated the consequences of TIP60-eGFP overexpression on UHRF1 and DNMT1 in HeLa cells in order to decipher the relationship between these epigenetic partners in the tumorigenesis process. Overexpression of TIP60 led to down-regulation of UHRF1 and DNMT1 in HeLa cells (Fig. 8a). UHRF1 levels were significantly reduced in TIP60-eGFP transfected cells as compared to that in untreated control cells, i.e., without any treatment or cells treated with jetPEI or transfected with eGFP alone (Fig. 8b). Similarly, DNMT1 levels were also significantly reduced in cells overexpressing TIP60-eGFP (Fig. 8c). It is interesting to observe that DNMT1 and UHRF1 levels were not affected by the overexpression of TIP60ΔMYST-eGFP in the nucleus which lacks the acetyltransferase domain of TIP60. Further, we also analyzed the effect of TIP60-eGFP overexpression on global DNA methylation levels. In accordance with the decrease in UHRF1 and DNMT1 levels, global DNA

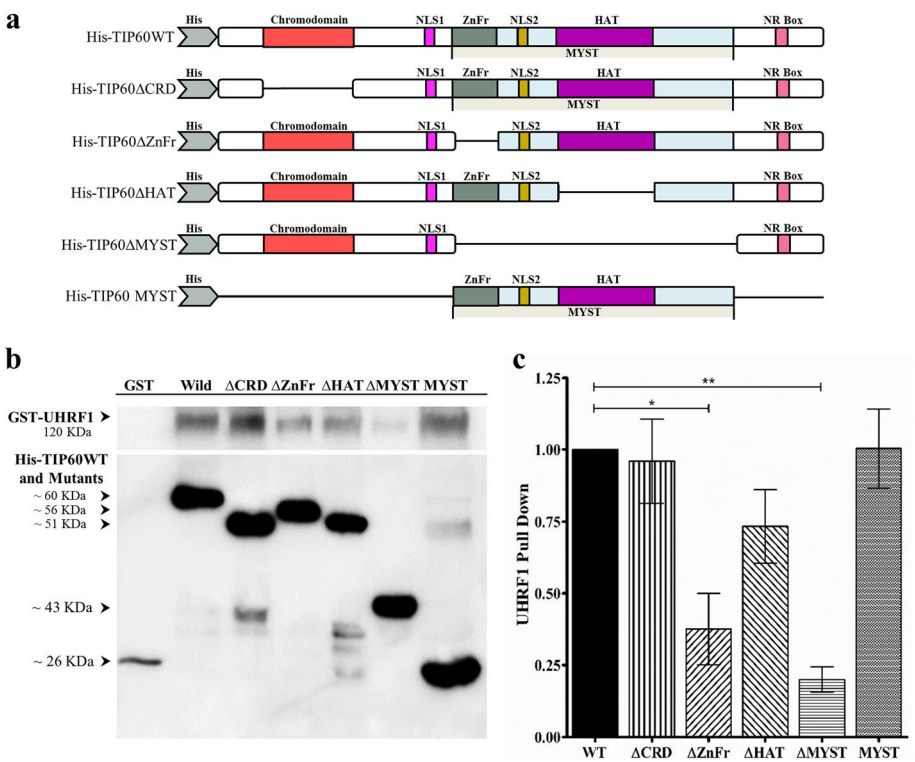

Fig. 4 In vitro pull-down analysis between His-TIP60WT/mutants and GST-UHRF1. **a**, Diagram showing His tag TIP60 wild type and mutants. **b** Western blot of in vitro pull-down assay. His tagged TIP60-WT or mutants were immobilized on Ni-NTA beads and incubated with UHRF1-GST. The complex recovered after washing were subjected to SDS PAGE and analyzed by Western blot. **c**. Western blot images were quantified by Image Studio Lite (Li-Core Biosciences USA) and statistically analyzed by using Student's *t*-test. Values are means ± SEM from three independent experiments (* $P < 0.05$, ** $P < 0.01$)

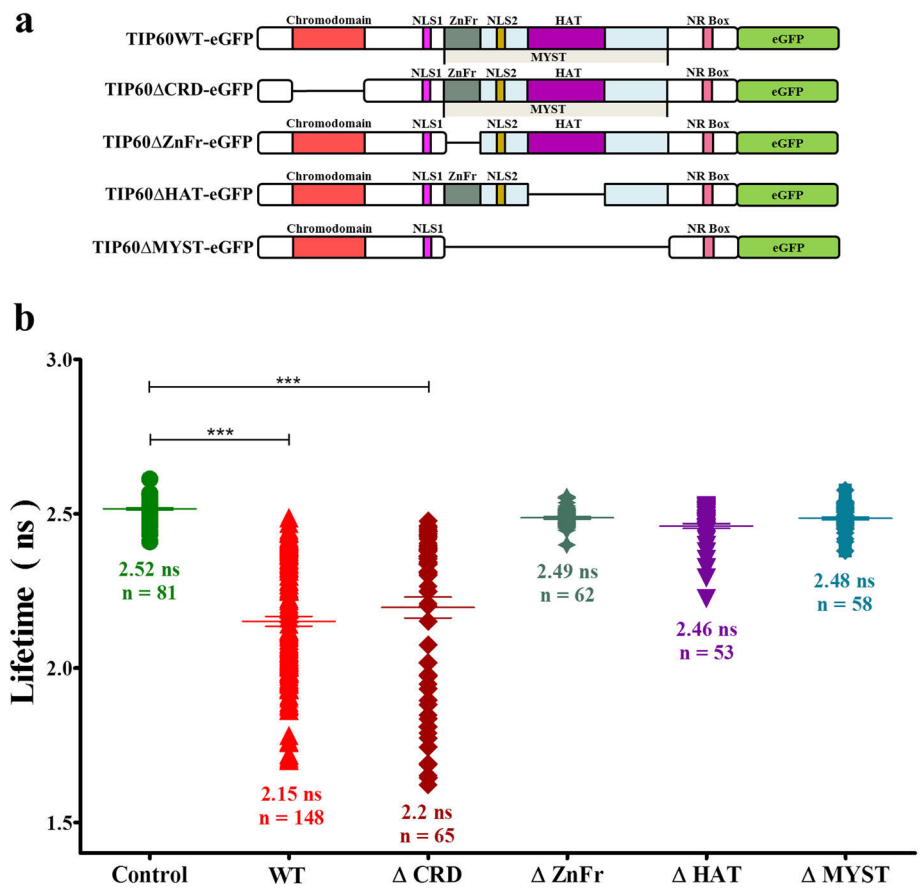

Fig. 5 Interaction between TIP60-eGFP WT/mutants and UHRF1 evidenced by FRET-FLIM. **a** Schematic diagram of TIP60WT/mutants tagged with eGFP at the C-terminus. **b** Lifetime distribution of TIP60-eGFP (●), TIP60 WT-eGFP + UHRF1-mCherry co-transfected cells (▲), TIP60 ΔCRD-eGFP + UHRF1-mCherry co-transfected cells (◆), TIP60 ΔZnFr-eGFP + UHRF1-mCherry co-transfected cells (✦), TIP60 ΔHAT-eGFP + UHRF1-mCherry co-transfected cells (▼), TIP60 ΔMYST-eGFP + UHRF1-mCherry co-transfected cells (✿). Values are means ± SEM from three to five independent experiments. For statistical analysis, a Student's *t*-test was performed (*** $P < 0.001$)

methylation also decreased by 26% after overexpression of TIP60WT-eGFP in 24 h of transfection (Fig. 8d). Overexpression of TIP60ΔCRD-eGFP also decreased the global DNA methylation by 21% (Fig. 8d), however, over expressing TIP60ΔZnFr-eGFP and TIP60ΔMYST-eGFP only lowered the DNA methylation by 9%. Overexpression of TIP60ΔHAT-eGFP had minimal effect on global DNA methylation which decreased only by 5% (Fig. 8d). Altogether these results suggest TIP60 as a regulator of DNMT1, UHRF1 and DNA methylation levels through its enzymatic activity.

Discussion

UHRF1 and TIP60 are part of large protein complexes and their conformation and association with other partners vary with the genomic activity and are regulated during cell cycle [46, 47]. Our results provided evidence for in vivo and in vitro interaction between UHRF1 and TIP60 protein by using the FLIM-FRET technique and pull-down assay. Furthermore, we could also show that MYST domain of TIP60 is playing a major role in its interaction with UHRF1. MYST domain is the conserved part of TIP60 containing a zinc finger involved in protein-protein interaction and a catalytic domain harboring its acetyltransferase activity [47]. In fact, through its MYST domain, TIP60 is able to acetylate both histones and non-histones proteins and regulates the activity of many proteins such as ATM and p53 [25, 36, 48]. Since p53-mediated apoptosis is dependent on its acetylation by TIP60 [35] therefore, interaction of TIP60 through its MYST domain with UHRF1 might impair many cellular functions. This may also explain how overexpressed UHRF1 in cancer negatively regulates the TIP60-p53 interplay in cells by preventing induction of cell cycle arrest and apoptosis. It is interesting to note that although chromodomain is not playing a direct role in its association with UHRF1 as indicated by FLIM and pull-down experiments, its removal can adversely also affect this interaction in vivo. According to two-component model, removal of chromodomain did not

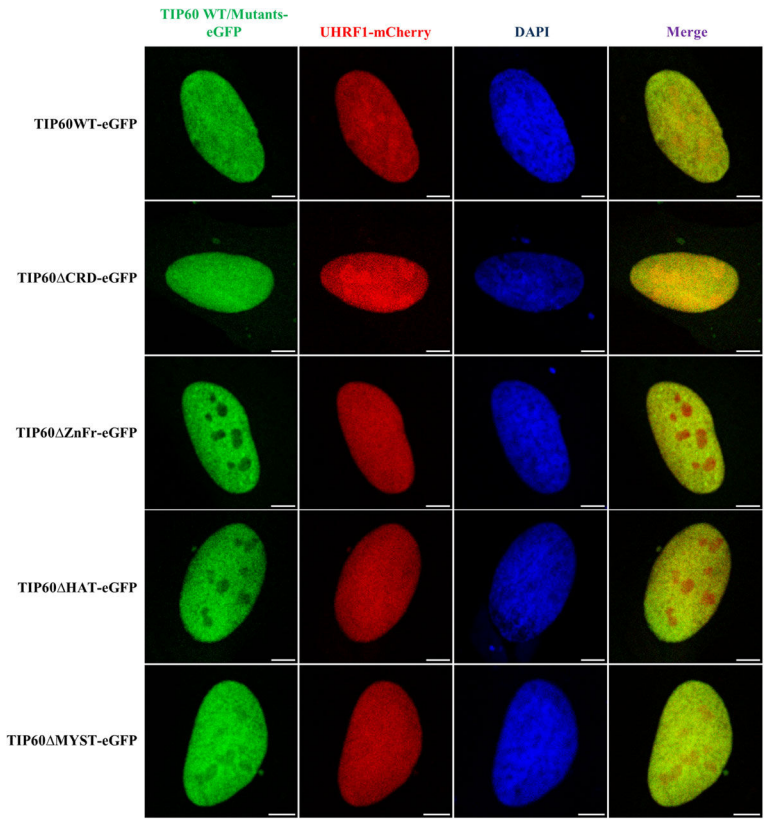

Fig. 6 Expression and localization of TIP60 mutants in HeLa cells. Confocal images show the expression and co-localization of TIP60WT-eGFP and mutants with UHRF1-mCherry in the HeLa cells with DAPI labeling. Green panel indicates TIP60 wild type or mutants tagged with eGFP, red panel shows UHRF1-mCherry, blue panel indicates DAPI and merge panel shows the composite of the TIP60-eGFP and UHRF1-mCherry panels. White bar indicates size of 5 μm

have a big impact on the mean lifetime of short component and FRET efficiencies as compared with wild type. However, the population interacting with UHRF1 was drastically reduced when chromodomain was removed from the structure of TIP60. Chromodomain helps TIP60 in reading out the histone marks and its loading to chromatin which may increase the possibility of TIP60 to interact with UHRF1 present in the same complex [49–51].

UHRF1 is a multi-domain protein which is essential for maintaining the DNA methylation during S phase of cell cycle by recruiting DNMT1 to the replication foci where it forms a multi protein complex with PCNA, DNMT1, TIP60, HDAC1, USP7 and other epigenetic partners [38, 52]. TIP60 is also well known for its role in DNA damage response to interstrand cross linkages or double strand breaks as TIP60-mediated H4K16 acetylation promotes DNA damage repair by homologous recombination (HR) pathway which dominates during the S phase of cell cycle [53, 54]. Recently the role of UHRF1 in DNA damage response has also been reported as it identifies interstrand cross linkages and double strand breaks and facilitates DNA damage repair by the same homologous recombination (HR) pathway through interaction with common partners such as FANCD2 and BRCA1 [55–57]. This predicts that UHRF1 and TIP60 may also work together in coherence to facilitate the DNA damage repair during S phase of cell cycle.

TIP60 along with UHRF1 is known to regulate levels of DNMT1 during cell cycle by inducing proteasomal degradation of DNMT1 through TIP60-mediated acetylation and subsequent ubiquitination by UHRF1 [19, 58, 59]. Accordingly, we have observed increased association of DNMT1 with UHRF1 in TIP60-eGFP transfected samples through co-immunoprecipitation experiments confirming the previous findings. DNMT1 is stabilized in cells by its direct association with USP7, a deubiquitinating enzyme which is present in the same complex. It has been recently reported that TIP60 impairs this protective association of USP7 with DNMT1 by acetylation [60]. Besides DNMT1, UHRF1 is also prevented from proteasomal degradation through its association with USP7 [16, 61, 62] and interruption of this association through cell cycle dependent kinase leads to proteasomal degradation of UHRF1 in M phase [16]. Zang and collaborators have recently suggested an identical role of

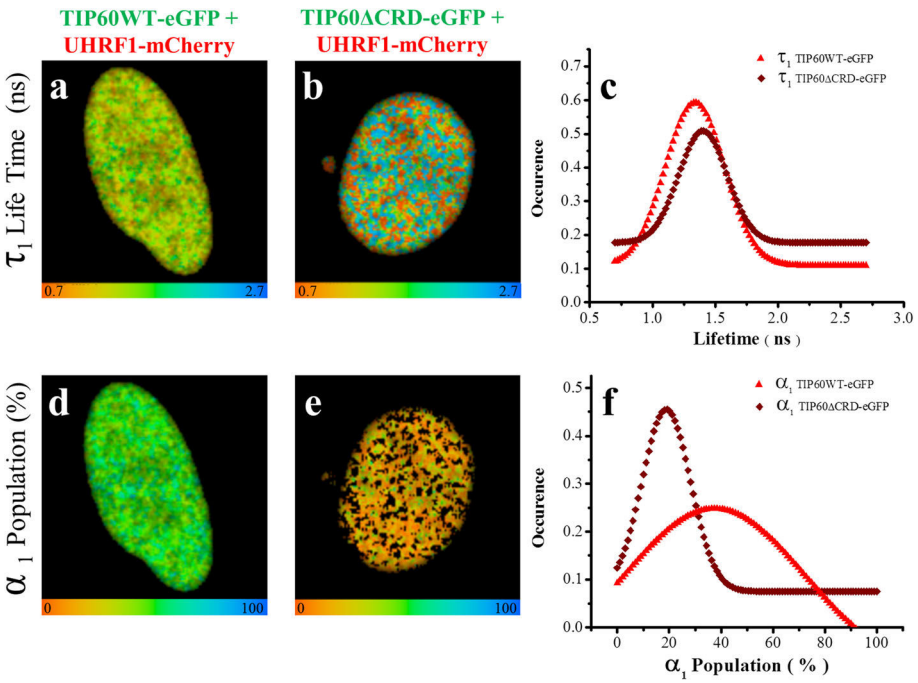

Fig. 7 Two component analyses of the fluorescence decays of TIP60WT-eGFP and TIP60ΔCRD-eGFP lifetime in presence of UHRF1-mCherry. Fluorescence decays were measured at each pixel for the respective cells by using bi-exponential model. In this model, the long-lived lifetime component (τ_2) was fixed to the lifetime of Tip6WT-eGFP when it is transfected alone in HeLa cells (2.52 ns). **a** 25 μm × 25 μm FLIM image of the distribution of τ_1 lifetimes of TIP60WT-eGFP in the presence of UHRF1-mCherry (corresponding to the component undergoing FRET). **b** 25 μm × 25 μm FLIM image of the distribution of τ_1 lifetimes of TIP60ΔCRD-eGFP in the presence of UHRF1-mCherry (corresponding to the component undergoing FRET). Color scale codes for lifetimes ranging from 0.7 ns (red) to 2.7 ns (blue). **c** Distribution of τ_1 lifetimes of TIP60WT-eGFP and TIP60ΔCRD-eGFP transfected cells in presence of UHRF1-mCherry. **d** 25 μm × 25 μm FLIM image of the population α_1 of TIP60WT-eGFP undergoing FRET in the presence of UHRF1-mCherry. **e** 25 μm × 25 μm FLIM image of the population α_1 of TIP60ΔCRD-eGFP undergoing FRET in the presence of UHRF1-mCherry. Color scale codes for population ranging from 0% (red) to 100% (blue). **f** Distribution of population α_1 for TIP60WT-eGFP and TIP60ΔCRD-eGFP transfected cells in presence of UHRF1-mCherry. Values indicated are from 148 TIP60WT-eGFP and UHRF1-mCherry co-transfected cells from five independent experiments and 65 TIP60ΔCRD-eGFP and UHRF1-mCherry co-transfected cells from three independent experiments

TIP60 in regulating the stability of UHRF1 as it regulates the stability of DNMT1. They demonstrated that UHRF1 can be acetylated by TIP60 at the K659 which lies in preferential binding area of USP7 and this acetylation greatly hampered the association of USP7 with UHRF1 [63]. Our results showed that TIP60 interacts with UHRF1 through its enzymatic MYST domain and overexpression of TIP60 in HeLa cells led to downregulation of UHRF1 suggesting another mechanism for the regulation of UHRF1 in cells.

TIP60 is found downregulated in different types of cancers and is believed to have tumor suppressor properties as oncovirus like HPV induces proliferation and tumorigenesis by destabilizing TIP60 in cervical cancer cells [42–45, 64–66]. Downregulation of TIP60 is associated with increased metastasis, decreased DNA damage response to oncogenes and poor survival of patients while enhanced TIP60 levels counters DNMT1-SNAIL2 driven epithelial to mesenchymal transition and inhibits metastasis [67]. UHRF1 on the other hand, is known to play an oncogenic role in cancer as its high expression in cancer is often related to downregulation of tumor suppressor genes through promoter hypermethylation [52, 68]. We observed that overexpression of UHRF1-mCherry decreases the protein level of TIP60-eGFP (Fig. 1d) which might be attributed to promoter hypermethylation or the E3 ligase activity of UHRF1 through which it can ubiquitinate TIP60 and may possibly reduce the level of TIP60-eGFP inside the cells [18]. This is in agreement with our previous findings where knock down of UHRF1 through siRNA upregulated the TIP60 levels in Jurkat cells [21]. It is also reported that targeting UHRF1 and DNMT1 can affect the global methylation [69, 70] and re-expression of tumor suppressor genes [2]. Our results showed that TIP60 overexpression in HeLa cells induced downregulation of UHRF1 and DNMT1, resulting in global DNA hypomethylation.

Conclusion

Epigenetic code replication machinery is a multi-protein complex which is actively involved in maintaining the epigenetic marks after the DNA replication. TIP60 and

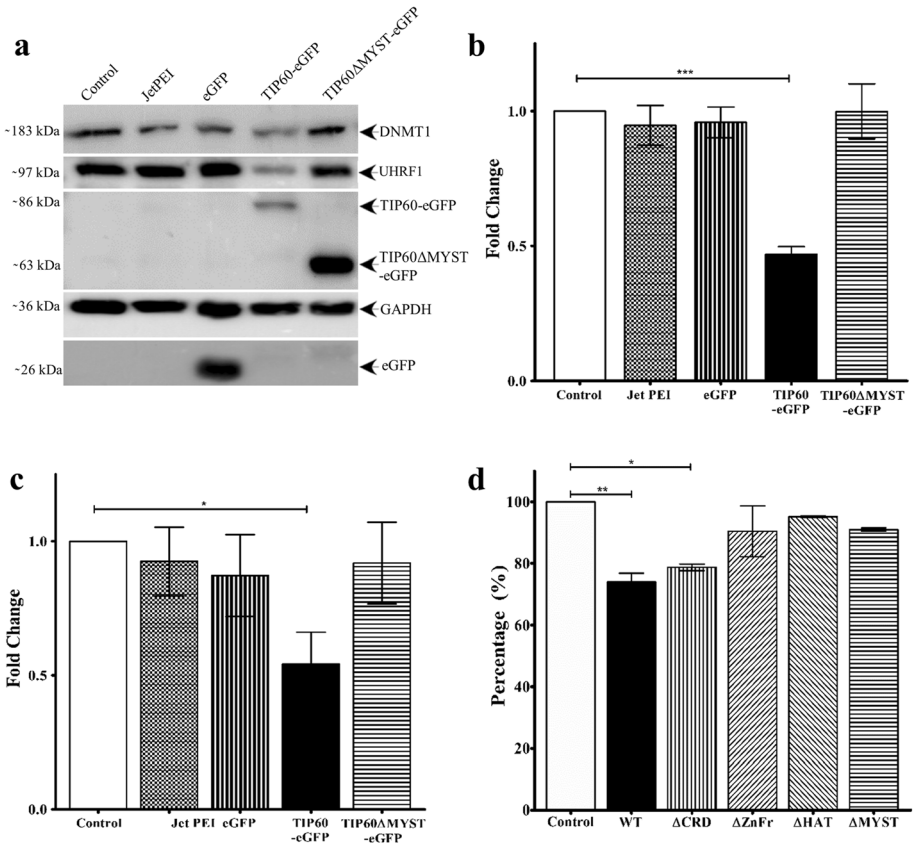

Fig. 8 TIP60 overexpression down-regulates its epigenetic partners UHRF1 and DNMT1. TIP60-eGFP was overexpressed in HeLa cells and the effect of this transient overexpression was compared to that of the control HeLa cells, HeLa cells with transfecting agent (JetPEI), HeLa cells with transfection of eGFP alone or TIP60**Δ**MYST-eGFP. **a** Western blot results showing down-regulation of UHRF1 and DNMT1 in TIP60-eGFP transfected cells. **b** Analysis of effect of TIP60-eGFP overexpression on UHRF1. **c**, Analysis of effect of TIP60-eGFP overexpression on DNMT1. Results indicated are from five independent experiments which are analyzed statistically by Student's *t*-test (* $P < 0.05$, ** $P < 0.01$, *** $P < 0.001$). **d** Effect of TIP60-eGFP overexpression on global DNA methylation. DNA was extracted from HeLa cells transfected with TIP60WT-eGFP and mutants and the methylation levels were compared to control HeLa cells. Results are indicated from three independent experiments and were analyzed by one-way ANOVA with post-hoc Tukey test. (* $P < 0.05$, ** $P < 0.01$, *** $P < 0.001$)

URHF1 are important members of this complex along with DNMT1. Here we conclude that TIP60 directly interacts with UHRF1 during the DNA replication phase of cell cycle and this interaction is dependent on the MYST domain of TIP60. Since UHRF1 interaction with TIP60 is known to perturb TIP60 mediated p53 activation, this study provides us with information to overcome this perturbation and counter the malicious transformations by utilizing the tumor suppressive role of TIP60. Finally, further investigations are required to fully decipher the dialogue within this three-way partnership involving UHRF1, DNMT1 and TIP60.

Abbreviations

ΔCRD: Chromodomain mutant; ΔHAT: Histone acetyltransferase domain mutant; ΔMYST: MYST domain mutant; ΔZnFr: Zinc Finger mutant; DNMT1: DNA methyl transferase 1; eGFP: Enhanced Green Fluorescent Protein; FLIM: Fluorescence Lifetime Imaging Microscopy; FRET: Fluorescence Resonance Energy Transfer; IP: Immunoprecipitation; TIP60: Tat interacting protein 60 kDa; UHRF1: Ubiquitin-like with PHD and RING Finger Domains 1; USP7: Ubiquitin specific protease 7; WB: Western Blotting; WT: Wild type

Acknowledgements

We thank Hugues de Rocquigny and Romain Vauchelles (Plate-forme d'Imagerie Quantitative - PIQ) for their technical support. WA and TA would also like to acknowledge funding support by the Higher Education Commission Pakistan for this work.

Funding

Our work was supported by the Agence Nationale de la Recherche (ANR-12-BS08–0003-02), the Fondation pour la Recherche Médicale (FRM DCM20111223038), Ligue contre le Cancer and by the grant ANR-10-LABX-0030-INRT, a French State fund managed by the Agence Nationale de la Recherche under the frame program Investissements d'Avenir ANR-10-IDEX-0002-02. WA and TA would also like to acknowledge funding support by the Higher Education Commission Pakistan for this work.

Availability of data and materials

Please contact corresponding author for data requests.

Authors' contributions
WA conducted most of the biochemical and cellular experiments with the help of LZ, AI and TA under the supervision of MM and CB. LR helped in the FLIM FRET experiments. WA, MA, CB and MM wrote most of the manuscript with the guidance and help of AH and YM. All authors read and approved the final manuscript.

Ethics approval and consent to participate
Not applicable

Consent for publication
Not applicable

Competing interests
The authors declare that they have no competing interests.

Publisher's Note
Springer Nature remains neutral with regard to jurisdictional claims in published maps and institutional affiliations.

Author details
[1]Laboratoire de Biophotonique et Pharmacologie, UMR 7213 CNRS, Faculté de Pharmacie, Université de Strasbourg, 74, Route du Rhin, 67401 Illkirch Cedex, France. [2]Institut de Génétique et de Biologie Moléculaire et Cellulaire, INSERM U964 CNRS UMR 7104, Université de Strasbourg, Illkirch, France. [3]Department of Biochemistry, Faculty of Science, King Abdulaziz University, Jeddah, Saudi Arabia. [4]Cancer Metabolism and Epigenetic Unit, Faculty of Science, King Abdulaziz University, Jeddah, Saudi Arabia. [5]BioTechnology Research Center (BTRC), Tripoli, Libya.

Received: 9 August 2017 Accepted: 4 December 2017
Published online: 21 December 2017

References
1. Hopfner R, Mousli M, Jeltsch JM, Voulgaris A, Lutz Y, Marin C, et al. ICBP90, a novel human CCAAT binding protein, involved in the regulation of topoisomerase IIalpha expression. Cancer Res. 2000;60(1):121–8.
2. Krifa M, Alhosin M, Muller CD, Gies JP, Chekir-Ghedira L, Ghedira K, et al. Limoniastrum guyonianum aqueous gall extract induces apoptosis in human cervical cancer cells involving p16 INK4A re-expression related to UHRF1 and DNMT1 down-regulation. J Exp Clin Cancer Res. 2013;32:30.
3. Arita K, Ariyoshi M, Tochio H, Nakamura Y, Shirakawa M. Recognition of hemi-methylated DNA by the SRA protein UHRF1 by a base-flipping mechanism. Nature. 2008;455(7214):818–21.
4. Avvakumov GV, Walker JR, Xue S, Li Y, Duan S, Bronner C, et al. Structural basis for recognition of hemi-methylated DNA by the SRA domain of human UHRF1. Nature. 2008;455(7214):822–5.
5. Hashimoto H, Horton JR, Zhang X, Bostick M, Jacobsen SE, Cheng X. The SRA domain of UHRF1 flips 5-methylcytosine out of the DNA helix. Nature. 2008;455(7214):826–9.
6. Liu X, Gao Q, Li P, Zhao Q, Zhang J, Li J, et al. UHRF1 targets DNMT1 for DNA methylation through cooperative binding of hemi-methylated DNA and methylated H3K9. Nat Commun. 2013;4:1563.
7. Nady N, Lemak A, Walker JR, Avvakumov GV, Kareta MS, Achour M, et al. Recognition of multivalent histone states associated with heterochromatin by UHRF1 protein. J Biol Chem. 2011;286(27):24300–11.
8. Nishiyama A, Yamaguchi L, Sharif J, Johmura Y, Kawamura T, Nakanishi K, et al. Uhrf1-dependent H3K23 ubiquitylation couples maintenance DNA methylation and replication. Nature. 2013;502(7470):249–53.
9. Qin W, Wolf P, Liu N, Link S, Smets M, La Mastra F, et al. DNA methylation requires a DNMT1 ubiquitin interacting motif (UIM) and histone ubiquitination. Cell Res. 2015;25(8):911–29.
10. Mousli M, Hopfner R, Abbady AQ, Monte D, Jeanblanc M, Oudet P, et al. ICBP90 belongs to a new family of proteins with an expression that is deregulated in cancer cells. Br J Cancer. 2003;89(1):120–7.
11. Ashraf W, Ibrahim A, Alhosin M, Zaayter L, Ouararhni K, Papin C, et al. The epigenetic integrator UHRF1: on the road to become a universal biomarker for cancer. Oncotarget. 2017;8:51946.
12. Boukhari A, Alhosin M, Bronner C, Sagini K, Truchot C, Sick E, et al. CD47 activation-induced UHRF1 over-expression is associated with silencing of tumor suppressor gene p16INK4A in glioblastoma cells. Anticancer Res. 2015;35(1):149–57.
13. Jeanblanc M, Mousli M, Hopfner R, Bathami K, Martinet N, Abbady AQ, et al. The retinoblastoma gene and its product are targeted by ICBP90: a key mechanism in the G1/S transition during the cell cycle. Oncogene. 2005; 24(49):7337–45.
14. Unoki M, Brunet J, Mousli M. Drug discovery targeting epigenetic codes: the great potential of UHRF1, which links DNA methylation and histone modifications, as a drug target in cancers and toxoplasmosis. Biochem Pharmacol. 2009;78(10):1279–88.
15. Wang F, Yang YZ, Shi CZ, Zhang P, Moyer MP, Zhang HZ, et al. UHRF1 promotes cell growth and metastasis through repression of p16(ink(4)a) in colorectal cancer. Ann Surg Oncol. 2012;19(8):2753–62.
16. Ma H, Chen H, Guo X, Wang Z, Sowa ME, Zheng L, et al. M phase phosphorylation of the epigenetic regulator UHRF1 regulates its physical association with the deubiquitylase USP7 and stability. Proc Natl Acad Sci U S A. 2012;109(13):4828–33.
17. Bronner C. Control of DNMT1 abundance in epigenetic inheritance by acetylation, ubiquitylation, and the histone code. Sci Signal. 2011;4(157):pe3.
18. Dai C, Shi D, Gu W. Negative regulation of the acetyltransferase TIP60-p53 interplay by UHRF1 (ubiquitin-like with PHD and RING finger domains 1). J Biol Chem. 2013;288(27):19581–92.
19. Du Z, Song J, Wang Y, Zhao Y, Guda K, Yang S, et al. DNMT1 stability is regulated by proteins coordinating deubiquitination and acetylation-driven ubiquitination. Sci Signal. 2010;3(146):ra80.
20. Guan D, Factor D, Liu Y, Wang Z, Kao HY. The epigenetic regulator UHRF1 promotes ubiquitination-mediated degradation of the tumor-suppressor protein promyelocytic leukemia protein. Oncogene. 2013;32(33):3819–28.
21. Achour M, Fuhrmann G, Alhosin M, Ronde P, Chataigneau T, Mousli M, et al. UHRF1 recruits the histone acetyltransferase Tip60 and controls its expression and activity. Biochem Biophys Res Commun. 2009;390(3):523–8.
22. Doyon Y, Selleck W, Lane WS, Tan S, Cote J. Structural and functional conservation of the NuA4 histone acetyltransferase complex from yeast to humans. Mol Cell Biol. 2004;24(5):1884–96.
23. Kamine J, Elangovan B, Subramanian T, Coleman D, Chinnadurai G. Identification of a cellular protein that specifically interacts with the essential cysteine region of the HIV-1 tat transactivator. Virology. 1996;216(2):357–66.
24. Lee KK, Workman JL. Histone acetyltransferase complexes: one size doesn't fit all. Nat Rev Mol Cell Biol. 2007;8(4):284–95.
25. Yamamoto T, Horikoshi M. Novel substrate specificity of the histone acetyltransferase activity of HIV-1-tat interactive protein Tip60. J Biol Chem. 1997;272(49):30595–8.
26. Gaughan L, Logan IR, Cook S, Neal DE, Robson CN. Tip60 and histone deacetylase 1 regulate androgen receptor activity through changes to the acetylation status of the receptor. J Biol Chem. 2002;277(29):25904–13.
27. Ikura T, Ogryzko VV, Grigoriev M, Groisman R, Wang J, Horikoshi M, et al. Involvement of the TIP60 histone acetylase complex in DNA repair and apoptosis. Cell. 2000;102(4):463–73.
28. Murr R, Loizou JI, Yang YG, Cuenin C, Li H, Wang ZQ, et al. Histone acetylation by Trrap-Tip60 modulates loading of repair proteins and repair of DNA double-strand breaks. Nat Cell Biol. 2006;8(1):91–9.
29. Squatrito M, Gorrini C, Amati B. Tip60 in DNA damage response and growth control: many tricks in one HAT. Trends Cell Biol. 2006;16(9): 433–42.
30. DeRan M, Pulvino M, Greene E, Su C, Zhao J. Transcriptional activation of histone genes requires NPAT-dependent recruitment of TRRAP-Tip60 complex to histone promoters during the G1/S phase transition. Mol Cell Biol. 2008;28(1):435–47.
31. Mo F, Zhuang X, Liu X, Yao PY, Qin B, Su Z, et al. Acetylation of aurora B by TIP60 ensures accurate chromosomal segregation. Nat Chem Biol. 2016; 12(4):226–32.
32. Niida H, Katsuno Y, Sengoku M, Shimada M, Yukawa M, Ikura M, et al. Essential role of Tip60-dependent recruitment of ribonucleotide reductase at DNA damage sites in DNA repair during G1 phase. Genes Dev. 2010; 24(4):333–8.
33. Taubert S, Gorrini C, Frank SR, Parisi T, Fuchs M, Chan HM, et al. E2F-dependent histone acetylation and recruitment of the Tip60 acetyltransferase complex to chromatin in late G1. Mol Cell Biol. 2004;24(10):4546–56.
34. Berns K, Hijmans EM, Mullenders J, Brummelkamp TR, Velds A, Heimerikx M, et al. A large-scale RNAi screen in human cells identifies new components of the p53 pathway. Nature. 2004;428(6981):431–7.

35. Sykes SM, Mellert HS, Holbert MA, Li K, Marmorstein R, Lane WS, et al. Acetylation of the p53 DNA-binding domain regulates apoptosis induction. Mol Cell. 2006;24(6):841–51.
36. Tang Y, Luo J, Zhang W, Gu W. Tip60-dependent acetylation of p53 modulates the decision between cell-cycle arrest and apoptosis. Mol Cell. 2006;24(6):827–39.
37. El Meshri SE, Dujardin D, Godet J, Richert L, Boudier C, Darlix JL, et al. Role of the nucleocapsid domain in HIV-1 Gag oligomerization and trafficking to the plasma membrane: a fluorescence lifetime imaging microscopy investigation. J Mol Biol. 2015;427(6 Pt B):1480–94.
38. Bostick M, Kim JK, Esteve PO, Clark A, Pradhan S, Jacobsen SE. UHRF1 plays a role in maintaining DNA methylation in mammalian cells. Science. 2007; 317(5845):1760–4.
39. Miura M, Watanabe H, Sasaki T, Tatsumi K, Muto M. Dynamic changes in subnuclear NP95 location during the cell cycle and its spatial relationship with DNA replication foci. Exp Cell Res. 2001;263(2):202–8.
40. Zhang J, Gao Q, Li P, Liu X, Jia Y, Wu W, et al. S phase-dependent interaction with DNMT1 dictates the role of UHRF1 but not UHRF2 in DNA methylation maintenance. Cell Res. 2011;21(12):1723–39.
41. Chakalova L, Debrand E, Mitchell JA, Osborne CS, Fraser P. Replication and transcription: shaping the landscape of the genome. Nat Rev Genet. 2005;6(9):669–77.
42. Bassi C, Li YT, Khu K, Mateo F, Baniasadi PS, Elia A, et al. The acetyltransferase Tip60 contributes to mammary tumorigenesis by modulating DNA repair. Cell Death Differ. 2016;23(7):1198–208.
43. Chen G, Cheng Y, Tang Y, Martinka M, Li G. Role of Tip60 in human melanoma cell migration, metastasis, and patient survival. J Invest Dermatol. 2012;132(11):2632–41.
44. Sakuraba K, Yasuda T, Sakata M, Kitamura YH, Shirahata A, Goto T, et al. Down-regulation of Tip60 gene as a potential marker for the malignancy of colorectal cancer. Anticancer Res. 2009;29(10):3953–5.
45. Sakuraba K, Yokomizo K, Shirahata A, Goto T, Saito M, Ishibashi K, et al. TIP60 as a potential marker for the malignancy of gastric cancer. Anticancer Res. 2011;31(1):77–9.
46. Gelato KA, Tauber M, Ong MS, Winter S, Hiragami-Hamada K, Sindlinger J, et al. Accessibility of different histone H3-binding domains of UHRF1 is allosterically regulated by phosphatidylinositol 5-phosphate. Mol Cell. 2014; 54(6):905–19.
47. Sapountzi V, Logan IR, Robson CN. Cellular functions of TIP60. Int J Biochem Cell Biol. 2006;38(9):1496–509.
48. Sun Y, Jiang X, Chen S, Fernandes N, Price BD. A role for the Tip60 histone acetyltransferase in the acetylation and activation of ATM. Proc Natl Acad Sci U S A. 2005;102(37):13182–7.
49. Kim CH, Kim JW, Jang SM, An JH, Seo SB, Choi KH. The chromodomain-containing histone acetyltransferase TIP60 acts as a code reader, recognizing the epigenetic codes for initiating transcription. Biosci Biotechnol Biochem. 2015;79(4):532–8.
50. Kim MY, Ann EJ, Kim JY, Mo JS, Park JH, Kim SY, et al. Tip60 histone acetyltransferase acts as a negative regulator of Notch1 signaling by means of acetylation. Mol Cell Biol. 2007;27(18):6506–19.
51. Sun Y, Jiang X, Xu Y, Ayrapetov MK, Moreau LA, Whetstine JR, et al. Histone H3 methylation links DNA damage detection to activation of the tumour suppressor Tip60. Nat Cell Biol. 2009;11(11):1376–82.
52. Alhosin M, Sharif T, Mousli M, Etienne-Selloum N, Fuhrmann G, Schini-Kerth VB, et al. Down-regulation of UHRF1, associated with re-expression of tumor suppressor genes, is a common feature of natural compounds exhibiting anti-cancer properties. J Exp Clin Cancer Res. 2011;30:41.
53. Renaud E, Barascu A, Rosselli F. Impaired TIP60-mediated H4K16 acetylation accounts for the aberrant chromatin accumulation of 53BP1 and RAP80 in Fanconi anemia pathway-deficient cells. Nucleic Acids Res. 2016;44(2):648–56.
54. Tang J, Cho NW, Cui G, Manion EM, Shanbhag NM, Botuyan MV, et al. Acetylation limits 53BP1 association with damaged chromatin to promote homologous recombination. Nat Struct Mol Biol. 2013;20(3):317–25.
55. Liang CC, Zhan B, Yoshikawa Y, Haas W, Gygi SP, Cohn MA. UHRF1 is a sensor for DNA interstrand crosslinks and recruits FANCD2 to initiate the Fanconi anemia pathway. Cell Rep. 2015;10(12):1947–56.
56. Tian Y, Paramasivam M, Ghosal G, Chen D, Shen X, Huang Y, et al. UHRF1 contributes to DNA damage repair as a lesion recognition factor and nuclease scaffold. Cell Rep. 2015;10(12):1957–66.
57. Zhang H, Liu H, Chen Y, Yang X, Wang P, Liu T, et al. A cell cycle-dependent BRCA1-UHRF1 cascade regulates DNA double-strand break repair pathway choice. Nat Commun. 2016;7:10201.
58. Qin W, Leonhardt H, Spada F. Usp7 and Uhrf1 control ubiquitination and stability of the maintenance DNA methyltransferase Dnmt1. J Cell Biochem. 2011;112(2):439–44.
59. Shamma A, Suzuki M, Hayashi N, Kobayashi M, Sasaki N, Nishiuchi T, et al. ATM mediates pRB function to control DNMT1 protein stability and DNA methylation. Mol Cell Biol. 2013;33(16):3113–24.
60. Cheng J, Yang H, Fang J, Ma L, Gong R, Wang P, et al. Molecular mechanism for USP7-mediated DNMT1 stabilization by acetylation. Nat Commun. 2015;6:7023.
61. Chen H, Ma H, Inuzuka H, Diao J, Lan F, Shi YG, et al. DNA damage regulates UHRF1 stability via the SCF(beta-TrCP) E3 ligase. Mol Cell Biol. 2013;33(6):1139–48.
62. Felle M, Joppien S, Nemeth A, Diermeier S, Thalhammer V, Dobner T, et al. The USP7/Dnmt1 complex stimulates the DNA methylation activity of Dnmt1 and regulates the stability of UHRF1. Nucleic Acids Res. 2011;39(19): 8355–65.
63. Zhang ZM, Rothbart SB, Allison DF, Cai Q, Harrison JS, Li L, et al. An Allosteric interaction links USP7 to Deubiquitination and chromatin targeting of UHRF1. Cell Rep. 2015;12(9):1400–6.
64. Gorrini C, Squatrito M, Luise C, Syed N, Perna D, Wark L, et al. Tip60 is a haplo-insufficient tumour suppressor required for an oncogene-induced DNA damage response. Nature. 2007;448(7157):1063–7.
65. Jha S, Vande Pol S, Banerjee NS, Dutta AB, Chow LT, Dutta A. Destabilization of TIP60 by human papillomavirus E6 results in attenuation of TIP60-dependent transcriptional regulation and apoptotic pathway. Mol Cell. 2010; 38(5):700–11.
66. Subbaiah VK, Zhang Y, Rajagopalan D, Abdullah LN, Yeo-Teh NS, Tomaic V, et al. E3 ligase EDD1/UBR5 is utilized by the HPV E6 oncogene to destabilize tumor suppressor TIP60. Oncogene. 2016;35(16):2062–74.
67. Zhang Y, Subbaiah VK, Rajagopalan D, Tham CY, Abdullah LN, Toh TB, et al. TIP60 inhibits metastasis by ablating DNMT1-SNAIL2-driven epithelial-mesenchymal transition program. J Mol Cell Biol. 2016;
68. Alhosin M, Omran Z, Zamzami MA, Al-Malki AL, Choudhry H, Mousli M, et al. Signalling pathways in UHRF1-dependent regulation of tumor suppressor genes in cancer. J Exp Clin Cancer Res. 2016;35(1):174.
69. Rothbart SB, Dickson BM, Ong MS, Krajewski K, Houliston S, Kireev DB, et al. Multivalent histone engagement by the linked tandem Tudor and PHD domains of UHRF1 is required for the epigenetic inheritance of DNA methylation. Genes Dev. 2013;27(11):1288–98.
70. Seo JS, Choi YH, Moon JW, Kim HS, Park SH. Hinokitiol induces DNA demethylation via DNMT1 and UHRF1 inhibition in colon cancer cells. BMC Cell Biol. 2017;18(1):14.

4.1.1 Supplementary Results

Interaction of the epigenetic integrator UHRF1 with the MYST domain of TIP60 inside the cell

Waseem Ashraf[1], Christian Bronner[2], Liliyana Zaayter[1], Tanveer Ahmad[1], Ludovic Richert[1], Mahmoud Alhosin[3,4], Abdulkhaleg Ibrahim[2,5], Ali Hamiche[2], Yves Mely[1] and Marc Mousli[1]

[1]Laboratoire de Biophotonique et Pharmacologie, UMR 7213 CNRS, Faculté de Pharmacie, Université de Strasbourg, 74, Route du Rhin, 67401 Illkirch Cedex, France. [2]Institut de Génétique et de Biologie Moléculaire et Cellulaire, INSERM U964 CNRS UMR 7104, Université de Strasbourg, Illkirch, France. [3]Department of Biochemistry, Faculty of Science, King Abdulaziz University, Jeddah, Saudi Arabia. [4]Cancer Metabolism and Epigenetic Unit, Faculty of Science, King Abdulaziz University, Jeddah, Saudi Arabia. [5]BioTechnology Research Center (BTRC), Tripoli, Libya.

Strength of interaction between GST-UHRF1 and His-TIP60 was also determined by varying the salt concentration in the *in-vitro* pull-down analysis. Increasing the salt concentration in the solution usually weakens the interaction between the two proteins. It was observed that there is a strong interaction between GST-UHRF1 and His-TIP60 protein and this interaction was strong enough to endure the 500 mM of NaCl in the interaction buffer (Figure 33).

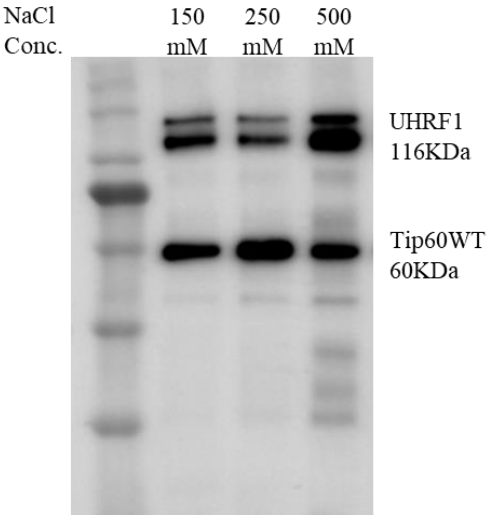

Figure 33: Western blot image of an in-vitro pull-down assay showing strong interaction between UHRF1 and TIP60 proteins which is stable up to 500 mM of NaCl.

Similarly, interaction between GST-UHRF1 and FLAG-MYST was also determined at different salt concentration and was found stable up till 1 M of NaCl concentration (Figure 34). This shows strong association between the UHRF1 and MYST domain of TIP60 protein.

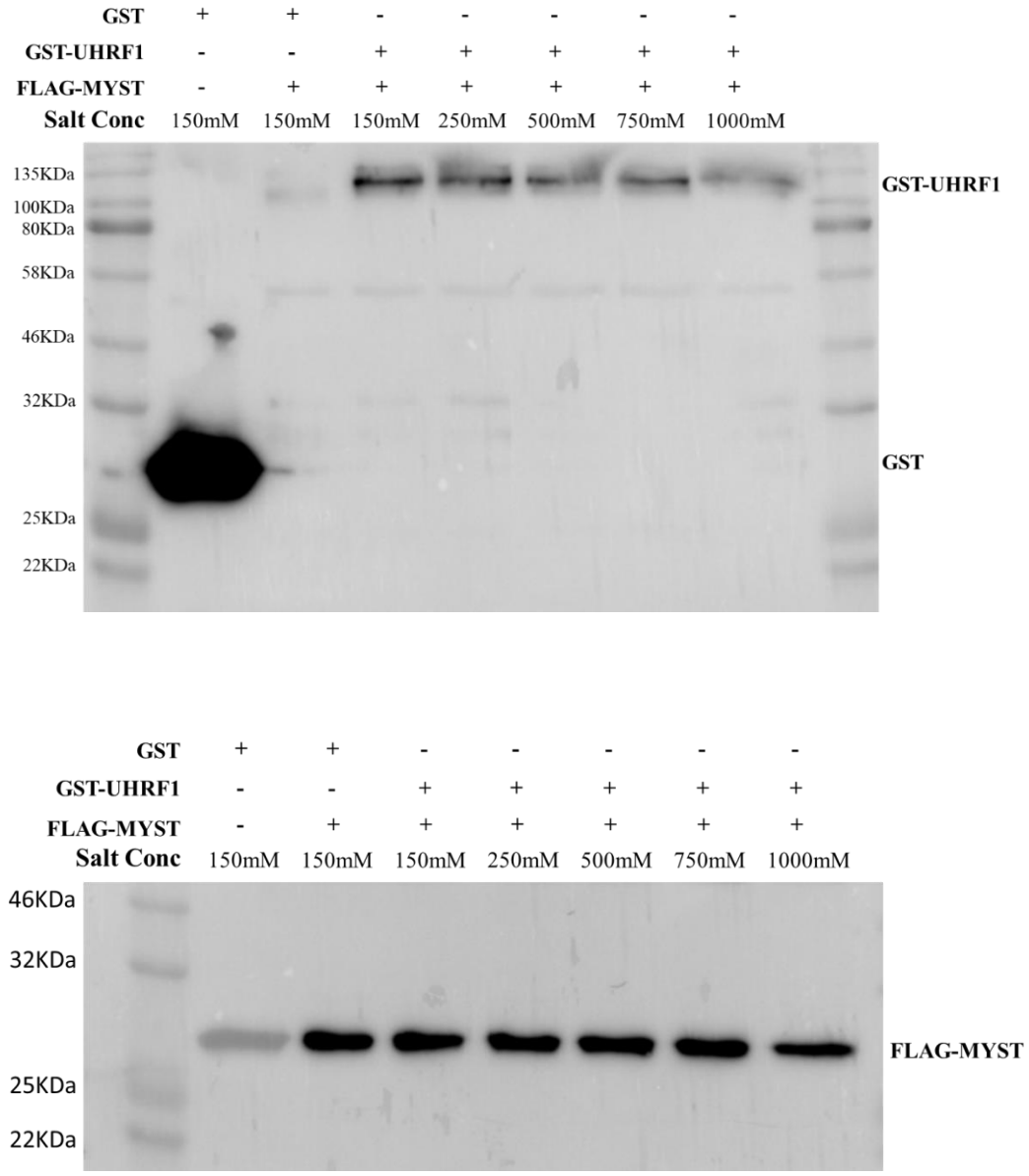

Figure 34: Interaction between UHRF1 and TIP60 at different salt concentration. Western blot analysis showing results of in-vitro pull down assays between GST-UHRF1 and His-TIP60 at different salt concentration. In upper image, blot is revealed by anti-GST antibody while the lower image represents the same blot revealed by anti-FLAG antibody.

Besides the other mutants of TIP60, we also prepared some mutants of TIP60 tagged with eGFP, affecting the localization of TIP60 protein inside the cells (Figure 35). TIP60 was predicted to have two nuclear localization signals (NLS) in its structure by PSORT II prediction program (Hass and Yankner, 2005). One nuclear localization signal PGRKRKS (NLS1) lies before the MYST domain at position 184 while the second signal RKGTISFFEIDGRKNKS (NLS2) starts at 295 and lies within the MYST domain of TIP60.

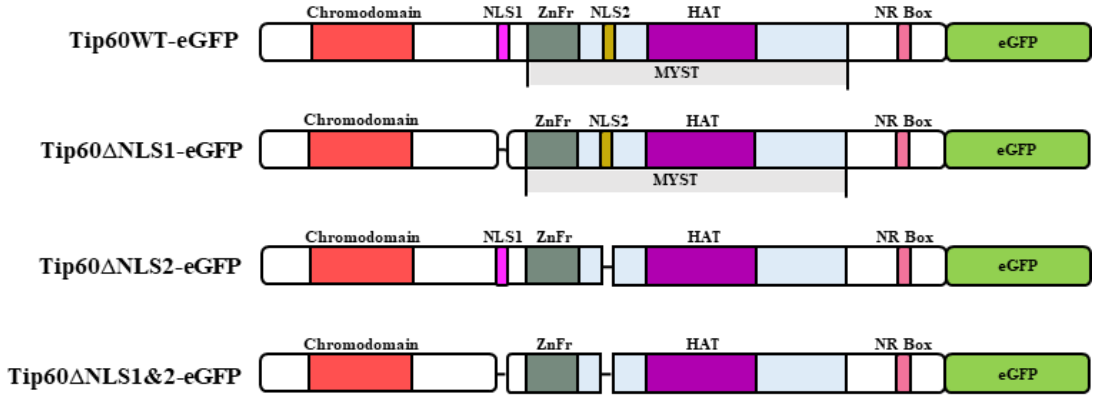

Figure 35: Schematic diagram of mutants of TIP60 affecting its nuclear localization.

Through confocal microscopy, we found that NLS1 is playing a major role in localization of the TIP60 protein to the nucleus of HeLa cells (Figure 36). Deletion of NLS1 resulted in distribution of the protein in both cytoplasm and nucleus of the HeLa cells. While deletion of other localization signal NLS2, did not affect the localization of the expressed eGFP tagged TIP60 protein. When both NLS sequences, *i.e.,* NLS1 & 2 were removed from the structure of TIP60 protein, it specifically localized to the cytoplasm and did not traverse to the nucleus of the cells (Figure 36).

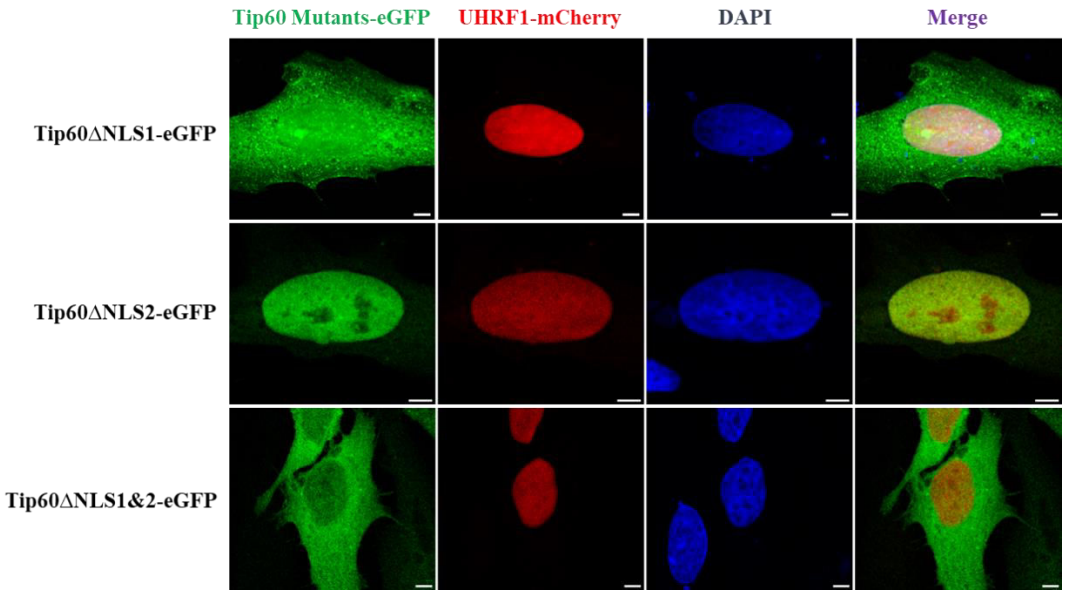

Figure 36: Confocal microscopy image showing localization of different mutants of TIP60 protein. White bar indicates size of 5 µm.

By using FLIM, we also analyzed the interaction of these mutants with UHRF1-mCherry, which specifically localize to the nucleus of cells. There was no significant change in the lifetime of eGFP in these mutants when transfected with UHRF1-mCherry as compared to the controls (Figure 37).

This is probably because of the change in localization of these proteins. TIP60ΔNLS1-eGFP and TIP60ΔNLS1&2-eGFP localized to cytoplasm where there was no UHRF1-mCherry and because of that, there was no global decrease in lifetime of eGFP. TIP60ΔNLS2-eGFP localized to the nucleus of HeLa cells but deletion of this fragment might have resulted in change in three-dimensional structure of the protein, which affected its interaction with UHRF1-mCherry in the nucleus of cells.

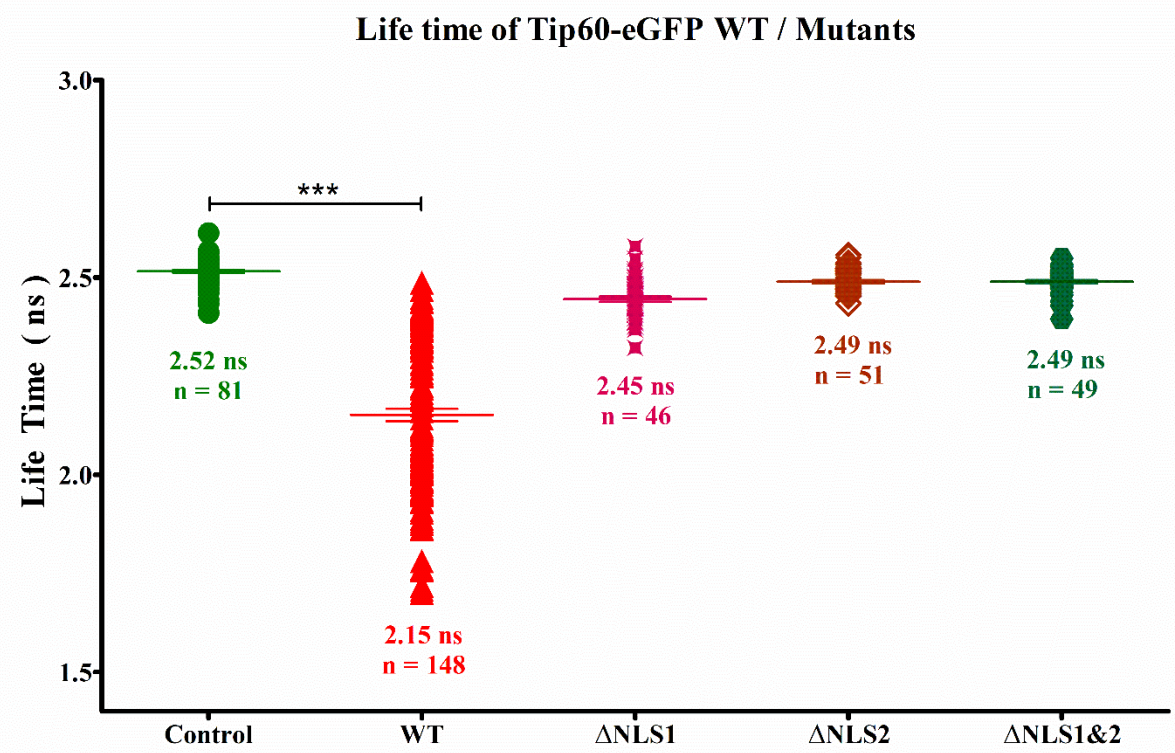

Figure 37: Interaction between Tip60-eGFP WT/mutants in FRET-FLIM analysis. Life time distribution of Tip60-eGFP (●), Tip60 WT-eGFP + UHRF1-mCherry co-transfected cells (▲), Tip60 ΔNLS1-eGFP + UHRF1-mCherry co-transfected cells (✖), Tip60 ΔNLS2-eGFP + UHRF1-mCherry co-transfected cells (◈) and Tip60 ΔNLS1&2-eGFP + UHRF1-mCherry co-transfected cells (⬣). Values are means ± SEM from three to five independent experiments. For statistical analysis, a Student's t-test was performed (*** p>0.001).

ADDITIONAL RESULTS

4.2 Interaction of TIP60 and UHRF1 at DNA damage area

4.2.1 Introduction

Many studies have stated the role of TIP60 in DNA damage response pathways where it is playing multiple roles to tailor the DNA damage response towards the HR pathway. TIP60 acetylates histones (H4K16) and (H2AK15) and prevents the loading of proteins such as 53BP1 which initiate the repair by the NHEJ pathway (Tang *et al.*, 2013, Jacquet *et al.*, 2016). TIP60 also acetylates H2AX at lysine 5 to promote the chromatin relaxation at the site of DNA damage, which facilitates the DNA repair mechanisms (Ikura *et al.*, 2007, Ikura *et al.*, 2015). Besides acetylating histones, TIP60 also activates other proteins through acetylation like ATM, which further recruits and activates other proteins (like NBS, CHK2, p53 and SMC1) to initiate the signaling cascade involved in DNA damage repair (Sun *et al.*, 2005). Thus, all this data present TIP60 as a key player in DNA damage response pathways.

Recently, role of UHRF1 has also been identified in the DNA damage response pathways (Liang *et al.*, 2015, Tian *et al.*, 2015, Zhang *et al.*, 2016a). In case of interstrand crosslinks it recognizes the anomalies in DNA structure through SRA domain and later recruits proteins such as FANCD2, ERCC1 and MUS81 to repair these damages (Liang *et al.*, 2015, Tian *et al.*, 2015). UHRF1 role in DSBs have also been identified where it is recruited to the site of damage by BRCA1 and facilitates the repair by HR pathway (Zhang *et al.*, 2016a). Since both TIP60 and UHRF1 are involved in DNA damage responses we decided to visualize the localization of both the proteins together at the site of DNA damage.

4.2.2 Results

4.2.2.1 Localization of endogenous UHRF1 and TIP60 to the site of DNA damage

First, we created localized double strand breaks as described in protocol by Suzuki *et al* (Suzuki *et al.*, 2011) and checked the localization of endogenous UHRF1 at these damage spots with reference to gamma-H2AX which is a well-known marker for DNA double-strand breaks. Briefly, HeLa cell were incubated with BrdU to make them sensitive to DNA damage and were then covered by isopore hydrophilic membrane with a pore size of 5 µm and irradiated by UVC lamp to induce the DNA damage at the sites exposed through the pores. The cells were then

fixed at different time intervals after the exposure and were labeled with fluorescent tagged antibodies to see the localization of proteins.

In our results we found that UHRF1 quickly accumulated at the sites of DNA damage indicated by the labeling of γH2AX (DNA damage marker) (Figure 38). It concentrated to the damage area within five minutes after the exposure to UVC (Figure 38), showing UHRF1 as one of the quick response proteins in the DNA damage pathway. Endogenous UHRF1 stayed at the of DNA damage site evidently for 15 and 30 minutes after the induction of damage as seen in (Figure 38). However, the accumulation of UHRF1 at these sites faded away after one hour of the UV exposure while the γH2AX marker labeling remained intense at these spots with the passage of time (indicated by white arrows, Figure 38).

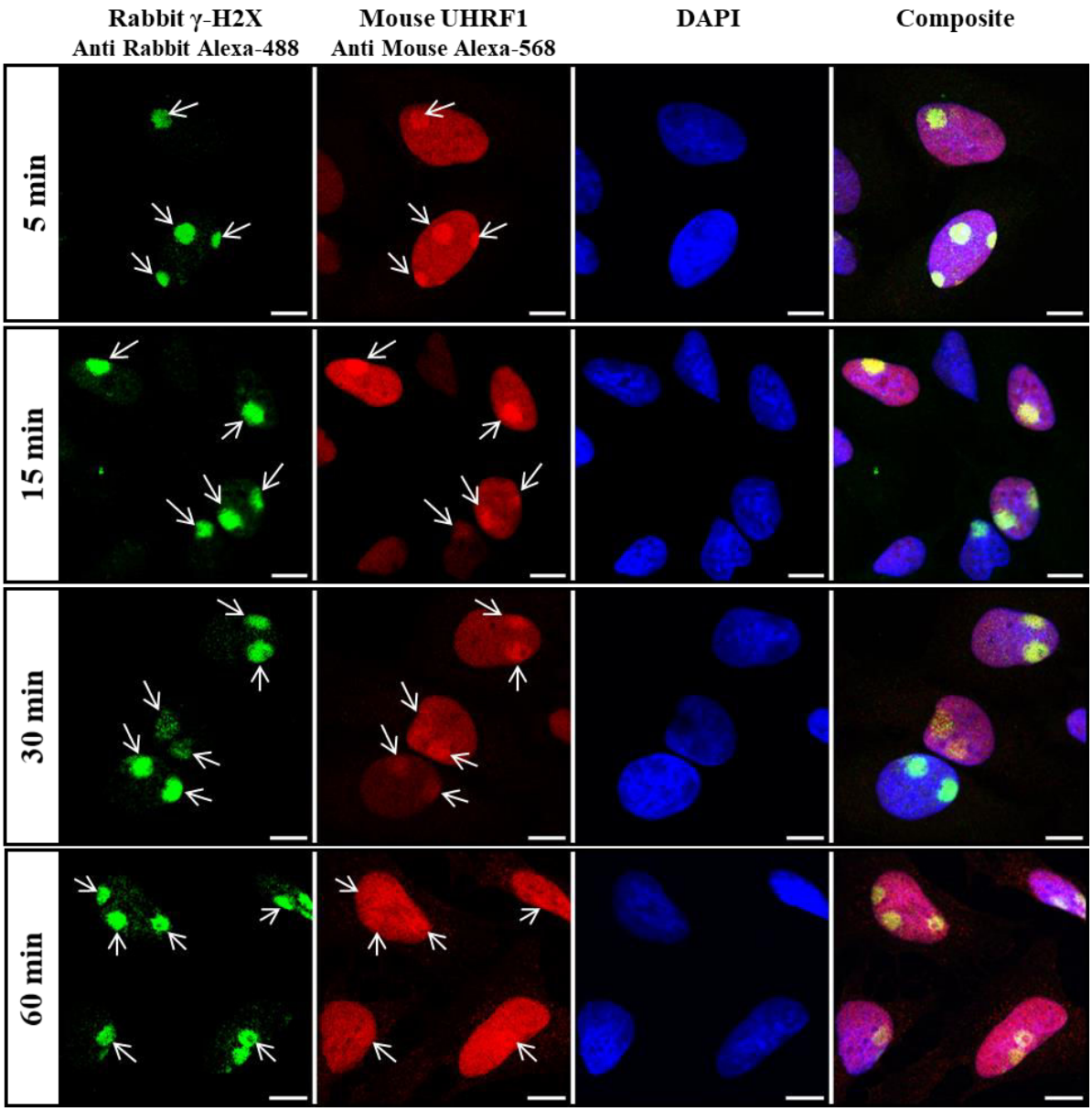

Figure 38: Confocal images showing localization of endogenous UHRF1 at the DNA damage spots. DSBs were induced in the HeLa cells by using UVC radiation. Cells were fixed at different time intervals after the induction of damage and subsequently labeled with specific antibodies to see the localization of proteins at DNA damage spots. Left panel of figure indicates the time after the induction of DNA damage when the cells were fixed. Green panel shows the fluorescence labeling of γH2AX, a well-known DNA damage marker with Alexa-488 conjugated secondary antibody. Red panel shows fluorescent labeling of endogenous UHRF1 with Alexa-568 conjugated secondary antibody. Blue panel is staining of nucleic acid by DAPI and composite is the merge of all the panels. White bar indicates size of 10 µm.

We repeated the same experiment with labeling of TIP60 besides UHRF1 to investigate the roles of both proteins together in the DNA damage response. It was observed that TIP60 also accumulated at the sites of DNA damage however, the staining of TIP60 at these spots varied in comparison to UHRF1. TIP60 did not localize as intensely as UHRF1 to all the DNA damage spots within 5 minutes predicting a relatively slow response of TIP60 as compared to UHRF1 (indicated by white arrows in 5 min panel, Figure 39). But unlike UHRF1, TIP60 stayed at the DNA damage spot for longer time than UHRF1. TIP60 staining showed that its accumulation at the damage spot was still identifiable after 1 hr while UHRF1 staining revealed that it is not concentrated on these spots after 1 hr but is rather homogenously distributed in the nucleus of cells (indicated by white arrows in 60 min panel, Figure 39).

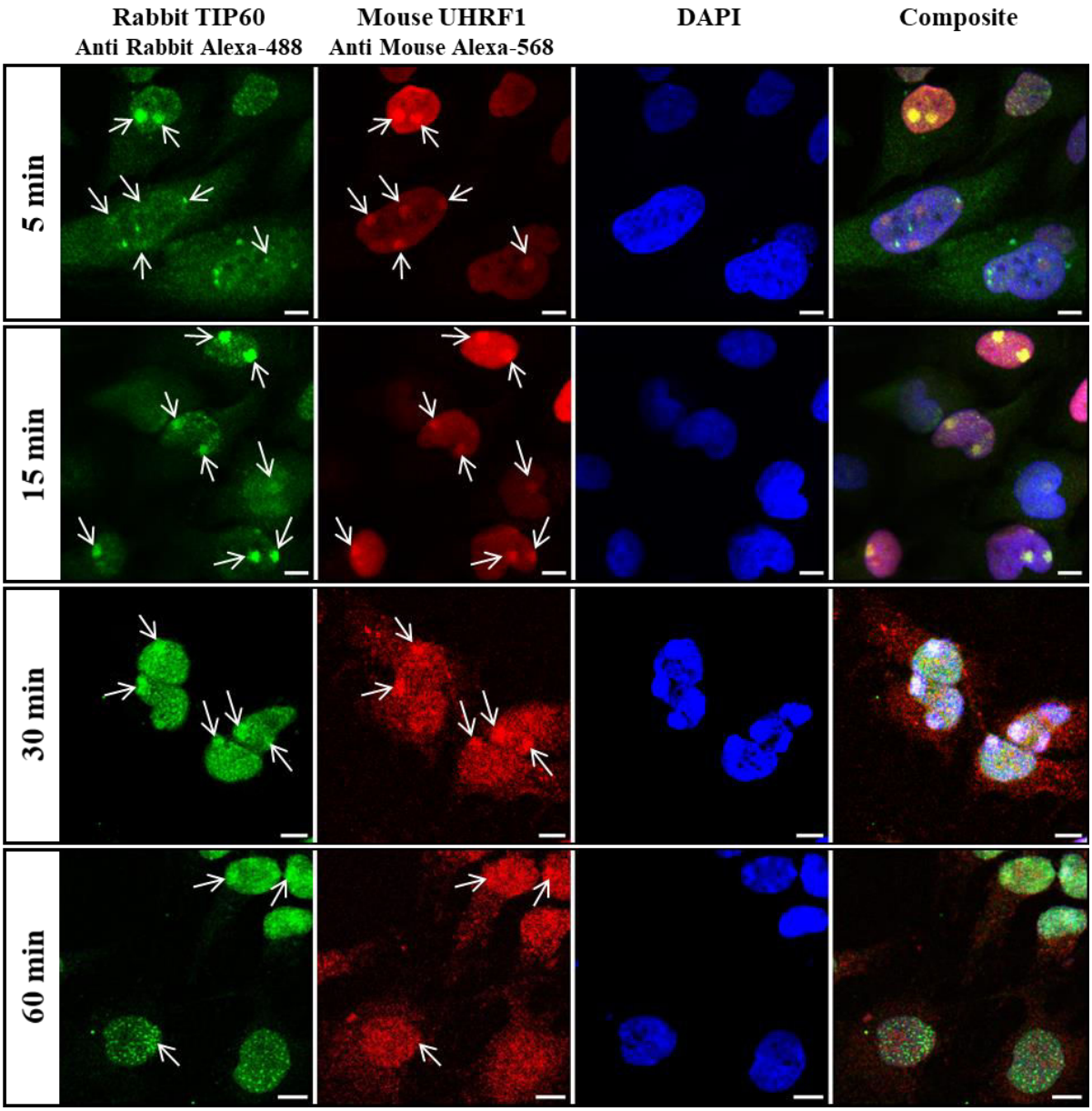

Figure 39: Confocal images showing localization of endogenous TIP60 with UHRF1 at the DNA damage spots. DSBs were induced in the HeLa cells by using UVC radiation. Cells were fixed at different time intervals after the induction of damage and subsequently labeled with specific antibodies to see the localization of proteins at DNA damage spots. Left panel of figure indicates the time after the induction of DNA damage when the cells were fixed. Green panel shows the fluorescent labeling of endogenous TIP60 with Alexa-488 conjugated secondary antibody. Red panel shows fluorescent labeling of endogenous UHRF1 with Alexa-568 secondary antibody. Blue panel is staining of nucleic acid by DAPI and composite is the merge of all the panels. White bar indicates size of 10 µm.

4.2.2.2 Localization of exogenous TIP60-eGFP and UHRF1-mCherry at the site of DNA damage

To further visualize the localization of UHRF1 and TIP60 at DNA damage spot we used live cell imaging to know the dynamics of these proteins at the damage site of chromatin. For this purpose, we transfected the cells with TIP60-eGFP and UHRF1-mCherry and induced double strand break along a straight line in the co-transfected cells with UV laser as described previously (Beck *et al.*, 2014). Localization of fluorescent-tagged TIP60 and UHRF1 proteins was monitored at the site of damage by fluorescent microscopy. Fluorescent intensity at the site of damage was determined and compared to the intensity before the induction of damage to quantify the localization of proteins at these spots.

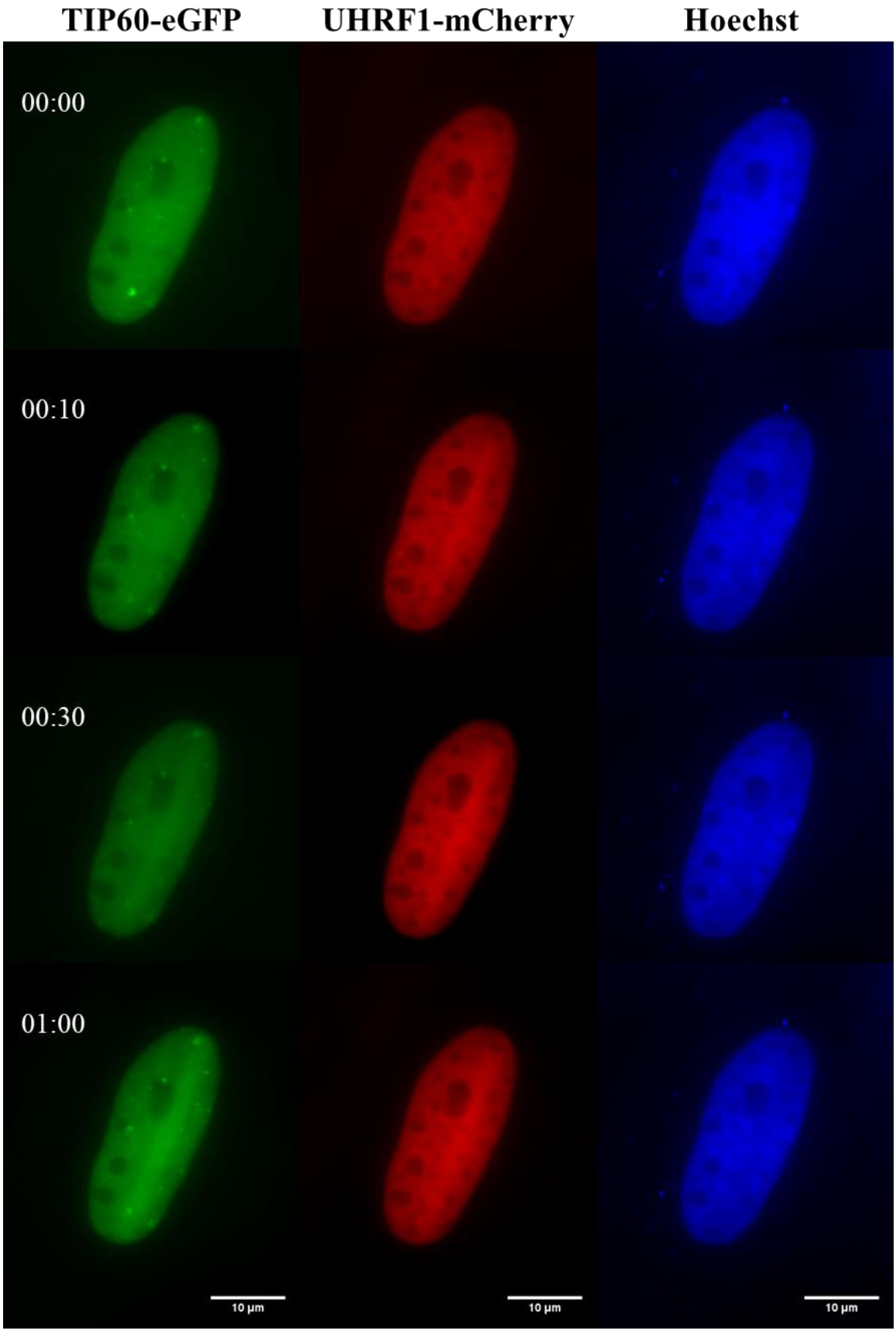
TIP60-eGFP
UHRF1-mCherry
Hoechst
00:00
00:10
00:30
01:00
10 µm
10 µm
10 µm

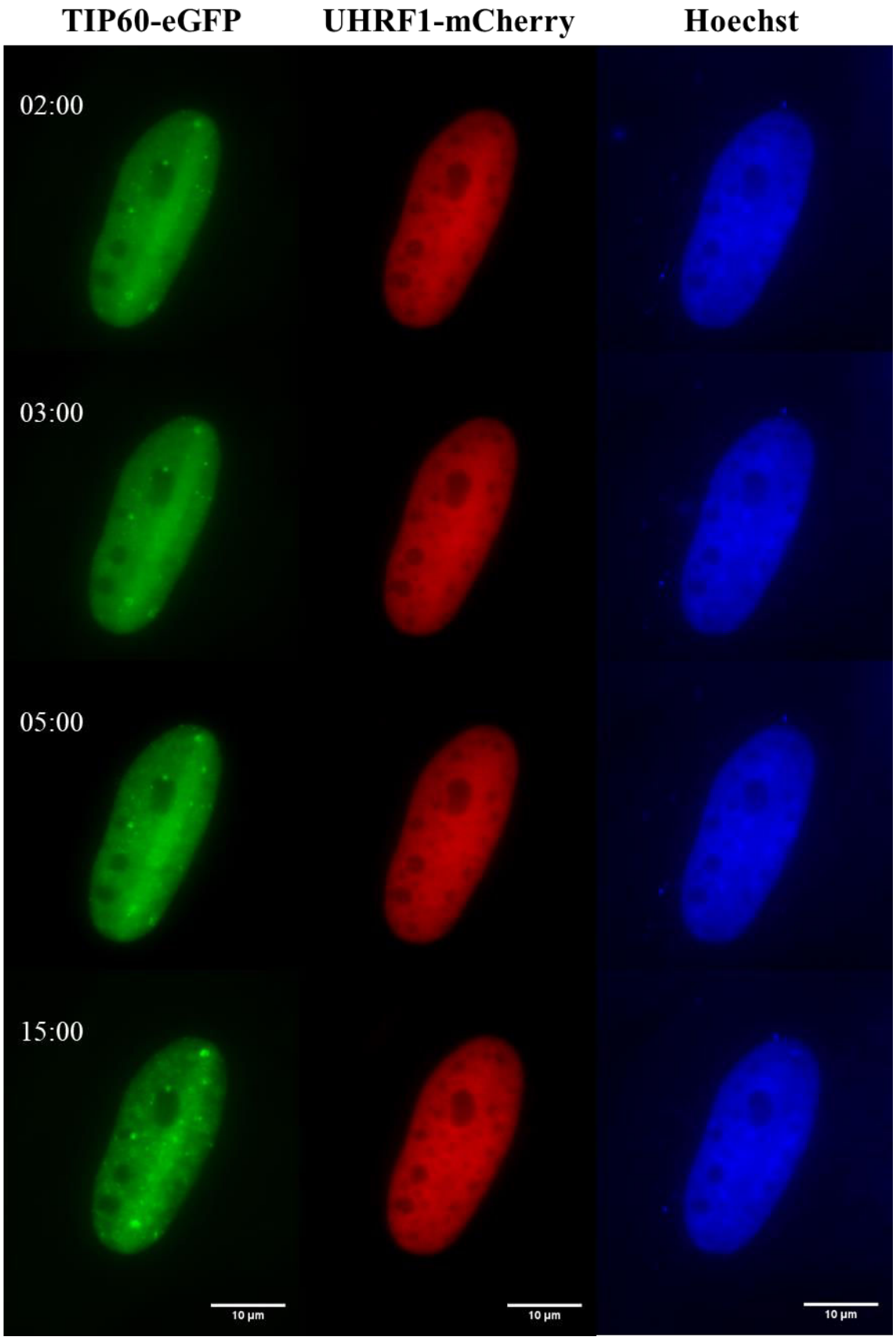
TIP60-eGFP
UHRF1-mCherry
Hoechst
02:00
03:00
05:00
15:00
10 µm
10 µm
10 µm

Figure 40: Localization of exogenous TIP60-eGFP and UHRF1-mCherry at the site of DNA damage. DNA damage is induced along a straight line by UV laser in the live co-transfected cells and dynamics of protein are monitored by taking images at short time intervals. TIP60-eGFP is indicated in green and UHRF1-mCherry in red while blue color indicates Hoechst staining of chromatin in nucleus. White bar indicates size of 10 µm.

With live cell imaging, similar dynamics of both proteins were observed at the DNA damage site as observed in fixed cells with endogenous proteins. Both proteins accumulated to the site of damage within 30 seconds after the DNA damage induction (Figure 40). Again, UHRF1 was quick in response as UHRF1-mCherry concentrated to the sites of damage within 10 seconds while TIP60-eGFP was relatively slow and its noticeable accumulation started to appear within 30 seconds after the induction of damage (Figure 40). Quantification of the relative fluorescent intensities of these exogenously expressed proteins confirmed the results seen with the endogenous proteins. UHRF1 was recruited to the sites of damage quickly and stayed for lesser time as compared to TIP60 (Figure 41). UHRF1-mCherry accumulation at the site of damage intensified within seconds of damage and later reduced to the basal levels at the end of 15 minutes. TIP60-eGFP on the other hand, appeared relatively late at the site of damage as compared to UHRF1 but it became more concentrated with the passage of time and remained intensified till the end of 15 minutes (Figure 41).

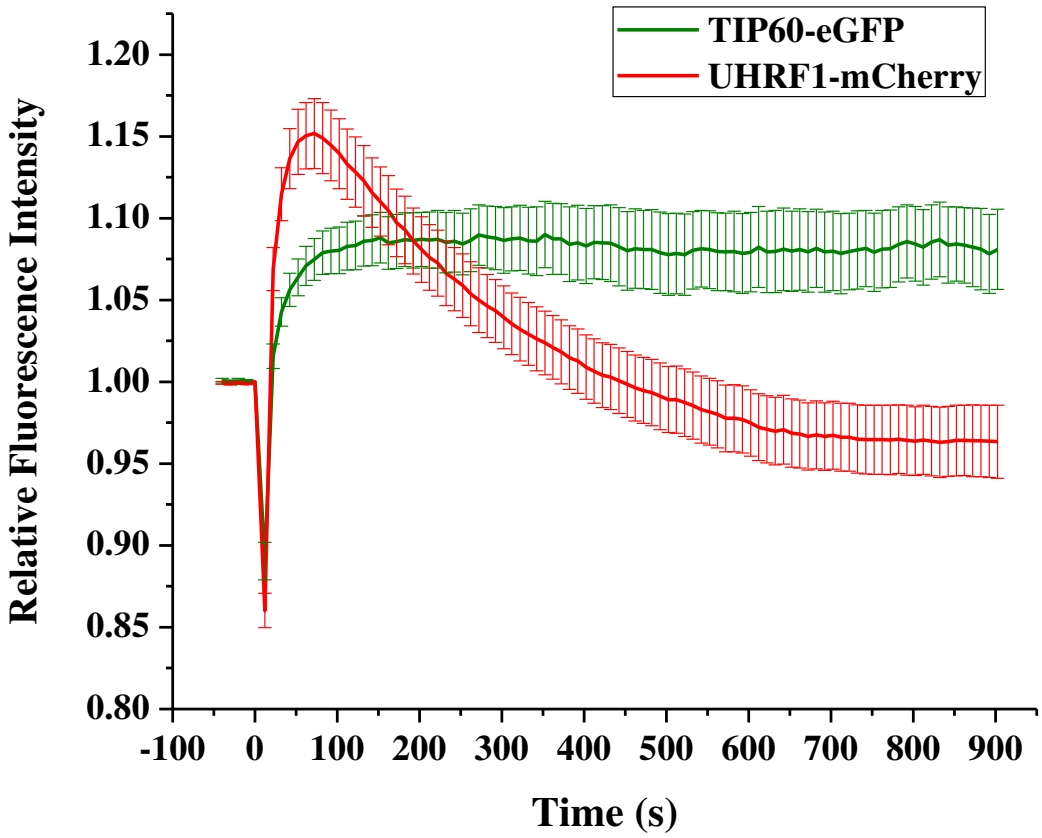

Figure 41: Dynamics of TIP60-eGFP and UHRF1-mCherry at the site of DNA damage. Graph shows relative fluorescence intensities of exogenously expressed TIP60-eGFP and UHRF1-mCherry at the site of damage measured before and after the induction of DNA damage plotted against time. Time scale is represented in seconds and zero value indicates the time when DNA damage was induced. Graph represents the average curve obtained from seventeen individual events along with ±SEM values.

4.2.3 Discussion

These results show an interesting behavior of UHRF1 and TIP60 in response to DNA damage. Early recruitment of UHRF1 to the site of DNA damage suggest its role as "detector" protein. It is well-known that UHRF1 is in close contact with chromatin during the S phase of cell cycle. It identifies the methylated cytosine on parent strand through its SRA domain and later recruits the DNMT1 to the newly formed daughter strand to maintain the DNA methylation patterns (Bostick *et al.*, 2007, Sharif *et al.*, 2007). Similarly, SRA domain of UHRF1 also identifies the interstrand crosslinks in the damaged DNA and enables the UHRF1 to recruit the specialized "effector" proteins to repair these anomalies (Liang *et al.*, 2015, Tian *et al.*, 2015). Our results predict that UHRF1 might be playing a similar role in detection of DSBs and may be bringing the TIP60 to the site of damage, which has well established role in DNA damage response. It

is also interesting to note that TIP60 favors the DSB repair by HR pathway, which dominates during the S and G2 phase of cell cycle (Jacquet *et al.*, 2016). Recently, UHRF1 has also been linked to promote the repair of DSBs by HR pathway (Zhang *et al.*, 2016a), which suggests that these proteins might be working in coherence to facilitate the repair of DSBs by HR pathway.

It is also noteworthy that TIP60 stays for longer time at the DNA damage sites as compared to UHRF1. Since TIP60 along with its complex is involved in various of steps of DNA damage repair this might explain the longer stay of TIP60 at these sites. In our results, we have also observed that increased levels of TIP60 downregulate UHRF1 in cells so increased accumulation of TIP60 at these spots might also be playing a role in quick eviction of UHRF1 from these sites.

4.3 Consequences of TIP60 overexpression in HeLa Cells

4.3.1 Introduction

TIP60 is considered to be a tumor suppressive protein as it plays a vital role in maintaining the integrity of genome and hinders the mechanisms involved in the malignant transformation of the cells (Gorrini *et al.*, 2007, Liu and Sun, 2011). In case of genotoxic insults, it modulates the DNA repair and ensures the genomic stability during the replication and other key cellular process. However, if genome suffers an irreparable damage, TIP60 activates molecular mechanisms to eliminate the rogue cells by halting their proliferation or inducing apoptosis (Legube *et al.*, 2004, Sykes *et al.*, 2006, Tang *et al.*, 2006). Mechanistically, TIP60 can activate p53 in acetylation dependent or independent manner, which in turn can lead to induction of apoptosis or cell cycle arrest respectively (Dai *et al.*, 2013). TIP60 also prevents oncogenesis by blocking the activity of proto-oncogenic transcription factors such as c-MYB and STAT3 and also hinders the epithelial to mesenchymal transition, a vital step in metastasis and invasion of transformed cells (Xiao *et al.*, 2003, Zhao *et al.*, 2012, Zhang *et al.*, 2016b).

Down regulation of TIP60 has been observed in many cancers and low levels of TIP60 are corelated with increase in proliferative and metastatic potential of tumors along with poor prognosis of disease (ME *et al.*, 2006, Gorrini *et al.*, 2007, Bassi *et al.*, 2016). TIP60 have been extensively studied in relation to human papillomavirus (HPV) induced cervical cancers where HPV oncogenic E6 protein destabilizes TIP60 protein to bypass TIP60-p53 mediated apoptosis and promotes malignant transformation (Jha *et al.*, 2010, Subbaiah *et al.*, 2016). HPV genome is integrated in the HeLa cells and constitutively expresses HPV18 E6 and E7 oncoproteins leading to lower levels of TIP60 and p53 in these cells (Jha *et al.*, 2010).

In our previous experiments, we overexpressed TIP60 in HeLa cervical cancer cells and observed downregulation of its interacting partners UHRF1 and DNMT1 proteins. It has been shown previously that UHRF1 is upregulated in cancers and it promotes oncogenesis by blocking the action of different tumor suppressor genes (Ashraf *et al.*, 2017b). Elevated levels of UHRF1 either repress the expression of different tumor suppressor genes via the promoter hypermethylation or interfere in the downstream signaling pathways initiated by these TSGs. Many studies have reported that downregulation of UHRF1 in cancer cells can lead to re-activation of tumor suppressor genes and inhibition of proliferation by induction of growth

arrest and apoptosis. So, therefore we decided to further study the effects of TIP60 overexpression in these cells.

4.3.2 Results

4.3.2.1 Effect of TIP60 overexpression on p73 and p53 tumor suppressor proteins.

The p53 is one of the key tumor suppressor proteins activated by TIP60 in response to stress signals. UHRF1, through its physical interaction with TIP60 is known to perturb the TIP60-mediated activation of p53 protein to override the mechanisms suppressing proliferation in cancer cells (Dai *et al.*, 2013). As UHRF1 levels are downregulated by TIP60 overexpression, we wanted to analyze the effect of this downregulation on interplay between TIP60 and p53.

It is also reported that p73, another well-known tumor suppressor gene regulates UHRF1 in cancer cells. Natural polyphenolic compounds (such as thymoquinone) induce p73 expression in cancer cells, which in turn plays a role in downregulation of UHRF1 (Alhosin *et al.*, 2010).

So, in order to decipher the mechanism of UHRF1 downregulation and its effect on TIP60-p53 pathway, we studied the effect of TIP60 overexpression on p53 and p73 proteins. It was observed that p73 was significantly upregulated in HeLa cells with TIP60-eGFP expression as compared to cells expressing eGFP alone or treated with transfecting agent (Figure 42 A, C). While in comparison to p73, there was no significant change in expression of p53 tumor suppressor gene in HeLa with overexpression of TIP60 (Figure 42 A, B).

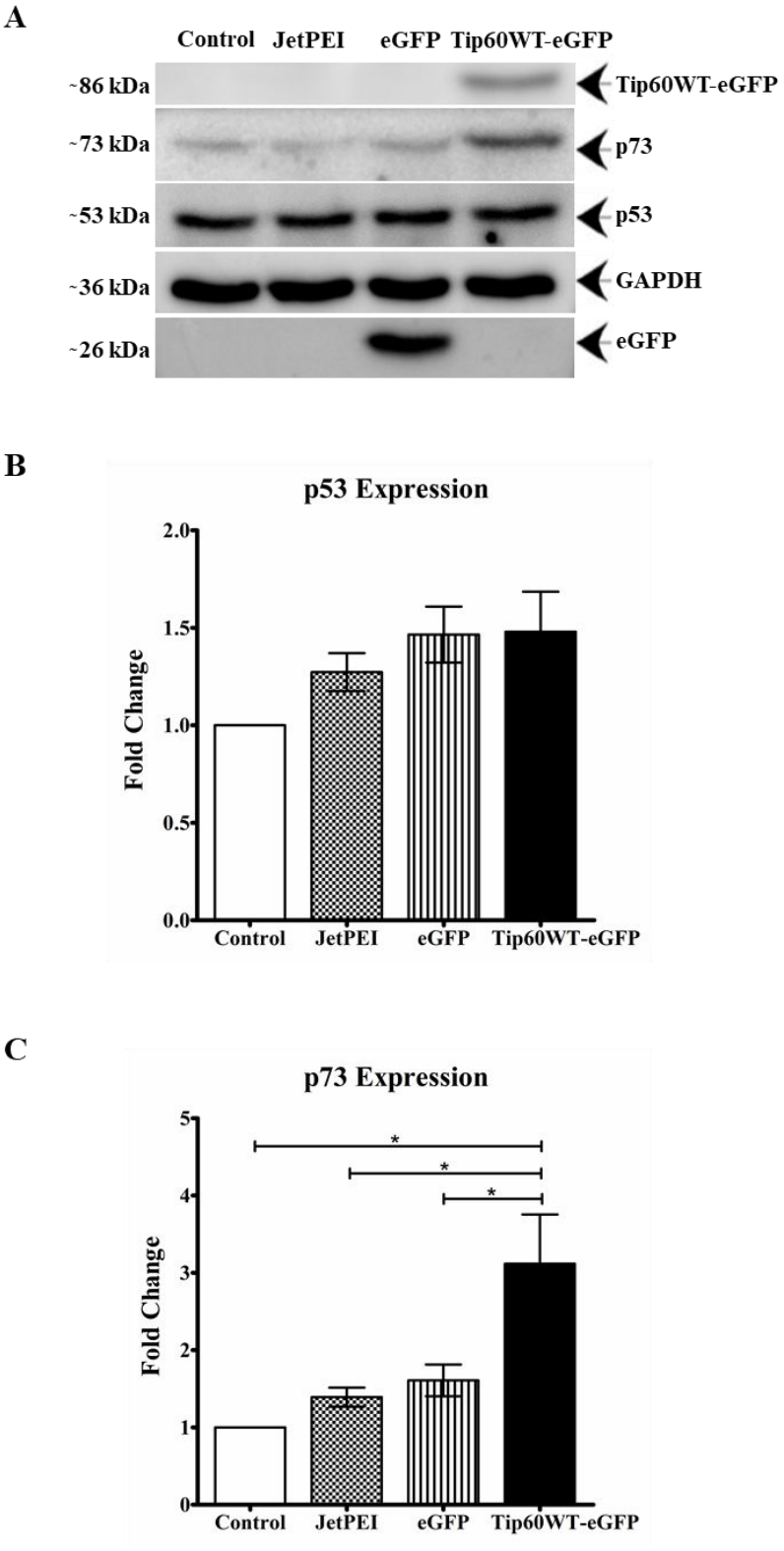

Figure 42: Effect of TIP60 overexpression on p53 and p73. A, Western blot showing expression of p53 and p73 in control, JetPEI treated, eGFP and TIP60 transfected HeLa cells. B, Analysis of TIP60-eGFP expression on p53. C, Analysis of TIP60-eGFP

expression on p73. Results indicated are from five independent experiments which are analyzed statistically by Student's t-test (* $P < 0.05$).

4.3.2.2 Effect of TIP60 overexpression on p53, p73 mediated apoptosis:

Next, we decided to study the effect of TIP60 overexpression on the downstream signaling pathways of p53 and p73 proteins. Both tumor suppressor proteins can induce apoptosis or cell cycle arrest in cancer cells upon activation.

To study the induction of apoptosis, we analyzed the cells transfected with TIP60-eGFP by FACS and compared it to the controls HeLa cells treated with transfecting agent in a similar way. Annexin- V-iFluor™ 350 conjugate and PI staining of cells helped us to detect the cells in early and late phases of apoptosis and also differentiated the cells undergoing necrosis. Our flow cytometry results showed that TIP60 overexpression reduced the viability of transfected cells from 88% in control to the 54% in TIP60-eGFP transfected samples. This overall decrease of 34% in cell viability after 24 hr of TIP60-eGFP transfection was also accompanied with 12% and 16% increase in early and late apoptotic cells fractions respectively (Figure 43).

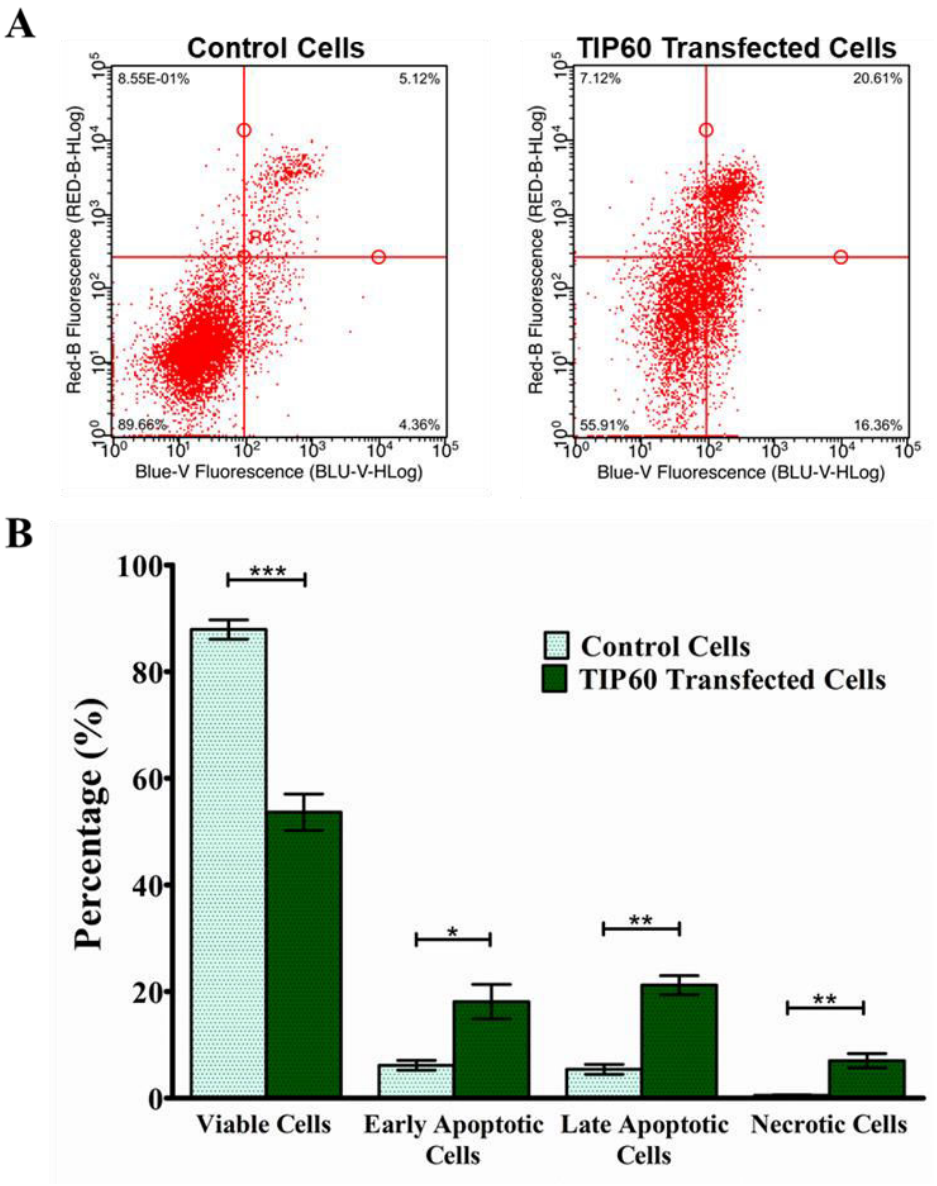

Figure 43: TIP60 overexpression induces apoptosis in HeLa cells. A, FACS analysis examining Annexin V-iFluor™ 350 and PI labeling in control HeLa cells (treated with jetPEI in identical manner) to cells transfected with TIP60-eGFP for 24 hr. B, Graph represents average values from three independent experiments which were statistically analyzed by Student's t-test (* $P < 0.05$, ** $P < 0.01$, *** $P < 0.001$).

To reaffirm these results, total cells collected in TIP-eGFP transfected samples were segregated into TIP60-eGFP positive and TIP60-eGFP negative cells by the presence eGFP fluorescence and the results were reanalyzed. This helped us to specifically determine the induction of apoptosis in cells overexpressing TIP60-eGFP as compared to the cells not expressing TIP60-eGFP in the same samples. It was revealed that average viability of TIP60-eGFP expressing cells was decreased by 39% as compared to the cells not expressing TIP60-eGFP while the

average transfection efficiency of TIP60-eGFP was 61% in these experiments (Figure 44). Cells in early and late phases of apoptosis were also increased by 20% and 19% respectively in TIP60 overexpressing cells, which is comparable to the global results (Figure 44).

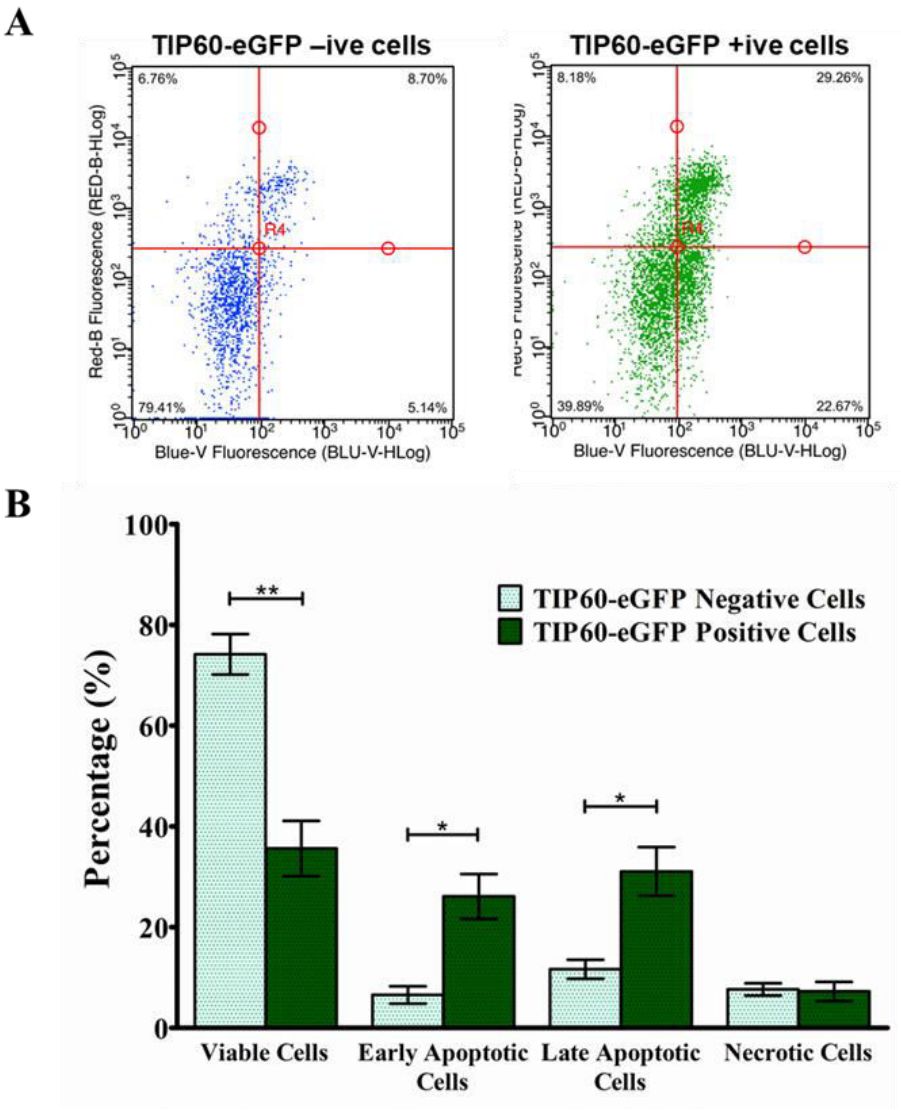

Figure 44: TIP60 overexpression induces apoptosis in HeLa cells. A, FACS analysis examining Annexin V-iFluor™ 350 and PI labeling in TIP60-eGFP negative cells to TIP60-eGFP positive cells in TIP60-eGFP transfected samples. B, Graph represents average values from three independent experiments which were statistically analyzed by Student's t-test (* $P < 0.05$, ** $P < 0.01$, *** $P < 0.001$).

p53 and p73 mediated apoptosis is generally attributed to activation of mitochondria dependent apoptotic pathway by transactivation of pro-apoptotic proteins (e.g. BAX protein) and downregulation of pro-survival proteins (e.g. BCL2). Therefore, we analyzed the expression of these proteins in TIP60-eGFP transfected samples and comparted it to control, JetPEI treated

or eGFP transfected HeLa cells. In our results, we observed that TIP60 overexpression led to induction of BAX protein and simultaneously downregulated the antiapoptotic BCL2 protein confirming the activation of apoptosis in the downstream signaling pathway (Figure 45).

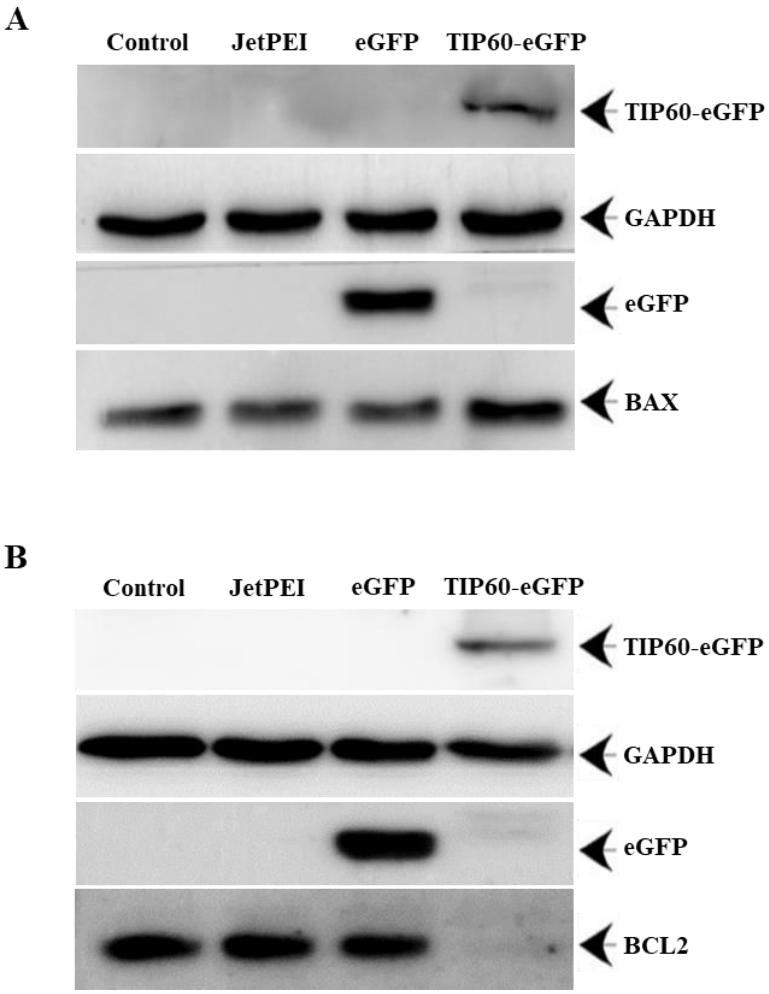

Figure 45: Effect of TIP60 overexpression on BAX and BCL2 proteins. A, Western blot image showing effect of TIP60 overexpression on BAX protein. B, Western blot image showing effect of TIP60 overexpression on BCL2 protein.

To further confirm the induction of apoptosis by TIP60-eGFP transfection, we checked the activation of caspase 3 and PARP in these cells. Western blot analysis of the protein collected from the samples revealed that indeed, TIP60-eGFP overexpression induced the activation of caspase 3 from precursor pro-caspase 3 protein, which in turn activated the cleavage of PARP to induce apoptosis (Figure 46).

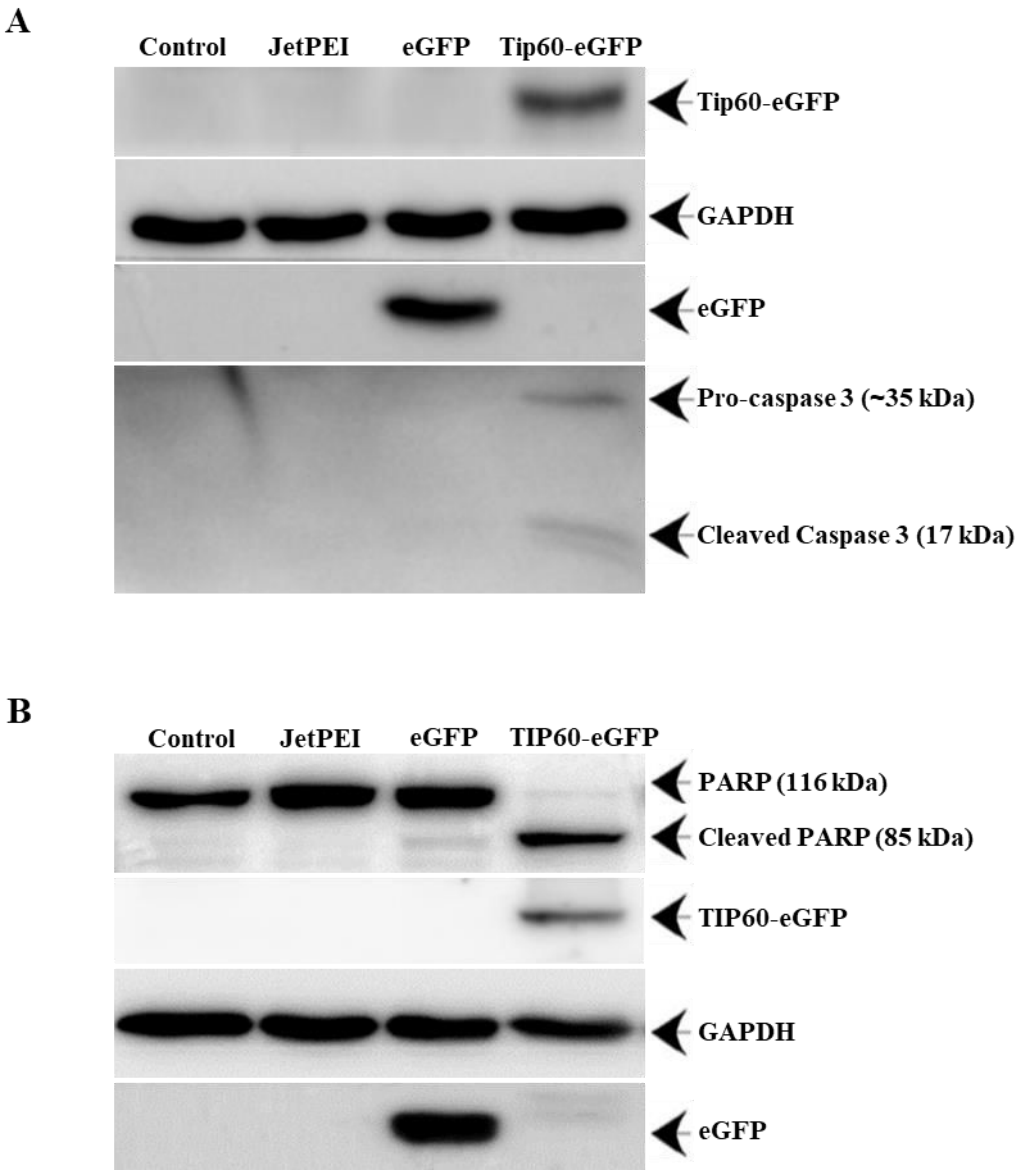

Figure 46: Effect of TIP60 overexpression on caspase 3 and PARP1 activation. A, Western blot image showing caspase 3 activation in response to TIP60 overexpression in HeLa cells. B, Western blot image showing effect of TIP60 overexpression on PARP activation.

4.3.2.3 Effect of TIP60 on p53 mediated cell cycle arrest:

Activation of p53 and p73 can also lead to cell cycle arrest and inhibit the proliferation of cancer cells by induction of p21 pathway. To check the induction of p21 protein, we analyzed its levels through western blot analysis and found a decrease in p21 levels in samples transfected with TIP60-eGFP plasmid as compared to control. However, this change was not significant when compared to HeLa cells treated with jetPEI or transfected with eGFP alone (Figure 47).

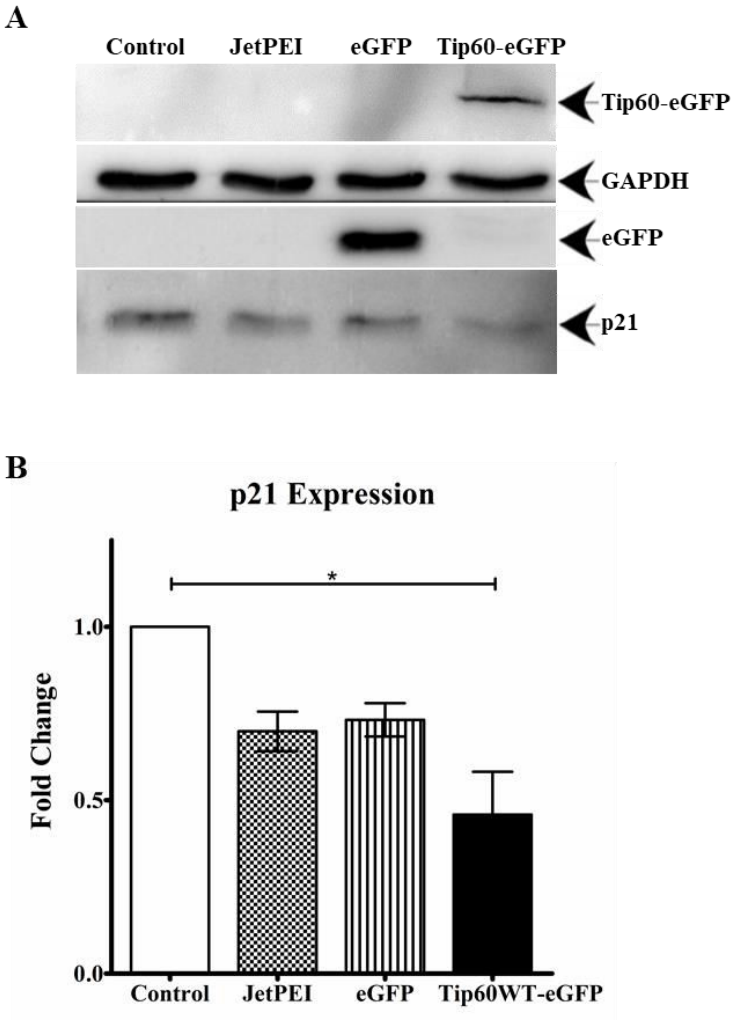

Figure 47: Effect of TIP60 overexpression on p21. A, Western blot showing expression of p21 in control, JetPEI treated, eGFP and TIP60 transfected HeLa cells. B, Statistical analysis of TIP60-eGFP expression on p21. Results indicated are from three independent experiments analyzed statistically by Student's t-test (* $P < 0.05$).

Moreover, cell cycle analysis was also done by using FACS to study the effect of TIP60 overexpression on proliferation of HeLa cells and it was revealed that cell cycle was not affected by the overexpression of TIP60-eGFP in HeLa cells (Figure 48).

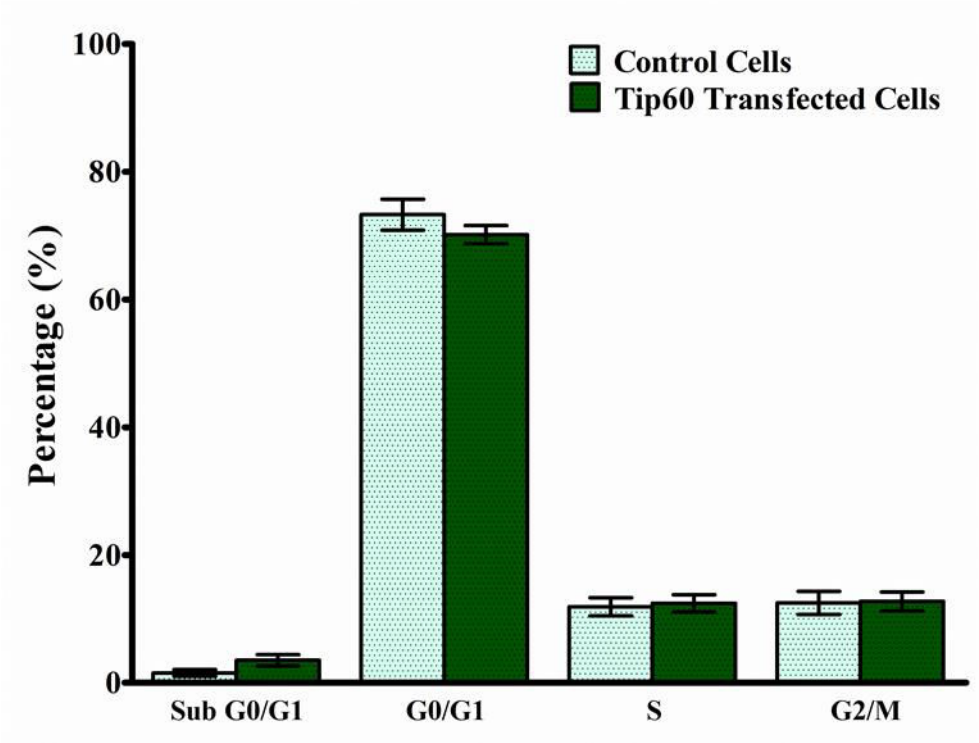

Figure 48: Effect of TIP60 overexpression on cell cycle distribution of HeLa cells.

These results conclude that overexpression of TIP60-eGFP induced apoptosis in HeLa cells by the activation of p53 and p73 tumor suppressor protein while it had no significant effect on the cell cycle distribution of these cells.

4.3.3 Discussion

These results highlight a tumor suppressive role of TIP60 in HeLa cells where its upregulation induces apoptosis by the activation of p73 and p53 mediated downstream signaling. TIP60 is essential for p53 mediated antitumor response as TIP60-dependent acetylation of p53 at K120 is necessary for transactivation of BAX and PUMA proteins (Sykes *et al.*, 2006). High levels of UHRF1 in cancers can inhibit this induction of apoptosis by blocking the interaction between TIP60 and p53 protein. Our results have revealed that UHRF1 can bind to the MYST domain of TIP60, compromising its ability to acetylate p53 and induction of apoptosis. Overexpression of TIP60 on the other hand can downregulate UHRF1 and induce apoptosis by activation of p53 and p73 mediated response to inhibit proliferation (Figure 49).

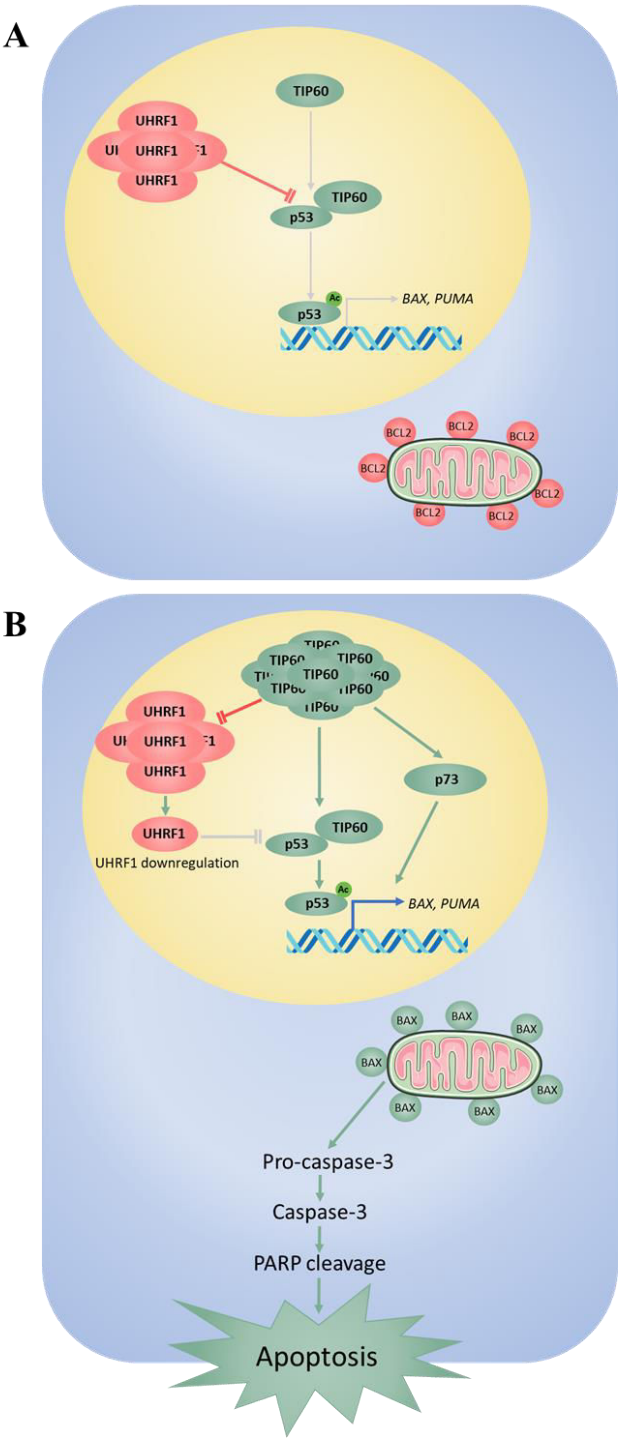

Figure 49: Schematic model of TIP60 mediated apoptosis in cancer cells. A, UHRF1 upregulation in cancer inhibits the TIP60 mediated activation of p53 and apoptosis. B, TIP60 overexpression downregulates UHRF1 and counters its inhibitory effect on induction of p73 and p53-mediated apoptosis. Dark lines indicate the activated pathways while the gray lines indicate the repressed pathways.

HeLa cells have low basal levels of TIP60 and p53 proteins because of the inherent expression of HPV E6 and E7 viral oncoprotein translated from the integrated HPV genome. HPV E6

protein promotes the proteasomal degradation of TIP60 through EDD1 E3 ligase and abrogates the p53 dependent activation of apoptotic pathways (Jha *et al.*, 2010, Subbaiah *et al.*, 2016). Downregulation of TIP60 by virus in cervical cancer not only inhibits the induction of apoptosis but also facilitates the immortalization of cells in response to viral proteins (Rajagopalan *et al.*, 2017). Indeed, retrospective analysis of a data set (GDS3233) submitted in GEO NCBI database regarding differential expression of genes in normal and cervical cancer tissues revealed to us that TIP60 is significantly downregulated in cervical cancer samples as compared with normal epithelial tissues (Figure 50).

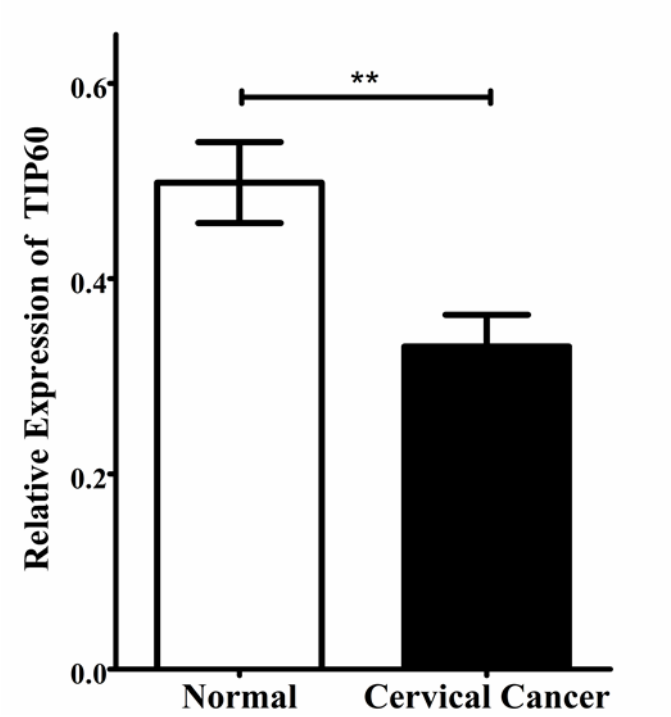

Figure 50: Downregulation of TIP60 in cervical cancer. Results are obtained by analyzing expression of TIP60 in a dataset (GDS3233) submitted to GEO NCBI database. Differential gene expression at mRNA level was observed in 20 normal squamous cervical epithelial samples and 20 cervical cancer tissues by using Affymetrix U133A oligonucleotide microarray (Scotto et al., 2008).

Therefore, overexpression of TIP60 in such transformed cells activated the p53 and p73 mediated BAX transactivation and initiated the downstream signaling cascade for induction of apoptosis. It is noteworthy that TIP60 also represses the expression of HPV E6 protein by recruiting Brd4, a cellular repressor complex to the promoters of HPV and virus tends to evade this phenomenon by degrading the TIP60 in first place (Jha *et al.*, 2010).

It is also interesting to note that expression of TIP60 also induced the expression of p73, which can also induce apoptosis by a similar pathway in cells (Yoon *et al.*, 2015). We also observed that overexpression of TIP60 downregulated UHRF1 in these cells. Previously, we have reported that increased expression of p73 results in downregulation of UHRF1 and is often accompanied with induction of apoptosis or cell cycle arrest (Alhosin *et al.*, 2010, Sharif *et al.*, 2010, Sharif *et al.*, 2012). However, with TIP60 over expression, we only observed the induction of apoptosis while no significant change in cell cycle distribution was detected. TIP60 through its interaction with p53 can induce the activation of p21-mediated growth arrest in an acetylation independent manner but it was not observed in HeLa cells over expressing TIP60.

CONCLUSION AND PRESPECTIVES

5 - CONCLUSION AND PERSPECTIVES

UHRF1 is a multidomain protein, involved in key epigenetic regulations including DNA methylation and histone modifications. During DNA replication, UHRF1 acts as "reader" to identify the methylated cytosine on parent strand through its SRA domain and recruits the DNMT1 to the daughter strand for maintenance of DNA methylation (Bostick *et al.*, 2007, Sharif *et al.*, 2007, Avvakumov *et al.*, 2008). This process is also guided by the TTD and PHD of UHRF1 which read the specific modifications at N-terminal tail of histone H3 (Hu *et al.*, 2011, Lallous *et al.*, 2011, Nady *et al.*, 2011, Rajakumara *et al.*, 2011, Wang *et al.*, 2011, Rothbart *et al.*, 2012, Liu *et al.*, 2013b). RING domain of UHRF1 functions as "writer" domain of UHRF1 as it ubiquitinates multiple lysine residue on H3 protein which serve as anchoring marks for the loading of DNMT1 to daughter strand of newly formed DNA (Nishiyama *et al.*, 2013, Qin *et al.*, 2015, Harrison *et al.*, 2016). Because of these epigenetic modifications, UHRF1 takes an active part in regulation of gene expression, DNA damage response, differentiation, embryonic development and organogenesis (Bronner *et al.*, 2013, Sidhu and Capalash, 2017). These different roles of UHRF1 are facilitated by its interaction with multiple epigenetic partners such as PCNA, DNMTs, HDACs, HATs, and USP7 which together form a multiprotein macromolecular complex on chromatin (Alhosin *et al.*, 2011).

TIP60 is one of such important interacting partner of UHRF1 and it was reported to be a part of the same epigenetic complex by our laboratory in 2009 (Achour *et al.*, 2009). It is a well-known acetyltransferase of MYST family and it is involved in multiple cellular activities such as regulation of gene expression, cell proliferation, DNA damage response and development (Sapountzi *et al.*, 2006, Judes *et al.*, 2015). TIP60 is also a multidomain protein and interacts with many other proteins to form a dynamic multiprotein complex endowed with chromatin remodeling activity (Doyon and Cote, 2004). In this project we have further explored the interaction between UHRF1 and TIP60 inside the cells and have tried to comprehend the mechanism underlying this interaction.

- **UHRF1 interacts with MYST domain of TIP60**

Our results have shown that UHRF1 interacts with MYST domain of TIP60 protein and both the proteins interact together in the DNA replication phase of cell cycle (Ashraf *et al.*, 2017a). Multiple biochemical and imaging techniques were utilized in this study to analyze the

interaction between UHRF1 and TIP60 proteins. Firstly, immunoprecipitation of UHRF1 and TIP60 indicated the presence of both proteins together in the same epigenetic complex in cells and later FLIM experiments helped to visualize the interaction between UHRF1 and TIP60 inside the nucleus of HeLa cells during the S phase of cell cycle. Finally, the *in vitro* pull-down assays confirmed the strong association between UHRF1 and MYST domain of TIP60 protein (Ashraf *et al.*, 2017a). Additionally, we have also observed that overexpression of TIP60 in HeLa cells downregulated the UHRF1 and DNMT1 levels and induced global hypomethylation in a MYST domain dependent manner (Ashraf *et al.*, 2017a).

MYST domain is the key structural component of TIP60 and is comprised of a zinc finger and histone acetyltransferase (HAT) activity motif. Besides TIP60, this highly conserved domain is also present in four other human acetyltransferase MOZ, MORF, HBO1 and MOF proteins (Avvakumov and Cote, 2007, Voss and Thomas, 2009). TIP60 interaction with UHRF1 through this MYST domain shows the probability that UHRF1 might be able to interact with these other MYST domain containing proteins. Indeed, a study has predicted an interaction between UHRF1 and MOF acetyltransferase whose MYST domain is 80% identical to TIP60 MYST domain in mammals (Ruan, 2015). However, this hypothesis needs further evaluation and the presences of these MYST domain containing proteins can be checked in UHRF1 complex immunoprecipitated from cells. Later, the possible interactions can be explored further by specifically designed studies.

- **UHRF1, TIP60 and DNMT1 are present in same epigenetic complex and interaction between UHRF1 and TIP60 prevails in S phase of cell cycle**

We also observed that UHRF1, TIP60 and DNMT1 are present in the same complex as predicted by the previous findings (Achour *et al.*, 2009, Dai *et al.*, 2013). It is interesting to note that besides decrease of DNMT1 in TIP60 overexpressed samples, more amount of DNMT1 was pulled-down with UHRF1 in these samples which confirms the close association of these three proteins in a same epigenetic complex.

UHRF1 and DNMT1 are well known for their involvement in maintenance of DNA methylation patterns during the S phase of cell cycle and are recruited to replication fork through their association with PCNA (Zhang *et al.*, 2011, Bronner *et al.*, 2013). In FLIM, we have observed that TIP60 is also a part of this complex and the interaction between TIP60 and UHRF also occurs during the DNA replication phase of cell cycle (Ashraf *et al.*, 2017a). Like

UHRF1, TIP60 can also interact with multiple common interacting partners (DNMT1 and USP7) and thus might also be involved in S phase specific nuclear activities including chromatin remodeling and maintenance of epigenetic code during chromatin replication. TIP60 facilitates the supply of dNTPs and histone proteins needed for the chromatin replication, failure to which can halt the DNA synthesis at replication forks (DeRan *et al.*, 2008, Niida *et al.*, 2010). Studies have reported that acetylation of histones can regulate the DNA replication by affecting the origin of replication and loosening of the compact chromatin organization (Unnikrishnan *et al.*, 2010, Ruan *et al.*, 2015). TIP60 can acetylate multiple histone residues (including H2AK5, H2AK15, H3K9, H3K14, H4K8, H4K12 and H4K16) (Sapountzi *et al.*, 2006, Jacquet *et al.*, 2016, Xu *et al.*, 2016, Zeng *et al.*, 2017) and thus might be involved in such regulatory events at the replication fork. TIP60 also plays a key role in repair of the DNA damages by FA and HR pathway that dominate during the S and G2/M phase of cell cycle. For this purpose, TIP60 is essentially loaded onto the chromatin where it acetylates H4K16 and H2AK15 residues and directs the recruitment of effector proteins (Ayrapetov *et al.*, 2014, Jacquet *et al.*, 2016). Cells deficient in TIP60 cannot repair the DNA damages and result in high number of stalled replication forks in genotoxic stress, leading to arrest in S phase of cell cycle (Su *et al.*, 2017). Recently, role of UHRF1 have been also discovered in DNA damage response against the interstrand cross linkage and double strand breaks as it also facilitates the repair by FA and HR repair mechanisms (Liang *et al.*, 2015, Zhang *et al.*, 2016a). This predicts that TIP60 and UHRF1 proteins may work in coordination with each other to maintain the genomic integrity during the DNA replication phase of cell cycle.

- **UHRF1 and TIP60 colocalize at the DNA damage areas**

In our experiments, UHRF1 and TIP60 were also visualized together at localized double strand breaks in DNA, confirming the association of both proteins at the DNA damage areas. However, difference in dynamics of both the proteins at DNA damage spots suggests that role of both proteins should be further explored in relevance to each other as UHRF1 might be helping to recruit TIP60 or TIP60 might be involved in eviction of UHRF1 from the DNA damage area. Evidences of early accumulation of UHRF1 on DNA damage sites in our results predict the role of UHRF1 as “detector” protein in DNA damage response which is also supported by the previous studies (Liang *et al.*, 2015, Tian *et al.*, 2015, Zhang *et al.*, 2015). Presence of specialized structural SRA domain in UHRF1 that is capable of detecting methylated cytosines and abnormalities in DNA like interstrand cross linkages while sliding

over the DNA strengthens this hypothesis. It is noteworthy that both UHRF1 and TIP60 proteins are also equipped with TTD and chromodomain respectively, that can recognize H3K9 methylation marks which are dynamically regulated at the site of DNA damage (Sun *et al.*, 2009). Therefore, the role of these domains in recruitment of UHRF1 and TIP60 to the DNA damage spot can also be explored further.

- **TIP60 overexpression activates apoptotic cascade in HeLa cells**

Both UHRF1 and TIP60 play a role in regulation of cell growth and proliferation and are deregulated in most of the cancers (Gorrini *et al.*, 2007, Alhosin *et al.*, 2011). UHRF1 is highly expressed in the proliferating and cancer tissues while TIP60 levels are mostly downregulated in tumors (Gorrini *et al.*, 2007, Ashraf *et al.*, 2017b). UHRF1 suppresses the activation of tumor suppressor genes in cancer while TIP60 is considered essential for the action of many TSGs such as p53 (Ashraf *et al.*, 2017b). In response to genotoxic insult or oncogenic stimulation TIP60 activates the p53 in an acetylation dependent or independent manner to induce apoptosis or cell cycle arrest respectively. Indeed, acetylation of p53 at K120 by TIP60 is indispensable for the transactivation of proapoptotic BAX and PUMA protein in p53 downstream signaling cascade (Sykes *et al.*, 2006, Tang *et al.*, 2006). Previously, it has been described that high levels of UHRF1 in cancers interfere in TIP60-p53 interplay and block the activation of p53 dependent antitumor activities (Dai *et al.*, 2013). Our results provide an insight to the mechanism and predicts that UHRF1 inhibits TIP60-mediated p53 acetylation and activation. UHRF1, by interacting with MYST domain of TIP60 can block its acetylation activity and disrupt the association between TIP60 and p53, resulting in failure to induce apoptosis. On the other hand, overexpression of TIP60 can bypass this inhibitory effect of UHRF1 and lead to transactivation of BAX and proapoptotic signaling cascade to induce cell death.

Contrary to previous findings, we also observed upregulation of p73 tumor suppressor protein by overexpression of TIP60 in HeLa cells (Kim *et al.*, 2008). p73 is the structural and functional analogue of p53 and is able to induce proapoptotic activity in p53 mutated or null cancer cells. Indeed, many anticancer drugs induce apoptosis in cancer cells through the activation of p73 dependent salvage pathways (Yoon *et al.*, 2015). There is a need to further explore the mechanism of TIP60 mediated induction of p73 in p53 deficient cells and its involvement in the apoptotic pathways.

- **TIP60 regulates DNMT1 and UHRF1 in cells**

In our findings, we also observed that overexpression of TIP60 led to downregulation of UHRF1 and DNMT1 in cells and this downregulation was dependent on the MYST domain of TIP60. DNMT1 is well known to be regulated by the UHRF1 and TIP60 in cells. It is also interesting to note that all the three proteins, *i.e.,* UHRF1, DNMT1 and TIP60 are protected from proteasomal degradation by their association with USP7 a deubiquitinating enzyme present in the same complex (Du *et al.*, 2010, Dar *et al.*, 2013, Zhang *et al.*, 2015). DNMT1 is degraded by the coordinated action of UHRF1 and TIP60. Mechanistically, DNMT1 is acetylated by TIP60, which lowers its association with USP7 and then UHRF1 via its enzymatic E3 ligase activity ubiquitinates DNMT1 and triggers DNMT1 degradation by the proteasomal pathway (Du *et al.*, 2010). In our results, we have seen a decrease in DNMT1 levels by TIP60 overexpression, which confirms the above mechanism and lower levels of UHRF1 also predicts a similar pathway for the regulation of UHRF1.

UHRF1 has the ability to auto-ubiquitinate itself and trigger its own degradation. However, it is saved from proteasomal degradation by its association with ubiquitin like domains (UBL1-2) of USP7. USP7 interacts with UHRF1 at the polybasic region between its SRA and RING domain and lysine 659 (isoform 2) of UHRF1 is considered to be critical for this interaction (Zhang *et al.*, 2015). TIP60 also interacts with UHRF1 in the same region and a study using a small polypeptide from that region has shown that TIP60 can acetylate K659 of UHRF1, which can drastically lower the affinity of acetylated polypeptide with USP7 (Dai *et al.*, 2013, Zhang *et al.*, 2015). This predicts the pathway by which overexpression of TIP60 might regulate the stability of UHRF1 in a mechanism similar to that of DNMT1 regulation which needs further investigation.

It is noteworthy that TIP60 levels are increased in cells after the completion of DNA methylation (Du *et al.*, 2010) and thus increased TIP60 levels at that time can compete with USP7 for binding to UHRF1 or by increased acetylation can dissociate USP7 from UHRF1 to make UHRF1 more prone to degradation (Figure 51).

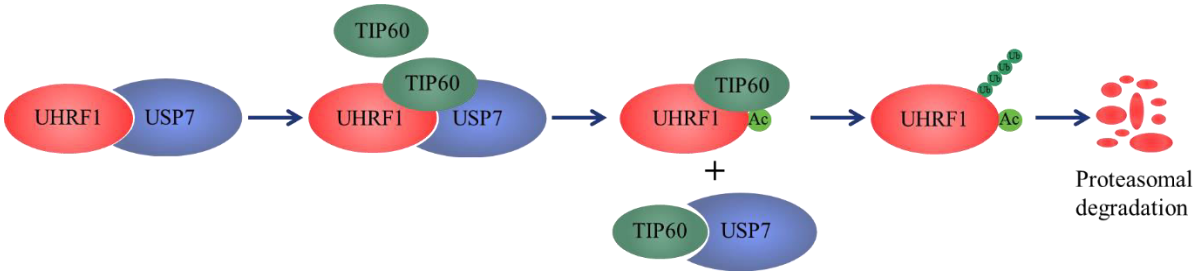

Figure 51: Proposed model for degradation of UHRF1. UHRF1 is stabilized in cells by its association with USP7. Increased level of TIP60 can interrupt this association between UHRF1 and USP7 by directly competing for the binding with UHRF1 or altering its interacting area with USP7 through acetylation. After dissociation of USP7, UHRF1 can be ubiquitinated and primed for proteasomal degradation by UHRF1 intrinsic E3 ligase activity or by other E3 ligase enzyme in nucleus.

In order to strengthen our hypothesis, we checked this model of UHRF1 regulation through *in-silico* docking of PBR region of UHRF1 with USP7 and TIP60 proteins. For this purpose, we utilized the Cluspro docking server which was rated as the best online server for protein-protein docking in the last CAPRI (Critical Assessment of PRediction of Interactions) evaluation meeting in 2016 (Kozakov *et al.*, 2017). First, we retrieved the crystal structure of UHRF1 PBR in complex with the Ubiquitin like domains (UBL1-3) of USP7 (PDB ID: 5C6D) (Figure 52 A) and simulated its docking on the Cluspro server to check the docking capabilities of this program. Cluspro predicted a similar binding model between UHRF1 PBR (taken as receptor) and USP7 (ubiquitin like domain 1-3) (taken as the ligand) (Figure 52 B) in its top most predicted model when compared to the reported crystal of interaction. UHRF1 PBR region was docked between the UBL1&2 of USP7 as it was shown to interact in the original crystal structure (Figure 52).

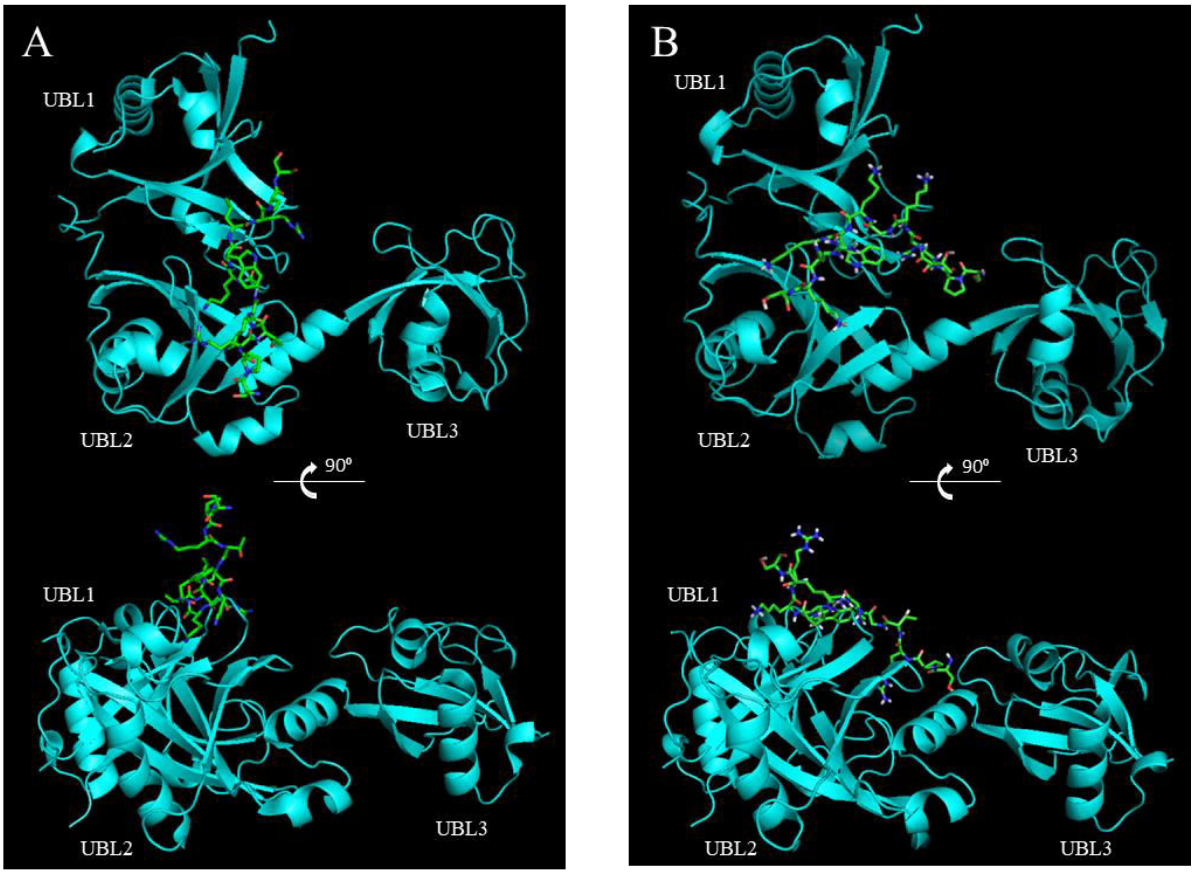

Figure 52: A, Crystal structure of UHRF1 PBR (green / sticks) in complex with UBL1-3 domains of USP7 (cyan / cartoon) (PDB ID: 5C6D). B, Predicted docking model of UHRF1 PBR (green / sticks) in interaction with UBL1-3 domains of USP7 (cyan / cartoon).

Crystal structure of USP7 was also aligned with the predicted model and root mean square (RMS) deviation was calculated for both structures. RMS is the measure of the structural similarity between the two structures and is calculated by taking square root of the mean of square of the distances between the matched atoms. Lower RMS value correspond to higher structural similarity. Low RMS values of 0.75 Å between USP7 crystal structure and predicted model also increased our confidence towards the docking server (Figure 53).

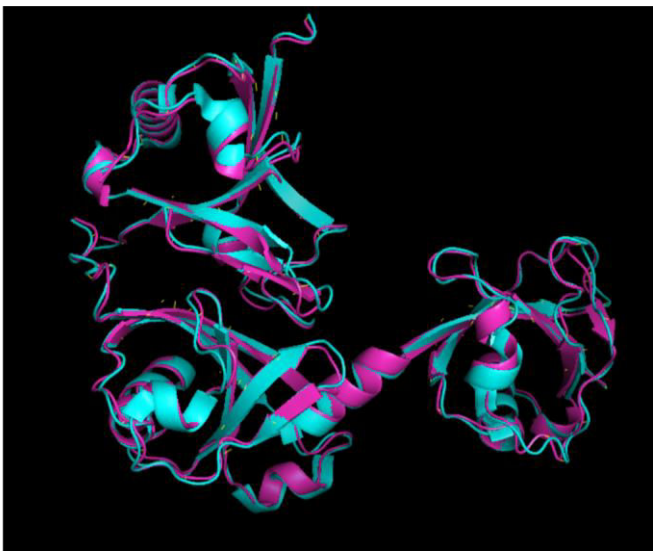

Figure 53: Structural alignment between UBL1-3 domains of USP1 in crystal (cyan) versus modeled structure (magenta).

As our results show interaction of UHRF1 with MYST domain of TIP60 so next, we retrieved the crystal structure of MYST domain of TIP60 protein (PDB ID: 2OU2) (Figure 54 A) and docked it with the PBR of UHRF1. The top most predicted binding model of this interaction revealed that UHRF1 PBR perfectly aligned in the catalytic HAT region (indicated in magenta) of TIP60 MYST domain (Figure 54 B).

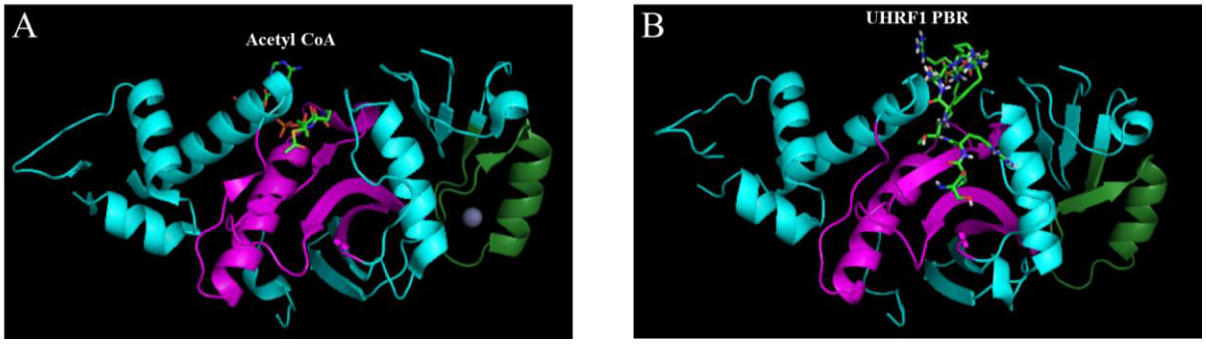

Figure 54: A, Crystal structure of Acetyl CoA (indicated in green sticks) in complex with MYST domain of TIP60 (indicated in cyan magenta and forest green cartoon) (PDB ID: 2OU2). B, Predicted docking model of UHRF1 PBR (indicated in green sticks) in complex with MYST domain of TIP60 (indicated in cyan magenta and forest green cartoon).

Predicted model of MYST domain was also well aligned with the original crystal structure of MYST domain and had low RMS value of 0.99 Å (Figure 55).

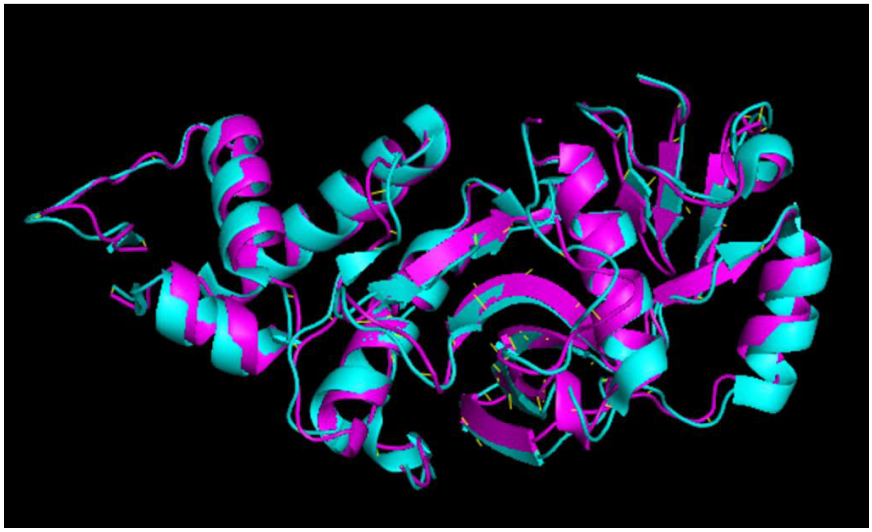

Figure 55: Structural alignment between TIP60 MYST domain in crystal (cyan) versus modeled structure (magenta).

Weighed scores were also predicted by this program which are dependent on the size of cluster (number of docked structures) and PIPER energies of the models. High number of docked structure with lower energies predict favorable binding between the two proteins (Kozakov *et al.*, 2017). When compared, models showing UHRF1 PBR interaction with MYST domain of TIP60 had better scores as compared to predicted model of UHRF1 PBR interaction with the USP7 protein (Figure 56). This predicts a relatively stronger chance of interaction between UHRF1 PBR with TIP60 MYST domain as compared to UHRF1 PBR interaction with USP7 UBL domains.

Weighed scores for best fit Models

USP7 / UHRF1(PBR)

Cluster	Members	Representative	Weighted Score
0	101	Center	-468.3
		Lowest Energy	-477.1
1	99	Center	-470.0
		Lowest Energy	-470.0
2	79	Center	-455.6
		Lowest Energy	-461.0
3	72	Center	-519.0
		Lowest Energy	-519.0
4	58	Center	-471.1
		Lowest Energy	-536.3
5	55	Center	-476.1
		Lowest Energy	-476.1
6	50	Center	-517.0
		Lowest Energy	-517.0
7	38	Center	-467.6
		Lowest Energy	-467.6
8	38	Center	-464.5
		Lowest Energy	-464.9
9	36	Center	-459.6
		Lowest Energy	-459.6

TIP60 / UHRF1(PBR)

Cluster	Members	Representative	Weighted Score
0	190	Center	-683.2
		Lowest Energy	-683.2
1	167	Center	-470.5
		Lowest Energy	-518.5
2	165	Center	-500.3
		Lowest Energy	-580.8
3	75	Center	-514.2
		Lowest Energy	-541.8
4	72	Center	-531.6
		Lowest Energy	-533.9
5	56	Center	-473.8
		Lowest Energy	-545.0
6	48	Center	-508.1
		Lowest Energy	-540.9
7	45	Center	-492.7
		Lowest Energy	-526.5
8	40	Center	-556.2
		Lowest Energy	-556.2
9	32	Center	-468.4
		Lowest Energy	-526.3

Figure 56: Weighed scores for the best fit models predicted by Cluspro server.

Hence, this *in-silico* modeling supports our idea that competitive binding of TIP60 through MYST domain can interfere in UHRF1 interaction with USP7 and can make UHRF1 more vulnerable for proteasomal degradation. However, this hypothesis needs further evaluation in cellular studies by checking the effect of TIP60 overexpression on UHRF1 association with USP7 and its degradation by ubiquitination pathway. Role of TIP60 mediated acetylation of UHRF1 can also be checked in reference to degradation of UHRF1, as in-silico docking predicts the localization of UHRF1 PBR at the active site of HAT domain of TIP60. Finally, the isothermal calorimetric or crystallization studies can be helpful in this regard to provide the conclusive evidence for this interaction and regulation of UHRF1.

Recently, it has been reported that TIP60 also regulates the activity of SP1 transcription factor. It acetylates SP1, which lowers its affinity to DNA and consequently represses the transcription from its targeted promoters (Rajagopalan *et al.*, 2017). Interestingly, SP1 upregulates UHRF1 expression in cancer (Wu *et al.*, 2015); therefore, inhibition of SP1 might also contribute to downregulation of UHRF1 in TIP60 dependent manner which can be later examined in following studies.

In our results, we have also observed that levels of exogenous TIP60 are lower when we co-transfected TIP60-eGFP with UHRF1-mCherry as compared to cells transfected with TIP60-eGFP alone. Similar findings were reported from our lab where targeting of UHRF1 by the siRNA increased the levels of endogenous TIP60 in Jurkat cells (Achour *et al.*, 2009). Overall, these results predict that besides working together in an epigenetic complex; TIP60 and UHRF1 are regulating each other in cells and have an antagonistic role in cancers. This hypothesis can be confirmed by analyzing the expression of TIP60 and UHRF1 in pathological specimen to see whether the deregulation in expression of both proteins is mutually correlated or independent of each other in cancers.

Finally, this study concludes TIP60 as a bona fide interacting partner of UHRF1 where TIP60 interacts with UHRF1 through its MYST domain and together they are present in the same epigenetic complex in S phase of cell cycle. Our results also predict a tumor suppressive role of TIP60 protein which can be exploited therapeutically to target UHRF1 which is deregulated in cancers. UHRF1 is primarily overexpressed in majority of cancers and is often associated with the silencing of tumor suppressor genes, aggressive tumor growth and poor prognosis (Achour *et al.*, 2009). This makes UHRF1 an attractive target for anticancer therapy. Inhibitors for other members of this complex such as DNMT1 and HDAC1 have already been marketed for anticancer therapy but their use is limited to few cancers because of low efficacy and safety profile (Batty *et al.*, 2009, Unoki, 2011). Basal expression of HDACs in normal cell and ubiquitous expression of DNMT1 in different organs create a significant challenge for targeting the cancer cells with high specificity (Bronner *et al.*, 2007, Unoki *et al.*, 2009a, Unoki, 2011). While targeting of UHRF1 in this complex can be beneficial as it is significantly upregulated in cancers and not expressed in fully differentiated cells or vital organs such as heart, liver, kidney, lungs and bladder (Unoki *et al.*, 2009b). UHRF1 also plays a pivotal role in the function of DNMT1 and HDAC1; so, targeting UHRF1 can give an added advantage to overcome the oncogenic role of these proteins. Various strategies can be adopted to target the UHRF1 including use of small molecules to bind its SRA domain, which will impair its function in DNA methylation or DNA damage response. Similarly, small molecules or peptides can be designed to target PBR region between SRA and RING domain which will block its association with USP7 and thus by promoting its degradation will suppress its oncogenic role in cancer cells.

REFERENCES

6 - REFERENCES

Achour, M., Fuhrmann, G., Alhosin, M., Ronde, P., Chataigneau, T., Mousli, M., Schini-Kerth, V.B. & Bronner, C., 2009. UHRF1 recruits the histone acetyltransferase Tip60 and controls its expression and activity. *Biochem Biophys Res Commun,* 390**,** 523-8.

Achour, M., Mousli, M., Alhosin, M., Ibrahim, A., Peluso, J., Muller, C.D., Schini-Kerth, V.B., Hamiche, A., Dhe-Paganon, S. & Bronner, C., 2013. Epigallocatechin-3-gallate up-regulates tumor suppressor gene expression via a reactive oxygen species-dependent down-regulation of UHRF1. *Biochem Biophys Res Commun,* 430**,** 208-12.

Adamowicz, M., Vermezovic, J. & D'adda Di Fagagna, F., 2016. NOTCH1 Inhibits Activation of ATM by Impairing the Formation of an ATM-FOXO3a-KAT5/Tip60 Complex. *Cell Rep,* 16**,** 2068-76.

Akhtar, A., Zink, D. & Becker, P.B., 2000. Chromodomains are protein-RNA interaction modules. *Nature,* 407**,** 405-9.

Alhosin, M., Abusnina, A., Achour, M., Sharif, T., Muller, C., Peluso, J., Chataigneau, T., Lugnier, C., Schini-Kerth, V.B., Bronner, C. & Fuhrmann, G., 2010. Induction of apoptosis by thymoquinone in lymphoblastic leukemia Jurkat cells is mediated by a p73-dependent pathway which targets the epigenetic integrator UHRF1. *Biochem Pharmacol,* 79**,** 1251-60.

Alhosin, M., Leon-Gonzalez, A.J., Dandache, I., Lelay, A., Rashid, S.K., Kevers, C., Pincemail, J., Fornecker, L.M., Mauvieux, L., Herbrecht, R. & Schini-Kerth, V.B., 2015. Bilberry extract (Antho 50) selectively induces redox-sensitive caspase 3-related apoptosis in chronic lymphocytic leukemia cells by targeting the Bcl-2/Bad pathway. *Sci Rep,* 5**,** 8996.

Alhosin, M., Omran, Z., Zamzami, M.A., Al-Malki, A.L., Choudhry, H., Mousli, M. & Bronner, C., 2016. Signalling pathways in UHRF1-dependent regulation of tumor suppressor genes in cancer. *J Exp Clin Cancer Res,* 35**,** 174.

Alhosin, M., Sharif, T., Mousli, M., Etienne-Selloum, N., Fuhrmann, G., Schini-Kerth, V.B. & Bronner, C., 2011. Down-regulation of UHRF1, associated with re-expression of tumor suppressor genes, is a common feature of natural compounds exhibiting anti-cancer properties. *J Exp Clin Cancer Res,* 30**,** 41.

Allfrey, V.G., Faulkner, R. & Mirsky, A.E., 1964. Acetylation and Methylation of Histones and Their Possible Role in the Regulation of Rna Synthesis. *Proc Natl Acad Sci U S A,* 51**,** 786-94.

Allis, C.D. & Jenuwein, T., 2016. The molecular hallmarks of epigenetic control. *Nat Rev Genet,* 17**,** 487-500.

Arima, Y., Hirota, T., Bronner, C., Mousli, M., Fujiwara, T., Niwa, S., Ishikawa, H. & Saya, H., 2004. Down-regulation of nuclear protein ICBP90 by p53/p21Cip1/WAF1-dependent DNA-damage checkpoint signals contributes to cell cycle arrest at G1/S transition. *Genes Cells,* 9**,** 131-42.

Arita, K., Ariyoshi, M., Tochio, H., Nakamura, Y. & Shirakawa, M., 2008. Recognition of hemi-methylated DNA by the SRA protein UHRF1 by a base-flipping mechanism. *Nature,* 455**,** 818-21.

Arita, K., Isogai, S., Oda, T., Unoki, M., Sugita, K., Sekiyama, N., Kuwata, K., Hamamoto, R., Tochio, H., Sato, M., Ariyoshi, M. & Shirakawa, M., 2012. Recognition of modification status on a histone H3 tail by linked histone reader modules of the epigenetic regulator UHRF1. *Proc Natl Acad Sci U S A,* 109**,** 12950-5.

Ashraf, W., Bronner, C., Zaayter, L., Ahmad, T., Richert, L., Alhosin, M., Ibrahim, A., Hamiche, A., Mely, Y. & Mousli, M., 2017a. Interaction of the epigenetic integrator UHRF1 with the MYST domain of TIP60 inside the cell. *J Exp Clin Cancer Res,* 36**,** 188.

Ashraf, W., Ibrahim, A., Alhosin, M., Zaayter, L., Ouararhni, K., Papin, C., Ahmad, T., Hamiche, A., Mely, Y., Bronner, C. & Mousli, M., 2017b. The epigenetic integrator UHRF1: on the road to become a universal biomarker for cancer. *Oncotarget,* 8**,** 51946-51962.

Auger, A., Galarneau, L., Altaf, M., Nourani, A., Doyon, Y., Utley, R.T., Cronier, D., Allard, S. & Cote, J., 2008. Eaf1 is the platform for NuA4 molecular assembly that evolutionarily links chromatin acetylation to ATP-dependent exchange of histone H2A variants. *Mol Cell Biol,* 28**,** 2257-70.

Avvakumov, G.V., Walker, J.R., Xue, S., Li, Y., Duan, S., Bronner, C., Arrowsmith, C.H. & Dhe-Paganon, S., 2008. Structural basis for recognition of hemi-methylated DNA by the SRA domain of human UHRF1. *Nature,* 455**,** 822-5.

Avvakumov, N. & Cote, J., 2007. The MYST family of histone acetyltransferases and their intimate links to cancer. *Oncogene,* 26**,** 5395-407.

Awasthi, S., Sharma, A., Wong, K., Zhang, J., Matlock, E.F., Rogers, L., Motloch, P., Takemoto, S., Taguchi, H., Cole, M.D., Luscher, B., Dittrich, O., Tagami, H., Nakatani, Y., Mcgee, M., Girard, A.M., Gaughan, L., Robson, C.N., Monnat, R.J., Jr. & Harrod, R., 2005. A human T-cell lymphotropic virus type 1 enhancer of Myc transforming potential stabilizes Myc-TIP60 transcriptional interactions. *Mol Cell Biol,* 25**,** 6178-98.

Ayrapetov, M.K., Gursoy-Yuzugullu, O., Xu, C., Xu, Y. & Price, B.D., 2014. DNA double-strand breaks promote methylation of histone H3 on lysine 9 and transient formation of repressive chromatin. *Proc Natl Acad Sci U S A,* 111**,** 9169-74.

Bassi, C., Li, Y.T., Khu, K., Mateo, F., Baniasadi, P.S., Elia, A., Mason, J., Stambolic, V., Pujana, M.A., Mak, T.W. & Gorrini, C., 2016. The acetyltransferase Tip60 contributes to mammary tumorigenesis by modulating DNA repair. *Cell Death Differ,* 23**,** 1198-208.

Batty, N., Malouf, G.G. & Issa, J.P., 2009. Histone deacetylase inhibitors as anti-neoplastic agents. *Cancer Lett,* 280**,** 192-200.

Beck, C., Boehler, C., Guirouilh Barbat, J., Bonnet, M.E., Illuzzi, G., Ronde, P., Gauthier, L.R., Magroun, N., Rajendran, A., Lopez, B.S., Scully, R., Boussin, F.D., Schreiber, V. & Dantzer, F., 2014. PARP3 affects the relative contribution of homologous recombination and nonhomologous end-joining pathways. *Nucleic Acids Res,* 42**,** 5616-32.

Berndsen, C.E., Albaugh, B.N., Tan, S. & Denu, J.M., 2007. Catalytic mechanism of a MYST family histone acetyltransferase. *Biochemistry,* 46**,** 623-9.

Bhoumik, A., Singha, N., O'connell, M.J. & Ronai, Z.A., 2008. Regulation of TIP60 by ATF2 modulates ATM activation. *J Biol Chem,* 283**,** 17605-14.

Bird, A., 2002. DNA methylation patterns and epigenetic memory. *Genes Dev,* 16**,** 6-21.

Bird, A., 2007. Perceptions of epigenetics. *Nature,* 447**,** 396-8.

Biswas, S. & Rao, C.M., 2017. Epigenetics in cancer: Fundamentals and Beyond. *Pharmacol Ther,* 173**,** 118-134.

Bostick, M., Kim, J.K., Esteve, P.O., Clark, A., Pradhan, S. & Jacobsen, S.E., 2007. UHRF1 plays a role in maintaining DNA methylation in mammalian cells. *Science,* 317**,** 1760-4.

Brady, M.E., Ozanne, D.M., Gaughan, L., Waite, I., Cook, S., Neal, D.E. & Robson, C.N., 1999. Tip60 is a nuclear hormone receptor coactivator. *J Biol Chem,* 274**,** 17599-604.

Bronner, C., Achour, M., Arima, Y., Chataigneau, T., Saya, H. & Schini-Kerth, V.B., 2007. The UHRF family: oncogenes that are drugable targets for cancer therapy in the near future? *Pharmacol Ther,* 115**,** 419-34.

Bronner, C., Krifa, M. & Mousli, M., 2013. Increasing role of UHRF1 in the reading and inheritance of the epigenetic code as well as in tumorogenesis. *Biochem Pharmacol,* 86**,** 1643-9.

Bronner, C., Trotzier, M.A., Filhol, O., Cochet, C., Rochette-Egly, C., Scholler-Guinard, M., Klein, J.P. & Mousli, M., 2004. The antiapoptotic protein ICBP90 is a target for protein kinase 2. *Ann N Y Acad Sci,* 1030**,** 355-60.

Charvet, C., Wissler, M., Brauns-Schubert, P., Wang, S.J., Tang, Y., Sigloch, F.C., Mellert, H., Brandenburg, M., Lindner, S.E., Breit, B., Green, D.R., Mcmahon, S.B., Borner, C., Gu, W. & Maurer, U., 2011. Phosphorylation of Tip60 by GSK-3 determines the induction of PUMA and apoptosis by p53. *Mol Cell,* 42**,** 584-96.

Chen, G., Cheng, Y., Tang, Y., Martinka, M. & Li, G., 2012. Role of Tip60 in human melanoma cell migration, metastasis, and patient survival. *J Invest Dermatol,* 132**,** 2632-41.

Chen, H., Ma, H., Inuzuka, H., Diao, J., Lan, F., Shi, Y.G., Wei, W. & Shi, Y., 2013. DNA damage regulates UHRF1 stability via the SCF(beta-TrCP) E3 ligase. *Mol Cell Biol,* 33**,** 1139-48.

Cheng, J., Yang, H., Fang, J., Ma, L., Gong, R., Wang, P., Li, Z. & Xu, Y., 2015. Molecular mechanism for USP7-mediated DNMT1 stabilization by acetylation. *Nat Commun,* 6**,** 7023.

Cheng, Z., Ke, Y., Ding, X., Wang, F., Wang, H., Wang, W., Ahmed, K., Liu, Z., Xu, Y., Aikhionbare, F., Yan, H., Liu, J., Xue, Y., Yu, J., Powell, M., Liang, S., Wu, Q., Reddy, S.E., Hu, R., Huang, H., Jin, C. & Yao, X., 2008. Functional characterization of TIP60 sumoylation in UV-irradiated DNA damage response. *Oncogene,* 27**,** 931-41.

Choudhary, C., Kumar, C., Gnad, F., Nielsen, M.L., Rehman, M., Walther, T.C., Olsen, J.V. & Mann, M., 2009. Lysine acetylation targets protein complexes and co-regulates major cellular functions. *Science,* 325**,** 834-40.

Chu, J., Loughlin, E.A., Gaur, N.A., Senbanerjee, S., Jacob, V., Monson, C., Kent, B., Oranu, A., Ding, Y., Ukomadu, C. & Sadler, K.C., 2012. UHRF1 phosphorylation by cyclin A2/cyclin-dependent kinase 2 is required for zebrafish embryogenesis. *Mol Biol Cell,* 23**,** 59-70.

Col, E., Caron, C., Chable-Bessia, C., Legube, G., Gazzeri, S., Komatsu, Y., Yoshida, M., Benkirane, M., Trouche, D. & Khochbin, S., 2005. HIV-1 Tat targets Tip60 to impair the apoptotic cell response to genotoxic stresses. *EMBO J,* 24**,** 2634-45.

Cole, H.A., Cui, F., Ocampo, J., Burke, T.L., Nikitina, T., Nagarajavel, V., Kotomura, N., Zhurkin, V.B. & Clark, D.J., 2016. Novel nucleosomal particles containing core histones and linker DNA but no histone H1. *Nucleic Acids Res,* 44**,** 573-81.

Compere, S.J. & Palmiter, R.D., 1981. DNA methylation controls the inducibility of the mouse metallothionein-I gene lymphoid cells. *Cell,* 25**,** 233-40.

Cui, H., Guo, M., Xu, D., Ding, Z.C., Zhou, G., Ding, H.F., Zhang, J., Tang, Y. & Yan, C., 2015. The stress-responsive gene ATF3 regulates the histone acetyltransferase Tip60. *Nat Commun,* 6**,** 6752.

D'adda Di Fagagna, F., 2008. Living on a break: cellular senescence as a DNA-damage response. *Nat Rev Cancer,* 8**,** 512-22.

Dai, C., Shi, D. & Gu, W., 2013. Negative regulation of the acetyltransferase TIP60-p53 interplay by UHRF1 (ubiquitin-like with PHD and RING finger domains 1). *J Biol Chem,* 288**,** 19581-92.

Daley, J.M. & Sung, P., 2014. 53BP1, BRCA1, and the choice between recombination and end joining at DNA double-strand breaks. *Mol Cell Biol,* 34**,** 1380-8.

Dar, A., Shibata, E. & Dutta, A., 2013. Deubiquitination of Tip60 by USP7 determines the activity of the p53-dependent apoptotic pathway. *Mol Cell Biol,* 33**,** 3309-20.

Dawson, M.A. & Kouzarides, T., 2012. Cancer epigenetics: from mechanism to therapy. *Cell,* 150**,** 12-27.

Deans, A.J. & West, S.C., 2011. DNA interstrand crosslink repair and cancer. *Nat Rev Cancer,* 11**,** 467-80.

Deran, M., Pulvino, M., Greene, E., Su, C. & Zhao, J., 2008. Transcriptional activation of histone genes requires NPAT-dependent recruitment of TRRAP-Tip60 complex to histone promoters during the G1/S phase transition. *Mol Cell Biol,* 28**,** 435-47.

Ding, G., Chen, P., Zhang, H., Huang, X., Zang, Y., Li, J., Li, J. & Wong, J., 2016. Regulation of Ubiquitin-like with Plant Homeodomain and RING Finger Domain 1 (UHRF1) Protein Stability by Heat Shock Protein 90 Chaperone Machinery. *J Biol Chem,* 291**,** 20125-35.

Djebali, S., Davis, C.A., Merkel, A., Dobin, A., Lassmann, T., Mortazavi, A., Tanzer, A., Lagarde, J., Lin, W., Schlesinger, F., Xue, C., Marinov, G.K., Khatun, J., Williams, B.A., Zaleski, C., Rozowsky, J., Roder, M., Kokocinski, F., Abdelhamid, R.F., Alioto, T., Antoshechkin, I., Baer, M.T., Bar, N.S., Batut, P., Bell, K., Bell, I., Chakrabortty, S., Chen, X., Chrast, J., Curado, J., Derrien, T., Drenkow, J., Dumais, E., Dumais, J., Duttagupta, R., Falconnet, E., Fastuca, M., Fejes-Toth, K., Ferreira, P., Foissac, S., Fullwood, M.J., Gao, H., Gonzalez, D., Gordon, A., Gunawardena, H., Howald, C.,

Jha, S., Johnson, R., Kapranov, P., King, B., Kingswood, C., Luo, O.J., Park, E., Persaud, K., Preall, J.B., Ribeca, P., Risk, B., Robyr, D., Sammeth, M., Schaffer, L., See, L.H., Shahab, A., Skancke, J., Suzuki, A.M., Takahashi, H., Tilgner, H., Trout, D., Walters, N., Wang, H., Wrobel, J., Yu, Y., Ruan, X., Hayashizaki, Y., Harrow, J., Gerstein, M., Hubbard, T., Reymond, A., Antonarakis, S.E., Hannon, G., Giddings, M.C., Ruan, Y., Wold, B., Carninci, P., Guigo, R. & Gingeras, T.R., 2012. Landscape of transcription in human cells. *Nature,* 489**,** 101-8.

Doyon, Y. & Cote, J., 2004. The highly conserved and multifunctional NuA4 HAT complex. *Curr Opin Genet Dev,* 14**,** 147-54.

Du, Z., Song, J., Wang, Y., Zhao, Y., Guda, K., Yang, S., Kao, H.Y., Xu, Y., Willis, J., Markowitz, S.D., Sedwick, D., Ewing, R.M. & Wang, Z., 2010. DNMT1 stability is regulated by proteins coordinating deubiquitination and acetylation-driven ubiquitination. *Sci Signal,* 3**,** ra80.

El Meshri, S.E., Dujardin, D., Godet, J., Richert, L., Boudier, C., Darlix, J.L., Didier, P., Mely, Y. & De Rocquigny, H., 2015. Role of the nucleocapsid domain in HIV-1 Gag oligomerization and trafficking to the plasma membrane: a fluorescence lifetime imaging microscopy investigation. *J Mol Biol,* 427**,** 1480-94.

Esteller, M., 2008. Epigenetics in cancer. *N Engl J Med,* 358**,** 1148-59.

Esteller, M., 2011. Non-coding RNAs in human disease. *Nat Rev Genet,* 12**,** 861-74.

Eymin, B., Claverie, P., Salon, C., Leduc, C., Col, E., Brambilla, E., Khochbin, S. & Gazzeri, S., 2006. p14ARF activates a Tip60-dependent and p53-independent ATM/ATR/CHK pathway in response to genotoxic stress. *Mol Cell Biol,* 26**,** 4339-50.

Fang, J., Cheng, J., Wang, J., Zhang, Q., Liu, M., Gong, R., Wang, P., Zhang, X., Feng, Y., Lan, W., Gong, Z., Tang, C., Wong, J., Yang, H., Cao, C. & Xu, Y., 2016. Hemi-methylated DNA opens a closed conformation of UHRF1 to facilitate its histone recognition. *Nat Commun,* 7**,** 11197.

Felle, M., Joppien, S., Nemeth, A., Diermeier, S., Thalhammer, V., Dobner, T., Kremmer, E., Kappler, R. & Langst, G., 2011. The USP7/Dnmt1 complex stimulates the DNA methylation activity of Dnmt1 and regulates the stability of UHRF1. *Nucleic Acids Res,* 39**,** 8355-65.

Ferry, L., Fournier, A., Tsusaka, T., Adelmant, G., Shimazu, T., Matano, S., Kirsh, O., Amouroux, R., Dohmae, N., Suzuki, T., Filion, G.J., Deng, W., De Dieuleveult, M., Fritsch, L., Kudithipudi, S., Jeltsch, A., Leonhardt, H., Hajkova, P., Marto, J.A., Arita, K., Shinkai, Y. & Defossez, P.A., 2017. Methylation of DNA Ligase 1 by G9a/GLP Recruits UHRF1 to Replicating DNA and Regulates DNA Methylation. *Mol Cell,* 67**,** 550-565 e5.

Frank, S.R., Parisi, T., Taubert, S., Fernandez, P., Fuchs, M., Chan, H.M., Livingston, D.M. & Amati, B., 2003. MYC recruits the TIP60 histone acetyltransferase complex to chromatin. *EMBO Rep,* 4**,** 575-80.

Fujisawa, T. & Filippakopoulos, P., 2017. Functions of bromodomain-containing proteins and their roles in homeostasis and cancer. *Nat Rev Mol Cell Biol,* 18**,** 246-262.

Gao, Y., Koppen, A., Rakhshandehroo, M., Tasdelen, I., Van De Graaf, S.F., Van Loosdregt, J., Van Beekum, O., Hamers, N., Van Leenen, D., Berkers, C.R., Berger, R., Holstege, F.C., Coffer, P.J., Brenkman, A.B., Ovaa, H. & Kalkhoven, E., 2013. Early adipogenesis is regulated through USP7-mediated deubiquitination of the histone acetyltransferase TIP60. *Nat Commun,* 4**,** 2656.

Gaughan, L., Brady, M.E., Cook, S., Neal, D.E. & Robson, C.N., 2001. Tip60 is a co-activator specific for class I nuclear hormone receptors. *J Biol Chem,* 276**,** 46841-8.

Gaughan, L., Logan, I.R., Cook, S., Neal, D.E. & Robson, C.N., 2002. Tip60 and histone deacetylase 1 regulate androgen receptor activity through changes to the acetylation status of the receptor. *J Biol Chem,* 277**,** 25904-13.

Gelato, K.A., Tauber, M., Ong, M.S., Winter, S., Hiragami-Hamada, K., Sindlinger, J., Lemak, A., Bultsma, Y., Houliston, S., Schwarzer, D., Divecha, N., Arrowsmith, C.H. & Fischle, W., 2014. Accessibility of different histone H3-binding domains of UHRF1 is allosterically regulated by phosphatidylinositol 5-phosphate. *Mol Cell,* 54**,** 905-19.

Gevry, N., Chan, H.M., Laflamme, L., Livingston, D.M. & Gaudreau, L., 2007. p21 transcription is regulated by differential localization of histone H2A.Z. *Genes Dev,* 21**,** 1869-81.

Gorrini, C., Squatrito, M., Luise, C., Syed, N., Perna, D., Wark, L., Martinato, F., Sardella, D., Verrecchia, A., Bennett, S., Confalonieri, S., Cesaroni, M., Marchesi, F., Gasco, M., Scanziani, E., Capra, M., Mai, S., Nuciforo, P., Crook, T., Lough, J. & Amati, B., 2007. Tip60 is a haplo-insufficient tumour suppressor required for an oncogene-induced DNA damage response. *Nature,* 448**,** 1063-7.

Guan, Z., Zhang, J., Song, S. & Dai, D., 2013. Promoter methylation and expression of TIMP3 gene in gastric cancer. *Diagn Pathol,* 8**,** 110.

Harrison, J.S., Cornett, E.M., Goldfarb, D., Darosa, P.A., Li, Z.M., Yan, F., Dickson, B.M., Guo, A.H., Cantu, D.V., Kaustov, L., Brown, P.J., Arrowsmith, C.H., Erie, D.A., Major, M.B., Klevit, R.E., Krajewski, K., Kuhlman, B., Strahl, B.D. & Rothbart, S.B., 2016. Hemi-methylated DNA regulates DNA methylation inheritance through allosteric activation of H3 ubiquitylation by UHRF1. *Elife,* 5.

Hashimoto, H., Horton, J.R., Zhang, X., Bostick, M., Jacobsen, S.E. & Cheng, X., 2008. The SRA domain of UHRF1 flips 5-methylcytosine out of the DNA helix. *Nature,* 455**,** 826-9.

Hass, M.R. & Yankner, B.A., 2005. A {gamma}-secretase-independent mechanism of signal transduction by the amyloid precursor protein. *J Biol Chem,* 280**,** 36895-904.

Hejna, J., Bruun, D., Pauw, D. & Moses, R.E., 2010. A FANCD2 domain activates Tip60-dependent apoptosis. *Cell Biol Int,* 34**,** 893-9.

Hejna, J., Holtorf, M., Hines, J., Mathewson, L., Hemphill, A., Al-Dhalimy, M., Olson, S.B. & Moses, R.E., 2008. Tip60 is required for DNA interstrand cross-link repair in the Fanconi anemia pathway. *J Biol Chem,* 283**,** 9844-51.

Helleday, T., Eshtad, S. & Nik-Zainal, S., 2014. Mechanisms underlying mutational signatures in human cancers. *Nat Rev Genet,* 15**,** 585-98.

Holbert, M.A. & Marmorstein, R., 2005. Structure and activity of enzymes that remove histone modifications. *Curr Opin Struct Biol,* 15**,** 673-80.

Holliday, R. & Pugh, J.E., 1975. DNA modification mechanisms and gene activity during development. *Science,* 187**,** 226-32.

Hopfner, R., Mousli, M., Jeltsch, J.M., Voulgaris, A., Lutz, Y., Marin, C., Bellocq, J.P., Oudet, P. & Bronner, C., 2000. ICBP90, a novel human CCAAT binding protein, involved in the regulation of topoisomerase IIalpha expression. *Cancer Res,* 60**,** 121-8.

Hotchkiss, R.D., 1948. The quantitative separation of purines, pyrimidines, and nucleosides by paper chromatography. *J Biol Chem,* 175**,** 315-32.

Hu, L., Li, Z., Wang, P., Lin, Y. & Xu, Y., 2011. Crystal structure of PHD domain of UHRF1 and insights into recognition of unmodified histone H3 arginine residue 2. *Cell Res,* 21**,** 1374-8.

Hu, R., Wang, E., Peng, G., Dai, H. & Lin, S.Y., 2013. Zinc finger protein 668 interacts with Tip60 to promote H2AX acetylation after DNA damage. *Cell Cycle,* 12**,** 2033-41.

Hu, Y., Fisher, J.B., Koprowski, S., Mcallister, D., Kim, M.S. & Lough, J., 2009. Homozygous disruption of the Tip60 gene causes early embryonic lethality. *Dev Dyn,* 238**,** 2912-21.

Huang, J., Stewart, A., Maity, B., Hagen, J., Fagan, R.L., Yang, J., Quelle, D.E., Brenner, C. & Fisher, R.A., 2014. RGS6 suppresses Ras-induced cellular transformation by facilitating Tip60-mediated Dnmt1 degradation and promoting apoptosis. *Oncogene,* 33**,** 3604-11.

Ikura, M., Furuya, K., Matsuda, S., Matsuda, R., Shima, H., Adachi, J., Matsuda, T., Shiraki, T. & Ikura, T., 2015. Acetylation of Histone H2AX at Lys 5 by the TIP60 Histone Acetyltransferase Complex Is Essential for the Dynamic Binding of NBS1 to Damaged Chromatin. *Mol Cell Biol,* 35**,** 4147-57.

Ikura, T., Ogryzko, V.V., Grigoriev, M., Groisman, R., Wang, J., Horikoshi, M., Scully, R., Qin, J. & Nakatani, Y., 2000. Involvement of the TIP60 histone acetylase complex in DNA repair and apoptosis. *Cell,* 102**,** 463-73.

Ikura, T., Tashiro, S., Kakino, A., Shima, H., Jacob, N., Amunugama, R., Yoder, K., Izumi, S., Kuraoka, I., Tanaka, K., Kimura, H., Ikura, M., Nishikubo, S., Ito, T., Muto, A., Miyagawa, K., Takeda, S., Fishel, R., Igarashi, K. & Kamiya, K., 2007. DNA damage-dependent acetylation and ubiquitination of H2AX enhances chromatin dynamics. *Mol Cell Biol,* 27**,** 7028-40.

Inbar-Feigenberg, M., Choufani, S., Butcher, D.T., Roifman, M. & Weksberg, R., 2013. Basic concepts of epigenetics. *Fertil Steril,* 99**,** 607-15.

Jacquet, K., Fradet-Turcotte, A., Avvakumov, N., Lambert, J.P., Roques, C., Pandita, R.K., Paquet, E., Herst, P., Gingras, A.C., Pandita, T.K., Legube, G., Doyon, Y., Durocher, D. & Cote, J., 2016. The TIP60 Complex Regulates Bivalent Chromatin Recognition by 53BP1 through Direct H4K20me Binding and H2AK15 Acetylation. *Mol Cell,* 62**,** 409-21.

Jakovcevski, M. & Akbarian, S., 2012. Epigenetic mechanisms in neurological disease. *Nat Med,* 18**,** 1194-204.

Jang, S.M., Kim, J.W., Kim, C.H., An, J.H., Johnson, A., Song, P.I., Rhee, S. & Choi, K.H., 2015a. KAT5-mediated SOX4 acetylation orchestrates chromatin remodeling during myoblast differentiation. *Cell Death Dis,* 6**,** e1857.

Jang, S.Y., Hong, D., Jeong, S.Y. & Kim, J.H., 2015b. Shikonin causes apoptosis by up-regulating p73 and down-regulating ICBP90 in human cancer cells. *Biochem Biophys Res Commun,* 465**,** 71-6.

Jenkins, Y., Markovtsov, V., Lang, W., Sharma, P., Pearsall, D., Warner, J., Franci, C., Huang, B., Huang, J., Yam, G.C., Vistan, J.P., Pali, E., Vialard, J., Janicot, M., Lorens, J.B., Payan, D.G. & Hitoshi, Y., 2005. Critical role of the ubiquitin ligase activity of UHRF1, a nuclear RING finger protein, in tumor cell growth. *Mol Biol Cell,* 16**,** 5621-9.

Jeong, K.W., Kim, K., Situ, A.J., Ulmer, T.S., An, W. & Stallcup, M.R., 2011. Recognition of enhancer element-specific histone methylation by TIP60 in transcriptional activation. *Nat Struct Mol Biol,* 18**,** 1358-65.

Jha, S., Vande Pol, S., Banerjee, N.S., Dutta, A.B., Chow, L.T. & Dutta, A., 2010. Destabilization of TIP60 by human papillomavirus E6 results in attenuation of TIP60-dependent transcriptional regulation and apoptotic pathway. *Mol Cell,* 38**,** 700-11.

Jin, B. & Robertson, K.D., 2013. DNA methyltransferases, DNA damage repair, and cancer. *Adv Exp Med Biol,* 754**,** 3-29.

Johnstone, R.W., 2002. Histone-deacetylase inhibitors: novel drugs for the treatment of cancer. *Nat Rev Drug Discov,* 1**,** 287-99.

Judes, G., Rifai, K., Ngollo, M., Daures, M., Bignon, Y.J., Penault-Llorca, F. & Bernard-Gallon, D., 2015. A bivalent role of TIP60 histone acetyl transferase in human cancer. *Epigenomics,* 7**,** 1351-63.

Jurkowska, R.Z., Jurkowski, T.P. & Jeltsch, A., 2011. Structure and function of mammalian DNA methyltransferases. *Chembiochem,* 12**,** 206-22.

Kaidi, A. & Jackson, S.P., 2013. KAT5 tyrosine phosphorylation couples chromatin sensing to ATM signalling. *Nature,* 498**,** 70-4.

Kamine, J., Elangovan, B., Subramanian, T., Coleman, D. & Chinnadurai, G., 1996. Identification of a cellular protein that specifically interacts with the essential cysteine region of the HIV-1 Tat transactivator. *Virology,* 216**,** 357-66.

Karagianni, P., Amazit, L., Qin, J. & Wong, J., 2008. ICBP90, a novel methyl K9 H3 binding protein linking protein ubiquitination with heterochromatin formation. *Mol Cell Biol,* 28**,** 705-17.

Kim, C.H., Kim, J.W., Jang, S.M., An, J.H., Seo, S.B. & Choi, K.H., 2015a. The chromodomain-containing histone acetyltransferase TIP60 acts as a code reader, recognizing the epigenetic codes for initiating transcription. *Biosci Biotechnol Biochem,* 79**,** 532-8.

Kim, J.H., Kim, B., Cai, L., Choi, H.J., Ohgi, K.A., Tran, C., Chen, C., Chung, C.H., Huber, O., Rose, D.W., Sawyers, C.L., Rosenfeld, M.G. & Baek, S.H., 2005. Transcriptional regulation of a metastasis suppressor gene by Tip60 and beta-catenin complexes. *Nature,* 434**,** 921-6.

Kim, J.W., Jang, S.M., Kim, C.H., An, J.H., Kang, E.J. & Choi, K.H., 2012. New molecular bridge between RelA/p65 and NF-kappaB target genes via histone acetyltransferase TIP60 cofactor. *J Biol Chem,* 287**,** 7780-91.

Kim, J.W., Song, P.I., Jeong, M.H., An, J.H., Lee, S.Y., Jang, S.M., Song, K.H., Armstrong, C.A. & Choi, K.H., 2008. TIP60 represses transcriptional activity of p73beta via an MDM2-bridged ternary complex. *J Biol Chem,* 283**,** 20077-86.

Kim, M.Y., Ann, E.J., Kim, J.Y., Mo, J.S., Park, J.H., Kim, S.Y., Seo, M.S. & Park, H.S., 2007. Tip60 histone acetyltransferase acts as a negative regulator of Notch1 signaling by means of acetylation. *Mol Cell Biol,* 27**,** 6506-19.

Kim, M.Y., Park, S.J., Shim, J.W., Yang, K., Kang, H.S. & Heo, K., 2015b. Naphthazarin enhances ionizing radiation-induced cell cycle arrest and apoptosis in human breast cancer cells. *Int J Oncol,* 46**,** 1659-66.

Kimura, A. & Horikoshi, M., 1998. Tip60 acetylates six lysines of a specific class in core histones in vitro. *Genes Cells,* 3**,** 789-800.

Kouzarides, T., 2007. Chromatin modifications and their function. *Cell,* 128**,** 693-705.

Kozakov, D., Hall, D.R., Xia, B., Porter, K.A., Padhorny, D., Yueh, C., Beglov, D. & Vajda, S., 2017. The ClusPro web server for protein-protein docking. *Nat Protoc,* 12**,** 255-278.

Krifa, M., Alhosin, M., Muller, C.D., Gies, J.P., Chekir-Ghedira, L., Ghedira, K., Mely, Y., Bronner, C. & Mousli, M., 2013. Limoniastrum guyonianum aqueous gall extract induces apoptosis in human cervical cancer cells involving p16 INK4A re-expression related to UHRF1 and DNMT1 down-regulation. *J Exp Clin Cancer Res,* 32**,** 30.

Krifa, M., Leloup, L., Ghedira, K., Mousli, M. & Chekir-Ghedira, L., 2014. Luteolin induces apoptosis in BE colorectal cancer cells by downregulating calpain, UHRF1, and DNMT1 expressions. *Nutr Cancer,* 66**,** 1220-7.

Kusch, T., Florens, L., Macdonald, W.H., Swanson, S.K., Glaser, R.L., Yates, J.R., 3rd, Abmayr, S.M., Washburn, M.P. & Workman, J.L., 2004. Acetylation by Tip60 is required for selective histone variant exchange at DNA lesions. *Science,* 306**,** 2084-7.

Lallous, N., Legrand, P., Mcewen, A.G., Ramon-Maiques, S., Samama, J.P. & Birck, C., 2011. The PHD finger of human UHRF1 reveals a new subgroup of unmethylated histone H3 tail readers. *PLoS One,* 6**,** e27599.

Lavin, M.F., Birrell, G., Chen, P., Kozlov, S., Scott, S. & Gueven, N., 2005. ATM signaling and genomic stability in response to DNA damage. *Mutat Res,* 569**,** 123-32.

Leduc, C., Claverie, P., Eymin, B., Col, E., Khochbin, S., Brambilla, E. & Gazzeri, S., 2006. p14ARF promotes RB accumulation through inhibition of its Tip60-dependent acetylation. *Oncogene,* 25**,** 4147-54.

Lee, M.S., Seo, J., Choi, D.Y., Lee, E.W., Ko, A., Ha, N.C., Yoon, J.B., Lee, H.W., Kim, K.P. & Song, J., 2013a. Stabilization of p21 (Cip1/WAF1) following Tip60-dependent acetylation is required for p21-mediated DNA damage response. *Cell Death Differ,* 20**,** 620-9.

Lee, M.T., Leung, Y.K., Chung, I., Tarapore, P. & Ho, S.M., 2013b. Estrogen receptor beta (ERbeta1) transactivation is differentially modulated by the transcriptional coregulator Tip60 in a cis-acting element-dependent manner. *J Biol Chem,* 288**,** 25038-52.

Legube, G., Linares, L.K., Lemercier, C., Scheffner, M., Khochbin, S. & Trouche, D., 2002. Tip60 is targeted to proteasome-mediated degradation by Mdm2 and accumulates after UV irradiation. *EMBO J,* 21**,** 1704-12.

Legube, G., Linares, L.K., Tyteca, S., Caron, C., Scheffner, M., Chevillard-Briet, M. & Trouche, D., 2004. Role of the histone acetyl transferase Tip60 in the p53 pathway. *J Biol Chem,* 279**,** 44825-33.

Legube, G. & Trouche, D., 2003. Identification of a larger form of the histone acetyl transferase Tip60. *Gene,* 310**,** 161-8.

Lemercier, C., Legube, G., Caron, C., Louwagie, M., Garin, J., Trouche, D. & Khochbin, S., 2003. Tip60 acetyltransferase activity is controlled by phosphorylation. *J Biol Chem,* 278**,** 4713-8.

Li, E., Bestor, T.H. & Jaenisch, R., 1992. Targeted mutation of the DNA methyltransferase gene results in embryonic lethality. *Cell,* 69**,** 915-26.

Li, H., Cuenin, C., Murr, R., Wang, Z.Q. & Herceg, Z., 2004. HAT cofactor Trrap regulates the mitotic checkpoint by modulation of Mad1 and Mad2 expression. *EMBO J,* 23**,** 4824-34.

Li, T., Wang, L., Du, Y., Xie, S., Yang, X., Lian, F., Zhou, Z. & Qian, C., 2018. Structural and mechanistic insights into UHRF1-mediated DNMT1 activation in the maintenance DNA methylation. *Nucleic Acids Res*.

Li, X.L., Meng, Q.H. & Fan, S.J., 2009. Adenovirus-mediated expression of UHRF1 reduces the radiosensitivity of cervical cancer HeLa cells to gamma-irradiation. *Acta Pharmacol Sin,* 30**,** 458-66.

Liang, C.C., Zhan, B., Yoshikawa, Y., Haas, W., Gygi, S.P. & Cohn, M.A., 2015. UHRF1 is a sensor for DNA interstrand crosslinks and recruits FANCD2 to initiate the Fanconi anemia pathway. *Cell Rep,* 10**,** 1947-56.

Liao, J., Karnik, R., Gu, H., Ziller, M.J., Clement, K., Tsankov, A.M., Akopian, V., Gifford, C.A., Donaghey, J., Galonska, C., Pop, R., Reyon, D., Tsai, S.Q., Mallard, W., Joung, J.K., Rinn, J.L., Gnirke, A. & Meissner, A., 2015. Targeted disruption of DNMT1, DNMT3A and DNMT3B in human embryonic stem cells. *Nat Genet,* 47**,** 469-78.

Lin, S.Y., Li, T.Y., Liu, Q., Zhang, C., Li, X., Chen, Y., Zhang, S.M., Lian, G., Liu, Q., Ruan, K., Wang, Z., Zhang, C.S., Chien, K.Y., Wu, J., Li, Q., Han, J. & Lin, S.C., 2012a. GSK3-TIP60-ULK1 signaling pathway links growth factor deprivation to autophagy. *Science,* 336**,** 477-81.

Lin, S.Y., Li, T.Y., Liu, Q., Zhang, C., Li, X., Chen, Y., Zhang, S.M., Lian, G., Liu, Q., Ruan, K., Wang, Z., Zhang, C.S., Chien, K.Y., Wu, J., Li, Q., Han, J. & Lin, S.C., 2012b. Protein phosphorylation-acetylation cascade connects growth factor deprivation to autophagy. *Autophagy,* 8**,** 1385-6.

Liu, N., Wang, J., Wang, J., Wang, R., Liu, Z., Yu, Y. & Lu, H., 2013a. ING5 is a Tip60 cofactor that acetylates p53 in response to DNA damage. *Cancer Res,* 73**,** 3749-60.

Liu, X., Gao, Q., Li, P., Zhao, Q., Zhang, J., Li, J., Koseki, H. & Wong, J., 2013b. UHRF1 targets DNMT1 for DNA methylation through cooperative binding of hemi-methylated DNA and methylated H3K9. *Nat Commun,* 4**,** 1563.

Liu, Z. & Sun, Y., 2011. Role of Tip60 tumor suppressor in DNA repair pathway. *Chinese Science Bulletin,* 56**,** 1212-1215.

Ma, H., Chen, H., Guo, X., Wang, Z., Sowa, M.E., Zheng, L., Hu, S., Zeng, P., Guo, R., Diao, J., Lan, F., Harper, J.W., Shi, Y.G., Xu, Y. & Shi, Y., 2012. M phase phosphorylation of the epigenetic regulator UHRF1 regulates its physical association with the deubiquitylase USP7 and stability. *Proc Natl Acad Sci U S A,* 109**,** 4828-33.

Mattera, L., Escaffit, F., Pillaire, M.J., Selves, J., Tyteca, S., Hoffmann, J.S., Gourraud, P.A., Chevillard-Briet, M., Cazaux, C. & Trouche, D., 2009. The p400/Tip60 ratio is critical for colorectal cancer cell proliferation through DNA damage response pathways. *Oncogene,* 28**,** 1506-17.

Me, L.L., Vidal, F., Gallardo, D., Diaz-Fuertes, M., Rojo, F., Cuatrecasas, M., Lopez-Vicente, L., Kondoh, H., Blanco, C., Carnero, A. & Ramon Y Cajal, S., 2006. New p53 related genes in human tumors: significant downregulation in colon and lung carcinomas. *Oncol Rep,* 16**,** 603-8.

Merlo, A., Herman, J.G., Mao, L., Lee, D.J., Gabrielson, E., Burger, P.C., Baylin, S.B. & Sidransky, D., 1995. 5' CpG island methylation is associated with transcriptional silencing of the tumour suppressor p16/CDKN2/MTS1 in human cancers. *Nat Med,* 1**,** 686-92.

Mistry, H., Tamblyn, L., Butt, H., Sisgoreo, D., Gracias, A., Larin, M., Gopalakrishnan, K., Hande, M.P. & Mcpherson, J.P., 2010. UHRF1 is a genome caretaker that facilitates the DNA damage response to gamma-irradiation. *Genome Integr,* 1**,** 7.

Miyamoto, N., Izumi, H., Noguchi, T., Nakajima, Y., Ohmiya, Y., Shiota, M., Kidani, A., Tawara, A. & Kohno, K., 2008. Tip60 is regulated by circadian transcription factor clock and is involved in cisplatin resistance. *J Biol Chem,* 283**,** 18218-26.

Mo, F., Zhuang, X., Liu, X., Yao, P.Y., Qin, B., Su, Z., Zang, J., Wang, Z., Zhang, J., Dou, Z., Tian, C., Teng, M., Niu, L., Hill, D.L., Fang, G., Ding, X., Fu, C. & Yao, X., 2016. Acetylation of Aurora B by TIP60 ensures accurate chromosomal segregation. *Nat Chem Biol,* 12**,** 226-32.

Mudbhary, R., Hoshida, Y., Chernyavskaya, Y., Jacob, V., Villanueva, A., Fiel, M.I., Chen, X., Kojima, K., Thung, S., Bronson, R.T., Lachenmayer, A., Revill, K., Alsinet, C., Sachidanandam, R., Desai, A., Senbanerjee, S., Ukomadu, C., Llovet, J.M. & Sadler, K.C., 2014. UHRF1 overexpression drives DNA hypomethylation and hepatocellular carcinoma. *Cancer Cell,* 25**,** 196-209.

Muto, M., Kanari, Y., Kubo, E., Takabe, T., Kurihara, T., Fujimori, A. & Tatsumi, K., 2002. Targeted disruption of Np95 gene renders murine embryonic stem cells hypersensitive to DNA damaging agents and DNA replication blocks. *J Biol Chem,* 277**,** 34549-55.

Myrianthopoulos, V., Cartron, P.F., Liutkeviciute, Z., Klimasauskas, S., Matulis, D., Bronner, C., Martinet, N. & Mikros, E., 2016. Tandem virtual screening targeting the SRA domain of UHRF1 identifies a novel chemical tool modulating DNA methylation. *Eur J Med Chem,* 114**,** 390-6.

Nady, N., Lemak, A., Walker, J.R., Avvakumov, G.V., Kareta, M.S., Achour, M., Xue, S., Duan, S., Allali-Hassani, A., Zuo, X., Wang, Y.X., Bronner, C., Chedin, F., Arrowsmith, C.H. & Dhe-Paganon, S., 2011. Recognition of multivalent histone states associated with heterochromatin by UHRF1 protein. *J Biol Chem,* 286**,** 24300-11.

Nagashima, M., Shiseki, M., Pedeux, R.M., Okamura, S., Kitahama-Shiseki, M., Miura, K., Yokota, J. & Harris, C.C., 2003. A novel PHD-finger motif protein, p47ING3, modulates p53-mediated transcription, cell cycle control, and apoptosis. *Oncogene,* 22**,** 343-50.

Naidu, S.R., Lakhter, A.J. & Androphy, E.J., 2012. PIASy-mediated Tip60 sumoylation regulates p53-induced autophagy. *Cell Cycle,* 11**,** 2717-28.

Nielsen, P.R., Nietlispach, D., Mott, H.R., Callaghan, J., Bannister, A., Kouzarides, T., Murzin, A.G., Murzina, N.V. & Laue, E.D., 2002. Structure of the HP1 chromodomain bound to histone H3 methylated at lysine 9. *Nature,* 416**,** 103-7.

Niida, H., Katsuno, Y., Sengoku, M., Shimada, M., Yukawa, M., Ikura, M., Ikura, T., Kohno, K., Shima, H., Suzuki, H., Tashiro, S. & Nakanishi, M., 2010. Essential role of Tip60-dependent recruitment of ribonucleotide reductase at DNA damage sites in DNA repair during G1 phase. *Genes Dev,* 24**,** 333-8.

Nishiyama, A., Yamaguchi, L., Sharif, J., Johmura, Y., Kawamura, T., Nakanishi, K., Shimamura, S., Arita, K., Kodama, T., Ishikawa, F., Koseki, H. & Nakanishi, M., 2013. Uhrf1-dependent H3K23 ubiquitylation couples maintenance DNA methylation and replication. *Nature,* 502**,** 249-53.

Okano, M., Bell, D.W., Haber, D.A. & Li, E., 1999. DNA methyltransferases Dnmt3a and Dnmt3b are essential for de novo methylation and mammalian development. *Cell,* 99**,** 247-57.

Pandey, A.K., Zhang, Y., Zhang, S., Li, Y., Tucker-Kellogg, G., Yang, H. & Jha, S., 2015. TIP60-miR-22 axis as a prognostic marker of breast cancer progression. *Oncotarget,* 6**,** 41290-306.

Parashar, G. & Capalash, N., 2016. Promoter methylation-independent reactivation of PAX1 by curcumin and resveratrol is mediated by UHRF1. *Clin Exp Med,* 16**,** 471-8.

Park, J.H., Sun, X.J. & Roeder, R.G., 2010. The SANT domain of p400 ATPase represses acetyltransferase activity and coactivator function of TIP60 in basal p21 gene expression. *Mol Cell Biol,* 30**,** 2750-61.

Patel, J.H., Du, Y., Ard, P.G., Phillips, C., Carella, B., Chen, C.J., Rakowski, C., Chatterjee, C., Lieberman, P.M., Lane, W.S., Blobel, G.A. & Mcmahon, S.B., 2004. The c-MYC oncoprotein is a substrate of the acetyltransferases hGCN5/PCAF and TIP60. *Mol Cell Biol,* 24**,** 10826-34.

Pei, J.H., Luo, S.Q., Zhong, Y., Chen, J.H., Xiao, H.W. & Hu, W.X., 2011. The association between non-Hodgkin lymphoma and methylation of p73. *Tumour Biol,* 32**,** 1133-8.

Pierce, B.A., 2012. *Genetics: A conceptual approach*: Macmillan.

Ponting, C.P., Oliver, P.L. & Reik, W., 2009. Evolution and functions of long noncoding RNAs. *Cell,* 136**,** 629-41.

Portela, A. & Esteller, M., 2010. Epigenetic modifications and human disease. *Nat Biotechnol,* 28**,** 1057-68.

Pray-Grant, M.G., Daniel, J.A., Schieltz, D., Yates, J.R., 3rd & Grant, P.A., 2005. Chd1 chromodomain links histone H3 methylation with SAGA- and SLIK-dependent acetylation. *Nature,* 433**,** 434-8.

Putnik, J., Zhang, C.D., Archangelo, L.F., Tizazu, B., Bartels, S., Kickstein, M., Greif, P.A. & Bohlander, S.K., 2007. The interaction of ETV6 (TEL) and TIP60 requires a functional histone acetyltransferase domain in TIP60. *Biochim Biophys Acta,* 1772**,** 1211-24.

Qin, W., Wolf, P., Liu, N., Link, S., Smets, M., La Mastra, F., Forne, I., Pichler, G., Horl, D., Fellinger, K., Spada, F., Bonapace, I.M., Imhof, A., Harz, H. & Leonhardt, H., 2015. DNA methylation requires a DNMT1 ubiquitin interacting motif (UIM) and histone ubiquitination. *Cell Res,* 25**,** 911-29.

Rajagopalan, D., Pandey, A.K., Xiuzhen, M.C., Lee, K.K., Hora, S., Zhang, Y., Chua, B.H., Kwok, H.S., Bhatia, S.S., Deng, L.W., Tenen, D.G., Kappei, D. & Jha, S., 2017. TIP60 represses telomerase expression by inhibiting Sp1 binding to the TERT promoter. *PLoS Pathog,* 13**,** e1006681.

Rajakumara, E., Wang, Z., Ma, H., Hu, L., Chen, H., Lin, Y., Guo, R., Wu, F., Li, H., Lan, F., Shi, Y.G., Xu, Y., Patel, D.J. & Shi, Y., 2011. PHD finger recognition of unmodified histone H3R2 links UHRF1 to regulation of euchromatic gene expression. *Mol Cell,* 43**,** 275-284.

Ran, Q. & Pereira-Smith, O.M., 2000. Identification of an alternatively spliced form of the Tat interactive protein (Tip60), Tip60(beta). *Gene,* 258**,** 141-6.

Ravichandran, P. & Ginsburg, D., 2015. Tip60 overexpression exacerbates chemotherapeutic drug treatment in breast, pancreatic, and lung cancer cell lines. *The FASEB Journal,* 29**,** 725.21.

Renaud, E., Barascu, A. & Rosselli, F., 2016. Impaired TIP60-mediated H4K16 acetylation accounts for the aberrant chromatin accumulation of 53BP1 and RAP80 in Fanconi anemia pathway-deficient cells. *Nucleic Acids Res,* 44**,** 648-56.

Riggs, A.D., 1975. X inactivation, differentiation, and DNA methylation. *Cytogenet Cell Genet,* 14**,** 9-25.

Riggs, A.D., Martienssen, R.A. & Russo, V.E.A., 1996. *Epigenetic mechanisms of gene regulation* New York: Cold Spring Harbor Laboratory Press.

Robertson, K.D., 2005. DNA methylation and human disease. *Nat Rev Genet,* 6**,** 597-610.

Rodriguez, J., Frigola, J., Vendrell, E., Risques, R.A., Fraga, M.F., Morales, C., Moreno, V., Esteller, M., Capella, G., Ribas, M. & Peinado, M.A., 2006. Chromosomal instability correlates with genome-wide DNA demethylation in human primary colorectal cancers. *Cancer Res,* 66**,** 8462-9468.

Rothbart, S.B., Krajewski, K., Nady, N., Tempel, W., Xue, S., Badeaux, A.I., Barsyte-Lovejoy, D., Martinez, J.Y., Bedford, M.T., Fuchs, S.M., Arrowsmith, C.H. & Strahl, B.D., 2012. Association of UHRF1 with methylated H3K9 directs the maintenance of DNA methylation. *Nat Struct Mol Biol,* 19**,** 1155-60.

Rottach, A., Frauer, C., Pichler, G., Bonapace, I.M., Spada, F. & Leonhardt, H., 2010. The multi-domain protein Np95 connects DNA methylation and histone modification. *Nucleic Acids Res,* 38**,** 1796-804.

Ruan, K., Yamamoto, T.G., Asakawa, H., Chikashige, Y., Kimura, H., Masukata, H., Haraguchi, T. & Hiraoka, Y., 2015. Histone H4 acetylation required for chromatin decompaction during DNA replication. *Sci Rep,* 5**,** 12720.

Ruan, Y., 2015. Investigating the regulation of UHRF1 in cell cycle. The University of Hong Kong (Pokfulam, Hong Kong).

Sakuraba, K., Yasuda, T., Sakata, M., Kitamura, Y.H., Shirahata, A., Goto, T., Mizukami, H., Saito, M., Ishibashi, K., Kigawa, G., Nemoto, H., Sanada, Y. & Hibi, K., 2009. Down-regulation of Tip60 gene as a potential marker for the malignancy of colorectal cancer. *Anticancer Res,* 29**,** 3953-5.

Sakuraba, K., Yokomizo, K., Shirahata, A., Goto, T., Saito, M., Ishibashi, K., Kigawa, G., Nemoto, H. & Hibi, K., 2011. TIP60 as a potential marker for the malignancy of gastric cancer. *Anticancer Res,* 31**,** 77-9.

Sapountzi, V., Logan, I.R. & Robson, C.N., 2006. Cellular functions of TIP60. *Int J Biochem Cell Biol,* 38**,** 1496-509.

Seo, J.S., Choi, Y.H., Moon, J.W., Kim, H.S. & Park, S.H., 2017. Hinokitiol induces DNA demethylation via DNMT1 and UHRF1 inhibition in colon cancer cells. *BMC Cell Biol,* 18**,** 14.

Shamma, A., Suzuki, M., Hayashi, N., Kobayashi, M., Sasaki, N., Nishiuchi, T., Doki, Y., Okamoto, T., Kohno, S., Muranaka, H., Kitajima, S., Yamamoto, K. & Takahashi, C., 2013. ATM mediates pRB function to control DNMT1 protein stability and DNA methylation. *Mol Cell Biol,* 33**,** 3113-24.

Sharif, J., Muto, M., Takebayashi, S., Suetake, I., Iwamatsu, A., Endo, T.A., Shinga, J., Mizutani-Koseki, Y., Toyoda, T., Okamura, K., Tajima, S., Mitsuya, K., Okano, M. & Koseki, H., 2007. The SRA protein Np95 mediates epigenetic inheritance by recruiting Dnmt1 to methylated DNA. *Nature,* 450**,** 908-12.

Sharif, T., Alhosin, M., Auger, C., Minker, C., Kim, J.H., Etienne-Selloum, N., Bories, P., Gronemeyer, H., Lobstein, A., Bronner, C., Fuhrmann, G. & Schini-Kerth, V.B., 2012. Aronia melanocarpa juice induces a redox-sensitive p73-related caspase 3-dependent apoptosis in human leukemia cells. *PLoS One,* 7**,** e32526.

Sharif, T., Auger, C., Alhosin, M., Ebel, C., Achour, M., Etienne-Selloum, N., Fuhrmann, G., Bronner, C. & Schini-Kerth, V.B., 2010. Red wine polyphenols cause growth inhibition and apoptosis in acute lymphoblastic leukaemia cells by inducing a redox-sensitive up-regulation of p73 and down-regulation of UHRF1. *Eur J Cancer,* 46**,** 983-94.

Sheridan, A.M., Force, T., Yoon, H.J., O'leary, E., Choukroun, G., Taheri, M.R. & Bonventre, J.V., 2001. PLIP, a novel splice variant of Tip60, interacts with group IV cytosolic phospholipase A(2), induces apoptosis, and potentiates prostaglandin production. *Mol Cell Biol,* 21**,** 4470-81.

Shin, S.H. & Kang, S.S., 2013. Phosphorylation of Tip60 Tyrosine 327 by Abl Kinase Inhibits HAT Activity through Association with FE65. *Open Biochem J,* 7**,** 66-72.

Shiota, M., Yokomizo, A., Masubuchi, D., Tada, Y., Inokuchi, J., Eto, M., Uchiumi, T., Fujimoto, N. & Naito, S., 2010. Tip60 promotes prostate cancer cell proliferation by translocation of androgen receptor into the nucleus. *Prostate,* 70**,** 540-54.

Sidhu, H. & Capalash, N., 2017. UHRF1: The key regulator of epigenetics and molecular target for cancer therapeutics. *Tumour Biol,* 39**,** 1010428317692205.

Simon, R.P., Robaa, D., Alhalabi, Z., Sippl, W. & Jung, M., 2016. KATching-Up on Small Molecule Modulators of Lysine Acetyltransferases. *J Med Chem,* 59**,** 1249-70.

Stefansson, O.A., Jonasson, J.G., Olafsdottir, K., Hilmarsdottir, H., Olafsdottir, G., Esteller, M., Johannsson, O.T. & Eyfjord, J.E., 2011. CpG island hypermethylation of BRCA1 and loss of pRb as co-occurring events in basal/triple-negative breast cancer. *Epigenetics,* 6**,** 638-49.

Struhl, K., 1998. Histone acetylation and transcriptional regulatory mechanisms. *Genes Dev,* 12**,** 599-606.

Su, J., Wang, F., Cai, Y. & Jin, J., 2016. The Functional Analysis of Histone Acetyltransferase MOF in Tumorigenesis. *Int J Mol Sci,* 17.

Su, W.P., Ho, Y.C., Wu, C.K., Hsu, S.H., Shiu, J.L., Huang, J.C., Chang, S.B., Chiu, W.T., Hung, J.J., Liu, T.L., Wu, W.S., Wu, P.Y., Su, W.C., Chang, J.Y. & Liaw, H., 2017. Chronic treatment with cisplatin induces chemoresistance through the TIP60-mediated Fanconi anemia and homologous recombination repair pathways. *Sci Rep,* 7**,** 3879.

Subbaiah, V.K., Zhang, Y., Rajagopalan, D., Abdullah, L.N., Yeo-Teh, N.S., Tomaic, V., Banks, L., Myers, M.P., Chow, E.K. & Jha, S., 2016. E3 ligase EDD1/UBR5 is utilized by the HPV E6 oncogene to destabilize tumor suppressor TIP60. *Oncogene,* 35**,** 2062-74.

Sun, Y., Jiang, X., Chen, S., Fernandes, N. & Price, B.D., 2005. A role for the Tip60 histone acetyltransferase in the acetylation and activation of ATM. *Proc Natl Acad Sci U S A,* 102**,** 13182-7.

Sun, Y., Jiang, X., Xu, Y., Ayrapetov, M.K., Moreau, L.A., Whetstine, J.R. & Price, B.D., 2009. Histone H3 methylation links DNA damage detection to activation of the tumour suppressor Tip60. *Nat Cell Biol,* 11**,** 1376-82.

Sun, Y., Xu, Y., Roy, K. & Price, B.D., 2007. DNA damage-induced acetylation of lysine 3016 of ATM activates ATM kinase activity. *Mol Cell Biol,* 27**,** 8502-9.

Suzuki, K., Yamauchi, M., Oka, Y., Suzuki, M. & Yamashita, S., 2011. Creating localized DNA double-strand breaks with microirradiation. *Nat Protoc,* 6**,** 134-9.

Sykes, S.M., Mellert, H.S., Holbert, M.A., Li, K., Marmorstein, R., Lane, W.S. & Mcmahon, S.B., 2006. Acetylation of the p53 DNA-binding domain regulates apoptosis induction. *Mol Cell,* 24**,** 841-51.

Szumiel, I. & Foray, N., 2011. Chromatin acetylation, beta-amyloid precursor protein and its binding partner FE65 in DNA double strand break repair. *Acta Biochim Pol,* 58**,** 11-8.

Tang, J., Cho, N.W., Cui, G., Manion, E.M., Shanbhag, N.M., Botuyan, M.V., Mer, G. & Greenberg, R.A., 2013. Acetylation limits 53BP1 association with damaged chromatin to promote homologous recombination. *Nat Struct Mol Biol,* 20**,** 317-25.

Tang, Y., Luo, J., Zhang, W. & Gu, W., 2006. Tip60-dependent acetylation of p53 modulates the decision between cell-cycle arrest and apoptosis. *Mol Cell,* 24**,** 827-39.

Tauber, M. & Fischle, W., 2015. Conserved linker regions and their regulation determine multiple chromatin-binding modes of UHRF1. *Nucleus,* 6**,** 123-32.

Taubert, S., Gorrini, C., Frank, S.R., Parisi, T., Fuchs, M., Chan, H.M., Livingston, D.M. & Amati, B., 2004. E2F-dependent histone acetylation and recruitment of the Tip60 acetyltransferase complex to chromatin in late G1. *Mol Cell Biol,* 24**,** 4546-56.

Tian, Y., Paramasivam, M., Ghosal, G., Chen, D., Shen, X., Huang, Y., Akhter, S., Legerski, R., Chen, J., Seidman, M.M., Qin, J. & Li, L., 2015. UHRF1 contributes to DNA damage repair as a lesion recognition factor and nuclease scaffold. *Cell Rep,* 10**,** 1957-66.

Trotzier, M.A., Bronner, C., Bathami, K., Mathieu, E., Abbady, A.Q., Jeanblanc, M., Muller, C.D., Rochette-Egly, C. & Mousli, M., 2004. Phosphorylation of ICBP90 by protein kinase A enhances topoisomerase IIalpha expression. *Biochem Biophys Res Commun,* 319**,** 590-5.

Unnikrishnan, A., Gafken, P.R. & Tsukiyama, T., 2010. Dynamic changes in histone acetylation regulate origins of DNA replication. *Nat Struct Mol Biol,* 17**,** 430-7.

Unoki, M., 2011. Current and potential anticancer drugs targeting members of the UHRF1 complex including epigenetic modifiers. *Recent Pat Anticancer Drug Discov,* 6**,** 116-30.

Unoki, M., Brunet, J. & Mousli, M., 2009a. Drug discovery targeting epigenetic codes: the great potential of UHRF1, which links DNA methylation and histone modifications, as a drug target in cancers and toxoplasmosis. *Biochem Pharmacol,* 78**,** 1279-88.

Unoki, M., Kelly, J.D., Neal, D.E., Ponder, B.A., Nakamura, Y. & Hamamoto, R., 2009b. UHRF1 is a novel molecular marker for diagnosis and the prognosis of bladder cancer. *Br J Cancer,* 101**,** 98-105.

Van Den Broeck, A., Nissou, D., Brambilla, E., Eymin, B. & Gazzeri, S., 2012. Activation of a Tip60/E2F1/ERCC1 network in human lung adenocarcinoma cells exposed to cisplatin. *Carcinogenesis,* 33**,** 320-5.

Verdin, E. & Ott, M., 2015. 50 years of protein acetylation: from gene regulation to epigenetics, metabolism and beyond. *Nat Rev Mol Cell Biol,* 16**,** 258-64.

Voss, A.K. & Thomas, T., 2009. MYST family histone acetyltransferases take center stage in stem cells and development. *Bioessays,* 31**,** 1050-61.

Wahlestedt, C., 2013. Targeting long non-coding RNA to therapeutically upregulate gene expression. *Nat Rev Drug Discov,* 12**,** 433-46.

Wang, C., Shen, J., Yang, Z., Chen, P., Zhao, B., Hu, W., Lan, W., Tong, X., Wu, H., Li, G. & Cao, C., 2011. Structural basis for site-specific reading of unmodified R2 of histone H3 tail by UHRF1 PHD finger. *Cell Res,* 21**,** 1379-82.

Wang, J. & Chen, J., 2010. SIRT1 regulates autoacetylation and histone acetyltransferase activity of TIP60. *J Biol Chem,* 285**,** 11458-64.

Wang, Q. & Goldstein, M., 2016. Small RNAs Recruit Chromatin-Modifying Enzymes MMSET and Tip60 to Reconfigure Damaged DNA upon Double-Strand Break and Facilitate Repair. *Cancer Res,* 76**,** 1904-15.

Wapenaar, H. & Dekker, F.J., 2016. Histone acetyltransferases: challenges in targeting bi-substrate enzymes. *Clin Epigenetics,* 8**,** 59.

Wu, S.M., Cheng, W.L., Liao, C.J., Chi, H.C., Lin, Y.H., Tseng, Y.H., Tsai, C.Y., Chen, C.Y., Lin, S.L., Chen, W.J., Yeh, Y.H., Huang, C.Y., Chen, M.H., Yeh, Y.C. & Lin, K.H., 2015. Negative modulation of the epigenetic regulator, UHRF1, by thyroid hormone receptors suppresses liver cancer cell growth. *Int J Cancer,* 137**,** 37-49.

Xiao, H., Chung, J., Kao, H.Y. & Yang, Y.C., 2003. Tip60 is a co-repressor for STAT3. *J Biol Chem,* 278**,** 11197-204.

Xiao, Y., Nagai, Y., Deng, G., Ohtani, T., Zhu, Z., Zhou, Z., Zhang, H., Ji, M.Q., Lough, J.W., Samanta, A., Hancock, W.W. & Greene, M.I., 2014. Dynamic interactions between TIP60 and p300 regulate FOXP3 function through a structural switch defined by a single lysine on TIP60. *Cell Rep,* 7**,** 1471-80.

Xu, F., Mao, C., Ding, Y., Rui, C., Wu, L., Shi, A., Zhang, H., Zhang, L. & Xu, Z., 2010. Molecular and enzymatic profiles of mammalian DNA methyltransferases: structures and targets for drugs. *Curr Med Chem,* 17**,** 4052-71.

Xu, S., Panikker, P., Iqbal, S. & Elefant, F., 2016. Tip60 HAT Action Mediates Environmental Enrichment Induced Cognitive Restoration. *PLoS One,* 11**,** e0159623.

Xu, Y., Liao, R., Li, N., Xiang, R. & Sun, P., 2014. Phosphorylation of Tip60 by p38alpha regulates p53-mediated PUMA induction and apoptosis in response to DNA damage. *Oncotarget,* 5**,** 12555-72.

Xu, Y. & Price, B.D., 2011. Chromatin dynamics and the repair of DNA double strand breaks. *Cell Cycle,* 10**,** 261-7.

Yamada, H.Y., 2012. *Human Tip60 (NuA4) Complex and Cancer*: INTECH Open Access Publisher.

Yamamoto, T. & Horikoshi, M., 1997. Novel substrate specificity of the histone acetyltransferase activity of HIV-1-Tat interactive protein Tip60. *J Biol Chem,* 272**,** 30595-8.

Yan, Y., Barlev, N.A., Haley, R.H., Berger, S.L. & Marmorstein, R., 2000. Crystal structure of yeast Esa1 suggests a unified mechanism for catalysis and substrate binding by histone acetyltransferases. *Mol Cell,* 6**,** 1195-205.

Yan, Y., Harper, S., Speicher, D.W. & Marmorstein, R., 2002. The catalytic mechanism of the ESA1 histone acetyltransferase involves a self-acetylated intermediate. *Nat Struct Biol,* 9**,** 862-9.

Yang, C., Wang, Y., Zhang, F., Sun, G., Li, C., Jing, S., Liu, Q. & Cheng, Y., 2013. Inhibiting UHRF1 expression enhances radiosensitivity in human esophageal squamous cell carcinoma. *Mol Biol Rep,* 40**,** 5225-35.

Yang, C., Wu, J. & Zheng, Y.G., 2012. Function of the active site lysine autoacetylation in Tip60 catalysis. *PLoS One,* 7**,** e32886.

Yang, J., Liu, K., Yang, J., Jin, B., Chen, H., Zhan, X., Li, Z., Wang, L., Shen, X., Li, M., Yu, W. & Mao, Z., 2017a. PIM1 induces cellular senescence through phosphorylation of UHRF1 at Ser311. *Oncogene,* 36**,** 4828-4842.

Yang, Y., Sun, J., Chen, T., Tao, Z., Zhang, X., Tian, F., Zhou, X. & Lu, D., 2017b. Tat-interactive Protein-60KDA (TIP60) Regulates the Tumorigenesis of Lung Cancer In Vitro. *Journal of Cancer,* 8**,** 2277-2281.

Yoon, M.K., Ha, J.H., Lee, M.S. & Chi, S.W., 2015. Structure and apoptotic function of p73. *BMB Rep,* 48**,** 81-90.

Yoon, S. & Eom, G.H., 2016. HDAC and HDAC Inhibitor: From Cancer to Cardiovascular Diseases. *Chonnam Med J,* 52**,** 1-11.

Zeng, S., Wang, Y., Zhang, T., Bai, L., Wang, Y. & Duan, C., 2017. E3 ligase UHRF2 stabilizes the acetyltransferase TIP60 and regulates H3K9ac and H3K14ac via RING finger domain. *Protein Cell,* 8**,** 202-218.

Zhang, H., Liu, H., Chen, Y., Yang, X., Wang, P., Liu, T., Deng, M., Qin, B., Correia, C., Lee, S., Kim, J., Sparks, M., Nair, A.A., Evans, D.L., Kalari, K.R., Zhang, P., Wang, L., You, Z., Kaufmann, S.H., Lou, Z. & Pei, H., 2016a. A cell cycle-dependent BRCA1-UHRF1 cascade regulates DNA double-strand break repair pathway choice. *Nat Commun,* 7**,** 10201.

Zhang, J., Gao, Q., Li, P., Liu, X., Jia, Y., Wu, W., Li, J., Dong, S., Koseki, H. & Wong, J., 2011. S phase-dependent interaction with DNMT1 dictates the role of UHRF1 but not UHRF2 in DNA methylation maintenance. *Cell Res,* 21**,** 1723-39.

Zhang, Y., Subbaiah, V.K., Rajagopalan, D., Tham, C.Y., Abdullah, L.N., Toh, T.B., Gong, M., Tan, T.Z., Jadhav, S.P., Pandey, A.K., Karnani, N., Chow, E.K., Thiery, J.P. & Jha, S., 2016b. TIP60 inhibits metastasis by ablating DNMT1-SNAIL2-driven epithelial-mesenchymal transition program. *J Mol Cell Biol*.

Zhang, Z.M., Rothbart, S.B., Allison, D.F., Cai, Q., Harrison, J.S., Li, L., Wang, Y., Strahl, B.D., Wang, G.G. & Song, J., 2015. An Allosteric Interaction Links USP7 to Deubiquitination and Chromatin Targeting of UHRF1. *Cell Rep,* 12**,** 1400-6.

Zhao, H., Jin, S. & Gewirtz, A.M., 2012. The histone acetyltransferase TIP60 interacts with c-Myb and inactivates its transcriptional activity in human leukemia. *J Biol Chem,* 287**,** 925-34.

Zheng, H., Seit-Nebi, A., Han, X., Aslanian, A., Tat, J., Liao, R., Yates, J.R., 3rd & Sun, P., 2013. A posttranslational modification cascade involving p38, Tip60, and PRAK mediates oncogene-induced senescence. *Mol Cell,* 50**,** 699-710.

LIST OF PUBLICATIONS

1- **Waseem Ashraf,** Abdulkhaleg Ibrahim, Mahmoud Alhosin, Liliyana Zaayter, Khalid Ouararhni, Christophe Papin, Tanveer Ahmad, Ali Hamiche, Yves Mély, Christian Bronner and Marc Mousli. "UHRF1: on the road to become a universal biomarker for cancer". Oncotarget 2017

2- **Waseem Ashraf**, Christian Bronner, Liliyana Zaayter, Tanveer Ahmad, Ludovic Richert, Mahmoud Alhosin, Abdulkhaleg Ibrahim, Ali Hamiche, Yves Mely and Marc Mousli. "Interaction of the Epigenetic Integrator UHRF1 with Tip60 through MYST domain during S Phase in Living Cells". Journal of experimental & clinical cancer research 2017

3- Liliyana Zaayter1, Mattia Mori, **Waseem Ashraf**, Christian Boudier, Vasyl Kilin, Krishna Gavvala, Tanveer Ahmad, Sylvia Eiler, Marc Ruff, Maurizio Botta, Christian Bronner, Marc Mousli and Yves Mély. "Targeting the base flipping activity of human UHRF1 decreases DNA methylation and impairs DNMT1 recruitment". (In preparation)

4- **Waseem Ashraf**, Mounira Krifa, Liliyana Zaayter, Tanveer Ahmad, Antonio Pizzi, Christian D. Muller, Yves Mély, Christina Bronner and Marc Mousli. "Maritime pine tannin extract exhibits anticancer properties by inducing expression of p73 and targeting DNA methylation machinery in cancer cells". (In preparation)

ANNEXURE

7 - ANNEXURE

Targeting of UHRF1 for anticancer therapy

Differentially high expression of UHRF1 in cancers and its putative role as an oncogene in cancer cells make UHRF1 an attractive target for anticancer therapy. During my PhD I also worked on two projects targeting UHRF1 by different approaches. In one approach, small synthetic molecules were screened against the known structure of UHRF1 SRA domain in order to find a potent and specific inhibitor of UHRF1. SRA is the key functional domain of UHRF1 involved in maintenance of DNA methylation patterns and repair mechanisms, thus targeting this domain can inhibit the UHRF1 functions in cell.

In second approach, we utilized an extract from Maritime pine bark to target the proliferation of anticancer cells. In our previous studies, plants extract rich in polyphenolic compounds have been proven effective against the cancer cells by targeting UHRF1 or DNA methylation maintenance machinery and we observed similar anticancer effects with tannins extracted from Maritime pine bark.

7.1 Manuscript II

Targeting the base flipping activity of human UHRF1 decreases DNA methylation and impairs DNMT1 recruitment

Liliyana Zaayter[1,#], Mattia Mori[2,#], Waseem Ashraf[1], Christian Boudier[1], Vasyl Kilin[1], Krishna Gavvala[1], Tanveer Ahmad[1], Sylvia Eiler[3], Marc Ruff[3], Maurizio Botta[3], Christian Bronner[3], Marc Mousli[1,*], Yves Mély[1,*]

[1] Laboratoire de Bioimagerie et Pathologies, UMR 7021 CNRS, Université de Strasbourg, Faculté de Pharmacie, Illkirch-France

[2] Dipartimento di Biotecnologie, Chimica e Farmacia, Università degli Studi di Siena, Via Aldo Moro 2, 53100, Siena, Italy.

[3] Institut de Génétique et de Biologie Moléculaire et Cellulaire (IGBMC), INSERM U964 CNRS UMR 7104, Université de Strasbourg, Illkirch-France.

[#] LZ and MM equally contributed to this work

*Authors to whom correspondence should be addressed: Yves Mély, yves.mely@unistra.fr; Marc Mousli, mousli@unistra.fr;

Abstract:

During DNA replication, Ubiquitin-like, containing PHD and RING fingers domains (UHRF1) plays key roles in the inheritance of methylation patterns to daughter strands by recognizing through its set and ring (SRA) domain the methylated CpGs and recruiting DNA methyltransferase1 (DNMT1). Herein, our goal is to identify UHRF1 inhibitors targeting the 5'-methylcytosine (5mC) binding pocket of the SRA domain to prevent the recognition and flipping of 5mC and hence, methylation aberrancies. For this, we used a multidisciplinary strategy combining virtual screening and molecular modeling with biophysical assays. The latter include a sensitive and selective base flipping assay, isothermal titration calorimetry, global DNA methylation assay and fluorescence lifetime imaging microscopy. We identified one active compound from the anthraquinone family, with a dose-response effect in the low micromolar range (IC_{50} = 4.4±0.5 μM) that was able to bind to the 5'-methylcytosine binding pocket of SRA and inhibit the base flipping process. Our results also showed that this hit impaired the interaction between UHRF1 and DNMT1 and decreased the overall methylation of DNA in cells, further highlighting base flipping as a critical event for DNMT1 recruitment. This study provides a proof of concept that UHRF1 can be a druggable target for anti-cancer therapy.

A- Introduction:

During the life of an organism, the genome undergoes a chain of epigenetic processes that shapes the function and morphology of a cell in a very diverse way. These epigenetic processes notably direct the gene expression patterns, establishing the identity of a cell that could be heritable for future generations. DNA methylation is a major epigenetic modification that controls the cell identity and fate, being responsible for many fundamental processes such as differentiation, genome imprinting and X chromosome inactivation [1-3]. This mark is also strongly involved in cancer [4, 5], as it is well recognized that DNA hypermethylation at specific loci is one of the hallmarks of tumorigenesis. Indeed, abnormal gain of DNA methylation in promoter regions of tumor suppressor genes plays a key role in their silencing and transcriptional repression [6, 7]. Therefore, in addition to the reversible nature of epigenetic mechanisms, unlike genetic ones, epigenetic mediators have gained considerable attention as pharmaceutical targets. Different strategies can be used to target DNA methylation as numerous actors are involved in this epigenetic process, but the most effective would be to interfere with early effectors involved in the duplication of the methylation patterns. In order to achieve a faithful transmission of these patterns, the DNA methylation machinery is coordinated by a macro-molecular protein complex [8, 9], in which UHRF1 (Ubiquitin-like, containing PHD and RING fingers domains) is the first effector. Indeed, UHRF1 binds specifically via its SET and RING-associated domain (SRA) to CpG motifs in the hemi-methylated (HM) DNA formed by the parent and daughter strands and flips out the 5'-methylcytosine (5mC) from the DNA helix [10, 11]. X-ray crystallography structures of SRA in complex with HM DNA helped to propose a model of DNA recognition and base flipping [10, 12, 13]. In these structures, SRA acts as a hand grasping the DNA duplex in its palm and through its NKR finger and its thumb, it flips out the 5mC into a binding pocket located in the palm. The flipped out 5mC is stabilized by pi-stacking interactions with two aromatic residues (Y478, Y466) [13]. Besides this, UHRF1 also binds to histone H3K9me3 via its tandem Tudor and PHD domain [14, 15]. These features promote the recruitment of DNA methyltransferase1 (DNMT1) to replication forks in the S phase of the cell cycle in order to ensure the maintenance of the methylation patterns in the newly formed DNA [11, 15, 16]. Alternatively, via the E3 ligase activity of its RING domain, UHRF1, can also mediate the ubiquitylation of H3K23 and H3K18, creating binding sites for DNMT1 [17, 18].

Numerous emerging therapeutic strategies focus on targeting DNA methylation [19], but till date, only demethylating agents targeting DNMT1 have been disclosed. These agents include FDA-approved nucleoside analogs (Azacytidine and Decitabine) [20, 21] and non-nucleoside inhibitors such as Hydralazine and Procainamide [22]. Several limitations upon their usage such as chemical instability, cytotoxicity and poor selectivity [23-25] stimulated the search of alternative treatments with improved efficacy and fewer side effects. Due to its key role in DNA methylation and its overexpression in almost every type of tumors [26], UHRF1 is perceived as a major target for anti-cancer therapy [27, 28]. Till date, several natural compounds have been reported to act on UHRF1 signaling pathways [9, 29, 30], but only two inhibitors have been identified to directly target the protein. One of these inhibitors is an uracil derivative that targets the SRA domain and perturbs the interaction with DNMT1 [31], while the second one, 4-benzylpiperidine-1-carboximidamide, targets the TTD groove and alters the binding of UHRF1 to H3K9me3 [32]. Finally, mitoxantrone, a topoisomerase II inhibitor, has also been reported to alter the binding of the SRA domain to HM DNA and induce hypomethylation with subsequent re-expression of tumor suppressor genes (TSGs) [33, 34].

In this context, our aim is to discover small molecule UHRF1 inhibitors that can fit into the 5mC binding pocket of the SRA domain. This binding mechanism is expected to impair the interaction of SRA to HM DNA and the subsequent flipping of 5mC. As a result, such inhibitors may prevent the recruitment of DNMT1 and hence, the transmission of the methylation marks, thereby improving the control of aberrant DNA methylation. To achieve this aim, we established a multidisciplinary strategy that includes virtual screening and molecular modeling together with biophysical assays and cellular studies. We found an active compound UM63 that shares some chemical features with mitoxantrone [35, 36]. Through binding to the 5mC binding pocket, UM63 prevented base flipping with an IC_{50} value in the low micromolar range. Moreover, UM63 inhibited the DNMT1/UHRF1 interaction and decreased the DNA methylation level in HeLa cells, thus emerging as a valuable UHRF1 inhibitor tool as well as a starting point for hit-to-lead optimization.

B- Materials and methods:

1- Materials

All compounds were dissolved in pure DMSO (Sigma Aldrich) and kept at -20°C. 4-Amino-1-(β-D-ribofuranosyl)-1,3,5-triazin-2(1*H*)-one and 5-Azacitidine ≥98 % (HPLC) were purchased from Sigma Aldrich. Wild-type SRA (residues 408-643) and SRA mutant (G488D) were expressed and purified in Escherichia coli BL21-pLysS (DE3) 3839 as previously described [37, 38]. Their concentration was calculated by using an extinction coefficient of 43,890 $M^{-1}cm^{-1}$ at 280 nm. DNA duplexes were obtained by annealing equal molar amounts of complementary oligonucleotides, and heating to 90°C for 5 min, and then cooling slowly down to room temperature. The following 12-bp duplex sequence was used **5'-GGGCCXGCAGGG-3' / 5'-CCCTGCGGGCCC-3'** with a single CpG site that was either non-methylated (X = C) or hemi-methylated (X = 5mC). Unlabeled oligonucleotides were purchased from IBA GmbH Nucleic Acids Product Supply (Germany) in a HPLC-purified form. Labeled 5'-GGGCCXGCAGGG-3' oligonucleotides with ^{th}G at position 7 were purchased from TriLink Biotechnologies (USA).

2- Absorption spectroscopy

Absorption spectra were recorded on a Cary 400 spectrophotometer (Varian). Extinction coefficients for the non-labeled sequences 5'-GGGCCCGCAGGG-3' and 5'-CCCTGCGGGCCC-3' were 112,500 $M^{-1}cm^{-1}$ and 97,300 $M^{-1}cm^{-1}$, respectively. Extinction coefficient for the single strand DNA sequence labeled with ^{th}G at position 7 was 103,000 $M^{-1}cm^{-1}$. Most experiments were performed at 20°C in 20 mM phosphate buffer pH 7.5, 50 mM NaCl, 1 mM EDTA, 2.5 mM TCEP and PEG 0.05%.

3- Molecular modeling.

The MolPort commercial library of compounds containing 6,504,839 entries in April 2015 was downloaded in SMILES format. Filtration was performed with the FILTER application implemented in OMEGA (version 2.5.1.4) from OpenEye [39, 40] using the SMARTS string corresponding to the aniline substructure as query: c1ccccc1[NH2]. Filtration of the initial library let to 30,947 molecules, whose protonation state was assigned by QUACPAC from OpenEye (version 1.6.3.1) [41]. Conformational analysis was performed with OMEGA (version 2.5.1.4) keeping all default settings and allowing the storage of up to 600 conformers per molecule. The crystallographic structure of the SRA domain of UHRF1 bound to methylated DNA was retrieved from the Protein Data Bank under the accession code 3CLZ and used as rigid receptor in molecular docking simulations [10]. Docking-based virtual

screening was performed with FRED from OpenEye (version 3.0.1) [42, 43] using default settings and retaining only the best pose of each docked molecule. In-depth docking investigation of UM63 was carried out with FRED, using the highest docking resolution settings and retaining 10 poses.

4- Steady-state fluorescence spectroscopy

Fluorescence spectra were recorded at 20°C on a FluoroLog (Jobin Yvon) or a Fluoromax 4 spectrofluorometer equipped with a thermostated cell compartment. Excitation was set at 330 nm. Spectra were corrected for buffer fluorescence, lamp fluctuations, and detector spectral sensitivity. To determine the percentage of inhibition for a given compound, the following formula was used:

$$\% \text{ inhibition} = \frac{I_{(DNA+SRA)} - I_{(DNA+SRA+inhibitor)}}{I_{(DNA+SRA)} - I_{(DNA)}} \qquad (1)$$

where $I_{DNA,}$ $I_{(DNA+SRA)}$ and $I_{(DNA+SRA+inhibitor)}$ correspond to the fluorescence intensity of DNA alone, DNA/SRA complex and DNA/SRA complex in the presence of inhibitor, respectively. For positive hits, the percentage of inhibition was measured at several hit concentrations in order to generate a dose-response curve. This curve was then fitted using:

$$\% \, inh = A_1 + \frac{(A_2 - A_1)}{1 + 10^{((\log(IC_{50}) - C) \times p)}} \qquad (2)$$

where A1 and A2 correspond to the percentage of inhibition in the absence and at saturating concentration of the hit, respectively. C is the concentration of the hit, IC_{50} corresponds to half maximal inhibitory concentration and p is the Hill coefficient. From the IC_{50} value, the inhibition constant of the compound (K_i) was then determined based on the Cheng and Prussof equation:

$$Ki = \frac{IC_{50}}{1 + \frac{[DNA]}{K_{d_{(SRA/DNA)}}}} \qquad (3)$$

where $K_{d_{(SRA/DNA)}}$ is the dissociation constant of SRA to the duplex and [DNA] is the DNA concentration.

In order to determine the binding constant of SRA to DNA in presence of the hits, a titration was performed by monitoring the changes in fluorescence anisotropy of a fixed amount of

labeled duplex in the presence of increasing concentrations of SRA. This titration was performed in the absence and in the presence of 10 µM of the positive hit. Anisotropy values were the average of 10 measurements. Excitation wavelength for thG was at 330 nm and emission was collected at 460 nm. The affinity constants were determined by fitting the fluorescence anisotropy changes to:

$$r = \frac{vRr_t - r_d(v-1)}{1+R_v-v} \qquad (4)$$

where r and r_d are the anisotropy values in the presence and absence of SRA, and r_t is the anisotropy at a saturating SRA concentration. R is the ratio of fluorescence intensity of the bound to the free forms and v is the fraction of bound SRA calculated as:

$$v = \frac{(K_a^{-1}+nL_t+P_t) - \sqrt{(K_a^{-1}+nL_t+P_t)^2 - 4nP_tL_t}}{2L_t} \qquad (5)$$

where K_a is the apparent affinity constant, Pt and Lt represent the total concentrations of SRA and thG-labeled duplex, respectively, and n represents the number of DNA binding sites per SRA [44].

5- Isothermal Titration Calorimetry

To determine the binding affinity of the hits to SRA or DNA, ITC was performed using a Nano ITC microcalorimeter (TA instruments). Experiments were performed at 20°C in 20 mM phosphate buffer pH 7.5, 50 mM NaCl. Solutions were prepared in a buffer containing less than 0.1% DMSO. Aliquots of 2.5 µL of 80 µM of SRA or HM duplex solution contained in the syringe were titrated into 8 µM of tested compound in the reaction cell. The heat flow (µcal × s $^{-1}$) resulting from the reaction between the two partners was recorded. Instrument control, data acquisition, and analysis were done with the NanoAnalyze and ITC run software provided by the manufacturer. The molar heat of binding ΔH^0 and the equilibrium dissociation constant K_d were obtained by fitting the normalized heat accompanying each injection [45] as a function of the total ligand / total hit molar ratio (X_{tot} / M_{tot} = X_r) to:

$$\frac{dQ}{V_0\, dX_{tot}} = \Delta H^0 \left(\frac{1}{2} + \frac{1-(1+r)/2 - X_r/2}{(X_r^2 - 2X_r(1-r) + (1+r)^2)^{1/2}}\right) \qquad (6)$$

Where V_0 is the volume of the reaction cell, Q is the released heat and $r = K_d / M_{tot}$

6- Stopped Flow

The kinetics of SRA-induced base flipping in the thG-labeled duplex was monitored using a stopped-flow apparatus (SFM-3, Bio-Logic, Claix, France). The thG excitation wavelength was set to 360 nm. Fluorescence intensity was followed above 425 nm using a long-pass filter (Kodak Wratten). The data recording frequency was 20 kHz. The dead time of the set-up was 2 ms. The kinetic curves were recorded after fast mixing of 100 µL of labeled DNA in one syringe and SRA in the absence or presence of UM63 in the other syringe. The final concentration of labeled DNA was 0.2 µM and the concentration of SRA was 1.5 µM. UM63 was tested at 10 µM and 25 µM. For dissociation experiments, 10 µM or 25 µM UM63 was added to a pre-formed DNA/SRA complex. Same parameters were used for both experiments. Data acquisition and processing were done with the Biokine software from the instrument manufacturer.

7- Cell culture

HeLa cells (ATCC, CCL-2) were grown in DMEM (Dulbecco's Modified Eagle's Medium) which was supplemented with 10% FBS (fetal bovine serum), in addition to penicillin (100 U/ml) and streptomycin (100 U/ml) (Invitrogen Corporation Pontoise, France). Cells were maintained in a humid atmosphere with 5% CO_2 at 37°C. Plasmids were transfected in HeLa cells with jetPEI™ (Life Technologies, Saint Aubin, France) according to the manufacturer's protocol.

8- Immunofluorescence Assay

HeLa cells were seeded on a cover glass and then treated for 24 h with UM63 or 5-Azacytidine (5-Aza), used as control. Cells were fixed with 4% paraformaldehyde for 15 minutes and then, permeabilized with 0.2% Triton X-100 for 15 min. Then, 4M HCl was added for 20 min to denature DNA. The medium was then neutralized with 100 mM Tris HCl pH = 8.5 for 10 min. Next, cells were blocked using 1% BSA and 0.05% Tween in PBS for 1 hour, before incubation with a primary antibody against 5mC (Actif Motif) overnight at 4°C. After washing three times with PBS, cells were incubated with secondary antibodies labeled with Alexa Fluor 488 (goat anti-mouse) for 20 min. Finally, cells were washed three times and imaged with a confocal Leica SPE microscope equipped with a 20× 0.7 N.A air immersion lens objective. The images were further processed with Image J software.

9- Fluorescence Lifetime Imaging Microscopy (FLIM)

For FLIM experiments, 10^5 cells were seeded in a µ-dish (Ibidi) with 35 mm wells and were co-transfected with 1 µg DNMT1-eGFP and 1 µg UHRF1-mCherry plasmids by using jetPEI™ reagent. After transfection, cells were treated with 10 µM of UM63 for 24 h. At the end of the treatment, cells were fixed with 4% paraformaldehyde. After fixation, cells were analyzed with a homemade two-photon excitation scanning microscope based on an Olympus IX70 inverted microscope with an 60× 1.2 NA water immersion objective operating in the descanned fluorescence collection mode as described [46, 47]. Two-photon excitation at 930 nm was provided by an Insight DeepSee laser (Spectra Physics). Fluorescence photons were collected using a short-pass filter with a cut-off wavelength of 680 nm (F75-680, AHF, Germany) and a band-pass filter of 520 ± 17 nm (F37-520, AHF, Germany). The fluorescence was directed to a fiber coupled APD (SPCM-AQR-14-FC, Perkin Elmer), which was connected to a time-correlated single photon counting module (SPC830, Becker & Hickl, Germany). FLIM data were analyzed using SPCImage v 4.9.7 (Becker & Hickel) and the Förster resonance energy transfer (FRET) efficiency was calculated according to $E=1-(\tau_{DA}/\tau_D)$, where τ_{DA} is the lifetime of the donor (eGFP) in the presence of acceptor (mCherry) and τ_D is the lifetime of eGFP in the absence of acceptor.

C- Results:

1- Selection of hits by virtual screening

With the aim to identify different chemotypes of UHRF1 inhibitors that target the 5mC binding pocket of the SRA domain, and based on structural information available from X-ray crystallography studies [10, 12, 13, 48], a diversity-oriented and structure-based virtual screening approach was established. The high resolution crystallographic structure of the human SRA domain of UHRF1 bound to HM DNA [10] was used as a rigid receptor in virtual screening. Analysis of the interactions established by the flipped 5mC in its narrow binding site within SRA revealed key pharmacophoric features such as the aromatic ring, which is pi-pi stacked to the side chain of Tyr478 in a parallel displaced geometry, and a number of polar groups able to establish H-bonds with the protein. These features were exploited to pre-screen the MolPort database of commercially available compounds (https://www.molport.com/shop/index, around 6.5M compounds in April 2015), and to enrich the test-set with compounds endowed with a high probability to mimic the binding of 5mC within the SRA binding site. In particular, the aniline substructure was selected for filtration of the database, which was accomplished through a SMARTS-based query with the FILTER

application of OMEGA from OpenEye [39, 40]. This operation decreased the overall size of the screening library up to around 31K molecules, which were submitted to conformational analysis with OMEGA (OpenEye) [39, 40] and were subsequently docked within the 5mC binding site by the FRED docking program from OpenEye [42, 43]. Top ranking 1,000 compounds were further selected for visual inspection. Moreover, to maximize chemical diversity, these molecules were clustered based on fingerprints and substructure search through a cheminformatics approach [49-51]. The combination between visual inspection and chemical diversity led to the selection of 26 small molecules for *in vitro* testing (Fig. S1).

2- Selection of hits by using an *in vitro* "base flipping assay"

To test the 26 compounds selected by virtual screening, we used a fluorescence-based assay highly sensitive to 5mC base flipping. This assay is based on the use of a HM DNA labeled by thienoguanosine (thG) (Fig. 2A), an isomorphic guanosine derivative that has been shown to perfectly replace the guanine residue next to the methylated cytosine in the CpG motif [52, 53]. Addition of SRA to this labeled DNA is accompanied by a 4-fold increase in the fluorescence intensity, as a result of the SRA-induced flipping of the 5mC residue (Fig. 2) [53]. Among the 26 compounds, UM63 was the most promising hit candidate, as it induced a concentration-dependent decrease in fluorescence intensity, suggesting that it could inhibit the SRA-induced base flipping with an IC_{50} value of 4.4 ±0.5 µM (Fig. 2B).

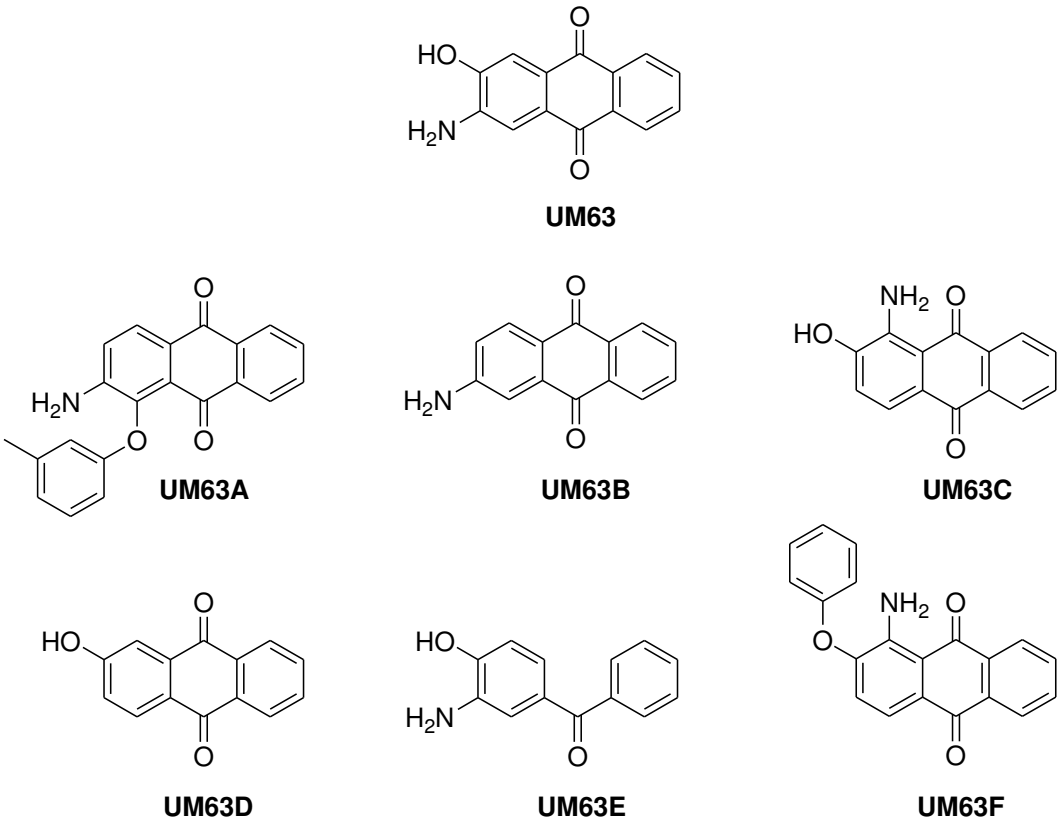

Figure 1. Chemical structure of the hit UM63 identified by virtual screening and six commercially available analogues of UM63 selected for *in vitro* tests.

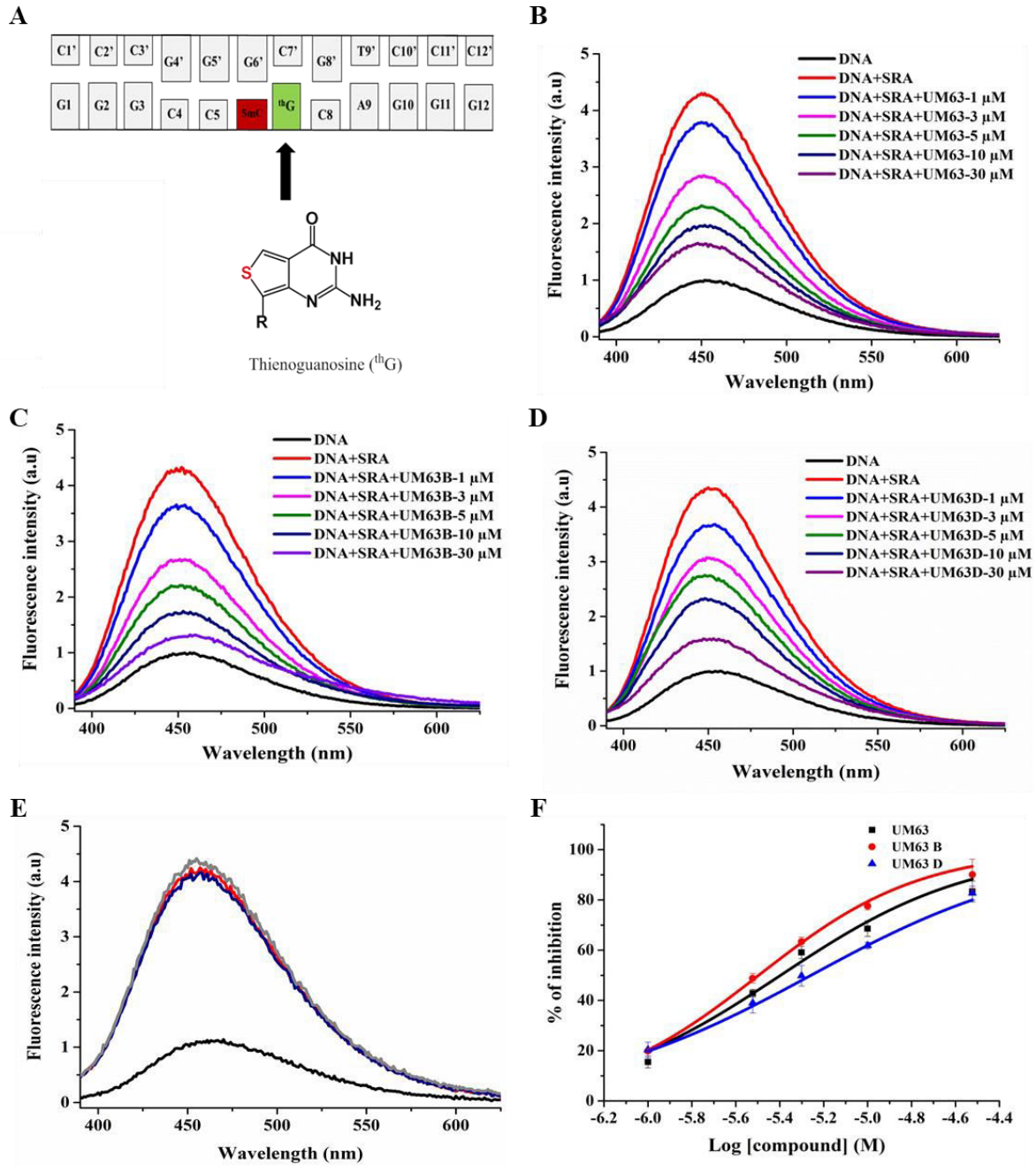

Figure 2. **Effects of compounds selected by virtual screening on the base flipping assay**. (**A**) Sequence of the thG-labeled HM duplex. The guanosine at position 7 substituted by thG is highlighted in green and the methylated cytosine is in red. Emission spectra of thG-labeled HM DNA (1 µM) in the absence (black) and in the presence of SRA (3 µM) before (red) and after addition of 1 µM (blue) , 3 µM (magenta) , 5 µM (green) , 10 µM (dark blue) or 30 µM (purple) of (**B**) UM63 (**C**) UM63B and (**D**) UM63D. (**E**) Emission spectra of HM thG-labeled DNA (1 µM) in the absence (black) and in the presence of SRA (3 µM) before (red) and after addition of 10 µM (dark blue) and 100 µM (grey) of UM63E. (**F**) Dose-response curve representing the inhibition of SRA base flipping activity by the selected compounds. The solid lines correspond to the fits of the experimental points by eq. (2). The IC_{50} values given

in the text are the mean ± S.E.M. of three independent experiments. Experiments were performed in phosphate buffer 20 mM, NaCl 50 mM, EDTA 1 mM, TCEP 2.5 mM, PEG 0.05%, pH 7.5.

To further substantiate the quality of the selected scaffold, six commercially available chemical derivatives of UM63, namely UM63A-F (Fig. 1) were selected and tested as well. Only UM63B and UM63D were able to inhibit the SRA-induced base flipping (Fig. 2C, D). Similarly to UM63, UM63B and UM63D inhibited the 5mC flipping in a concentration-dependent manner with IC_{50} values of 3.3 ±0.3 µM and 6.1 ±0.7 µM respectively (Fig. 2C, D). Noticeably, the thG fluorescence decrease was not due to a quenching by these compounds, since none of them modified the fluorescence of the labeled duplexes in the absence of SRA (Fig. S2). The corresponding K_i values calculated from eq. (3) were respectively 1.45 ±0.15, 1.05 ±0.1 and 2.0 ±0.2 µM for UM63, UM63B and UM63D, indicating that the three compounds have similar potency in inhibiting the SRA-induced base flipping. As the three compounds have similar chemical structures, this strongly suggests that their activity is related to a specific pharmacophore. As UM63B has been reported to be carcinogenic [54], this compound was discontinued and the subsequent assays were performed only with UM63 and UM63D.

3- Binding parameters of the positive hits to SRA and HM DNA

In order to determine whether the inhibitory effect of UM63 and UM63D on SRA-induced base flipping is related to their binding to SRA, we analyzed by ITC the thermodynamic binding parameters of UM63 and UM63D for SRA. ITC titration of UM63 by SRA (Fig. 3A) showed that the reaction is exothermic (ΔH = -10.9 KJ/mol), with a K_d value of 0.73 ± 0.03 µM and a 1:1 stoichiometry. The reaction was also characterized by a positive entropy ΔS, suggesting that formation of the SRA/UM63 complex is partly driven by release of ions and water molecules. In contrast, the interaction of UM63D with wild-type SRA was heat-silent (data not shown), preventing the determination of its K_d value.

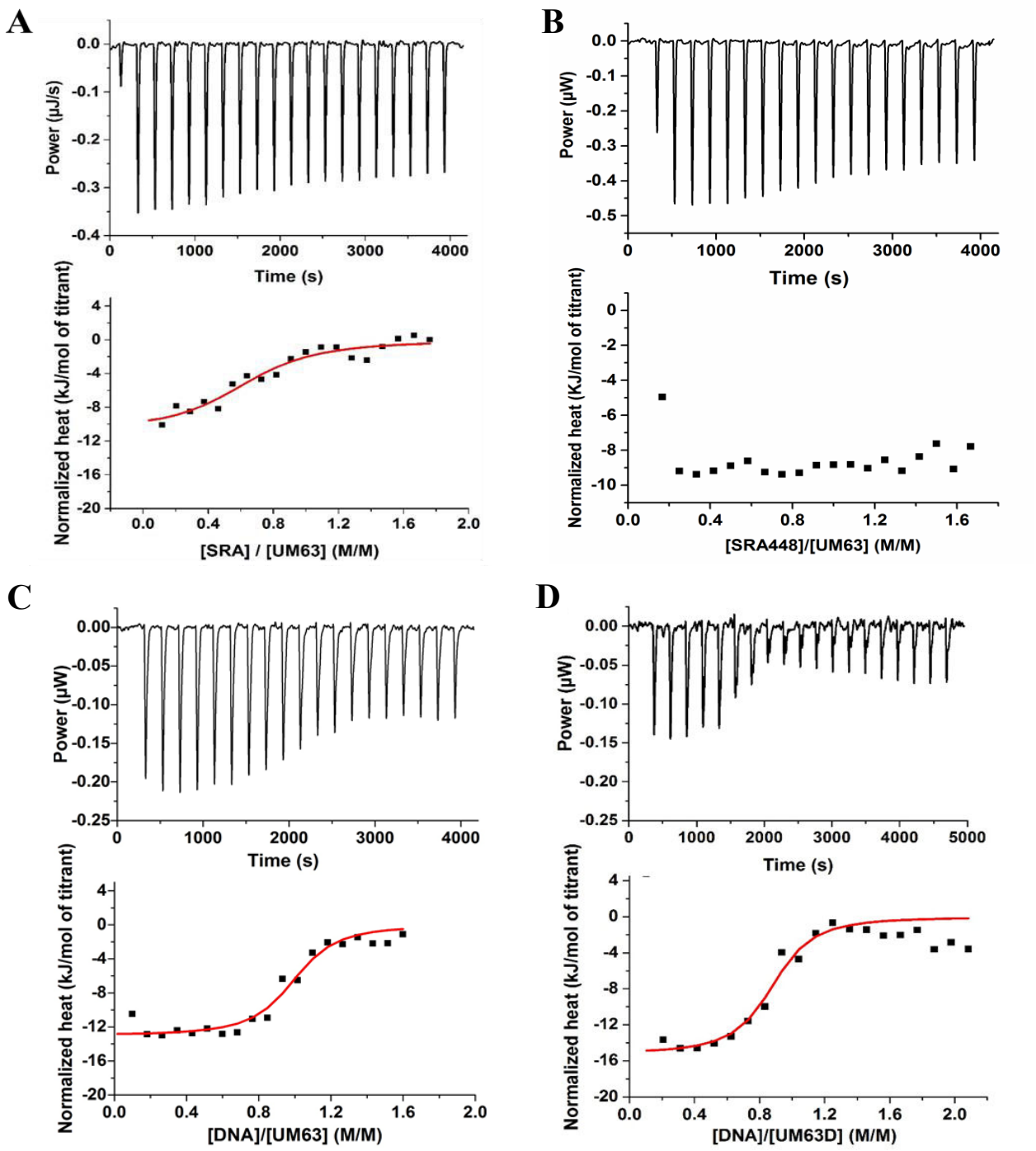

Figure 3. Binding of UM63 and UM63D to SRA and HM DNA, as monitored by Isothermal Titration Calorimetry. Representative ITC titration curves of 8 µM UM63 by (**A**) SRA and (**B**) SRA-G448D. The protein concentration in the syringe was 80 µM. Titration of 8 µM of (**C**) UM63 and (**D**) UM63D by HM DNA. The HM DNA concentration in the syringe was 80 µM. During titration, the area of the power peaks regularly decreases, reaching a plateau value that corresponds to the dilution heats of (**A**) SRA, (**B**) SRA-G448D or (**C, D**) HM DNA into the buffer alone. The red curves were fitted to the experimental heat

quantities using equation (6). Experiments were performed at 20°C in 20 mM phosphate buffer, NaCl 50 mM, pH=7.4.

In a next step, to further explore the base-flipping inhibition mechanism of UM63 and UM63D, we examined their possible interaction with DNA (Fig. 3C, D). The binding of both compounds to DNA was found to be exothermic (ΔH = -13.03 and -15.25 kJ/mol for UM63 and UM63D, respectively) with K_d values of 0.13 ± 0.01 µM and 0.15 ± 0.08 µM for UM63 and UM63D, respectively. These strong affinities could be rationalized by the fact that anthraquinones are DNA intercalators [55]. UM63 was clearly confirmed as a DNA intercalator by its ability to displace ethidium bromide (EtBr) from DNA (Fig. S3). However, the DNA intercalating properties of these compounds appear marginal in the base flipping inhibition, since UM63E (Fig. 2D) binds to DNA with an affinity comparable to UM63 and UM63D (Fig. S4) but is unable to inhibit the SRA-driven base flipping of HM DNA. From the demonstration of its binding to SRA, UM63 was selected for further studies.

4- UM63 binds to the SRA binding pocket and decreases the affinity of SRA to DNA

To experimentally evidence that UM63 targets the 5mC binding pocket on SRA, we replaced the wild-type SRA with a SRA G448D mutant where the glycine 448 residue is replaced by a more bulky aspartic acid to block the binding pocket and prevent base flipping [10, 53]. As expected, only marginal binding was observed with this mutant (Fig. 3B), confirming that the 5mC binding pocket of SRA is the target of UM63, in line with molecular modeling predictions.

To further explore the base flipping inhibition by UM63, we investigated by the stopped-flow technique how UM63 alters the kinetics of SRA-induced 5mC flipping in the thG-labeled DNA [53]. In line with our previous study [53], the kinetic trace of the thG-labeled DNA in the presence of SRA showed a slow component with a rate constant of ~ 6.5 s^{-1} attributed to the 5mC base flipping process (Fig. 4, red curve). Addition of UM63 only marginally decreases the kinetic rate constant, but efficiently reduces the final fluorescence plateau in a concentration-dependent manner (Fig. 4 compare blue and magenta curves with the red curve). This decrease in the plateau is consistent with the spectra in Figure 2 and the co-existence of a UM63-bound SRA population that is unable to flip the 5mC base with a population of free SRA that flips 5mC with unaltered kinetics. With increasing UM63 concentrations, the population of free active SRA decreases, explaining the decrease in the final plateau. As expected, the

negative compound UM63E did not induce any change in the kinetics or the final plateau (Fig. S5).

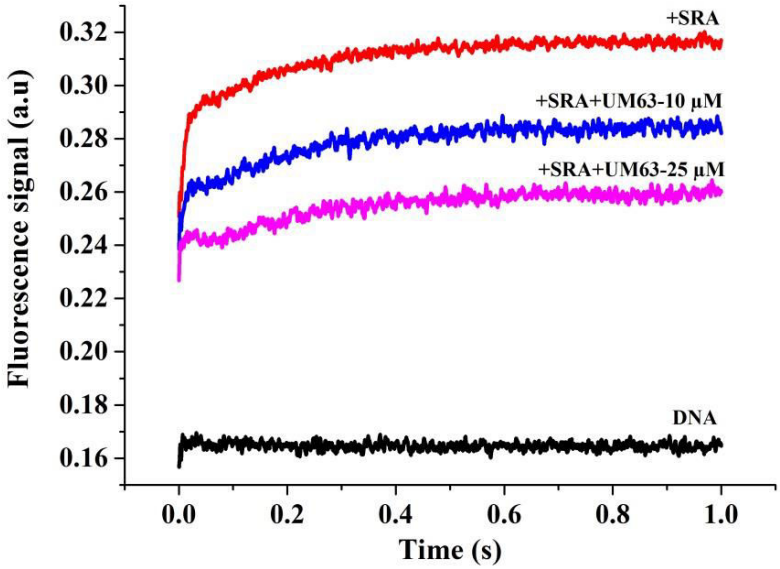

Figure 4. Effect of UM63 on the base flipping kinetics of the SRA domain. Kinetic traces were monitored by the stopped-flow technique. The black trace corresponds to the thG-labeled HM duplex mixed with buffer. The red trace describes the interaction of the thG-labeled HM duplex with SRA. The blue and magenta traces describe the kinetics of interaction of thG-labeled HM duplex with SRA in the presence of 10 µM and 25 µM of UM63. The final concentrations of thG-labeled HM DNA and SRA were 0.2 µM and 1.5 µM, respectively. Experiments were performed in phosphate buffer 20 mM, NaCl 50 mM, TCEP 2.5 mM, pH 7.5.

To determine whether the binding of UM63 to the binding pocket may alter the DNA binding properties of SRA, we performed binding experiments using the non-methylated version of the DNA duplex in Fig 2A. As no base flipping occurs with this non-methylated duplex [53], the effect of UM63 on the binding process only can be explored. Accordingly, we titrated by fluorescence anisotropy the thG-labeled non-methylated DNA with increasing concentrations of SRA in the absence or in the presence of 10 µM UM63. In the absence of UM63, the dissociation constant K_d of SRA to DNA was found to be 0.43 ±0.04 µM, close to the previously reported value [53]. Addition of UM63 shifted the titration curve to higher SRA concentrations (Fig. 5A) and decreased the apparent affinity of SRA to DNA ($K_{d_{(app)}}$ = 1.04 ± 0.15 µM), indicating that UM63 alters the binding properties of SRA to DNA. In contrast, no competition

was observed when the thG-labeled DNA was titrated by the SRA-G448D mutant (Fig. 5B), confirming that UM63 is unable to bind to this SRA mutant.

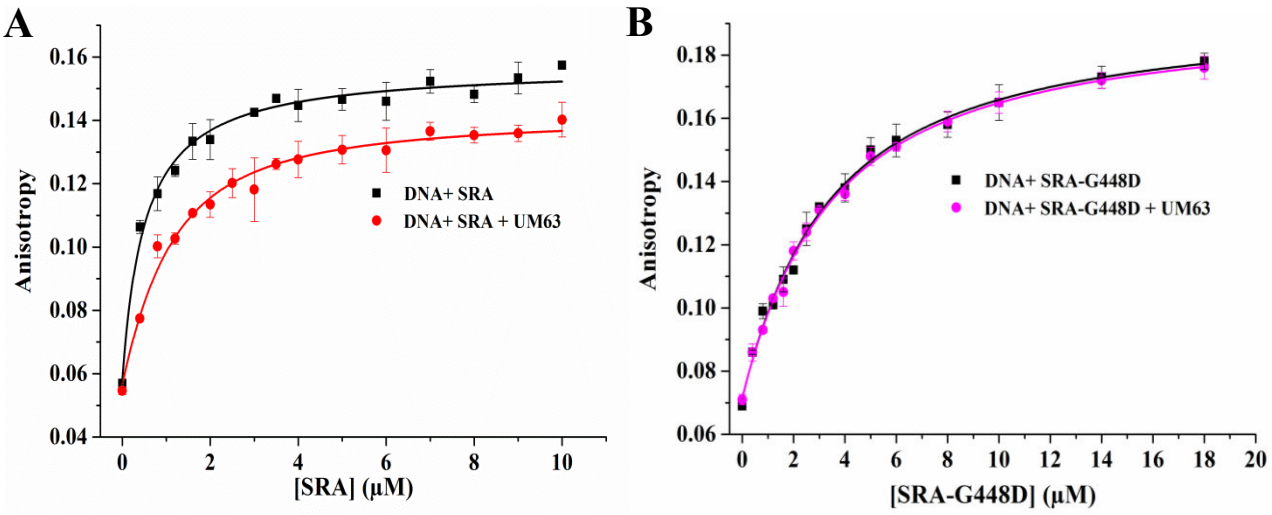

Figure 5. Effect of UM63 on the binding of SRA and SRA-G448D to non-methylated DNA, as monitored by fluorescence anisotropy. (A) Titration of 1 µM DNA with SRA in the absence (black) or in the presence of 10 µM UM63 (red). (**B**) Titration of 1 µM DNA with SRA-G448D in the absence (black) or in the presence of 10 µM UM63 (magenta). Experimental points are represented as means ± S.E.M for n=3 independent experiments. The solid lines correspond to the fits of the experimental data to equation (4) and (5).

To confirm that UM63 decreases the affinity for SRA to DNA, we added 10 µM or 25 µM of UM63 to the preformed complex of SRA with the thG-labeled HM duplex and monitored the changes in thG fluorescence with time (Fig. 6). With both concentrations, the time-dependent decrease in thG fluorescence intensity was similar to that previously observed when the complex was challenged with an excess of non-labeled DNA [53], indicating a dissociation of the complex, as a result of the decrease in the affinity of DNA when UM63 binds to the SRA binding pocket. Independently of the UM63 concentration, a dissociation rate constant of 8 s^{-1} was observed, in good agreement with the 3 s^{-1} rate constant of the flipping back of the 5mC residue, the rate-limiting step of the dissociation of the SRA/HM DNA complex [53]. As expected, the negative compound UM63E inactive on base flipping (Fig. 2E) was unable to affect the SRA/HM DNA complex (Fig. S6), when added at a 10 µM concentration.

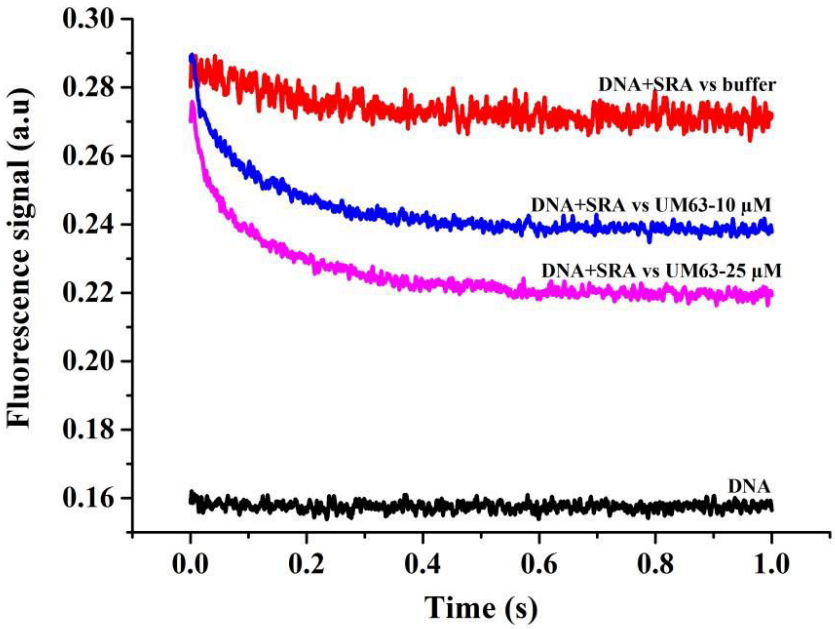

Figure 6. Dissociation kinetics of the DNA/SRA complex by UM63. The dissociation curves were measured by the stopped-flow technique after addition of 10 µM (blue curve) and 25 µM (magenta curve) of UM63 to a complex formed by 0.2 µM of thG-labeled HM duplex and 1.5 µM SRA. The red and black curves correspond to the DNA/SRA complex and the DNA alone mixed with buffer, respectively.

5- Binding mode of UM63 to SRA binding pocket

The interaction of UM63 within the binding site of 5mC on SRA was further investigated by molecular modeling simulations. Compared to the virtual screening setting, a more accurate docking simulation was carried out with the FRED docking program to predict the possible binding mode of UM63. These simulations clearly show that UM63 acts as 5mC mimetic, being pi-pi stacked with the side chain of Tyr478 and H-bonded to key residues that are also contacted by the flipped 5mC and the backbone of HM DNA [10] such as Asp469, Thr479, Gly448, Gly465 and Ala463 (Fig. 7). It is worth noting that the distal phenyl ring of the anthraquinone core occupies a region near the entrance of the binding site, where it sterically overlaps with the crystallographic binding of DNA phosphate backbone. The overlap is particularly important at the level of the 5mC nucleotide, which may further explain the decreased affinity of DNA to SRA in the presence of UM63 (Fig. S7). The phenol group of UM63 does not participate in H-bonding to the SRA and points towards partially accessible sub-pockets of the 5mC binding site, thus representing a possible site for hit-to-lead optimization. In contrast, the amino group

and the quinone moiety are well adapted to interact with SRA residues and could less easily be modified or substituted. Overall, the binding mode of UM63 predicted by molecular docking is highly comparable to the crystallographic binding mode of 5mC. It is also consistent with the lack of detectable binding of UM63 to the G448D mutant of SRA, because the Asp488 side chain in the mutant SRA occupies the binding site and thus prevents UM63 interaction by steric hindrance.

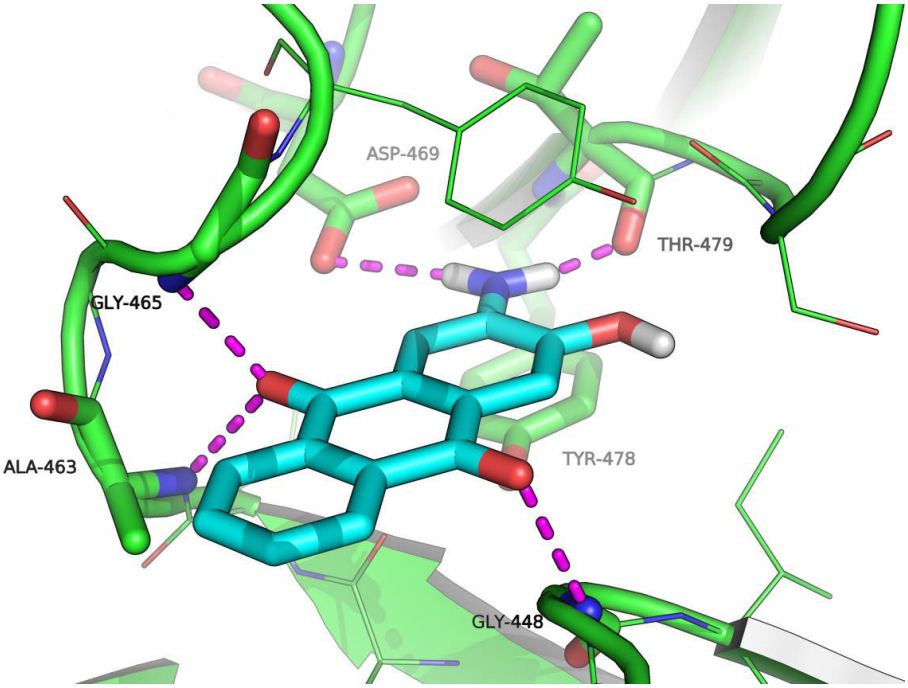

Figure 7. Docking-based binding mode of UM63 within the 5mC binding site of SRA. UM63 is shown as cyan sticks, and the crystallographic structure of SRA (PDB 3CLZ) is show as green cartoon. Residues within 5 Å from UM63 are shown as lines, while residues contacted by UM63 via H-bond or pi-pi stacking are shown in sticks and are labeled (residue numbering corresponds to the scheme adopted in the crystallographic structure). H-bonds are highlighted by magenta dashed lines.

6- Inhibition of SRA activity by UM63 is associated with a decrease in global DNA methylation

As our *in vitro* experiments and molecular modeling revealed that UM63 competes with the binding of SRA to the HM DNA and inhibits the flipping of the 5mC base, we hypothesized that UM63 should induce genomic DNA demethylation. Global DNA methylation was estimated by an immunofluorescence assay using a specific monoclonal antibody against 5mC and Alexa488-labeled secondary antibodies (Fig 8A). Based on the mean fluorescence intensity of Alexa488, the global DNA methylation level was found to decrease after 24 h treatment with

UM63 at 10 µM (Fig. 8B). The decrease in fluorescence (37%) was comparable to that induced by 10 µM of Azacytidine (44%), a DNMT1 inhibitor taken as a positive control. This decrease in global genomic methylation may tentatively be related to the effect of UM63 on the SRA/HM DNA complexes.

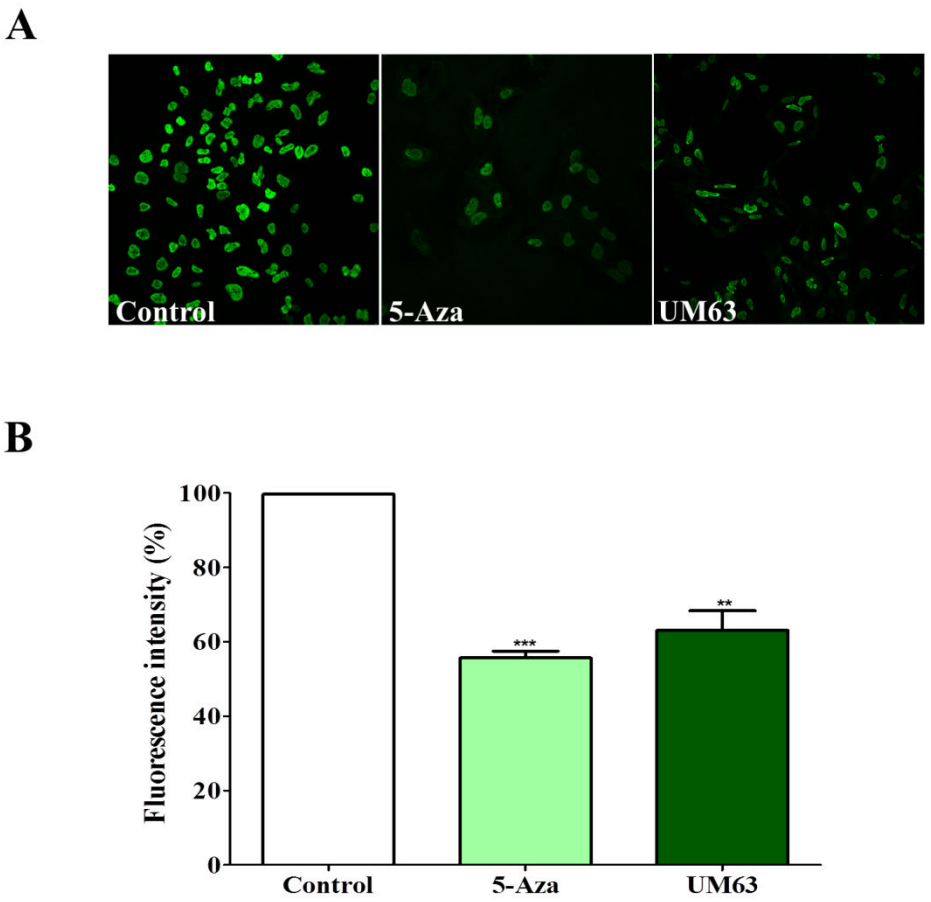

Figure 8. Effect of UM63 on global DNA methylation in HeLa cells. (**A**) Immunostaining of 5-mC in HeLa cells. Non-treated HeLa cells served as negative control, while cells treated with 10 µM 5-Azacytidine were used as a positive control and were compared to cells treated with 10 µM of UM63. The cells were fixed after treatment and labeled by anti-5mC antibodies and Alexa488-labeled secondary antibodies before visualization in confocal microscopy (**B**) Mean fluorescence intensities representing the amount of methylated cytosines in genomic DNA. Values are means ±S.E.M. for three independent experiments; statistically significant: * $p < 0.05$; ** $p < 0.01$; *** $p < 0.001$ (versus untreated group).

7- UM63 prevents the interaction between UHRF1 and DNMT1 in cells

The observed inhibition of DNA methylation by UM63 could be the result of the inhibition of 5mC flipping by UHRF1, which in turn prevents the recruitment of DNMT1 that is responsible of DNA methylation. To test this hypothesis, we used the FRET-FLIM technique to monitor

the interaction between DNMT1 and UHRF1 inside the nucleus, after transfection of HeLa cells with DNMT1-eGFP and UHRF1-mCherry (Fig. 9). FRET between eGFP and mCherry only occurs when they are less than 8 nm apart, a distance corresponding to intermolecular protein–protein interactions [46–48]. By measuring the fluorescence decay at each pixel of the cell, the FLIM technique allows extracting the fluorescence lifetime (τ) that, in contrast to fluorescence intensity, does not depend on the instrumentation or the concentration of fluorophores. The lifetime of the DNMT1-eGFP was 2.54 ± 0.01 ns in cells transfected with DNMT1-eGFP alone. The lifetime of eGFP was reduced to 2.19 ± 0.02 ns when DNMT1-eGFP was co-transfected with UHRF1-mCherry (Fig.9B). This corresponds to a FRET efficiency of 13.7 ± 0.8%, clearly indicating that UHRF1 and DNMT1 interact in the cell nucleus (Fig. 9B). In the same conditions, the lifetime of DNMT1-eGFP in cells treated with 10 µM UM63 was 2.44 ± 0.01 ns, corresponding to a FRET efficiency of only 3.4 ± 0.3% (Fig. 9A, B, C), a value considered as non-significant [56]. This strong decrease in FRET strongly suggests that UM63 efficiently prevents the interaction of UHRF1 with DNMT1, in full line with our hypothesis. Thus, by interacting with the 5mC binding pocket of SRA, UM63 may inhibit base flipping and thus the recruitment of DNMT1.

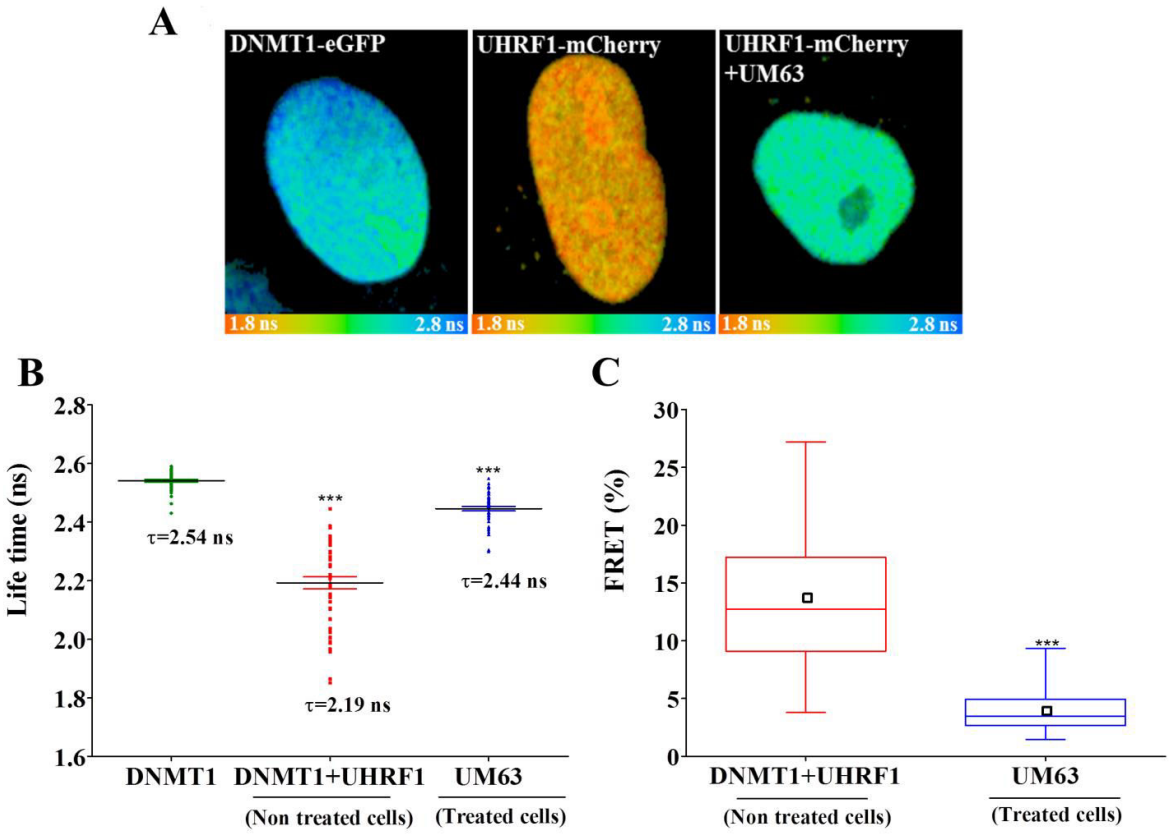

Figure 9. Effect of UM63 on DNMT1/UHRF1 interaction, as assessed by FRET-FLIM. (**A**) 30 µm x 30 µm FLIM images of HeLa cells transfected with DNMT1-eGFP or co-transfected with UHRF1-mCherry without or with UM63 treatment. The lifetime values are shown by using a color code ranging from red (1.8 ns) to blue (2.8 ns). (**B**, **C**) Effect of UM63 on FRET efficiency**. (B)** Distribution of lifetimes expressed as means ±S.E.M. of three independent experiments in treated and non treated samples. The horizontal lines show the mean values. **(C)** FRET efficiencies calculated from the average lifetime values of at least 50 cells in three independent experiments. Box-and-whiskers plots represent the FRET efficiency in non-treated and treated cells. Whiskers represent the minimum and maximum values. The boxes define the interquartile range that extends from the 25th to the 75th percentile, whereas the horizontal lines and square show the median values and the mean, respectively. Statistical significance: * $p < 0.05$; ** $p < 0.01$; *** $p < 0.001$ (versus untreated group).

D- Discussion:

UHRF1 plays a key role in the inheritance of methylation marks during DNA replication by reading the DNA sequence, sensing hemi-methylated CpG motifs and promoting the flipping of 5mC residues. Base flipping induced by the SRA domain of UHRF1 is thought to be the key event for recruiting the DNMT1 enzyme that will methylate the opposite cytosine on the daughter strand. In this context, the aim of the present work was to probe the druggability of

UHRF1 by identifying small molecules that can inhibit its activity and thus block the inheritance of the methylation patterns during cell replication. To reach this aim, we combined virtual screening to select molecules able to bind to the 5mC binding pocket on the SRA domain and a fluorescence-based screening assay monitoring the SRA-induced base flipping to evaluate the molecules selected by virtual screening. Through this approach, we selected three molecules from the anthraquinone family (UM63, UM63B and UM63D) that were observed to inhibit the SRA-induced based flipping with *K*i values in the low µM range. From these 3 compounds, we discarded UM63B that was reported to be carcinogenic. The two others were tested by ITC for their binding to SRA and DNA. UM63 was found to be the most interesting compound, as its binding to the wild-type SRA but not to the G448D mutant confirmed its binding to the 5mC binding pocket of SRA. This conclusion was further rationalized by molecular modeling, which indicates that UM63 mimics 5mC in the SRA pocket, being stabilized through a pi-pi stacking with the side chain of Tyr478 and several H-bonds to key SRA residues also contacted by methylated DNA. UM63 can also bind to DNA with a 0.1 µM dissociation constant, likely through intercalation (Fig. S5). However, as a similar high affinity for DNA was observed with UM63E, a compound structurally related to UM63 that has no effect on base flipping, the inhibitory effect of UM63 is thought to be mainly the consequence of its binding to the 5mC binding pocket of SRA. The binding of UM63 to the 5mC binding pocket was further shown to hinder the binding of SRA to DNA, as supported by the decrease in affinity of SRA for DNA in the presence of UM63 (Fig. 5A) and the dissociation of the SRA/DNA complexes by UM63 (Fig. 6). In addition, the inability of UM63 to hinder the binding of the G448D SRA mutant to DNA further confirmed that the intercalation of UM63 into the DNA has only a marginal effect on the binding of SRA (Fig. 5B).

Interestingly, treatment of HeLa cells with UM63 was found to prevent the interaction between UHRF1 and DNMT1 (Fig. 9), clearly. This is likely a consequence of the binding of UM63 to the SRA domain of UHRF1, which prevents the recognition of the methylated sites and the recruitment of DNMT1 through a direct interaction between SRA and the replication foci targeting sequence (RFTS) domain of DNMT1 [57]. Indeed, the interaction of the SRA domain of UHRF1 with the CpG site is mandatory to trigger the conversion of the “closed form” of UHRF1 to its “open form” which is able to interact with DNMT1 [58]. UM63 likely keeps UHRF1 in its closed form, unable to interact with DNMT1. Furthermore, our data clearly highlight the base flipping as a critical event for the recruitment of DNMT1 by UHRF1. As

previously suggested [53], the base flipping is thought to allow UHRF1 to stall at the CpG sites, thus providing sufficient time to recruit DNMT1. In addition, it is likely that the structural changes of the SRA domain connected to the base flipping process, such as the motion of the NKR finger are instrumental for DNMT1 recruitment by UHRF1.

By altering two crucial steps in the replication of DNA methylation patterns, namely the interaction of UHRF1 with HM DNA and the recruitment of DNMT1, UM63 is thought to decrease the DNA methylation status of the cell. In line with this hypothesis, UM63 was found to decrease the global DNA methylation level by about 40% in HeLa cells. A similar effect was observed when UHRF1 was knocked-down with shRNAs in HeLa cells [59], highlighting the key role of UHRF1 in the maintenance of the DNA methylation level. These findings strongly suggest that UM63 is pharmacologically able to target UHRF1 and thus prevent aberrant DNA methylation, such as hypermethylation of TSG promoters that is frequently observed in cancer development. UM63 may thus have the same effect as interference RNAs that knockdown UHRF1 and reactivates the expression of TSGs and inhibits oncogenesis [30, 61, 62]. Similarly, natural products such as flavonoids derived from *Limoniastrum guyonianum* and luteolin have been shown to downregulate UHRF1 and subsequently reduce the global methylation levels in cervical cancer cells, with a reexpression of TSGs and inhibition of cell proliferation [63].

Altogether, these findings suggest that UM63 acts as an UHRF1 inhibitor that binds to the 5mC binding pocket of the SRA domain, and prevents the flipping of 5mC as well as the recruitment of DNMT1 to the DNA replication foci. As a result, UM63 induces a decrease in the global methylation of DNA in the cell. This compound thus appears as potential candidate to serve as a starting point/lead to design more selective and efficient inhibitors of UHRF1. Such inhibitors can be pharmaceutically applied against different pathologies including cancers, in which UHRF1 is highly expressed and promotes tumor development and progression by epigenetically silencing the tumor suppressor genes.

Acknowledgements:

We thank Ludovic Richert for his help in FLIM experiments. We thank the ANR (SMFLUONA, ANR-17-CE11-0036-01) for financial support. LZ and KG were supported by fellowships from Lebanese government and FRM, respectively. W.A. and T.A. were supported by fellowships from HEC (Pakistan).

References:

1. Ehrlich M: **Expression of various genes is controlled by DNA methylation during mammalian development**. *Journal of cellular biochemistry* 2003, **88**(5):899-910.
2. Okamoto I, Otte AP, Allis CD, Reinberg D, Heard E: **Epigenetic dynamics of imprinted X inactivation during early mouse development**. *Science* 2004, **303**(5658):644-649.
3. Murphy SK, Jirtle RL: **Imprinting evolution and the price of silence**. *BioEssays : news and reviews in molecular, cellular and developmental biology* 2003, **25**(6):577-588.
4. Feinberg AP, Ohlsson R, Henikoff S: **The epigenetic progenitor origin of human cancer**. *Nature reviews Genetics* 2006, **7**(1):21-33.
5. Klose RJ, Bird AP: **Genomic DNA methylation: the mark and its mediators**. *Trends in biochemical sciences* 2006, **31**(2):89-97.
6. Baylin SB, Jones PA: **A decade of exploring the cancer epigenome - biological and translational implications**. *Nature reviews Cancer* 2011, **11**(10):726-734.
7. Sandoval J, Esteller M: **Cancer epigenomics: beyond genomics**. *Current opinion in genetics & development* 2012, **22**(1):50-55.
8. Bronner C, Krifa M, Mousli M: **Increasing role of UHRF1 in the reading and inheritance of the epigenetic code as well as in tumorogenesis**. *Biochemical pharmacology* 2013, **86**(12):1643-1649.
9. Alhosin M, Sharif T, Mousli M, Etienne-Selloum N, Fuhrmann G, Schini-Kerth VB, Bronner C: **Down-regulation of UHRF1, associated with re-expression of tumor suppressor genes, is a common feature of natural compounds exhibiting anti-cancer properties**. *Journal of experimental & clinical cancer research : CR* 2011, **30**:41.
10. Avvakumov GV, Walker JR, Xue S, Li Y, Duan S, Bronner C, Arrowsmith CH, Dhe-Paganon S: **Structural basis for recognition of hemi-methylated DNA by the SRA domain of human UHRF1**. *Nature* 2008, **455**(7214):822-825.
11. Sharif J, Muto M, Takebayashi S, Suetake I, Iwamatsu A, Endo TA, Shinga J, Mizutani-Koseki Y, Toyoda T, Okamura K *et al*: **The SRA protein Np95 mediates epigenetic inheritance by recruiting Dnmt1 to methylated DNA**. *Nature* 2007, **450**(7171):908-912.
12. Arita K, Ariyoshi M, Tochio H, Nakamura Y, Shirakawa M: **Recognition of hemi-methylated DNA by the SRA protein UHRF1 by a base-flipping mechanism**. *Nature* 2008, **455**(7214):818-821.
13. Hashimoto H, Horton JR, Zhang X, Bostick M, Jacobsen SE, Cheng X: **The SRA domain of UHRF1 flips 5-methylcytosine out of the DNA helix**. *Nature* 2008, **455**(7214):826-829.
14. Cheng J, Yang Y, Fang J, Xiao J, Zhu T, Chen F, Wang P, Li Z, Yang H, Xu Y: **Structural insight into coordinated recognition of trimethylated histone H3 lysine 9 (H3K9me3) by the plant homeodomain (PHD) and tandem tudor domain (TTD) of UHRF1 (ubiquitin-like, containing PHD and RING finger domains, 1) protein**. *The Journal of biological chemistry* 2013, **288**(2):1329-1339.
15. Liu X, Gao Q, Li P, Zhao Q, Zhang J, Li J, Koseki H, Wong J: **UHRF1 targets DNMT1 for DNA methylation through cooperative binding of hemi-methylated DNA and methylated H3K9**. *Nature communications* 2013, **4**:1563.
16. Bostick M, Kim JK, Esteve PO, Clark A, Pradhan S, Jacobsen SE: **UHRF1 plays a role in maintaining DNA methylation in mammalian cells**. *Science* 2007, **317**(5845):1760-1764.
17. Nishiyama A, Yamaguchi L, Sharif J, Johmura Y, Kawamura T, Nakanishi K, Shimamura S, Arita K, Kodama T, Ishikawa F *et al*: **Uhrf1-dependent H3K23 ubiquitylation couples maintenance DNA methylation and replication**. *Nature* 2013, **502**(7470):249-253.

18. Qin W, Wolf P, Liu N, Link S, Smets M, La Mastra F, Forne I, Pichler G, Horl D, Fellinger K *et al*: **DNA methylation requires a DNMT1 ubiquitin interacting motif (UIM) and histone ubiquitination**. *Cell research* 2015, **25**(8):911-929.
19. Yang X, Lay F, Han H, Jones PA: **Targeting DNA methylation for epigenetic therapy**. *Trends in pharmacological sciences* 2010, **31**(11):536-546.
20. Issa JP, Kantarjian H: **Azacitidine**. *Nature reviews Drug discovery* 2005, **Suppl**:S6-7.
21. Kantarjian H, Issa JP, Rosenfeld CS, Bennett JM, Albitar M, DiPersio J, Klimek V, Slack J, de Castro C, Ravandi F *et al*: **Decitabine improves patient outcomes in myelodysplastic syndromes: results of a phase III randomized study**. *Cancer* 2006, **106**(8):1794-1803.
22. Chuang JC, Yoo CB, Kwan JM, Li TW, Liang G, Yang AS, Jones PA: **Comparison of biological effects of non-nucleoside DNA methylation inhibitors versus 5-aza-2'-deoxycytidine**. *Molecular cancer therapeutics* 2005, **4**(10):1515-1520.
23. Foulks JM, Parnell KM, Nix RN, Chau S, Swierczek K, Saunders M, Wright K, Hendrickson TF, Ho KK, McCullar MV *et al*: **Epigenetic drug discovery: targeting DNA methyltransferases**. *Journal of biomolecular screening* 2012, **17**(1):2-17.
24. Jung Y, Park J, Kim TY, Park JH, Jong HS, Im SA, Robertson KD, Bang YJ, Kim TY: **Potential advantages of DNA methyltransferase 1 (DNMT1)-targeted inhibition for cancer therapy**. *Journal of molecular medicine* 2007, **85**(10):1137-1148.
25. Palii SS, Van Emburgh BO, Sankpal UT, Brown KD, Robertson KD: **DNA methylation inhibitor 5-Aza-2'-deoxycytidine induces reversible genome-wide DNA damage that is distinctly influenced by DNA methyltransferases 1 and 3B**. *Molecular and cellular biology* 2008, **28**(2):752-771.
26. Ashraf W, Ibrahim A, Alhosin M, Zaayter L, Ouararhni K, Papin C, Ahmad T, Hamiche A, Mely Y, Bronner C *et al*: **The epigenetic integrator UHRF1: on the road to become a universal biomarker for cancer**. *Oncotarget* 2017.
27. Bronner C, Achour M, Arima Y, Chataigneau T, Saya H, Schini-Kerth VB: **The UHRF family: oncogenes that are drugable targets for cancer therapy in the near future?** *Pharmacology & therapeutics* 2007, **115**(3):419-434.
28. Unoki M: **Current and potential anticancer drugs targeting members of the UHRF1 complex including epigenetic modifiers**. *Recent patents on anti-cancer drug discovery* 2011, **6**(1):116-130.
29. Alhosin M, Abusnina A, Achour M, Sharif T, Muller C, Peluso J, Chataigneau T, Lugnier C, Schini-Kerth VB, Bronner C *et al*: **Induction of apoptosis by thymoquinone in lymphoblastic leukemia Jurkat cells is mediated by a p73-dependent pathway which targets the epigenetic integrator UHRF1**. *Biochemical pharmacology* 2010, **79**(9):1251-1260.
30. Alhosin M, Omran Z, Zamzami MA, Al-Malki AL, Choudhry H, Mousli M, Bronner C: **Signalling pathways in UHRF1-dependent regulation of tumor suppressor genes in cancer**. *Journal of experimental & clinical cancer research : CR* 2016, **35**(1):174.
31. Myrianthopoulos V, Cartron PF, Liutkeviciute Z, Klimasauskas S, Matulis D, Bronner C, Martinet N, Mikros E: **Tandem virtual screening targeting the SRA domain of UHRF1 identifies a novel chemical tool modulating DNA methylation**. *European journal of medicinal chemistry* 2016, **114**:390-396.
32. Houliston RS, Lemak A, Iqbal A, Ivanochko D, Duan S, Kaustov L, Ong MS, Fan L, Senisterra G, Brown PJ *et al*: **Conformational dynamics of the TTD-PHD histone reader module of UHRF1 reveals multiple histone binding states, allosteric regulation and druggability**. *The Journal of biological chemistry* 2017.
33. Parker BS, Cutts SM, Nudelman A, Rephaeli A, Phillips DR, Sukumar S: **Mitoxantrone mediates demethylation and reexpression of cyclin d2, estrogen receptor and 14.3.3sigma in breast cancer cells**. *Cancer biology & therapy* 2003, **2**(3):259-263.

34. Walker DA, Wyhs N, Giovinazzo H, Yegnasubramanian S, Nelson WG: **Abstract 5390: Development of a high-throughput screening assay to identify UHRF1 inhibitors via time-resolved fluorescence resonance energy transfer (TR-FRET)**. *Cancer research* 2014, **74**(19 Supplement):5390-5390.
35. Evison BJ, Sleebs BE, Watson KG, Phillips DR, Cutts SM: **Mitoxantrone, More than Just Another Topoisomerase II Poison**. *Medicinal research reviews* 2016, **36**(2):248-299.
36. Das A, Roy S, Mondal P, Datta A, Mahali K, Loganathan G, Dharumadurai D, Sengupta PS, Akbarsha MA, Guin PS: **Studies on the interaction of 2-amino-3-hydroxy-anthraquinone with surfactant micelles reveal its nucleation in human MDA-MB-231 breast adinocarcinoma cells**. *RSC Advances* 2016, **6**(34):28200-28212.
37. Delagoutte B, Lallous N, Birck C, Oudet P, Samama JP: **Expression, purification, crystallization and preliminary crystallographic study of the SRA domain of the human UHRF1 protein**. *Acta crystallographica Section F, Structural biology and crystallization communications* 2008, **64**(Pt 10):922-925.
38. Achour M, Mousli M, Alhosin M, Ibrahim A, Peluso J, Muller CD, Schini-Kerth VB, Hamiche A, Dhe-Paganon S, Bronner C: **Epigallocatechin-3-gallate up-regulates tumor suppressor gene expression via a reactive oxygen species-dependent down-regulation of UHRF1**. *Biochemical and biophysical research communications* 2013, **430**(1):208-212.
39. Hawkins PC, Skillman AG, Warren GL, Ellingson BA, Stahl MT: **Conformer generation with OMEGA: algorithm and validation using high quality structures from the Protein Databank and Cambridge Structural Database**. *J Chem Inf Model* 2010, **50**(4):572-584.
40. **OMEGA 2.5.1.4: OpenEye Scientific Software, Santa Fe, NM. http://www.eyesopen.com**.
41. **QUACPAC 1.6.3.1: OpenEye Scientific Software, Santa Fe, NM. http://www.eyesopen.com.** In.
42. McGann M: **FRED pose prediction and virtual screening accuracy**. *J Chem Inf Model* 2011, **51**(3):578-596.
43. **FRED 3.0.1 OpenEye Scientific Software, Santa Fe, NM. http://www.eyesopen.com**.
44. Rochel N, Ciesielski F, Godet J, Moman E, Roessle M, Peluso-Iltis C, Moulin M, Haertlein M, Callow P, Mely Y *et al*: **Common architecture of nuclear receptor heterodimers on DNA direct repeat elements with different spacings**. *Nature structural & molecular biology* 2011, **18**(5):564-570.
45. Wiseman T, Williston S, Brandts JF, Lin LN: **Rapid measurement of binding constants and heats of binding using a new titration calorimeter**. *Analytical biochemistry* 1989, **179**(1):131-137.
46. El Meshri SE, Dujardin D, Godet J, Richert L, Boudier C, Darlix JL, Didier P, Mely Y, de Rocquigny H: **Role of the nucleocapsid domain in HIV-1 Gag oligomerization and trafficking to the plasma membrane: a fluorescence lifetime imaging microscopy investigation**. *Journal of molecular biology* 2015, **427**(6 Pt B):1480-1494.
47. Clamme JP, Azoulay J, Mely Y: **Monitoring of the formation and dissociation of polyethylenimine/DNA complexes by two photon fluorescence correlation spectroscopy**. *Biophysical journal* 2003, **84**(3):1960-1968.
48. Qian C, Li S, Jakoncic J, Zeng L, Walsh MJ, Zhou MM: **Structure and hemimethylated CpG binding of the SRA domain from human UHRF1**. *J Biol Chem* 2008, **283**(50):34490-34494.
49. Stahl M, Mauser H: **Database clustering with a combination of fingerprint and maximum common substructure methods**. *J Chem Inf Model* 2005, **45**(3):542-548.
50. Mori M, Tottone L, Quaglio D, Zhdanovskaya N, Ingallina C, Fusto M, Ghirga F, Peruzzi G, Crestoni ME, Simeoni F *et al*: **Identification of a novel chalcone derivative that inhibits Notch signaling in T-cell acute lymphoblastic leukemia**. *Sci Rep* 2017, **7**(1):2213.
51. Mori M, Kovalenko L, Malancona S, Saladini F, De Forni D, Pires M, Humbert N, Real E, Botzanowski T, Cianferani S *et al*: **Structure-Based Identification of HIV-1 Nucleocapsid**

Protein Inhibitors Active against Wild-Type and Drug-Resistant HIV-1 Strains. *ACS Chem Biol* 2018, **13**(1):253-266.

52. Shin D, Sinkeldam RW, Tor Y: **Emissive RNA alphabet**. *Journal of the American Chemical Society* 2011, **133**(38):14912-14915.
53. Kilin V, Gavvala K, Barthes NP, Michel BY, Shin D, Boudier C, Mauffret O, Yashchuk V, Mousli M, Ruff M *et al*: **Dynamics of Methylated Cytosine Flipping by UHRF1**. *Journal of the American Chemical Society* 2017, **139**(6):2520-2528.
54. National Toxicology P: **Bioassay of 2-aminoanthraquinone for possible carcinogenicity**. *National Cancer Institute carcinogenesis technical report series* 1978, **144**:1-117.
55. Hsin LW, Wang HP, Kao PH, Lee O, Chen WR, Chen HW, Guh JH, Chan YL, His CP, Yang MS *et al*: **Synthesis, DNA binding, and cytotoxicity of 1,4-bis(2-amino-ethylamino)anthraquinone-amino acid conjugates**. *Bioorganic & medicinal chemistry* 2008, **16**(2):1006-1014.
56. Becker W: **The Bh TCSPC Handbook**: Becker & Hickl; 2014.
57. Bashtrykov P, Jankevicius G, Jurkowska RZ, Ragozin S, Jeltsch A: **The UHRF1 protein stimulates the activity and specificity of the maintenance DNA methyltransferase DNMT1 by an allosteric mechanism**. *The Journal of biological chemistry* 2014, **289**(7):4106-4115.
58. Fang J, Cheng J, Wang J, Zhang Q, Liu M, Gong R, Wang P, Zhang X, Feng Y, Lan W *et al*: **Hemi-methylated DNA opens a closed conformation of UHRF1 to facilitate its histone recognition**. *Nature communications* 2016, **7**:11197.
59. Rothbart SB, Krajewski K, Nady N, Tempel W, Xue S, Badeaux AI, Barsyte-Lovejoy D, Martinez JY, Bedford MT, Fuchs SM *et al*: **Association of UHRF1 with methylated H3K9 directs the maintenance of DNA methylation**. *Nature structural & molecular biology* 2012, **19**(11):1155-1160.
60. Unoki M, Nishidate T, Nakamura Y: **ICBP90, an E2F-1 target, recruits HDAC1 and binds to methyl-CpG through its SRA domain**. *Oncogene* 2004, **23**(46):7601-7610.
61. Zhou L, Shang Y, Jin Z, Zhang W, Lv C, Zhao X, Liu Y, Li N, Liang J: **UHRF1 promotes proliferation of gastric cancer via mediating tumor suppressor gene hypermethylation**. *Cancer biology & therapy* 2015, **16**(8):1241-1251.
62. Jin W, Chen L, Chen Y, Xu SG, Di GH, Yin WJ, Wu J, Shao ZM: **UHRF1 is associated with epigenetic silencing of BRCA1 in sporadic breast cancer**. *Breast cancer research and treatment* 2010, **123**(2):359-373.
63. Krifa M, Pizzi A, Mousli M, Chekir-Ghedira L, Leloup L, Ghedira K: **Limoniastrum guyonianum aqueous gall extract induces apoptosis in colorectal cancer cells by inhibiting calpain activity**. *Tumour biology : the journal of the International Society for Oncodevelopmental Biology and Medicine* 2014, **35**(8):7877-7885.

Supporting Information

Targeting the base flipping activity of human UHRF1 decreases DNA methylation and impairs DNMT1 recruitment

Liliyana Zaayter[1,#], Mattia Mori[2,#], Waseem Ashraf[1], Christian Boudier[1], Vasyl Kilin[1], Krishna Gavvala[1], Tanveer Ahmad[1], Sylvia Eiler[3], Marc Ruff[3], Maurizio Botta[3], Christian Bronner[3], Marc Mousli[1,*], Yves Mély[1,*]

[1] Laboratoire de Bioimagerie et Pathologies, UMR 7021 CNRS, Université de Strasbourg, Faculté de Pharmacie, Illkirch-France

[2] Dipartimento di Biotecnologie, Chimica e Farmacia, Università degli Studi di Siena, Via Aldo Moro 2, 53100, Siena, Italy.

[3] Institut de Génétique et de Biologie Moléculaire et Cellulaire (IGBMC), INSERM U964 CNRS UMR 7104, Université de Strasbourg, Illkirch-France.

[#] LZ and MM equally contributed to this work

*Authors to whom correspondence should be addressed: Yves Mély, yves.mely@unistra.fr; Marc Mousli, mousli@unistra.fr;

- **Hits selection in silico**

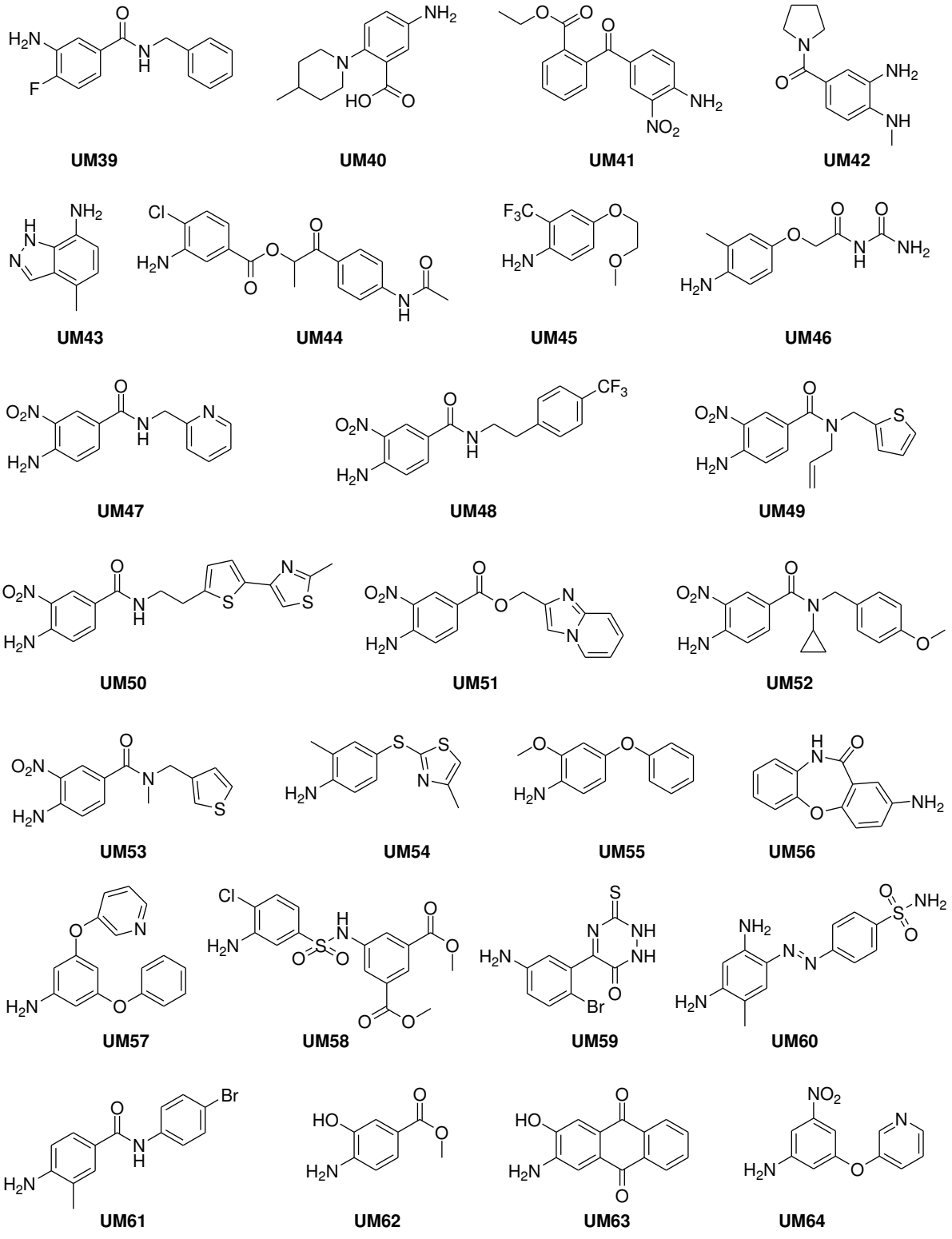

Figure S1. Chemical structure of putative hits UM39–UM64 selected by virtual screening.

- **Effect of UM63, UM63B and UM63D on the fluorescence of thG-labeled HM DNA duplexes**

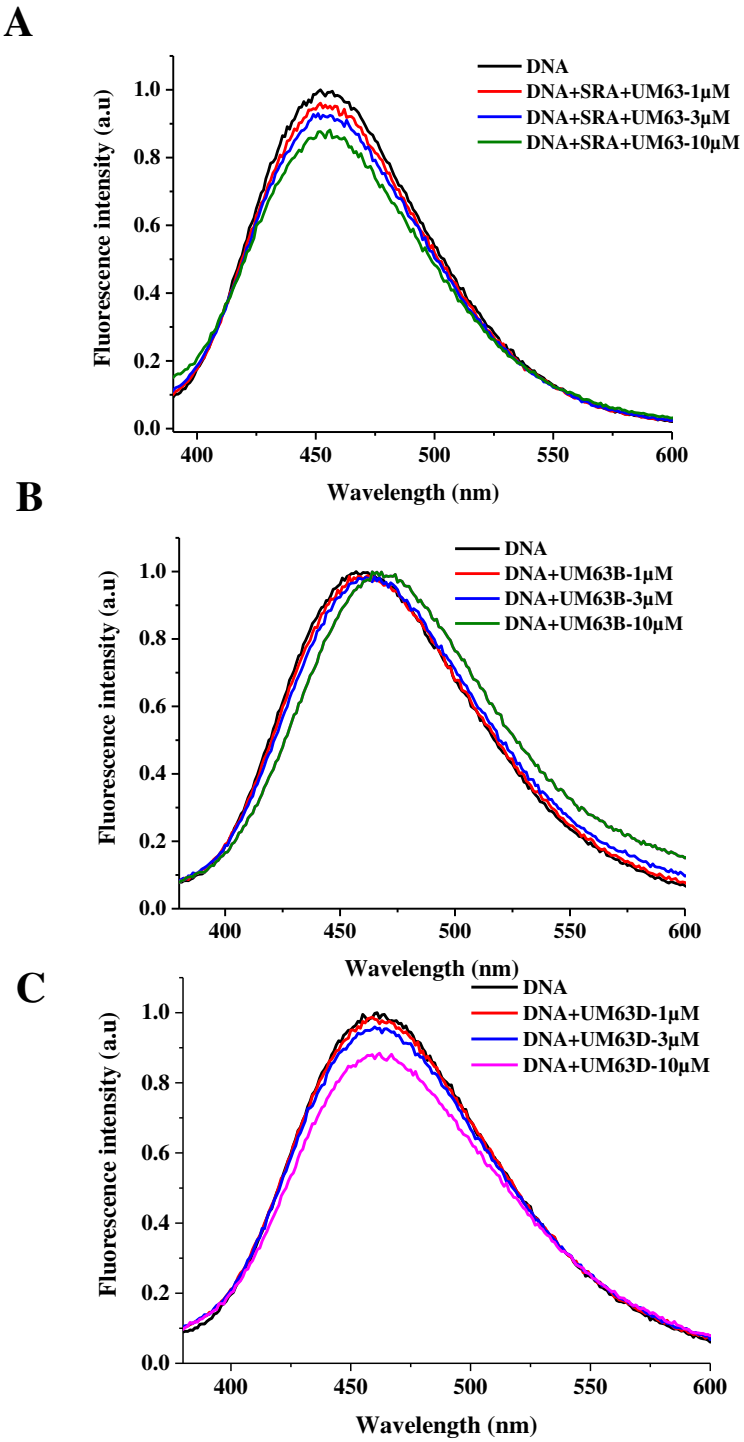

Figure S2. Effect of UM63, UM63B and UM63D on the emission spectrum of the thG-labeled HM duplex. Emission spectra of 1 μM thG-labeled duplex in the absence (black) and in the presence of different concentrations of (**A**) UM63 (**B**) UM63B or (**C**) UM63D. Excitation was at 330 nm.

UM63 competes with Ethidium bromide (EtBr) to bind to DNA:

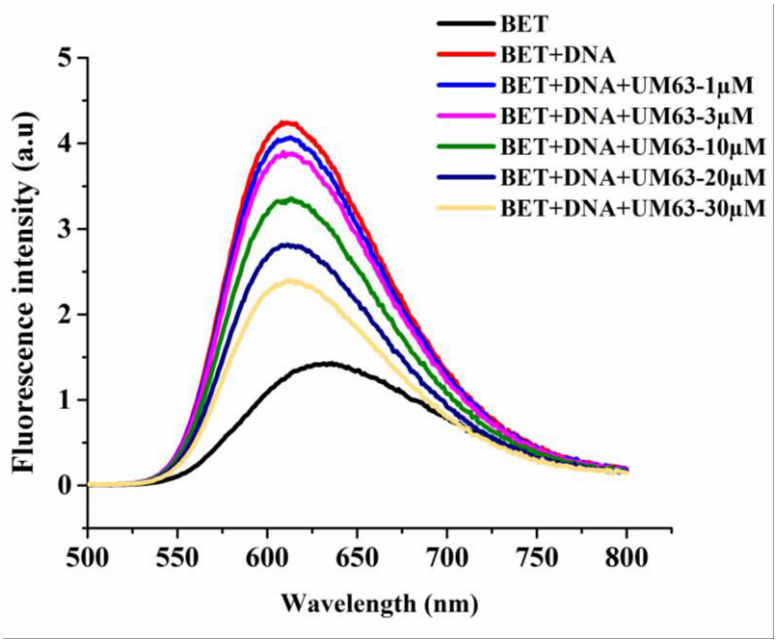

Figure S3. **UM63 competition with EtBr for DNA intercalation**. Fluorescence emission spectra of 1 μM EtBr free (black line) or bound to 1 μM DNA before (red) and after addition of different concentrations of UM63.

- **Binding of UM63E to HM DNA**

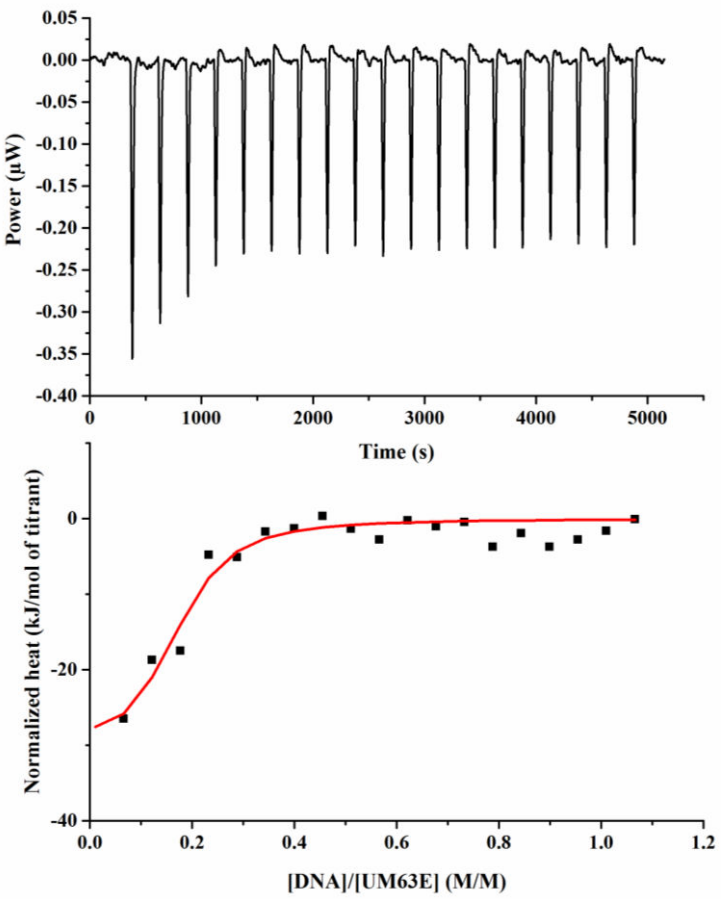

Figure S4. Binding of UM63E to HM DNA as monitored by Isothermal Titration Calorimetry. Representative ITC titration curve of 12 µM of UM63E by HM DNA. The concentration of HM DNA in the syringe was 80 µM. The red curve was fitted to the experimental heat quantities using equation (6) giving a K_d value of 0.25 µM and ΔH=-31.5 kJ/mol.

- **Effect of UM63E on the base flipping kinetics of the SRA domain**

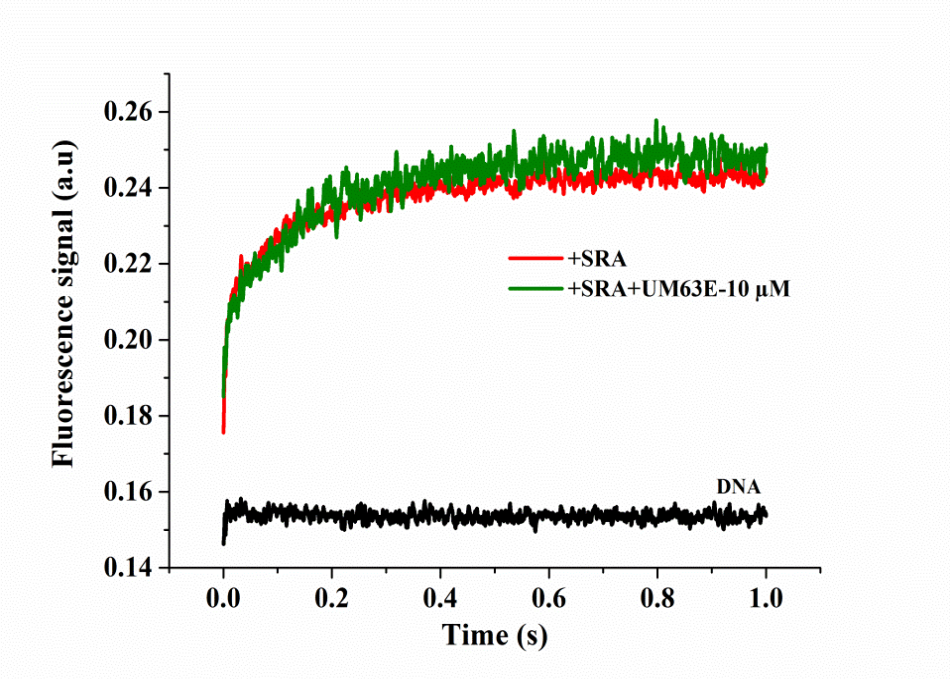

Figure S5. Effect of UM63E on the base flipping kinetics of the SRA domain. Kinetic curves were obtained by the stopped flow technique, monitoring the fluorescence of the thG-labeled HM duplex. The black curve corresponds to 0.2 µM HM duplex mixed with buffer. The red and green traces correspond to the mixing of 0.2 µM HM duplex with 1.5 µM SRA, respectively in the absence and the presence of 10 µM UM63E.

- **Effect of UM63E on the SRA/HM DNA complex**

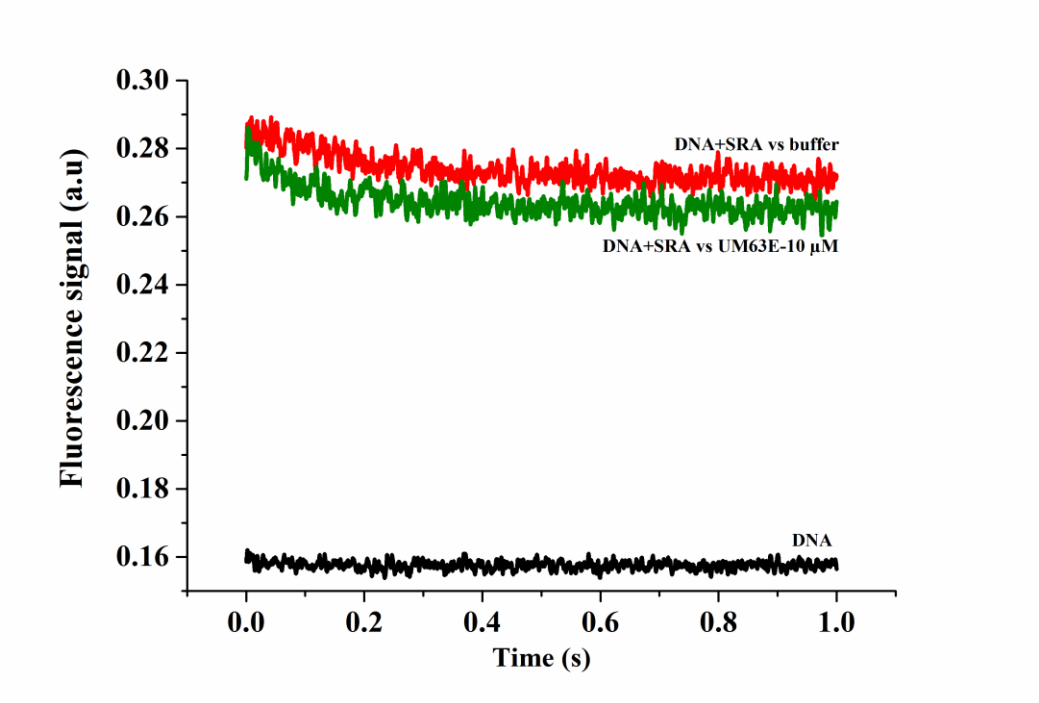

Figure S6. **Effect of UM63E on the SRA/HM DNA complex.** The dissociation of the SRA/HM DNA complex was monitored by the stopped flow technique after addition of 10 µM (green curve) of UM63E to the complex. The black curve corresponds to the DNA alone mixed with buffer. The concentrations of SRA and thG-labeled DNA were 0.2 µM and 1.5 µM, respectively.

- **Overlap of UM63 and HM DNA binding sites on SRA**

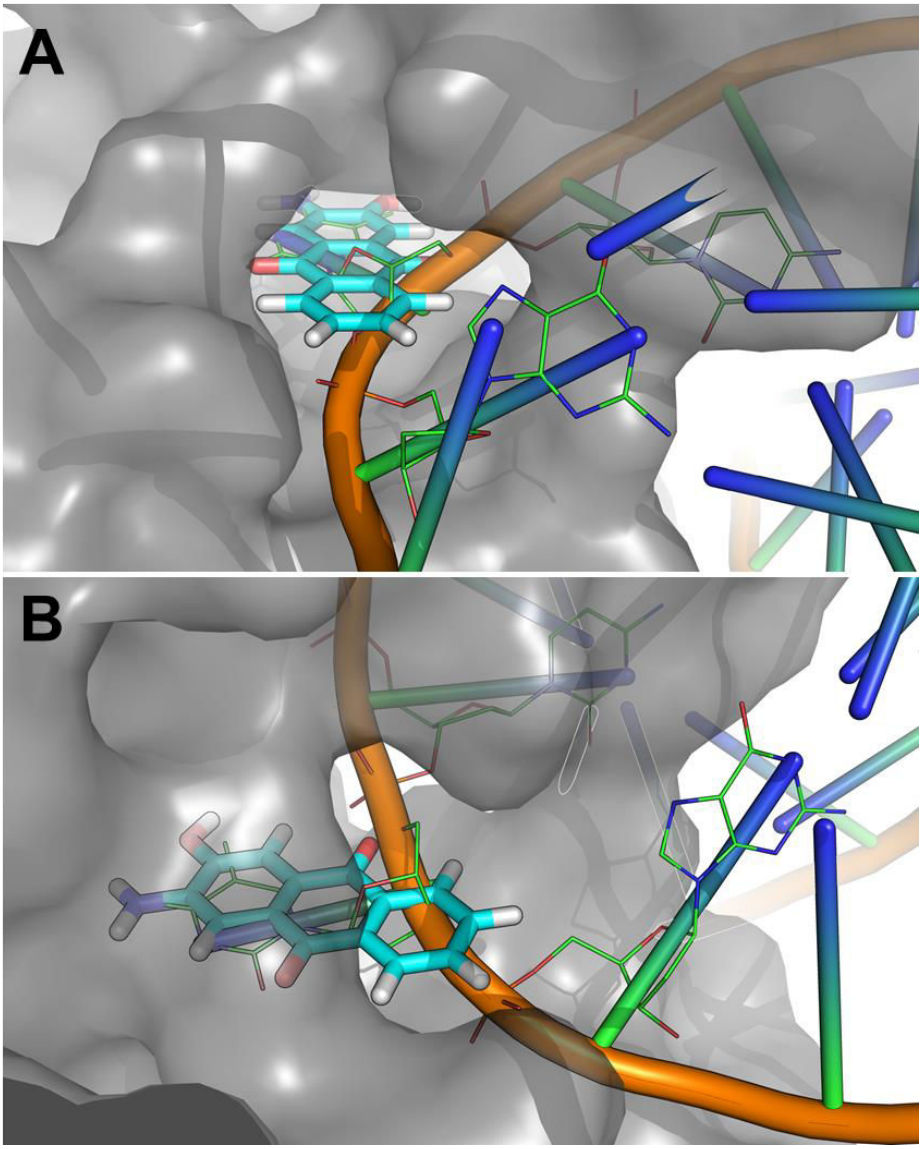

Figure S7. **UM63 and HM DNA partially overlap at the entrance of 5mC binding site on SRA**. Front (A) and side view (B) of the steric overlapping between the docking pose of UM63 and the crystallographic pose of HM DNA. UHRF1 is shown as gray surface, UM63 as cyan sticks with explicit H atoms. Crystallographic HM DNA is shown as cartoon, 5mC and the two flanking based are showed as lines.

Manuscript III

7.2 Manuscript III

Maritime pine tannin extract from bark exhibits anticancer properties by inducing expression of p73 and targeting UHRF1 and DNMT1 of epigenetic machinery in cancer cells.

Waseem Ashraf [1], Mounira Krifa [1,2], Liliyana Zaayter [1], Tanveer Ahmad [1], Antonio Pizzi [3,] Christian D. Muller [4], Yves Mély [1], Christina Bronner [5], Marc Mousli [1*]

[1]Laboratory of Bioimaging and Pathologies, UMR 7021 CNRS, Université de Strasbourg, Faculté de Pharmacie, Illkirch-France

[2]Division of Pharmacognosy and Molecular Biology, Faculty of Pharmacy at Monastir, Monastir, Tunisia

[3]ENSTIB/LERMAB, Epinal, France

[4]UMR 7200 CNRS, Laboratoire d'Innovation Thérapeutique, Université de Strasbourg, Faculte´ de Pharmacie, Illkirch, France

[5]Institut de Génétique et de Biologie Moléculaire et Cellulaire (IGBMC), INSERM U964 CNRS UMR 7104, Université de Strasbourg, Illkirch-France

*Correspondence: marc.mousli@unistra.fr
Laboratory of Bioimaging and Pathologies UMR 7021 CNRS,
Faculté de Pharmacie, 74, Route du Rhin, 67401 Illkirch
Cedex, France

ABSTRACT

Maritime pine bark is a rich source of polyphenolic compounds and it is commonly employed as herbal supplement worldwide. This study was designed to check the potential of maritime pine tannin extract (MPTE) for anticancer therapy and to determine the underlying mechanism of action. Our results demonstrated an inhibitory effect of MPTE on the proliferation of cancer cells as its treatment induced cell cycle arrest in G2/M phase. Treatment with MPTE also induced apoptosis in a concentration-dependent manner in cancer cells as evident by an enhanced activation of caspase 3 and cleavage of PARP along with downregulation of antiapoptotic protein BCL2. MPTE showed a pro-oxidant role in cancer cells and promoted the expression of p73 tumor suppressor gene in p53-deficient cells. It also downregulated the protooncogenic UHRF1 and DNMT1, mediators of DNA methylation machinery and reduced global methylation levels in HeLa cells. Altogether, our results show that maritime pine tannin extract can play a favorable role in treatment of cancers which can be explored by pharmaceutical industry for anticancer therapy.

INTRODUCTION

Cancer related diseases are among the major causes of death around the world. Though modern therapies have improved the patient care and therapeutic outcomes, still the majority of tumors are untreatable (Ferlay *et al.*, 2015, Gali-Muhtasib *et al.*, 2015). Continuous efforts are being made to find effective and safer therapies for cancer related disease. Naturally occurring compounds from plants are being thoroughly explored for this purpose and many drugs of natural origin have entered the clinical use (Wang *et al.*, 2012). Indeed, some of the effective anticancer drugs such as vincristine, vinblastine, docetaxel, paclitaxel are derivatives of plant kingdom and are in clinical use today for diverse types of cancers (Greenwell and Rahman, 2015). Treatment with these anticancer drugs inhibit the proliferation of tumors by halting the cell cycle and inducing the apoptosis (Moudi *et al.*, 2013, Iqbal *et al.*, 2017, Xie and Zhou, 2017).

Pinus *pinaster* (synonym Pinus *maritimus,* maritime pine) tree is well-known in traditional herbal medicine for multiple biological activities. Maritime pine trees are commonly found in Mediterranean countries such as France, Spain and Portugal, and in some northern African countries including Tunisia, Algeria and Morocco (Chupin *et al.*, 2013). Its bark is rich in polyphenolic compounds and is believed to possess anti-inflammatory, antioxidant, antidiabetic, anticancer and antiallergic properties (Packer *et al.*, 1999). The dry extract from bark is available commercially by the name of Pycnogenol® and is commonly indicated for multiple disease including asthma, allergies, skin disease, diabetes, osteoarthritis, erectile dysfunction and venous disease (Rohdewald, 2015). Polyphenolic constituents of this extract are divided into monomer or condensed (procyanidin) flavonoids. Monomers are generally catechin, epicatechin, epigallocatechin and epicatechin gallate along with small proportions of fisetinidin and taxifolin while the procyanidin are polymer of flavan-3-ol units of (+)-catechin or epicatechin of various lengths (Navarrete *et al.*, 2010, Chupin *et al.*, 2013, de la Luz Cadiz-Gurrea *et al.*, 2014).

Anticancer activities of French maritime pine bark have been predicted in few studies owing to its polyphenolic content. It induced apoptosis in breast cancer cells, leukemic and fibrosarcoma cells and also prevented the oncogenic transformation of ovarian cells on exposure to carcinogenic talc (Huynh and Teel, 2000, Huang *et al.*, 2005, Buz'Zard and Lau, 2007, Harati *et al.*, 2015). Treatment with bark extract also lowered the incidence of side effects related to

anticancer therapy (Belcaro *et al.*, 2008). Despite a beneficial role of maritime pine bark in cancer suggested by theses studies, a detailed study on anticancer properties of this bark content is lacking.

Caners cells are well known for their tendency to evade the normal growth regulatory mechanisms to proliferate indefinitely by escaping the immune system and simultaneously invading the surrounding tissues. Besides different genetic alterations, various epigenetic perturbations in response to endogenous or exogenous stress signals, also predispose the normal cells to acquire these oncogenic properties (Dawson and Kouzarides, 2012). Unlike the genetic abnormalities, epigenetic alterations can be reversed and led to the foundation of new class of compounds that can target these epigenetic alterations to treat cancer. Aberrant hypermethylation of the promoters of tumor suppressor genes is one of the hallmarks of cancer as it represses the function of these genes and leads to unopposed proliferation of cancer tissues (Sharma *et al.*, 2010, Sandoval and Esteller, 2012). DNMT1 and UHRF1 are the integral part of the DNA methylation machinery. UHRF1 identifies the hemi-methylated cytosine on the parent DNA strand and recruits the DNMT1 to the non-methylated cytosine at the daughter strand for the transfer of methylation pattern to newly form strand during the DNA replication (Bronner *et al.*, 2013). UHRF1 and DNMT1 levels are also upregulated in cancers which make them attractive target for anticancer therapy (Unoki, 2011, Ashraf *et al.*, 2017). Currently, 5-azacytidine and 5-aza-2'-deoxycytidine (Decitabine) two DNMTs inhibitor are already in market for the treatment of cancers by targeting this DNA methylation machinery (Pechalrieu *et al.*, 2017). Among many compounds of plant origin, few polyphenolic compounds such as epigallocatechin-3-gallate (EGCG) and luteolin have been reported for their ability to target this UHRF1/DNMT1 tandem to correct the faulty methylation pattern in cells and induce antiproliferative response in cancer cells (Fang *et al.*, 2003, Achour *et al.*, 2013, Krifa *et al.*, 2013).

Here, in this article we analyzed the anticancer activity of maritime pine tannin extract. Polyphenolic compounds present in this bark inhibited the proliferation of cancer cells by inducing arrest in G2/M phase of cell cycle. MPTE treatment also induced the activation of p73 tumor suppressor genes and activated the apoptotic pathway in in HeLa cells. This extract also downregulated the levels of epigenetic proteins UHRF1 and DNMT1 which are involved in maintenance of DNA methylation and ultimately led to global hypomethylation of these cells.

MATERIAL AND METHODS

1. Maritime Pine Tannin Extract Preparation:

Maritime pine (Pinus maritimus) bark was obtained from Landes, the southwest region of France. It was dried initially and crushed mildly to form coarse chips of bark which were later completely dried till a constant weight was obtained. Tannins were extracted from dried ground bark by completely immersing it in 2% sodium bisulphite and 0.5% sodium bicarbonate water solution with continuous stirring in an industrial reactor (Biolandes, France). Final solution was spray-dried to obtain the tannins in the form of dark reddish-brown powder which was later used for studies.

2. Cell Culture and MPTE treatment:

HeLa cells (ATCC, CCL-2), U2OS and fibroblast were cultured in DMEM (Dulbecco's Modified Eagle's Medium), supplemented with 10% FBS (fetal bovine serum), in addition to penicillin (100 U/ml) and streptomycin (100 U/ml) (Invitrogen). Cells were maintained at 37°C in a humid atmosphere with a continuous supply of CO_2 maintained at 5%.

MPTE solutions were always freshly prepared for the treatment of cells. 10 mg of extract powder was first mixed with 50 µL of DMSO by sonication and later this solution was then diluted in 10 mL of preheated DMEM by brief vortex to obtain a concentration of 1 mg/mL. Extract solution was then sterilized by passing through Millex-GP, 0,22 µm syringe filters (Merck-Millipore) and diluted to required concentrations with additional DMEM media. Prepared solutions of desired concentration were then added to seeded cells while the control samples were replaced with fresh media, without the addition of extract.

3. Antibodies:

Different antibodies used in this study include mouse monoclonal anti-PARP (BD Biosciences Pharmingen), rabbit polyclonal anti-caspase3 (Cell Signaling), mouse monoclonal anti-UHRF1 engineered as described previously (Hopfner *et al.*, 2000), mouse monoclonal anti-DNMT1 (Proteogenix France), mouse monoclonal anti-BCL-2 (Merck-Millipore), mouse monoclonal anti-GAPDH (Merck Millipore), polyclonal anti-mouse (Promega) and polyclonal anti-rabbit (promega) antibodies.

4. Cellular Proliferation Test:

Effect of MPTE treatment on cellular proliferation was assayed by help of colorimetric MTT assay. In this assay, viable cells are identified by their ability to reduce the tetrazolium dye MTT 3-(4,5-dimethylthiazol-2-yl)-2,5-diphenyltetrazolium bromide to insoluble purple color

formazan crystals. These crystals are later dissolved in DMSO and quantified by measuring absorption at 570 nm. Cell were seeded in 96 well plate at a density of $5x10^3$ cells per well and incubated with different concentrations (12.5, 25, 50, 75, 100, 150, 300, 400 and 500 µg/mL) of MPTE extract. Negative control wells were also replaced with fresh media without addition of extract. After 24 hr of treatment, old media was replaced by 100 µL of MTT (5mg/10mL) containing media in each well and incubated for further 4 hr. Formazan crystals formed after incubation with MTT were later dissolved in 100 µL of DMSO and the absorption at 570 nm was determined by Xenius plate reader. Each experiment was repeated three times and percentage viability in the treated samples was calculated with reference to untreated samples. The cytotoxicity was expressed as IC_{50}, which is the concentration required to reduce the absorbance of treated cells by 50% with reference to the control (untreated cells). Average IC_{50} values were then statistically determined from the dose response curves obtained in Origin software (version 8.6)

5. Cell Cycle and Apoptosis Analysis:

For cell cycle analysis, HeLa cells were seeded in 6-well plate at a density of 10^5 cells per well and were treated with 75, 150 and 300 µg/mL of MPTE along with control samples. At the end of 24 hr of treatment, cells were washed with PBS and mildly trypsinized to collect the cells which were fixed with BD cellfix (BD Biosciences) reagent. Fixed cells were then incubated with FxCycle™ PI/RNase staining solution (Thermo Fisher Scientific) for 20 mins before analysis with guava easyCyte™ flow cytometer (Merck Millipore). Fractions of cells in different phase of cell cycle were quantified by using InCyte Software for Guava® (Merck Millipore).

For apoptosis analysis, cells were seeded and treated as mentioned above. Cells from the plate and culture media were collected and incubated with PI and annexin V-FITC™ (Miltenyi Biotec) for 20 mins to label the cells undergoing apoptosis. These cells were then analyzed by guava easyCyte™ flow cytometer (Merck Millipore) to determine the percentage of cells in different phase of apoptosis.

6. Analysis of reactive oxygen species (ROS) production:

HeLa cells were seeded and treated in 6-well plate as described in pervious section. ROS production was determined by dihydroethidium (DHE) staining through flow cytometry. Cells were incubated with 10 µM concentration of DHE for 30 mins at 37°C before collection and analysis by guava easyCyte™ flow cytometer (Merck Millipore).

7. Western Blot:

HeLa cells were seeded in a 6-well plate and treated with 75, 150 and 300 µg/mL of MPTE for 24 hr as described earlier. After treatment, cells were collected by trypsinization and incubated with lysis buffer 10 mM Tris-HCl pH 7.5, 150 mM NaCl, 1 mM EDTA and 1% NP40 supplemented with protease inhibitors (complete mini EDTA free protease inhibitor cocktail tablets, Roche Germany) for 30 min on ice to harvest the proteins. After quantifying the isolated proteins by help of standard BSA curve, 40 µg of total protein lysate from each sample was resolved on 10% SDS-PAGE and transferred onto PVDF membranes. Membranes were blocked for 1 hr with 3% blotting-grade blocker (Bio-Rad) in TBST buffer before incubating them overnight with the primary antibodies at 4°C. Membranes were then washed with TBST for three times and incubated with respective secondary antibodies for 1 hr at room temperature. After washing the membranes with TBST, membranes were imaged with the help of chemiluminescent ECL system (Clarity™ ECL western blotting substrate, Biorad, 170-5060) on ImageQuant™ LAS 4000 system (GE Healthcare). Images were quantified using the Image Studio Lite (LiCore Biosciences, USA).

8. Global Methylation Assay:

For global methylation assay HeLa cells were seeded in six well plate and treated as described earlier. DNA was extracted from the treated and non-treated samples by using QIAamp® DNA Kit (Qiagen). 200 µg of the purified DNA from each sample was then analyzed for global methylation levels by using Sigma's Imprint® methylated DNA quantification kit (Sigma-Aldrich) according to manufacturer's protocol.

9. Statistical Analysis:

All experiments were repeated three times and results between groups were statistically compared by one-way ANOVA with post-hoc Tukey test using GraphPad-Prism (version 5.04) and Origin (version 8.6) software.

RESULTS

1. Effect of Maritime Pine tannin extract (MPTE) on cell proliferation

Firstly, the effect of maritime pine tannin extract on cellular proliferation was determined by MTT assay on different cell lines including cervical cancer cell line HeLa, osteosarcoma U2OS cells, and normal fibroblasts cells. Cells were treated with 12.5, 25, 50, 75, 100, 150, 300, 400 and 500 µg/mL of extract for 24 hr and the inhibitory effect was determined by comparing the cell viability with the untreated cells. Results of MTT assay showed that MPTE inhibited the proliferation of these cells in a dose dependent manner (Fig. 1). IC_{50} values were graphically determined for each cell line and it was observed that MPTE significantly reduced the proliferation of HeLa and U2OS cells at relatively low concentration (Fig. 1A-B) as compared to normal fibroblast cells (Fig. 1C). The mean IC_{50} values for HeLa and U2OS cells were 153 ± 16 µg/mL and 218 ± 5 µg/mL respectively as compared to normal fibroblast cells in which the IC_{50} value was 490 ± 26 µg/mL. This shows a selective response of MPTE towards the rapidly dividing cancer cells and prompted us to evaluate its antitumor potential in HeLa cells.

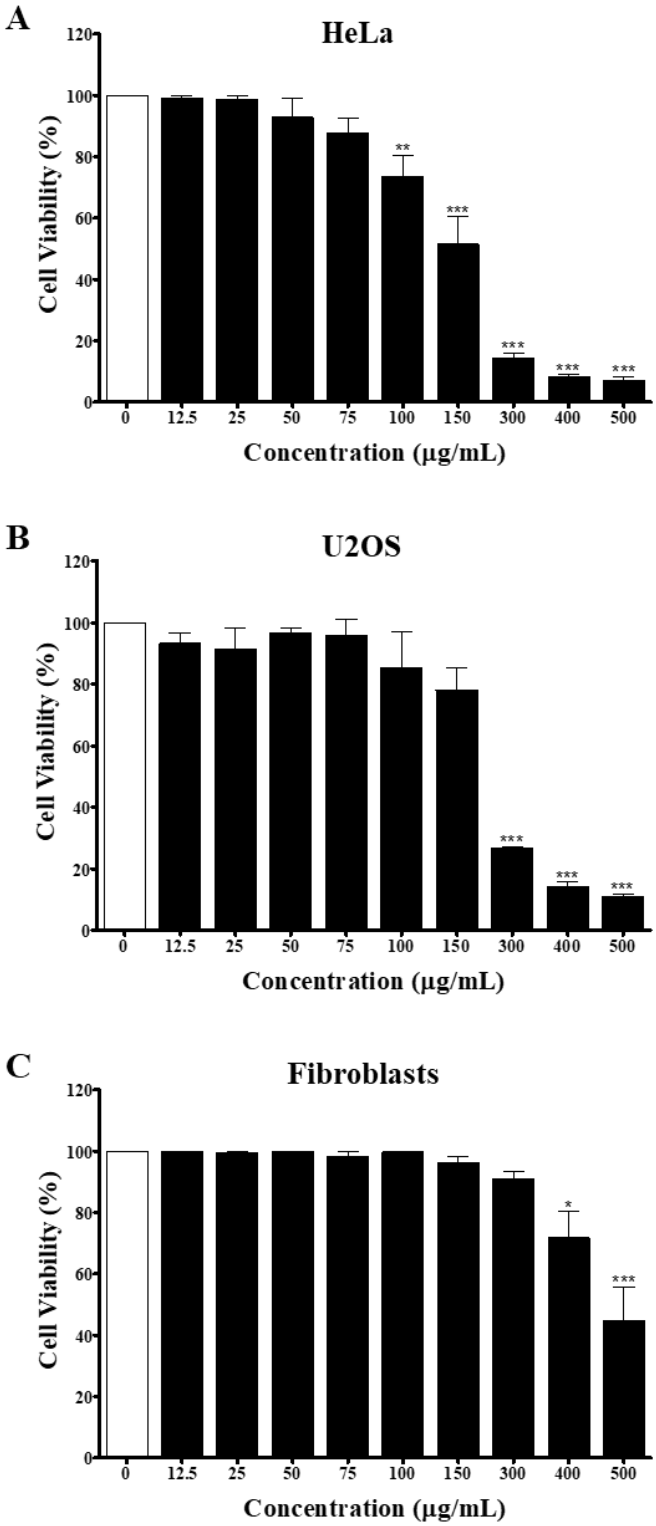

Figure 1. MPTE inhibits the proliferation of cancer cells. HeLa (A), U2OS (B) and fibroblasts cells (C) were treated with MPTE for 24 hr and the inhibition of proliferation was determined by colorimetric MTT assay. Values are represented in terms of percentage with reference to untreated samples serving as control. Values shown are mean

± SEM of three independent experiments. Statistical significance is represented as * P < 0.05, ** P < 0.01, *** P < 0.001 versus the corresponding control group.

2. MPTE induces cell cycle arrest in G2/M phase

In order to further explore the inhibitory effect of MPTE on cellular proliferation we analyzed the distribution of cells treated with 75, 150 and 300 µg/mL of MPTE in different phases of cell cycle and compared it to controls. FACS analysis revealed that treatment of MPTE for 24 hr reduced the cellular population in G0/G1 phase while the population in G2/M phase was increased in a dose dependent manner (Fig. 2). Indeed, cellular fraction in G0/G1 phase was significantly reduced from 57% in control cells to 30% and 27% in cells treated with 150 and 300 µg/mL of MPTE respectively. While the cellular population in G2/M phase significantly increased from 18% in control cells to 38% and 34% in HeLa cells treated with 150 and 300 µg/mL of MPTE respectively. This suggests that treatment of MPTE inhibits proliferation of cells by inducing cell cycle arrest at G2/M phase.

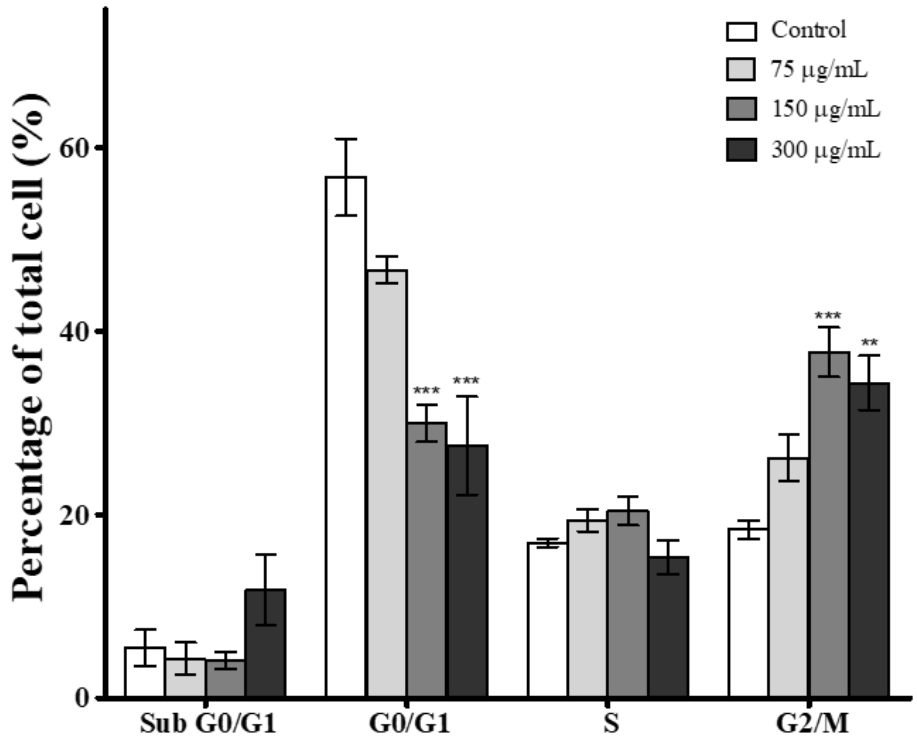

Figure 2. MPTE treatment induced cell cycle arrest. HeLa cells were treated with indicated concentrations of MPTE for 24 hr and distribution of cells in different phases of cell cycle were determined by fluorescence cell cytometry analysis. Cellular distribution in each phase was represented in terms of percentage relative to the total number of cells. Values are expressed as mean ± SEM of three independent experiments.

Statistical significance is represented as * $P < 0.05$, ** $P < 0.01$, *** $P < 0.001$ versus the corresponding control group.

3. MPTE treatment induced apoptosis in cells

The potential cytotoxic effect of MPTE treatment was also determined by FACS through labelling of annexin-FITC and propidium iodide. Treatment with MPTE decreased the viability of cells and induced apoptosis in HeLa cells in a concentration dependent manner (Fig. 3A). Viable cells were significantly reduced from 92% in control cells to 76%, 48% and 27% in cells treated with 75, 150 and 300 µg/mL of MPTE respectively. Accordingly, the early apoptotic cells were also increased from 1.8% in control to 8%, 8.7% and 5.2% in cells treated with 75, 150 and 300 µg/mL of MPTE respectively (Fig. 3A). The percentage of late apoptotic cells and necrotic cells also increased significantly by 24 hr treatment with 150 and 300 µg/mL of MPTE showing the ability of this extract to induce death in proliferating cells (Fig. 3A).

We also confirmed the induction of apoptosis by analyzing the activation of caspase 3, cleavage of PARP and levels of antiapoptotic protein like BCL2 in the proteins isolated from control and MPTE treated cells (Fig. 3B). Western blot analysis revealed evident activation of caspase 3 from its precursor protein after treating the cells with 150 µg/mL or higher concentration of MPTE. PARP cleavage also became visible in response to MPTE treatment and became more prominent with increasing concentration of MPTE. Indeed, BCL2 levels were also found evidently reduced with treatment of MPTE. These results confirmed the induction of apoptosis in response to MPTE treatment.

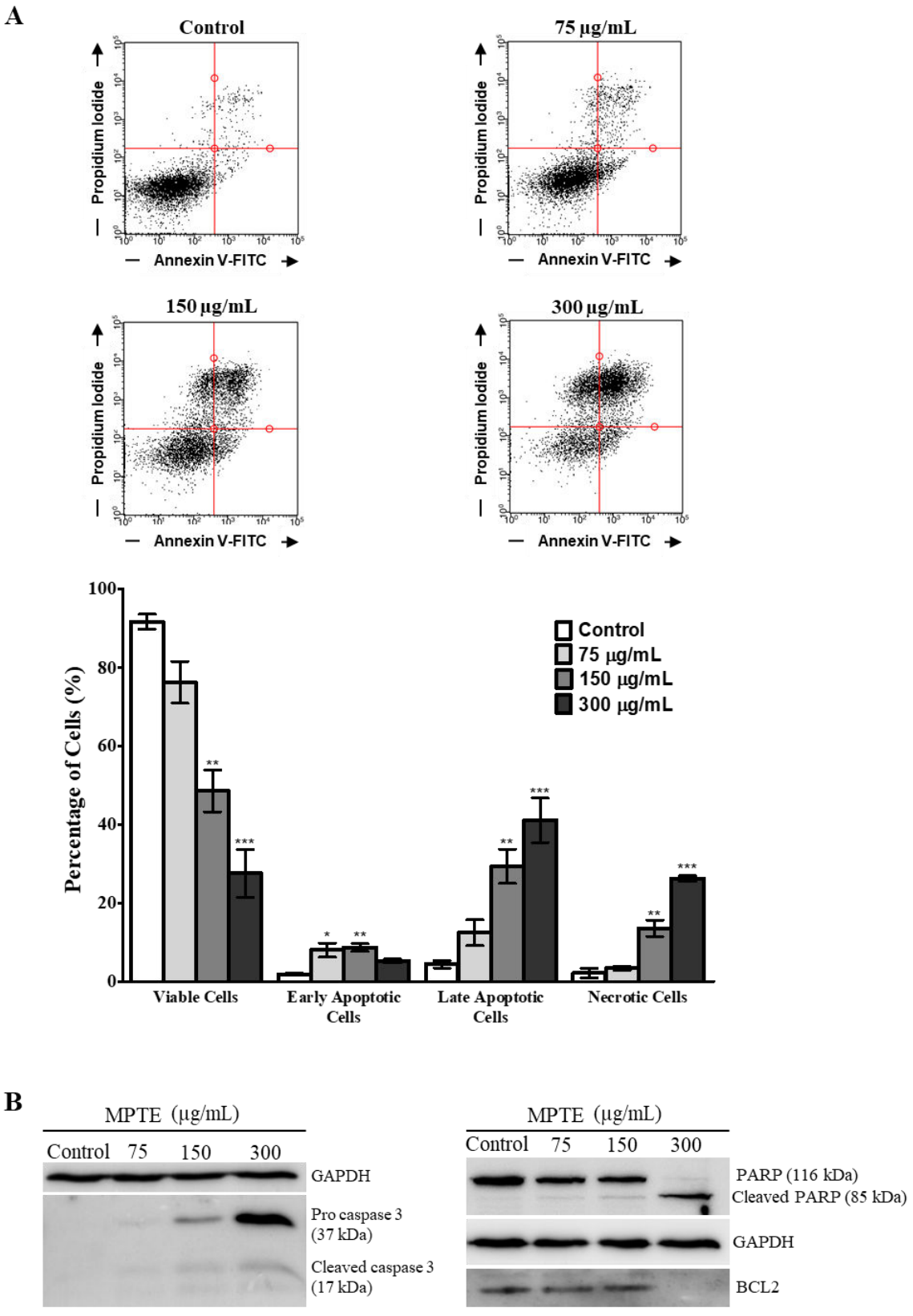

Figure 3. MPTE treatment induced apoptosis in HeLa cells. A, HeLa cells were incubated with indicated concentrations of MPTE for 24 hr and viable cells along with fraction of cells undergoing apoptosis were determined by annexin V-FITC and PI labeling through

FACS. Values are expressed as mean ± SEM of three independent experiments. Statistical significance is represented as * P < 0.05, ** P < 0.01, *** P < 0.001 versus the corresponding control group. B, Western blots showing cleavage of procaspase 3 and PARP along with downregulation of BCL2 protein with treatment MPTE in HeLa cells.

4. MPTE treatment induced ROS generation

In order to further determine the mechanism of apoptosis, we checked the levels of reactive oxygen species (ROS) generation in cells treated with MPTE by using dihydroethidium (DHE) staining in flow cytometry. DHE gets oxidized inside the cells on exposure to ROS and changes to 2-hydroxyethidium or ethidium which gets incorporated into the DNA and fluorescently labels the cells. Flow cytometry analysis of HeLa cells treated with MPTE revealed significant production of ROS when incubated with higher concentrations of MPTE for 24 hr (Fig. 4A-B). Indeed, the ROS levels increased by 1.5 and 2 folds with the 24 hr treatment of 150 and 300 µg/mL of MPTE respectively as compared to controls (Fig. 4B). The granularity of the cells is usually increased with ROS generation and is often considered as indicator of senescence or apoptosis (Gosselin *et al.*, 2009). Side scatter plot revealed that granularity of cells increased after 24 hr with the treatment of 150 and 300 µg/mL of MPTE in a pattern similar to increase in ROS levels indicating that high ROS levels by MPTE treatment induced apoptosis in these cells (Fig. 4C-D).

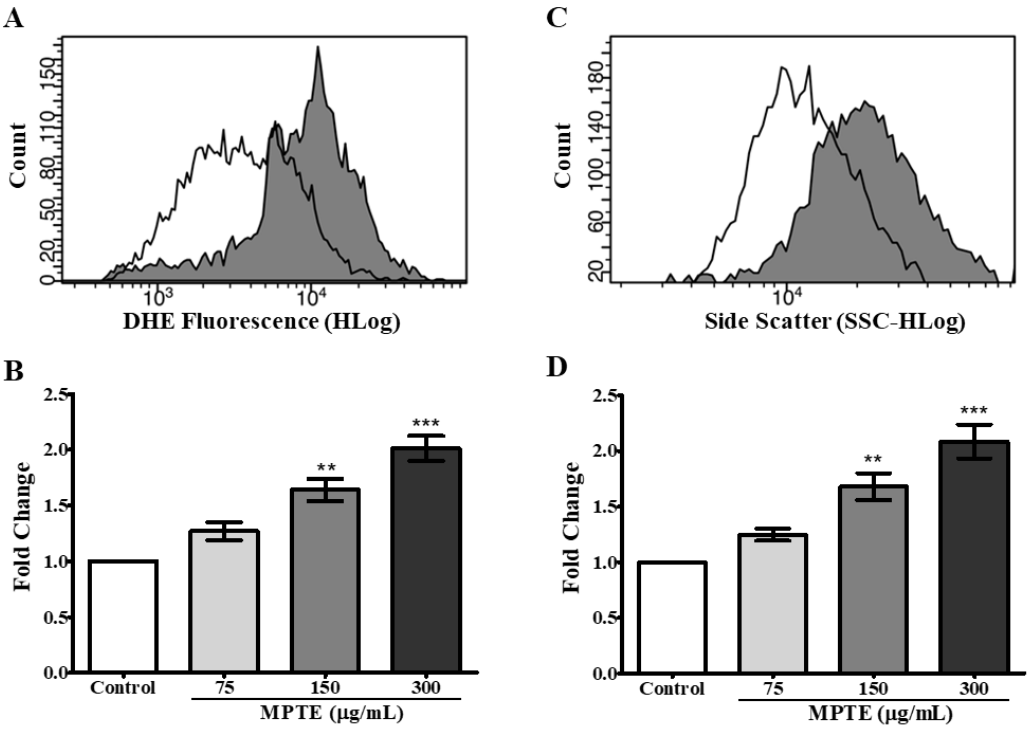

Figure 4. MPTE treatment increased ROS levels and granularity in treated cells. A, Cytogram showing DHE labeling in control (represented by white area under graph) and MPTE treated cells (300 µg/mL, represented by gray area under graph). B, Bar graph showing fold change in DHE labeling by treatment of MPTE at different concentration with respect to control. C, Cytogram showing side scatter in control (represented by white area under graph) and MPTE treated cells (300 µg/mL, represented by gray area under graph). D, Bar graph showing fold change in side scatter by treatment of MPTE at different concentration with respect to control. Values indicated are from three independent experiments and were analyzed by one-way ANOVA with post-hoc Tukey test. (* $P < 0.05$, ** $P < 0.01$, *** $P < 0.001$).

5. MPTE treatment upregulated p73 and downregulated UHRF1 and DNMT1 in HeLa cells

Previously, it has been reported that naturally occurring polyphenolic compounds inhibit the proliferation and activate apoptosis in p53 deficient cancer cells by inducing the expression of its analogue p73 (Alhosin *et al.*, 2010, Achour *et al.*, 2013). So, to check this effect as possible mechanism for induction of cell cycle arrest and apoptosis we evaluated the effect of MPTE treatment on expression of p73 in these cells. Cells were treated with 75, 150 and 300 µg/mL of MPTE for 24 hr and western blot results of the proteins isolated from these cells revealed that treatment of MPTE induced upregulation of p73 in HeLa cells (Fig. 5A-B). Increase in p73 expression was found most significant with treatment of 300 µg/mL of MPTE which upregulated p73 levels by five folds as compared to controls (Fig. 5B).

In our previous studies, we have observed that polyphenolic compounds can also target the UHRF1/DNMT1 tandem responsible for the maintenance of DNA methylation patterns in cells through tumor suppressor genes such as p53 and p73 (Alhosin *et al.*, 2010, Achour *et al.*, 2013). So, we also analyzed the levels of these epigenetic proteins after MPTE exposure to cells and observed significant downregulation of UHRF1 and DNMT1 in a dose dependent manner (Fig. 5A, C-D). Treatment with 75 µg/mL of MPTE induced significant decrease in UHRF1 and DNMT1 levels as compared to controls which became more prominent with higher concentration of extract (Fig. 5C-D).

Since, UHRF1 and DNMT1 are primarily involved in the maintenance of DNA methylation pattern during the replication, we also checked the effect of UHRF1 and DNMT1 downregulation on global DNA methylation level in cells by using Imprint® Methylated DNA Quantification assay. After treatment with different concentration of extract for 24 hr, our

results indicated a decrease in the global methylation levels (Fig. 5E). The effect was more prominent at concentration of 150 µg/mL, as the global methylation levels were averagely 25% less than the levels in control samples. Treatment with 300 µg/mL of MPTE for 24 hr further reduced the global methylation levels by 33% when compared with control samples.

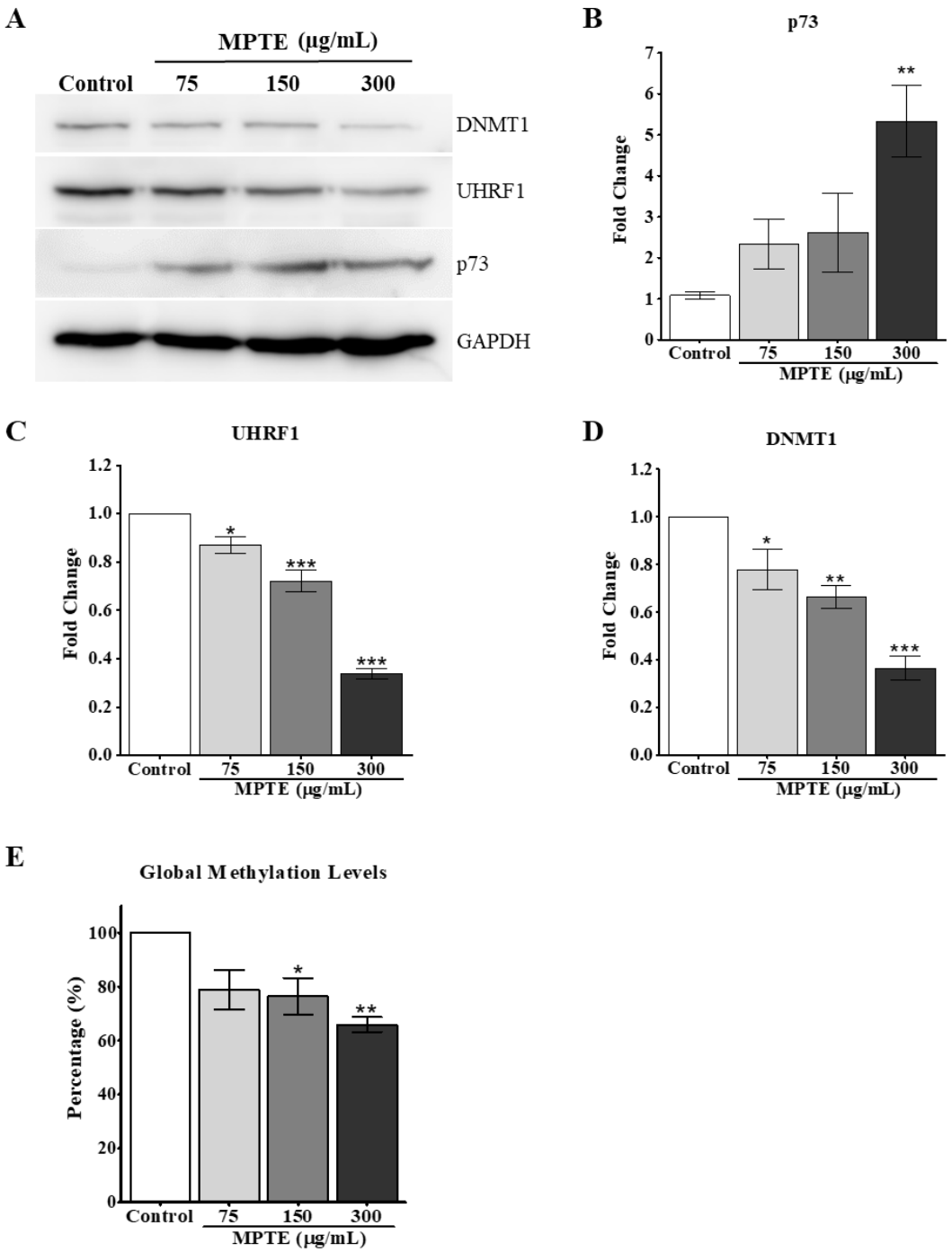

Figure 5. MPTE upregulated p73 along with downregulation of UHRF1 and DNMT1 in cancer cells. A, Western blot analysis of proteins isolated from HeLa cells were treated

with 75, 150 and 300 µg/mL of MPTE for 24 hr along with untreated cells. B, Effect of MPTE treatment on p73 levels with respect to controls. C, Effect of MPTE treatment on UHRF1 levels with respect to controls. D, Effect of MPTE treatment on DNMT1 levels with respect to controls. E, Effect of MPTE treatment on global methylation levels. Values indicated are from three independent experiments and were analyzed by one-way ANOVA with post-hoc Tukey test. (* $P < 0.05$, ** $P < 0.01$, *** $P < 0.001$).

DISCUSSION

Many studies have shown a beneficial role of polyphenolic plant products in prevention and cure of cancers. Such products are now being thoroughly explored for their possible application in treatment of tumors by identifying their active ingredients and their possible mechanism of action (Asensi *et al.*, 2011, Zhou *et al.*, 2016). Maritime pine bark has been previously reported to induce differentiation and apoptosis in cancer cells (Huynh and Teel, 2000, Huang *et al.*, 2005, Buz'Zard and Lau, 2007, Harati *et al.*, 2015). The aim of this study was to check the potential of tannin extract from its bark for the anticancer therapy. MPTE has been well characterized chemically, MALDI-TOF and 13C NMR analysis of this extract revealed that it contains mixture of condensed tannins (procyanidins) made up of varying subunits of catechin, epicatechin, epigallocatechin, epicatechin gallate and fisetinidin monomers (Fig. 6) (Navarrete *et al.*, 2010).

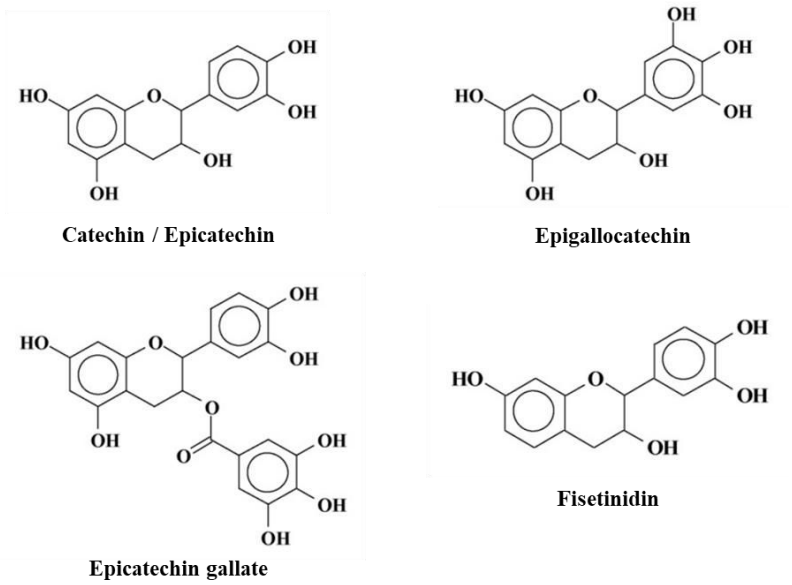

Figure 6. Major catechol monomers forming the procyanidins oligomers in maritime pine tannin extract.

Different physiological properties of maritime pine bark extract such as antioxidant, anti-inflammatory, antidiabetic and cardioprotective effects have been attributed to the presence of these polyphenolic compounds (Packer *et al.*, 1999, Rohdewald, 2015). These compounds are also present in naturally different combinations in leaves of green tea where they have shown their anticancer properties in different studies (Achour *et al.*, 2013, Yang and Wang, 2016). It is also observed that these compounds work better in the form of natural combination in plant product rather than tested individually, as in combination they are effective at lower dose and cause less toxicity (Bode and Dong, 2009).

In our results we observed that treatment with MPTE inhibited the proliferation of cervical cancer HeLa and osteosarcoma U2OS cell lines at low concentration as compared to the primary fibroblasts showing a specific response towards the rapidly proliferating cancer cells. Inhibition of proliferation on treatment with MPTE also resulted in accumulation of the cells in G2/M phase which is commonly observed by the treatment of anticancer compounds (Senese *et al.*, 2014). Catechins and other polyphenolic compounds and from different plant sources have also been reported to induce arrest in G2/M phase of cell cycle in similar studies (Shan *et al.*, 2015, Takanashi *et al.*, 2017). Along with it, MPTE also induced apoptosis in HeLa cells as indicated by increased labeling of annexin V and PI in flow cytometry analysis. Western blot results further confirmed the induction of apoptosis as it revealed the activation of caspase 3 and cleavage of PARP in a dose dependent manner in MPTE treated cells. Levels of pro-survival protein BCL2 were also decreased on MPTE treatment which is necessary for the maintenance of mitochondrial membrane integrity. Loss of BCL2 results in release of cytochrome c and thus leads to apoptosis. In a similar manner, many polyphenolic compounds e.g. (-) epigallocatechin gallate, butein and curcumin have been shown to induce apoptosis in variety of cancer cells by activating caspase 3 and PARP cleavage along with downregulation of BCL-2 protein (Halder *et al.*, 2008, Chen *et al.*, 2012, Wang *et al.*, 2015, Zhu *et al.*, 2015, Wang *et al.*, 2018).

Contrary to previously reported antioxidant activity of maritime pine bark extract, we observed a pro-oxidant role of MPTE in cancer cells which was evident by dose dependent increase in ROS staining with treatment of MPTE (Packer *et al.*, 1999). Polyphenols rich extracts from tea leaves, grapes, fruits and berries have already been reported to induce ROS production and induce apoptosis in cancer cells besides having predominantly antioxidant effect in normal cells (Leon-Gonzalez *et al.*, 2015). Polyphenols can act as both antioxidant or pro-oxidant depending

upon the nature of cells. In normal cells, polyphenolic compounds prevent the cellular material from oxidative stress because of its anti-oxidant activity while in cancer cells they may behave as pro-oxidant compound and can kill the tumor cells because of high pH and increased level of redox active transient metals (Leon-Gonzalez *et al.*, 2015, Eghbaliferiz and Iranshahi, 2016). This specific targeting of cancer cells makes the polyphenolic compounds an interesting candidate for anticancer therapy. Increased ROS is also associated with increase granularity in the cells indicating the early signs of apoptosis as previously it has been reported that increase in ROS generation leads to senescence by increased granulation of cells (Gosselin *et al.*, 2009, Raghuram *et al.*, 2010).

It is also interesting to note that treatment of MPTE induced the expression of p73, tumor suppressor genes in p53 deficient HeLa cells. Previously, it has been shown that increase ROS production can activate the p73 expression in HeLa cells and induce apoptosis through mitochondrial pathway by activation of caspase 9 and 3 (Singh *et al.*, 2007). Activation of p73 has also been observed with different plant products including thymoquinone, epigallocatechin-3-gallate and polyphenolic extracts from grapes and berries in p53 deficient cancer cells where it induced apoptosis by p73 dependent mechanism (Alhosin *et al.*, 2010, Sharif *et al.*, 2012, Achour *et al.*, 2013, Leon-Gonzalez *et al.*, 2017).

Earlier, we have observed in different studies that p53 and p73 also negatively regulates the epigenetic mediator UHRF1 in cancer cells (Alhosin *et al.*, 2010, Achour *et al.*, 2013). In this study, we also observed downregulation of UHRF1 upon MPTE treatment in HeLa cells along with upregulation of p73, correlating with the previous data. UHRF1 is mostly found upregulated in cancers and promotes oncogenesis of cells by facilitating their passage through cell cycle (Ashraf *et al.*, 2017). High levels of UHRF1 directly interferes in function of tumor suppressor genes (TSGs) or induces downregulation of variety of TSGs through their promoter hypermethylation. UHRF1 upregulation in cancer cells also makes the cells resistive to anticancer therapy by facilitating the DNA damage repair, highlighting its potential as a target for anticancer therapy (Bronner *et al.*, 2013, Ashraf *et al.*, 2017). Therefore, knockdown of UHRF1 by siRNA or other plant products such as ECGC, thymoquinone or polyphenolic extracts induced the apoptosis in cancer cells and improved the response of resistive tumor cells to anticancer therapy (Alhosin *et al.*, 2010, Achour *et al.*, 2013, Bronner *et al.*, 2013). In our current study, we observed a downregulation of UHRF1 with chatechin and epicatechin associated monomers and polymers enriched in MPTE and we observed blockade of cells in

G2/M phase which is in agreement with a previous finding where depletion of UHRF1 resulted in cell cycle arrest in G2/M phase of cell cycle (Tien *et al.*, 2011). MPTE also downregulated the expression of DNMT1, important epigenetic partner of UHRF1. It is through the mutual coordination with DNMT1 that UHRF1 silences different TSGs through promoter hypermethylation (Unoki, 2011, Bronner *et al.*, 2013). We have also observed that downregulation of UHRF1 and DNMT1 was followed by global hypomethylation on treatment with MPTE. Catechol containing dietary polyphenols have been well described previously to interfere in the DNA methylation process (Stefanska *et al.*, 2012). Catechol groups can be methylated by catechol-O-methyltransferase (COMT) to methylated catechols. This process depletes the S-adenosyl-L-methionine (SAM), the methyl group donor in the body for DNA methylation and converts it into S-adenosyl-L-homocysteine (SAH) which is a potent inhibitor of DNA methylation by feedback mechanism (Lee and Zhu, 2006). Additionally, gallic acid moiety containing catechol analogues such as (-)-epigallocatechin-3-O-gallate can also directly inhibit DNMT1 by tethering into the hydrophilic binding pocket of DNMT1 through Mg^{+2} stabilized interaction (Lee *et al.*, 2005, Fang *et al.*, 2007). MPTE is rich in this catechol containing compounds and by affecting the important actors of DNA methylation machinery including UHRF1 and DNMT1; it can interfere in the global methylation patterns of the cells.

In conclusion, our study showed the anticancer properties of maritime pine tannin extract and demonstrated that MPTE specifically inhibited the proliferation of cancer cells and induced cell cycle arrest in G2/M phase of HeLa cells along with ROS mediated activation of mitochondrial apoptotic pathway. MPTE increased the expression of p73 tumor suppressor gene while it downregulated oncogenic UHRF1 and DNMT1 in cancer cells and reduced the global DNA methylation levels. Maritime pine bark extract has been used in traditional herbal medicine for a long time. Easy availability in nature along with unique capability to inhibit cancer cells and regulate the DNA methylation patterns make MPTE an interesting candidate for pharmaceutical research to explore it for anticancer therapy.

REFERENCES

Achour, M., Mousli, M., Alhosin, M., Ibrahim, A., Peluso, J., Muller, C.D., Schini-Kerth, V.B., Hamiche, A., Dhe-Paganon, S. & Bronner, C., 2013. Epigallocatechin-3-gallate up-regulates tumor

suppressor gene expression via a reactive oxygen species-dependent down-regulation of UHRF1. *Biochem Biophys Res Commun,* 430**,** 208-12.

Alhosin, M., Abusnina, A., Achour, M., Sharif, T., Muller, C., Peluso, J., Chataigneau, T., Lugnier, C., Schini-Kerth, V.B., Bronner, C. & Fuhrmann, G., 2010. Induction of apoptosis by thymoquinone in lymphoblastic leukemia Jurkat cells is mediated by a p73-dependent pathway which targets the epigenetic integrator UHRF1. *Biochem Pharmacol,* 79**,** 1251-60.

Asensi, M., Ortega, A., Mena, S., Feddi, F. & Estrela, J.M., 2011. Natural polyphenols in cancer therapy. *Crit Rev Clin Lab Sci,* 48**,** 197-216.

Ashraf, W., Ibrahim, A., Alhosin, M., Zaayter, L., Ouararhni, K., Papin, C., Ahmad, T., Hamiche, A., Mely, Y., Bronner, C. & Mousli, M., 2017. The epigenetic integrator UHRF1: on the road to become a universal biomarker for cancer. *Oncotarget,* 8**,** 51946-51962.

Belcaro, G., Cesarone, M.R., Genovesi, D., Ledda, A., Vinciguerra, G., Ricci, A., Pellegrini, L., Gizzi, G., Ippolito, E., Dugall, M., Cacchio, M., Di Renzo, A. & Stuard, S., 2008. Pycnogenol may alleviate adverse effects in oncologic treatment. *Panminerva Med,* 50**,** 227-34.

Bode, A.M. & Dong, Z., 2009. Epigallocatechin 3-gallate and green tea catechins: United they work, divided they fail. *Cancer Prev Res (Phila),* 2**,** 514-7.

Bronner, C., Krifa, M. & Mousli, M., 2013. Increasing role of UHRF1 in the reading and inheritance of the epigenetic code as well as in tumorogenesis. *Biochem Pharmacol,* 86**,** 1643-9.

Buz'zard, A.R. & Lau, B.H., 2007. Pycnogenol reduces talc-induced neoplastic transformation in human ovarian cell cultures. *Phytother Res,* 21**,** 579-86.

Chen, Y.H., Yeh, C.W., Lo, H.C., Su, S.L., Hseu, Y.C. & Hsu, L.S., 2012. Generation of reactive oxygen species mediates butein-induced apoptosis in neuroblastoma cells. *Oncol Rep,* 27**,** 1233-7.

Chupin, L., Motillon, C., Charrier-El Bouhtoury, F., Pizzi, A. & Charrier, B., 2013. Characterisation of maritime pine (Pinus pinaster) bark tannins extracted under different conditions by spectroscopic methods, FTIR and HPLC. *Industrial Crops and Products,* 49**,** 897-903.

Dawson, M.A. & Kouzarides, T., 2012. Cancer epigenetics: from mechanism to therapy. *Cell,* 150**,** 12-27.

De La Luz Cadiz-Gurrea, M., Fernandez-Arroyo, S. & Segura-Carretero, A., 2014. Pine bark and green tea concentrated extracts: antioxidant activity and comprehensive characterization of bioactive compounds by HPLC-ESI-QTOF-MS. *Int J Mol Sci,* 15**,** 20382-402.

Eghbaliferiz, S. & Iranshahi, M., 2016. Prooxidant Activity of Polyphenols, Flavonoids, Anthocyanins and Carotenoids: Updated Review of Mechanisms and Catalyzing Metals. *Phytother Res,* 30**,** 1379-91.

Fang, M., Chen, D. & Yang, C.S., 2007. Dietary polyphenols may affect DNA methylation. *J Nutr,* 137**,** 223S-228S.

Fang, M.Z., Wang, Y., Ai, N., Hou, Z., Sun, Y., Lu, H., Welsh, W. & Yang, C.S., 2003. Tea polyphenol (-)-epigallocatechin-3-gallate inhibits DNA methyltransferase and reactivates methylation-silenced genes in cancer cell lines. *Cancer Res,* 63**,** 7563-70.

Ferlay, J., Soerjomataram, I., Dikshit, R., Eser, S., Mathers, C., Rebelo, M., Parkin, D.M., Forman, D. & Bray, F., 2015. Cancer incidence and mortality worldwide: sources, methods and major patterns in GLOBOCAN 2012. *Int J Cancer,* 136**,** E359-86.

Gali-Muhtasib, H., Hmadi, R., Kareh, M., Tohme, R. & Darwiche, N., 2015. Cell death mechanisms of plant-derived anticancer drugs: beyond apoptosis. *Apoptosis,* 20**,** 1531-62.

Gosselin, K., Deruy, E., Martien, S., Vercamer, C., Bouali, F., Dujardin, T., Slomianny, C., Houel-Renault, L., Chelli, F., De Launoit, Y. & Abbadie, C., 2009. Senescent keratinocytes die by autophagic programmed cell death. *Am J Pathol,* 174**,** 423-35.

Greenwell, M. & Rahman, P.K., 2015. Medicinal Plants: Their Use in Anticancer Treatment. *Int J Pharm Sci Res,* 6**,** 4103-4112.

Halder, B., Bhattacharya, U., Mukhopadhyay, S. & Giri, A.K., 2008. Molecular mechanism of black tea polyphenols induced apoptosis in human skin cancer cells: involvement of Bax translocation and mitochondria mediated death cascade. *Carcinogenesis,* 29**,** 129-38.

Harati, K., Slodnik, P., Chromik, A.M., Behr, B., Goertz, O., Hirsch, T., Kapalschinski, N., Klein-Hitpass, L., Kolbenschlag, J., Uhl, W., Lehnhardt, M. & Daigeler, A., 2015. Proapoptotic effects of pycnogenol on HT1080 human fibrosarcoma cells. *Int J Oncol,* 46**,** 1629-36.

Hopfner, R., Mousli, M., Jeltsch, J.M., Voulgaris, A., Lutz, Y., Marin, C., Bellocq, J.P., Oudet, P. & Bronner, C., 2000. ICBP90, a novel human CCAAT binding protein, involved in the regulation of topoisomerase IIalpha expression. *Cancer Res,* 60**,** 121-8.

Huang, W.W., Yang, J.S., Lin, C.F., Ho, W.J. & Lee, M.R., 2005. Pycnogenol induces differentiation and apoptosis in human promyeloid leukemia HL-60 cells. *Leuk Res,* 29**,** 685-92.

Huynh, H.T. & Teel, R.W., 2000. Selective induction of apoptosis in human mammary cancer cells (MCF-7) by pycnogenol. *Anticancer Res,* 20**,** 2417-20.

Iqbal, J., Abbasi, B.A., Mahmood, T., Kanwal, S., Ali, B., Shah, S.A. & Khalil, A.T., 2017. Plant-derived anticancer agents: A green anticancer approach. *Asian Pacific Journal of Tropical Biomedicine,* 7**,** 1129-1150.

Krifa, M., Alhosin, M., Muller, C.D., Gies, J.P., Chekir-Ghedira, L., Ghedira, K., Mely, Y., Bronner, C. & Mousli, M., 2013. Limoniastrum guyonianum aqueous gall extract induces apoptosis in human cervical cancer cells involving p16 INK4A re-expression related to UHRF1 and DNMT1 down-regulation. *J Exp Clin Cancer Res,* 32**,** 30.

Lee, W.J., Shim, J.Y. & Zhu, B.T., 2005. Mechanisms for the inhibition of DNA methyltransferases by tea catechins and bioflavonoids. *Mol Pharmacol,* 68**,** 1018-30.

Lee, W.J. & Zhu, B.T., 2006. Inhibition of DNA methylation by caffeic acid and chlorogenic acid, two common catechol-containing coffee polyphenols. *Carcinogenesis,* 27**,** 269-77.

Leon-Gonzalez, A.J., Auger, C. & Schini-Kerth, V.B., 2015. Pro-oxidant activity of polyphenols and its implication on cancer chemoprevention and chemotherapy. *Biochem Pharmacol,* 98**,** 371-80.

Leon-Gonzalez, A.J., Jara-Palacios, M.J., Abbas, M., Heredia, F.J. & Schini-Kerth, V.B., 2017. Role of epigenetic regulation on the induction of apoptosis in Jurkat leukemia cells by white grape pomace rich in phenolic compounds. *Food Funct,* 8**,** 4062-4069.

Moudi, M., Go, R., Yien, C.Y. & Nazre, M., 2013. Vinca alkaloids. *Int J Prev Med,* 4**,** 1231-5.

Navarrete, P., Pizzi, A., Pasch, H., Rode, K. & Delmotte, L., 2010. MALDI-TOF and 13C NMR characterization of maritime pine industrial tannin extract. *Industrial Crops and Products,* 32**,** 105-110.

Packer, L., Rimbach, G. & Virgili, F., 1999. Antioxidant activity and biologic properties of a procyanidin-rich extract from pine (Pinus maritima) bark, pycnogenol. *Free Radic Biol Med,* 27**,** 704-24.

Pechalrieu, D., Etievant, C. & Arimondo, P.B., 2017. DNA methyltransferase inhibitors in cancer: From pharmacology to translational studies. *Biochem Pharmacol,* 129**,** 1-13.

Raghuram, G.V., Pathak, N., Jain, D., Panwar, H., Pandey, H., Jain, S.K. & Mishra, P.K., 2010. Molecular mechanisms of isocyanate induced oncogenic transformation in ovarian epithelial cells. *Reprod Toxicol,* 30**,** 377-86.

Rohdewald, P.J., 2015. Update on the clinical pharmacology of Pycnogenol(R). *Medical Research Archives*.

Sandoval, J. & Esteller, M., 2012. Cancer epigenomics: beyond genomics. *Curr Opin Genet Dev,* 22**,** 50-5.

Senese, S., Lo, Y.C., Huang, D., Zangle, T.A., Gholkar, A.A., Robert, L., Homet, B., Ribas, A., Summers, M.K., Teitell, M.A., Damoiseaux, R. & Torres, J.Z., 2014. Chemical dissection of the cell cycle: probes for cell biology and anti-cancer drug development. *Cell Death Dis,* 5**,** e1462.

Shan, H.M., Shi, Y. & Quan, J., 2015. Identification of green tea catechins as potent inhibitors of the polo-box domain of polo-like kinase 1. *ChemMedChem,* 10**,** 158-63.

Sharif, T., Alhosin, M., Auger, C., Minker, C., Kim, J.H., Etienne-Selloum, N., Bories, P., Gronemeyer, H., Lobstein, A., Bronner, C., Fuhrmann, G. & Schini-Kerth, V.B., 2012. Aronia melanocarpa juice induces a redox-sensitive p73-related caspase 3-dependent apoptosis in human leukemia cells. *PLoS One,* 7**,** e32526.

Sharma, S., Kelly, T.K. & Jones, P.A., 2010. Epigenetics in cancer. *Carcinogenesis,* 31**,** 27-36.

Singh, M., Sharma, H. & Singh, N., 2007. Hydrogen peroxide induces apoptosis in HeLa cells through mitochondrial pathway. *Mitochondrion,* 7**,** 367-73.

Stefanska, B., Karlic, H., Varga, F., Fabianowska-Majewska, K. & Haslberger, A., 2012. Epigenetic mechanisms in anti-cancer actions of bioactive food components--the implications in cancer prevention. *Br J Pharmacol,* 167**,** 279-97.

Takanashi, K., Suda, M., Matsumoto, K., Ishihara, C., Toda, K., Kawaguchi, K., Senga, S., Kobayashi, N., Ichikawa, M., Katoh, M., Hattori, Y., Kawahara, S.I., Umezawa, K., Fujii, H. & Makabe, H., 2017. Epicatechin oligomers longer than trimers have anti-cancer activities, but not the catechin counterparts. *Sci Rep,* 7**,** 7791.

Tien, A.L., Senbanerjee, S., Kulkarni, A., Mudbhary, R., Goudreau, B., Ganesan, S., Sadler, K.C. & Ukomadu, C., 2011. UHRF1 depletion causes a G2/M arrest, activation of DNA damage response and apoptosis. *Biochem J,* 435**,** 175-85.

Unoki, M., 2011. Current and potential anticancer drugs targeting members of the UHRF1 complex including epigenetic modifiers. *Recent Pat Anticancer Drug Discov,* 6**,** 116-30.

Wang, H., Khor, T.O., Shu, L., Su, Z.Y., Fuentes, F., Lee, J.H. & Kong, A.N., 2012. Plants vs. cancer: a review on natural phytochemicals in preventing and treating cancers and their druggability. *Anticancer Agents Med Chem,* 12**,** 1281-305.

Wang, J., Pan, Y., Hu, J., Ma, Q., Xu, Y., Zhang, Y., Zhang, F. & Liu, Y., 2018. Tea polyphenols induce S phase arrest and apoptosis in gallbladder cancer cells. *Braz J Med Biol Res,* 51**,** e6891.

Wang, J., Xie, Y., Feng, Y., Zhang, L., Huang, X., Shen, X. & Luo, X., 2015. (-)-Epigallocatechingallate induces apoptosis in B lymphoma cells via caspase-dependent pathway and Bcl-2 family protein modulation. *Int J Oncol,* 46**,** 1507-15.

Xie, S. & Zhou, J., 2017. Harnessing Plant Biodiversity for the Discovery of Novel Anticancer Drugs Targeting Microtubules. *Front Plant Sci,* 8**,** 720.

Yang, C.S. & Wang, H., 2016. Cancer Preventive Activities of Tea Catechins. *Molecules,* 21.

Zhou, Y., Zheng, J., Li, Y., Xu, D.P., Li, S., Chen, Y.M. & Li, H.B., 2016. Natural Polyphenols for Prevention and Treatment of Cancer. *Nutrients,* 8.

Zhu, L., Han, M.B., Gao, Y., Wang, H., Dai, L., Wen, Y. & Na, L.X., 2015. Curcumin triggers apoptosis via upregulation of Bax/Bcl-2 ratio and caspase activation in SW872 human adipocytes. *Mol Med Rep,* 12**,** 1151-6.

RÉSUMÉ DE THÈSE

8 - RÉSUMÉ DE THÈSE

8.1 Introduction :

Le cancer est une croissance incontrôlée de cellules anormales chez l'homme qui est déclenchée par des altérations génétiques et des modulations épigénétiques. Des processus épigénétiques comme la méthylation de l'ADN, la modification des histones et l'expression de l'ARN non codant régulent la dynamique de l'expression des gènes. La reprogrammation de processus épigénétiques par divers facteurs peut conduire à une transformation cellulaire maligne soit en induisant l'expression d'oncogènes, soit en arrêtant l'expression de gènes suppresseurs de tumeur (TSGs). Contrairement aux altérations génétiques, les anomalies épigénétiques sont réversibles et peuvent être explorées comme des cibles thérapeutiques potentielles pour prévenir et traiter les cancers.

UHRF1 (Ubiquitin-like, containing PHD and ring finger 1) est une protéine multi-domaines (Figure I) impliquée dans la régulation épigénétique de l'expression des gènes. Elle est fortement exprimée dans la plupart des cellules cancéreuses et inhibe l'expression des gènes suppresseurs de tumeurs tels que *p16INK4A, p14ARF, RB1* et *p73* par l'hypermethylation de leurs promoteurs. UHRF1, par son interaction et sa coordination avec divers autres effecteurs dans le nucléosome, a la capacité de contrôler des processus épigénétiques importants tels que la méthylation de l'ADN et les modifications post-traductionnelles des histones. Normalement, UHRF1 identifie l'ADN hémi-méthylé grâce à son domaine SRA et elle interagit avec la marque épigénétique H3K9me3 présente sur les histones grâce aux domaines Tudor et PHD. Elle réplique les CpG méthylés dans l'ADN nouvellement formé en recrutant la DNMT1. En outre, UHRF1 interagit également avec les histones méthyl-transférases et les histones désacétylases pour modifier les profils de méthylation et d'acétylation des histones. De nombreuses autres protéines comme PCNA, USP7, BRCA1, Tip60 sont également connues pour être présentes dans le même complexe que celui d'UHRF1 et ensemble elles sont impliquées dans différentes activités cellulaires, incluant la régulation de la transcription des gènes et la réparation des ADN endommagés.

Tip60 est une acétyltransférase importante qui joue un rôle clé dans la régulation de la transcription des gènes et la réparation des dommages de l'ADN, la régulation du cycle cellulaire et l'apoptose. Il s'agit d'une protéine multi-domaines (Figure I) qui, grâce à son domaine catalytique MYST, peut acétyler une variété de protéines, y compris les histones (H2AK5, H3K14 et H4K), la p53, l'ATM et la DNMT1. TIP60. Il a été démontré par notre équipe qu'elle est présente dans le même complexe

épigénétique avec UHRF1 comme partenaire privilégié. Elle joue un rôle clé dans la régulation de l'activité de la DNMT1 dans les cellules. Aussi, l'interaction entre UHRF1 et Tip60 est responsable de l'arrêt de prolifération dépendante de la p53 et de l'apoptose. Par conséquent, ce projet vise à mieux comprendre l'interaction UHRF1-TIP60 dans les cellules HeLa, ce qui aidera à élucider les rôles de ces deux acteurs dans les cellules normales et cancéreuses.

Figure I : Schéma des différents domaines d'UHRF1 et Tip60.

8.2 Objectifs :

Les principaux objectifs de ce projet étaient les suivants:

1. Visualiser l'interaction entre UHRF1 et TIP60 dans les cellules par microscopie d'imagerie à temps de vie de fluorescence (FLIM). TIP60 et UHRF1 sont impliqués dans la replication de l'ADN dans la phase S, la réplication du code épigénétique et la réparation des dommages de l'ADN. Ainsi, l'étude de l'interaction de ces protéines au cours de la phase S peut aider à comprendre la fonction de ces protéines ensemble dans cette phase du cycle cellulaire.

2. Identifier les domaines de TIP60 interagissant avec UHRF1 à l'aide des mutants de Tip60.

3. Etudier le rôle de Tip60 dans la réparation des lésions de l'ADN.

Nous avons également étudier la colocalisation de TIP60 et UHRF1 sur les cassures double brin d'ADN afin de vérifier si les deux protéines travaillent en cohérence les unes avec les autres pendant la réponse aux dommages de l'ADN ou non?

4. Vérifier l'effet de la surexpression de TIP60 dans les cellules cancéreuses. La TIP60 est censée exercer un rôle suppresseur de tumeur en inhibant directement la prolifération ou favorisant l'expression des autres TSG. TIP60 se trouve sous-exprimée dans la plupart des cellules cancéreuses et la surexpression de cette protéine dans ces cellules tumorales pourrait restaurer le fonctionnement normal des autres TSGs et peut empêcher la prolifération des cellules cancéreuses.

8.3 Méthodologie et Résultats :

Pour évaluer l'interaction Tip60-UHRF1 dans les cellules, nous avons utilisé la technique FRET-FLIM dans les cellules HeLa transfectées avec Tip60-eGFP et UHRF1-mCherry. Tip60-eGFP agissait comme fluorophore donneur tandis qu'UHRF1-mCherry agissait comme un fluorophore accepteur, car les spectres d'émission de l'eGFP se trouve dans les spectres d'excitation de mCherry. Selon le principe FLIM-FRET, le temps de vie du fluorophore donneur est significativement réduit si le fluorophore accepteur est à proximité étroite du fluorophore donneur. Nos expériences montrent que le temps de vie de Tip60-eGFP a été significativement réduit en présence de UHRF1-mCherry confirmant la présence des deux protéines à proximité l'une de l'autre (<10 nm). L'interaction entre les protéines fluorescentes exogènes avec les protéines endogènes a également été vérifiée par des expériences de co-immunoprécipitation afin de montrer la fonctionnalité de ces protéines. Nous avons pu observer que la protéine Tip60-eGFP exogène était immunoprécipitée avec UHRF1 endogène et UHRF1-mCherry exogène, alors que la protéine UHRF1-mCherry exogène était immunoprécipitée avec Tip60 endogène et Tip60-eGFP exogène. Dans des expériences réciproques, l'extraction de TIP60-eGFP a entraîné une co-immunoprécipitation de protéines UHRF1 endogènes et UHRF1-mCherry exogènes montrant que l'interaction est spécifique entre les protéines UHRF1 et TIP60.

La DNMT1 a été également co-immunoprécipité avec les protéines UHRF1 et TIP60 montrant la présence des trois protéines dans le même complexe épigénétique.

Tip60 et UHRF1 sont impliquées dans des activités cellulaires importantes au cours de la phase de réplication de l'ADN du cycle cellulaire, l'interaction entre Tip60-eGFP et UHRF1-mCherry a également été étudiée en phase S du cycle cellulaire en utilisant la technique FRET FLIM. Les cellules en phase S ont été identifiées par « Clic-iT EdU » et un taux plus élevé de FRET a été observé dans les cellules en phase S indiquant une forte interaction des deux protéines dans cette phase (Figure II).

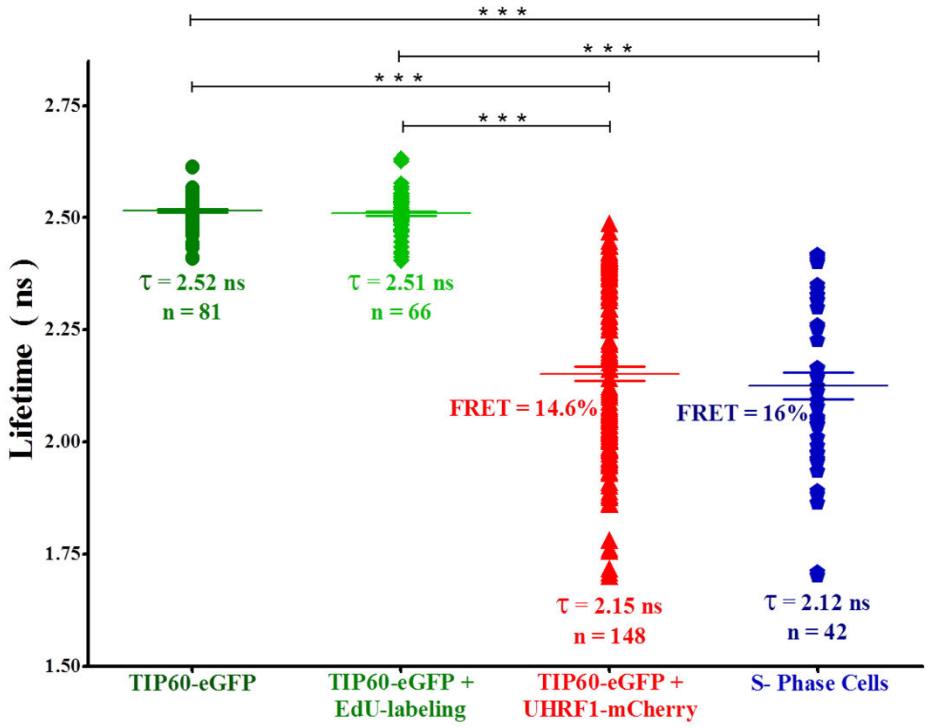

Figure II : L'interaction entre TIP60-eGFP et UHRF1-mCherry dans la phase S du cycle cellulaire des cellules HeLa. Distribution du temps de vie de fluorescence de TIP60-eGFP (●), des cellules TIP60-eGFP marquées par EdU (◆), des cellules co-transfectées par TIP60-eGFP + UHRF1-mCherry (▲) et des cellules co-transfectées dans la phase S du cycle cellulaire (⬟). Les valeurs sont les moyennes ± SEM de cinq expériences indépendantes. Pour l'analyse statistique, un test t Student a été réalisé (*** P <0,001).

Différents mutants de TIP60 ont également été construits dans cette étude afin de trouver le domaine d'interaction de TIP60 avec UHRF1. L'analyse FLIM-FRET de ces mutants de TIP60 marqués par eGFP prédit que toute délétion dans le domaine MYST de TIP60 entraîne une perte de son interaction avec UHRF1. La délétion du chromodomaine de TIP60 a également réduit son interaction avec UHRF1 dans les cellules. Ceci a été confirmé par une étude *in vitro* «pulldown assay avec des mutants de His-TIP60. Cette étude montre que l'interaction de TIP60 avec UHRF1 dépend fortement de son doigt de zinc et de son domaine MYST entier (Figure III).

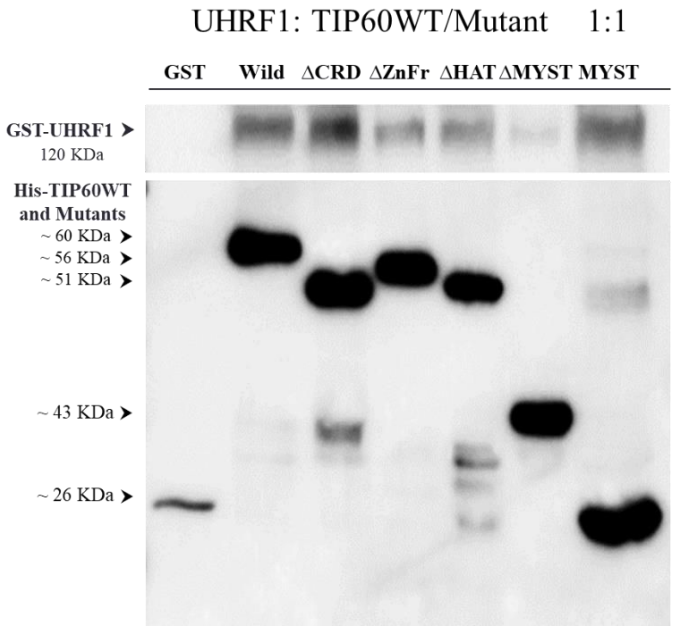

Figure III : Analyse de l'interaction *in vitro* entre His-TIP60WT / mutants et la GST-UHRF1.

Comme UHRF1 et TIP60 sont impliqués dans la réponse aux dommages de l'ADN, nous avons vérifié l'interaction de ces deux protéines sur les sites de l'ADN endommagé. Nous avons utilisé des techniques spécifiques pour induire des cassures localisées de double brin d'ADN et vérifié le recrutement de protéines endogènes et exogènes de UHRF1 et TIP60 à ces sites d'ADN endommagés. Nos résultats indiquent une colocalisation des deux protéines aux cassures double brin d'ADN. UHRF1 est recruté précocement sur les sites de l'ADN endommagé, suivi du recrutement de TIP60. La localisation de TIP60 a été suivie plus tard par la disparition d'UHRF1 du site d'endommagé de l'ADN suggérant que TIP60 joue un rôle dans la régulation d'UHRF1 (Figure IV).

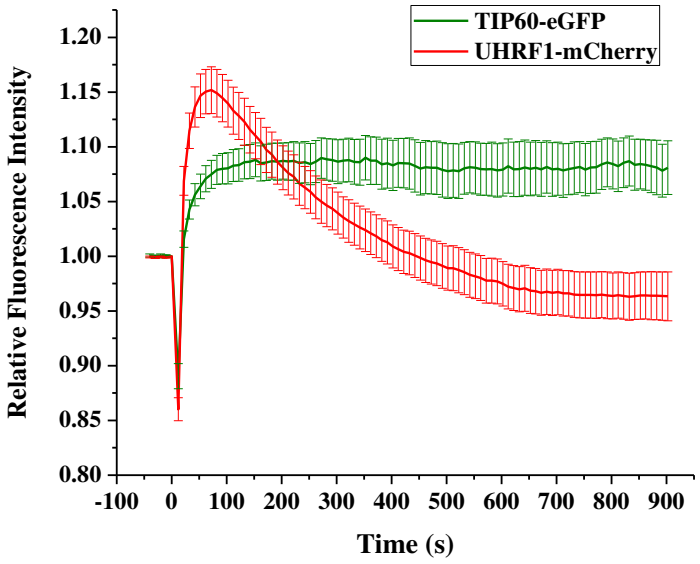

Figure IV : Dynamique de l'accumulation de TIP60-eGFP et UHRF1-mCherry sur le site de l'endommagement de l'ADN.

Comme Tip60 exerce une activité inhibitrice sur les TSGs et qu'elle se trouve faiblement exprimée dans les cancers, nous avons étudié l'effet de son surexpression dans des cellules HeLa. L'expression d'UHRF1 et d'autres protéines importantes dans la modulation épigénétique et la régulation du cycle cellulaire comme DNMT1 et p21, ont été inhibées lorsque Tip60-eGFP est surexprimée. En outre, la sur-expression de Tip60 a également induit un effet apoptotique dans les cellules par une activation de la cascade apoptotique médiée par p53/p73, accompagnée par une diminution de la stabilité mitochondriale, une activation protéolytique accrue de la caspase 3 et un clivage de la PARP et a inhibé la prolifération cellulaire (Figure V).

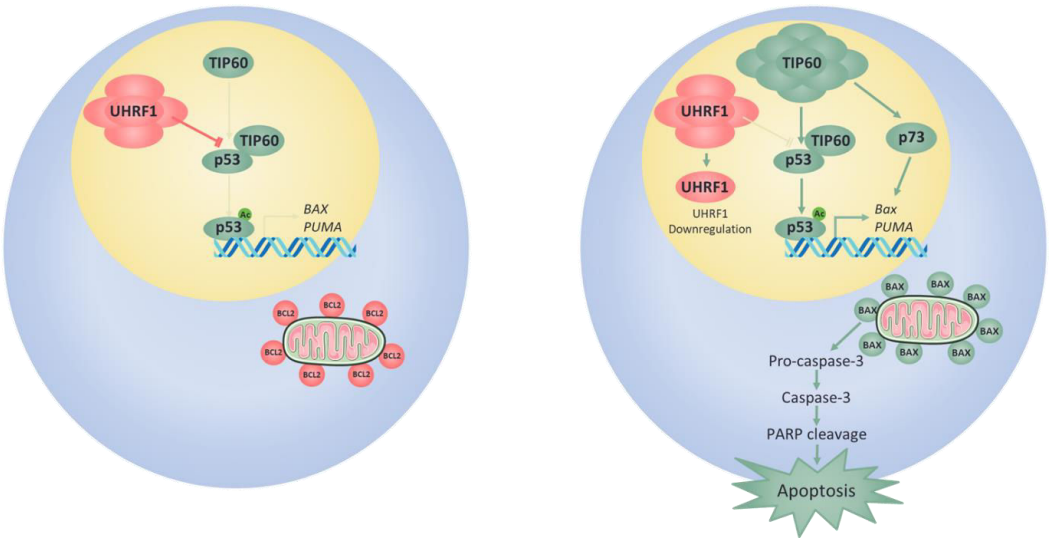

Figure V : Modèle proposé d'apoptose médiée par TIP60 dans les cellules cancéreuses.

8.4 Conclusion et Perspectives :

Nos résultats montrent qu'UHRF1 est un partenaire avec TIP60. Elle interagit directement avec le domaine MYST de la protéine TIP60. Le domaine MYST est hautement conservé dans d'autres histones acétyltransférases, y compris MOZ, MORF, HBO1 et MOF, ce qui suggère la possibilité d'UHRF1 d'interagir avec ces protéines dans les cellules.

Cette étude met également en évidence le rôle des protéines UHRF1 et TIP60 dans la réparation des sites d'ADN endommagés avec des cinétiques différentes. D'autres études peuvent être réalisées ultérieurement pour étudier les mécanismes responsables du recrutement de ces protéines sur les sites de dommages à l'ADN.

En outre, nos résultats suggèrent aussi un rôle suppresseur de tumeur de TIP60 en régulant les niveaux d'expressions des protéines UHRF1 et DNMT1 et par l'activation de p73 et de la cascade apoptotique. L'analyse *in silico* suggère aussi que TIP60 peut réguler la stabilité d'UHRF1 par un mécanisme de régulation similaire à celui de la DNMT1.

TIP60 peut interférer sur le rôle protecteur d'USP7 avec UHRF1 et peut donc jouer un rôle dans sa la dégradation par la voie du protéasome (Figure VI).

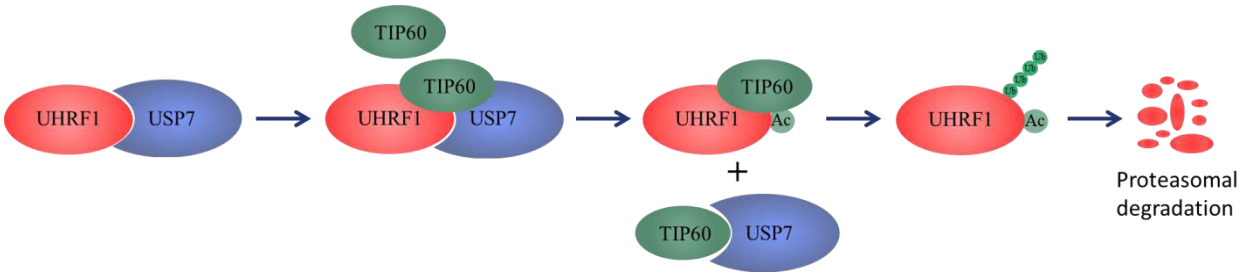

Figure VI : Modèle proposé pour la dégradation d'UHRF1 induite par TIP60.

Waseem ASHRAF

Mécanismes d'interaction de l'intégrateur épigénétique UHRF1 avec l'acétyltransférase TIP60

Résumé

UHRF1 est une protéine nucléaire responsable du maintien et de la régulation de l'épigénome des cellules. Elle favorise la prolifération cellulaire et est surexprimée dans la plupart des cancers. TIP60, l'un des partenaires le plus important d'UHRF1, est impliqué dans le remodelage de la chromatine et la régulation transcriptionnelle grâce à son activité acétyltransférase. Ensemble, les deux protéines régulent la stabilité et l'activité d'autres protéines telles que la DNMT1 et la p53. Le but de cette étude était d'explorer le mécanisme d'interaction entre UHRF1 et TIP60 en visualisant cette interaction dans les cellules. La microscopie par imagerie à temps de vie de fluorescence et d'autres techniques de biologie moléculaire ont été utilisées. Les résultats ont montré que UHRF1 interagit directement avec le domaine MYST de TIP60 et cette interaction se produit dans la phase S du cycle cellulaire. Les deux protéines ont également montré une réponse similaire aux dommages à l'ADN, ce qui prédit une cohérence dans leur fonction dans le mécanisme de réparation de l'ADN. La surexpression de TIP60 a également induit la baisse du niveau d'UHRF1 et de DNMT1 ainsi qu'une induction d'apoptose dans les cellules ce qui suggère un rôle de TIP60 dans la régulation des fonctions oncogéniques d'UHRF1.

Résumé en anglais

UHRF1 is a nuclear protein maintaining and regulating the epigenome of cells. Its promotes proliferation and is found upregulated in most of cancers. TIP60 is one of the important interacting partner of UHRF1 and is involved in chromatin remodeling and transcriptional regulation through its acetyltransferase activity. Together they regulate the stability and activity of other proteins such as DNMT1 and p53. The aim of this thesis was to explore the mechanism of interaction between UHRF1 and TIP60 by visualizing this interaction in cells. Fluorescent lifetime imaging microscopy and other molecular biology techniques were employed for this purpose. Results of this study showed that UHRF1 interacts directly to the MYST domain of TIP60 and this interaction prevails in the S-phase of cell cycle. Both proteins also showed a similar response to DNA damage predicting a coherence in their function in DNA repair mechanism. Overexpression of TIP60 also downregulated UHRF1 and DNMT1 and induced apoptosis in cells suggesting a role of TIP60 in regulation of oncogenic functions of UHRF1.

Keywords: UHRF1, TIP60, Protein-Protein interaction, DNMT1, FLIM, FRET, DNA methylation, Histone acetyltransferase (HAT)